Evaluation of a Novel Intradermal Delivery System for the Treatment of Pressure Ulcers

Abigail Omolu, BSc

Thesis submitted to University College London for the

Degree of Doctor of Philosophy

December 2016

Declaration

I, Abigail Omolu, confirm that the work presented in this thesis is my own. Where information has been derived from other sources, I confirm that this has been indicated in the thesis.

Signed:

……..

A.M.N Omolu

Acknowledgements

I have been extremely fortunate to have been able to work with so many varied and interesting research groups throughout my Ph.D. I have had the pleasure of meeting and collaborating with a wide variety of people that have also become good friends over the years. I will remember this time fondly.

Firstly, I am very grateful to my supervisor Dr. Richard Day for his on-going support, guidance and knowledge. He has contributed greatly to my research and I would like to thank him for all his efforts. He has been there every step of the way and has made my Ph.D. such a wonderful and creative experience. I would also like to thank Professor Simon Gaisford for all his help (and patience!) in teaching me the fundamentals of pharmaceutics.

I have had the utmost pleasure in collaborating with several national and international research groups and institutions, and would like to thank the following principal investigators and members of their team: Dr. Maryse Bailly (Department of Cell Biology, Institute of Ophthalmology, London, UK), Professor Lynne Regan (Department of Molecular Biophysics and Biochemistry, Yale University, Connecticut, USA), Dr. Richard Jackson (UCL Healthcare Biomagnetics Laboratories, Royal Institution of Great Britain, London, UK), Dr. Roger Narayan (Joint Department of Biomedical Engineering, University of North Carolina and North Carolina State University, North Carolina, USA) and Lissie Webster and the medical team at the Spinal Cord Injuries and Neurorehabilitation Unit, Northern General Hospital (Sheffield, UK).

For their technical support I thank Dr Christopher Thrasivoulou for his assistance in carrying out *in vivo* surgical procedures, Tim Robson for his invaluable help with processing my histological samples, Dr Sunny Gill for his help developing HPLC methods, and Dr Nicky Mordan and Dr Mark Turmaine for their guidance in scanning electron microscopy.

A special thank you to He Li, Laxmi Kerai, I-Hui Yang, Asma Buanz and Ashley Schloss who kindly took time out of their own experiments to teach me the techniques that I have used throughout my research.

My thanks extend to fellow post-doc and Ph.D. students Nina Parmar, Pauline Guhmann, Panos Sofokleous, Yani Angelopoulos, Jenny Kechagia and Daniel Gilmartin. I wish them all the best in the completion of their research and all their future endeavours.

Abstract

Background

Pressure ulcers, a form of chronic wound, represent a significant health and resource burden in elderly and immobilised patient populations. Pressure ulcers have been shown to exhibit high matrix metalloproteinase (MMP) activity which prevents normal wound healing and doxycycline, as an MMP inhibitor, offers a potential novel treatment. Intradermal delivery of doxycycline could help treat the earliest stages of wound development and prevent further wound progression. The skin, however, has a natural barrier function which prevents the diffusion of large exogenous molecules. Microneedle rollers offer a minimally invasive technique to transiently permeabilise the skin, creating microscopic pores that act as conduits for doxycycline diffusion.

Methods

The research described in this thesis focusses on the repurposing of existing microneedle rollers for the intradermal delivery of doxycycline as a pressure ulcer treatment. Firstly, the effect of microneedle length and application method on micropore formation and rate of drug permeation was investigated using the recently-launched artificial membrane Strat-M^{TM} and compared with excised biological tissue. Next, the biological effects of doxycycline and its transmembrane delivery were modelled in a dermal tissue equivalent (DTE) model, formed from collagen and dermal fibroblasts, by assessing changes DTE contractile behaviour and matrix metalloproteinase (MMP) activity. This simplified *in vitro* model was further developed to better emulate the pressure ulcer microenvironment by introducing: (i) mechanical loading using a bespoke metal weight, (ii) glucose deprivation through the use of glucose-free media, and (iii) inflammatory cells, specifically macrophages, through co-culture. Investigations progressed to a preliminary *in vivo* surgical wound model using compression by magnets to determine the biological effects of pressure in a whole organism. This pre-existing model was established in our lab for future investigations of microneedle-mediated doxycycline delivery. Finally, the repurposing of the existing non-invasive imaging technology optical coherence tomography (OCT) for pressure ulcer evaluation was explored in an observational clinical audit.

Results

The results demonstrate that microneedle rollers significantly enhance the transmembrane delivery of doxycycline with significant effect on tissue-equivalent contraction and MMP activity. Results from the pressure ulcer models corroborate previous findings that the pressure ulcer microenvironment augments MMP activity. Lastly, OCT is shown to detect subsurface biomarkers of skin in the earliest stages of pressure ulcer development, most suitable for treatment with doxycycline.

Table of Contents

List of Tables

List of Figures

List of Abbreviations

α2MG	Alpha-2 macroglobulin
ACCA	Alpha-cyano-4-hydroxy-3-methoxycinnamic acid
AMPA	4-Aminophenylmercuric acetate
ANOVA	Analysis of variance
APC	Antigen-presenting cell
API	Active pharmaceutical ingredient
ATP	Adenosine triphosphate
BSA	Bovine serum albumin
BMI	Body mass index
BMZ	Basement membrane zone
CCP	Critical closing pressure
CSLM	Confocal scanning laser microscopy
CT	Computerised tomography
DMEM	Dulbecco's modified Eagle's medium
DMSO	Dimethyl sulfoxide
DOX	Doxycycline
DTI	Deep tissue injury
ECM	Extracellular matrix
EPUAP	European Pressure Ulcer Advisory Panel
Ethd-1	Ethidium homodimer-1
Ex/Em	Excitation/emission (*in reference to fluorescence signals*)
FBS	Fetal bovine serum
FDA	Food and Drug Administration
FITC	Fluorescein isothiocyanate
FMPCL	Fibroblast (and) macrophage-populated collagen lattices
FPCL	Fibroblast-populated collagen lattices
H&E	Hemotoxylin and eosin
HPLC	High-performance liquid chromatography
IDD	Intradermal delivery
IL	Interleukin
IR	Ischemia-reperfusion
Mφ	Macrophage
MDVSN	Medical Devices and Vulnerable Skin Network
MMP	Matrix metalloproteinase
NPUAP	National Pressure Ulcer Advisory Panel
O.C.T.	Optimum cutting temperature
OCT	Optical coherence tomography

List of Abbreviations

OGD(R)	Oxygen/glucose deprivation (reperfusion)
MALDI-TOF	Matrix-assisted laser desorption/Ionisation time-of-flight
MCP-1	Monochemoattractant protein-1
MMPRS	Matrixmetalloproteinase recognition site
MRI	Magnetic resonance imaging
NA	Numerical aperture
PBS	Phosphate-buffered saline
PFA	Paraformaldehyde
PMA	Phorbol myristate acetate
PSA	Penicillin/ streptomycin/ amphotericin
PU	Pressure ulcer
ROI	Region of interest
ROS	Reactive oxygen species
RPM	Rotations per minute
RPMI	Rosswell Park Memorial Institute
SC	Stratum corneum
SCI	Spinal cord injury
SEM *(imaging)*	Scanning electron microscopy
SEM *(stats.)*	Standard error of the mean
SEM *(scanner*)	Sub-epidermal moisture
SEMA	Sonophoresis-enhanced microneedle arrays
SPE	Solid phase extraction
TACE	TNFα-converting enzyme
TDD	Transdermal drug delivery
TEV	Tobacco etch virus
TFA	Trifluoroacetic acid
TGF	Tissue growth factor
TIMP	Tissue inhibitor of metalloproteinases
TNF	Tissue necrosis factor
UDMA	Urethane dimethacrylate

Dedication

To my loving family.

Thesis Overview

Interdisciplinary nature of the thesis

This thesis was completed as part of the newly formed London Interdisciplinary Doctoral (LIDo) training programme and was funded by the Biotechnology and Biological Sciences Research Council (BBSRC). An integral part of the LIDo Ph.D. programme is to demonstrate interdisciplinarity throughout the body of research undertaken, especially with regards to the methods and approaches used in answering research questions. To achieve this, several national and international collaborations were undertaken to combine the expertise of different specialist research groups and institutions with a common aim of developing novel biotechnologies for medical and clinical applications. As a result, a range of scientific disciplines (including protein chemistry, pharmaceutics, clinical imaging and cell biology) were introduced, in an integrated way, to the research which was primarily based at the Applied Biomedical Engineering Group (UCL). The BBSRC itself puts emphasis on "New Ways of Working" and encourages the union of traditionally disparate research fields for the rapid development of cutting edge technologies.

Thesis chapter outline

The overall direction of the research was to explore novel bioengineering technologies in the prevention, treatment and evaluation of pressure ulcers which could supersede the current conventional therapies and nursing care practices. The thesis is sub-divided into five experimental chapters encompassing four major areas: (i) the development and investigation of biotechnologies that could deliver suitable drugs locally, (ii) investigation of an active pharmaceutical ingredient (API) efficacious as a treatment for pressure ulcers, (iii) the development of a simple yet informative non-human *in vivo* model of the pressure ulcer that could help bridge the gap between *in vitro* models and clinical studies, and (iv) the repurposing of existing imaging tools to improve upon current pressure ulcer evaluation. A summary of the thesis chapters are as follows:

General Introduction — The literature review provides an overview of pressure ulcers in the clinical setting, discussing their aetiology, presentation, complications and traditional clinical care (including current prevention methods and treatments). Fundamental aspects of human skin are detailed to provide a background on healthy skin structure and architecture. The pathophysiological mechanisms behind pressure ulcer development are also detailed and doxycycline is introduced as a potential therapeutic. Intradermal drug delivery methods are also discussed. Finally, the review assesses the current research models of the human pressure ulcer, detailing their advantages and limitations.

Chapter 2 — Assessment of a Microneedle Roller System to Enhance Transmembrane Delivery of Doxycycline. This chapter introduces the microneedle roller system used throughout the research. The ability of the microneedles to enhance the transmembrane delivery of doxycycline are investigated using Franz diffusion cell permeation studies.

Chapter 3 — Microneedle-Enhanced Transmembrane Delivery of Doxycycline to a Dermal Tissue Equivalent. In this chapter, doxycycline is delivered to a cell-based *in vitro* model of the human dermis. This was carried out so that the permeability of the membrane to doxycycline could be monitored through doxycycline's biological effects. The effect of microneedling on cell viability is also explored.

Chapter 4 — Modelling the Pressure Ulcer Microenvironment in an *In Vitro* FPCL System. In direct continuation of Chapter 3, the *in vitro* human dermis model is developed to better reflect the environmental conditions that result in pressure development.

Chapter 5 — An *In Vivo* Preclinical Surgical Model of Early Stage Pressure Ulcers. This chapter details experimental pressure ulcer formation in a preclinical model using surgical implantation of magnets for compression in which the effects of microneedling and doxycycline can be explored.

Chapter 6 — Optical Coherence Tomography for the Non-invasive Evaluation of Pressure Ulcers. This chapter focusses on repurposing a non-destructive *in vivo* imaging tool to identify changes in the skin that could be linked to pressure ulcer development and validates the technical feasibility of this approach in humans.

Overall Discussion — This chapter unites the entire body of research and discusses the thesis' contribution to knowledge. It also discusses how the work as a whole could be used to develop new technologies for clinical applications.

Research hypothesis

The overall research hypothesis is:

"Intradermal delivery of doxycycline by microneedles is a promising tool for treating and preventing the development of early stage pressure ulcers."

Chapter 1 General Introduction

1.1 An introductory clinical background to pressure ulcers

1.1.1 What are pressure ulcers and who do they affect?

Pressure ulcers, also known as decubitus ulcers, pressure sores, bed sores and more recently pressure injury, constitute one of the three major groups of chronic wounds alongside diabetic ulcers and venous leg ulcers[1]. Pressure ulcers are most commonly seen in two patient populations, the bed-ridden elderly in long-term care and immobilised patients with spinal cord injuries (SCI) in the acute care setting. Pressure ulcers are pathophysiologically different to other skin disorders and wounds that may display similar physical characteristics such as incontinence-associated dermatitis, intertriginous dermatitis, medical adhesive-related skin injury and traumatic wounds. Despite current treatments and management protocols, the prevalence/incidence of pressure ulcers remains high[2]. This suggests that either the true etiology has yet to be ascertained, hindering development of effective treatments at the research level, or the current preventative measures are being insufficiently implemented at the clinical level.

1.1.2 Prevalence, incidence and cost of pressure ulcers

Pressure ulcers occur across many healthcare settings including in the hospital and at long-term care facilities such as nursing homes. Worldwide, the highest incidence (the number of individuals with new pressure ulcers divided by the number of individuals at risk) is in the hospital, while the highest prevalence (the number of individuals with a pressure ulcer divided by the number of individuals at risk) is in long-term care facilities[3]. The prevalence rates of pressure ulcers in UK ranges from 5–32% in hospital settings and up to 22% in long-term care facilities[4]. Though a lot of the literature on pressure ulcers reports on ulcer development in elderly populations under long-term medical care, pressure ulcers also occur in the acute health setting in both adults and children[5,6]. Critically ill patients in intensive care units are often

confined to beds for long periods of time due to sedation or ventilation and are susceptible to developing pressure ulcers[7].

About 60% of pressure ulcers have been reported to occur in hospitals[8,9]. The wards which are at greatest risk of pressure ulcer development occurring in newly admitted patients are the orthopedics wards and intensive care units[3]. Pressure ulcers that arise in hospital will typically occur within the first two weeks of patient hospitalisation. For example, about 75% of new pressure ulcers occur in this time period in orthopedic patient populations[10]. This suggests that initial injury on ward admission is more crucial to pressure ulcer development than the length of time spent in the hospital[3]. Understanding when and where the pressure ulcer developed is important in determining where the deficit in care may lie since pressure ulcers are often deemed preventable adverse events, with their emergence representing a potential failure of care[11]. A new pressure ulcer may be categorised as community-acquired if it develops within three days of ward admission, and hospital-acquired (a HAPU) if it develops from three days after ward admission. In the UK, pressure ulcers represent a leading resource burden on the National Health Service (NHS) with annual costs having being estimated between £1.4–£2.5 billion in 2004, approximately 4% of the total NHS expenditure[12]. Much of this cost has been attributed to nurse time[3]. Importantly, the worse a pressure ulcer becomes the more costly it becomes to treat and manage[12].

1.1.3 Clinical pressure ulcer aetiology and pathogenesis

In the clinical setting, pressure ulcers are understood to be caused by prolonged periods of immobility where the body weight is concentrated at a few points. In normal situations of immobility, such as during sleep, the body responds to the increase in pressure at these points through neurological feedback, causing periodic changes in position[13]. In several situations, such as in heavily anesthetised or immobilised patients, or in patients with neurological pathologies (such as a spinal cord injury [SCI]), where sensation is decreased or absent, these feedback mechanisms are either not in place or not functioning properly leading to impaired and delayed responses to increased pressure. The localised and sustained mechanical loading to the skin and underlying tissues then results in soft tissue breakdown, worsening with increasing duration and resulting in a more severe wound[14].

The anatomic sites most susceptible to consistent unrelieved pressure are weight bearing points that come into contact with surfaces over bony prominences, and these are the regions where the vast majority of pressure ulcers develop (**Figure 1.1**)[15]. Approximately 95% of all pressure ulcers occur in the lower parts of the body, most commonly the sacrum (lowermost part of the back), coccyx (tail bone), calcaneus (heel), ischial tuberosities (sitting bones), greater

trochanters (lateral aspect of the upper thighs), buttocks, and hips[3]. Pressure ulcers can also develop on the elbows, occiput (back of the head), ears, and hallux (big toe)[16]. The most common site for pressure ulcer occurrence is the sacrum (36% of ulcers) followed by the heel (30% of ulcers)[17]. The anatomic site where a pressure ulcer is most likely to develop is dependent on the resting position that the immobilised patient is placed in. Supine positons, where patients are placed on their backs, typically have pressure ulcers develop on the heel, sacrum and buttocks. In lateral positions, where patients are laid on their sides, vulnerable sites to pressure ulcer development are the trochanteric regions. In prone positions, where the patient is rested on their front, the hips are the most vulnerable sites. Wheelchair users and patients seated upright have a different distribution of pressure than those laid horizontally[18]. Vulnerable sites in this seated positions are the ischial tuberosities and sacrum. Hospitalised patients will be typically placed in a supine resting position but may be repositioned during long surgical procedures[19].

1.1.4 Intrinsic and extrinsic risk factors

The etiology behind pressure ulcer development is multifactorial. A combination of extrinsic and intrinsic factors results in pressure ulcer formation[13]. Extrinsic factors are the environmental conditions that the patient exists in which increase the risk of pressure ulcer development. Such factors include pressure (the leading contributing factor) in combination with prolonged immobility, friction, shearing and moisture at susceptible regions. Intrinsic factors are the risk factors which make the individual particularly susceptible to developing a pressure ulcer. These include old age, neuropathy (decreased or absent sensations), particular medications, nutritional factors, incontinence and the presence of acute illness. It is evident that the greatest intrinsic risk factor for developing pressure ulcers is old age. People aged 70 years and older are most vulnerable to developing pressure ulcers due to several age-related factors including a reduced blood supply, aging of the skin and a higher rate of immobility compared with the general population[20]. This is reflected in the statistic that two out of every three pressure ulcers develops in this demographic[21,22].

Figure 1.1 — Pressure points and pressure distribution in four different resting positions. Adapted from "Pressure ulcers: Back to basics," by K. Agrawal and N. Chauhan, 2012, Indian Journal of Plastic Surgery, 45, pp. 249.

Figure 1.2 — The most common anatomic sites for pressure ulcer occurrence: (A) Back (posterior aspect) of the heel. **(B)** Sole (plantar aspect) of the heel. **(C)** Sacral region (lower back). **(D)** Buttocks. Pressure ulcers are also known to occur at the hips, trochanteric and coccygeal regions, and elbows. Adapted from "Morphological characteristics of the human skin over posterior aspect of heel in the context of pressure ulcer development," H. Arao *et al.*, 2013, Journal of Tissue Viability, 22, p. 43.

1.1.5 Risk assessment scales

On admittance into hospital care, several risk assessment scales are available to help medical staff determine the likelihood of the admitted patient developing a pressure ulcer. The first risk assessment scale for pressure ulcers was the Norton scale, developed in 1962, followed by the Waterlow scale (1985) and Braden scale (1987)[23]. Of the three, the Braden and Waterlow scales have been the two most commonly used to date – Braden more so in the USA, and Waterlow more so in the UK[24]. The Waterlow scale assesses eight factors: build/weight, height, skin type/visual risk areas, gender/age, continence, mobility, appetite, medication, and special risk factors (tissue malnutrition, neurological deficit, major surgery/ trauma)[25]. The scale identifies three 'at risk' categories based on how high the patient scores ('at risk', 'high risk' and 'very high risk'). Higher scores indicate a higher risk. The Braden scale assesses six factors: sensory perception, activity, mobility, moisture, nutrition, and friction/shear[26]. The scale identifies four 'at risk' categories based on how high the patient scores ('at risk', 'moderate risk', 'high risk' and 'very high risk') with lower scores indicating a higher risk[23]. The intention of these scales is to serve as a tool to be used alongside clinical judgement in predicting pressure ulcer risk in hospitalised patients. Any indication of risk from these scales should be followed with the appropriate action by the clinical staff. Despite their utility, these scales have been met with much criticism in recent years including poor inter-rater reliability and limited validity in predicting pressure ulcer risk[24,27].

1.1.6 Clinical presentation and traditional pressure ulcer staging

Traditionally, there are four clinical stages of pressure ulcer progression in order of increasing severity, with stage 1 being the least severe and stage 4 being the most severe (**Figure 1.3**). Staging is based on qualitative aspects of the wound that can be observed by clinical staff and has been outlined in guidelines made by bodies such as the National Pressure Ulcer Advisory Panel (NPUAP), the European Pressure Ulcer Advisory Panel (EPUAP) and the Pan Pacific Pressure Injury Alliance (PPPIA). With reference to the NPUAP staging system, stage 1 is the pre-ulcerous stage where the wound presents as a unblanchable erythema at susceptible regions with the skin remaining intact. This may appear differently in more darkly pigmented skin. Changes in temperature, sensation or firmness may also precede these visual changes. By stage 2, the skin surface has been breached, with partial thickness skin loss. The epidermis is compromised and the underlying dermis exposed. At this stage the ulcer is often described as 'superficial' as there is no visible involvement of subcutaneous tissue. The ulcer presents as an abrasion, blister or shallow cavity with no presence of granulation tissue, eschar (black scab-like tissue) or slough (yellow pus).

Stage 3 refers to full-thickness skin loss, with subcutaneous tissue necrosis or damage, which may extend down to, but not through, the underlying fascia. By stage 4 the pressure ulcer has progressed deep into the tissue, so much so that muscle and bones and sometimes even tendons and joints may be exposed or destroyed. Pressure ulcers may be classified as unstageable if full-thickness tissue and skin loss cannot be confirmed due to obscuration of the wound bed by slough or eschar. Debridement of this material may reveal a stage 3 or 4 pressure ulcer. The final category, deep tissue [pressure] injury (DTI), describes suspected deep tissue damage of unknown depth observable only as purple, deep red or maroon localised area of discolored intact skin. DTI can remain undetected for days or weeks until the discoloration is visible and in darkly pigmented skin may not be visible at all[28]. Notably, the NPUAP recently announced a change in terminology in their staging system, updating the term 'pressure ulcer' to 'pressure-related injury'. The rationale behind this change was that the term 'pressure-related injury' more accurately describes tissue injury of both intact skin and ulcerated skin, while the term 'pressure ulcer' described open ulcers and was not clearly inclusive of injured intact skin.

Table 1 — Description of pressure related-injury stage from the most recent guidelines published by the NPUAP (2016).

Pressure related-injury stage	Stage description
1	Unblanchable erythema of intact skin with tactile changes in skin temperature, tissue condition and/or sensation.
2	Partial thickness skin loss with exposed dermis.
3	Full-thickness skin loss (with subcutaneous tissue necrosis or damage).
4	Full thickness skin loss – muscle, bones, tendons and joints may be exposed and/or destroyed.
Unstageable	Obscured full-thickness skin and tissue loss.
Deep tissue pressure injury	Persistent unblanchable deep red, maroon, or purple discoloration.

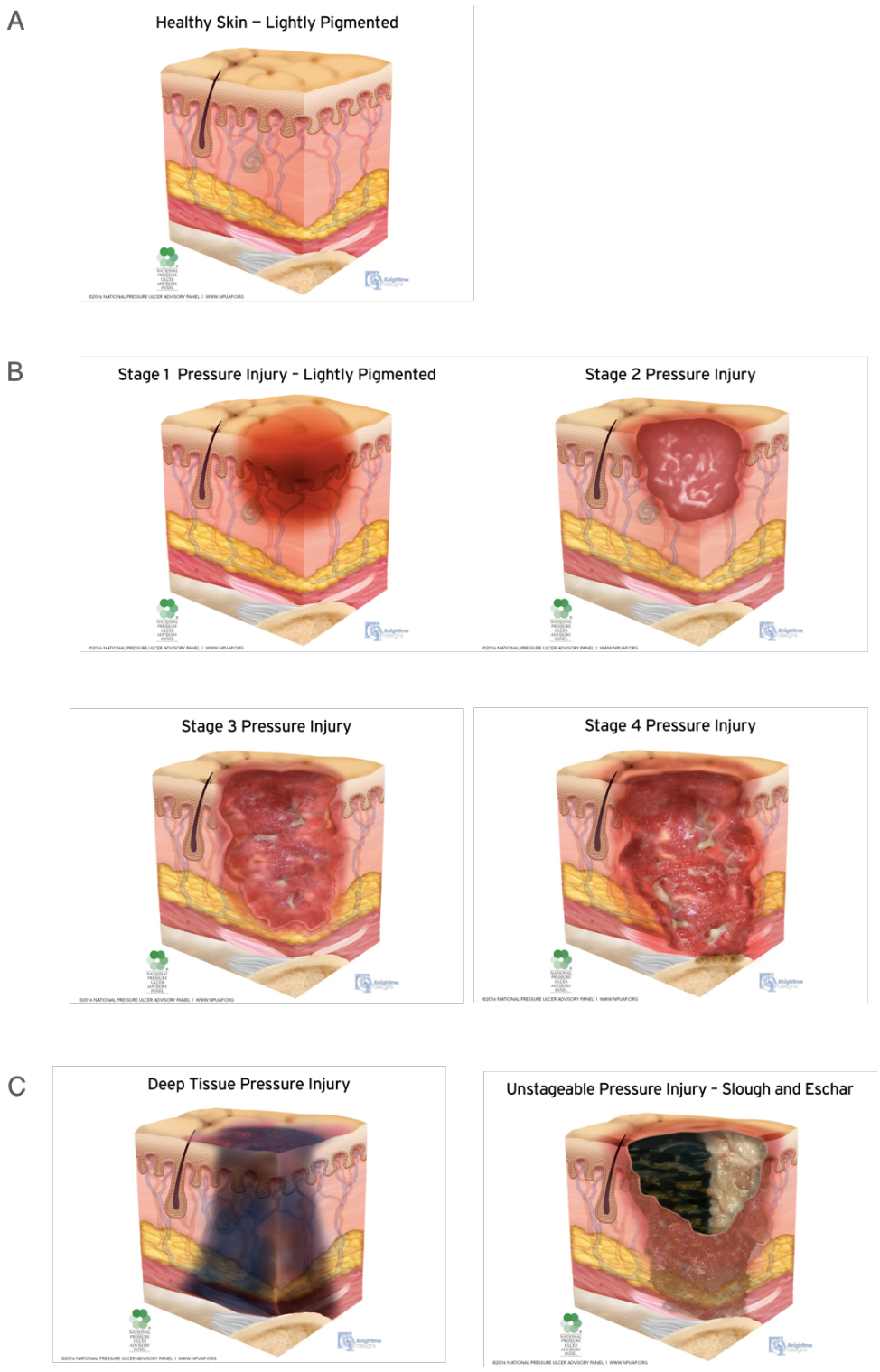

Figure 1.3 — Schematic representation of the NPUAP's updated scoring system of pressure-related injury: (A) Healthy, lightly-pigmented skin. **(B)** The four stages of pressure ulcer development. Stage 1 represents tissue injury of intact skin while stages 2, 3 and 4 represent open ulcers of increasing severity. **(C)** Two additional pressure-related categories - unstageable pressure ulcers where eschar and/or slough is obscuring the wound bed and deep tissue [pressure] injury (DTI) where the skin is intact but there is tissue breakdown in the underlying layers. From "Pressure Injury Staging Illustrations," NPUAP Free Resource Staging Illustrations, 2016, (http://www.npuap.org/resources/educational-and-clinical-resources/pressure-injury-staging-illustrations).

1.1.7 Medical complications of pressure ulcers

The morbidity and mortality associated with pressure ulcers mainly occur in the later pressure ulcer stages and are attributed to serious medical complications including cellulitis, blood poisoning, bone and joint infections, and gas gangrene (**Figure 1.4**)[29]. The occurrence of pressure ulcers increases mortality in patients in both acute and long-term care settings[3]. In some cases, the pressure ulcer itself does not cause death since it occurs in critically ill patients who are already more likely to die. The presence of pre-existing or co-existing illness is also likely to worsen the effect of pressure ulcers, especially in the critically ill and frail patient. Sepsis is one of the more serious consequences of pressure ulcers since it frequently results in death. Osteomyelitis, infection of bone, is a common complication of pressure ulcers and has been reported in 38% of patients with infected pressure ulcers[30]. A consequence of such an infection may be amputation, to prevent further spread of infection throughout the body and to salvage as much of the remaining uninfected limb as possible. In fact, amputation is a serious complication of other chronic wounds as well, especially the diabetic foot ulcer.

1.1.8 Traditional clinical care: preventative measures, intervention methods and treatments

Traditional approaches to pressure ulcer prevention include strategies to prevent the effect of external risk factors that cause pressure, shear, moisture and friction on vulnerable regions of skin. These include specialised pressure-redistributing mattresses, removal and replacement of wet bedding, especially for incontinent patients, and periodic turning of patients every one to two hours to relieve pressure, by nursing staff[3]. Once developed, treatment of the pressure ulcer varies depending on wound severity. It is important to debride unstable necrotic tissue and slough within an ulcer to prevent bacterial colonisation and to allow healing to occur[3]. Surgical intervention is indicated in the case of large, open and cavitied pressure ulcers. The procedure involves debriding the ulcer and suturing together the perimeter of healthy skin. Occlusive dressings supplemented with antimicrobial agents and wound healing promoters are also available. These techniques are explored further in this section.

Pressure ulcer prevention

Pressure ulcer prevention begins with identifying patients that are at risk of developing a pressure ulcer and understanding which factors are most likely to promote pressure ulcer development in that individual. Preventing pressure ulcer development in these at-risk patient populations is the next step. There are several ways this is accomplished – through adapting the patient's external environment and through improving the patient's health. Decreasing the moisture, friction, shear, and pressure that the patient experiences is deemed fundamental in

pressure ulcer prevention. The most traditional method of relieving pressure is through patient repositioning. Though there is no defined time interval for patient repositioning, it is reported that patients are typically turned once every one to two hours[31]. This repositioning helps relieve the pressure on weight-bearing anatomic sites in particular resting positions (**Figure 1.2**).

Between patient repositioning intervals, a common pressure ulcer prevention method is the use of specialised mattresses that redistribute, relieve or reduce pressure. The market is brimming with many types of mattresses made from a variety of materials and foams. Conventional mattresses are static but there are also dynamic-powered devices, such as alternating air mattresses, that use an electric air pump to promote the uniform distribution of pressure over the body surfaces[32]. These more dynamic and electricity-powered mattresses are generally more expensive options. Additionally, bony prominences can be directly point-protected from high pressures using foams, pillows, wedges or elevation devices over the region, for example through the use of a heel protection device[16,33].

In combination with pressure, moisture can macerate and injure the skin. In patients, moisture comes from three major sources: sweat, wound drainage and incontinence (both urinary and fecal)[3,34]. The effects of moisture can be managed in patients through removal and prevention of excessive moisture build-up at vulnerable sites such as around the buttocks and especially within the gluteal folds. This includes regular changing of incontinence pads and devices, and wiping down of areas that have accumulated moisture. The patient's nutritional status is also deemed important as poor nutritional status may impair wound healing[35]. Therefore, improving the patient's health through nutritional and vitamin supplements may help prevent the development of new ulcers and prevent existing ones from worsening[36].

Pressure ulcer management and treatment

Treatment of pressure ulcers is multi-fold. Many treatment options are aimed at late stage pressure ulcers (stages 3 and 4) where there is a high risk of mortality and life-threatening complications such as infection. One of the most important treatments is the removal of necrotic debris from the wound. By this stage of pressure ulcer development, phagocytosis by the host's immune cells is insufficient to remove the dead tissue. Therefore, debridement is essential to prevent establishment of bacterial colonies and biofilms, and to promote wound healing. There are several methods used to debride pressure ulcers including mechanical and surgical debridement. Of the two, surgical debridement is the most rapid method of removing necrotic tissue, though both methods can cause damage to healthy tissue or may insufficiently clean the wound[3]. During surgical debridement dead tissue is cut away from the wound. This procedure can be performed at the bedside or may need to be carried out in an operating theatre. During

mechanical debridement, fluid force is used to remove necrotic tissue from the wound. This includes wound irrigation systems using pulsed lavage where a handheld device delivers normal saline at safe pressures to force out the debris[1].

Ultrasound-assisted wound therapy uses a combination of surgical and mechanical debridement[37]. During this type of treatment, ultrasonic waves are passed over the surface of the wound *via* a saline filled pressure wave to separate the necrotic tissue from the healthy skin in the wound bed[16]. Autolytic debridement, using occlusive dressings[38], enzymatic debridement, using exogenous enzymes[35], and biological debridement, using maggot therapy[39,40], are viable longer term treatments options. Once an ulcer has been debrided, the remaining cavity may need to be surgically closed. This is done either by suturing the perimeter of healthy tissue or though flap surgery[36]. Alternatively, the pressure ulcer may be left to heal by secondary intention and managed with the use of dressings. A multitude of dressings are available and are chosen depending on the characteristics of the wound such as its depth and drainage. Transparent polymer films may be used on uninfected wounds that have little to no drainage, hydrocolloid dressings for shallow wounds with moderate drainage and foams or alginates for deeper wounds with heavier drainage[16]. The wound may also be packed with gauze[16].

Management of bacterial colonisation with the use of antibiotics is an important protocol in pressure ulcer treatment. Infection control is crucial to aid wound healing and prevent life-threatening complications such as bacteremia. Though it may be difficult to determine if a pressure ulcer is infected, a foul odour is usually indicative of the presence of anaerobic organisms[3]. Patients may also present with systemic symptoms of infection such as fever or organ failure[16]. Presence of bacteria in the wound has been shown to worsen pressure ulcers and topical antibiotics may be required if a pressure ulcer fails to progress toward healing. Notably, quantitative microbiology has been shown to be a poor predictor of clinical infection in chronic wounds[41], and the species of colonising bacteria is likely to be more significant to the severity of the infection[42,43].

Limitations of current pressure ulcer care

Despite the multitude of current pressure ulcer prevention methods, there is some doubt surrounding their efficacy. Furthermore, many of the prevention and treatment options that have been outlined here are outdated or contraindicated in many patients. For example, practical issues have been encountered with current treatment methods; whilst surgical repair of developed ulcers results in rapid resolution, there is an inability of frail patients to tolerate the procedure as well as the procedure being costly and resulting in frequent recurrence[35]. There is

also no consensus in the literature or amongst researchers on the efficacy of patient turning and repositioning in preventing pressure ulcers[44]. In some situations, such as is with certain SCIs, immobilisation precludes the need to reposition the patient. The efficacy of pressure-redistributing mattresses in order to prevent pressure ulcers is also debatable[3]. There are data to suggest that the use of specialised mattresses does not reduce the incidence of pressure ulcers and that there is no considerable difference in pressure ulcer occurrence between dynamic and static mattresses[45]. Several studies have also concluded that there does not seem to be a benefit of one over the other[46–48]. There is also limited evidence to suggest that improvement in nutritional status (another prevention method) has a significant impact in preventing pressure ulcers. Despite an epidemiological association between poor nutritional status and pressure ulcers, nutritional supplementation has proved disappointing with several observational studies reporting that it did not have an effect on the development of pressure ulcers[49,50]. In one study there was shown to be no statistically significant difference in prevalence, incidence or mortality of pressure ulcers between critically ill patients given oral supplements and those who had not[49,50].

Alternative approaches to pressure ulcer resolution

A potential approach to pressure ulcer resolution involves targeting pressure ulcers at a molecular level, that is, to interfere with the pathways that are involved in its etiopathogenesis and which promote wound development. Adjunctive therapies can be used alongside primary treatment in pressure ulcer management. Hyperbaric oxygen therapy, for example, involves the delivery of oxygen to improve tissue oxygenation and promote wound healing through stimulation of fibroblasts and epithelisation[51]. Electrical stimulation, though not widely used in clinical practice, is a method used to stimulate the cellular processes involved in wound healing through the use of electrical currents[37,52]. Growth factors required in the wound healing process such as platelet-derived growth factor (PDGF), endothelial growth factor (EGF) and vascular endothelial growth factor (VEGF), have been shown to be degraded in the presence of increased levels of elastases in chronic wound fluid[53] and bacterial proteases[54]. Increasing local levels of growth factors by delivering them to the wound, or through the use of protease inhibitors, has proved promising in chronic wound treatment[55]. Wound chemotherapy is a fast-growing area of adjunctive therapy and is explored further in section: **1.4 Pharmacological treatment of pressure ulcers**, ***p. 59.***

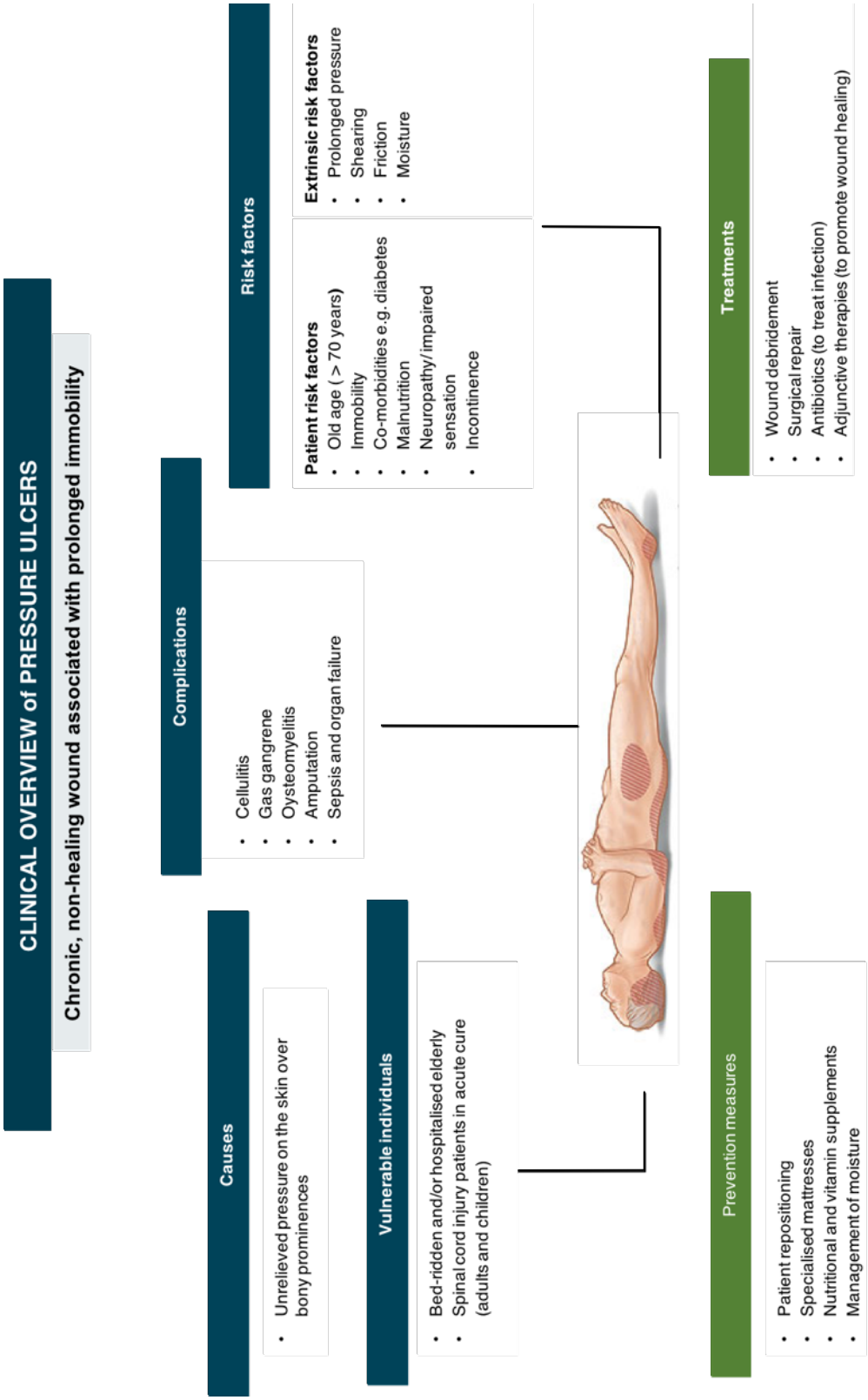

Figure 1.4 — Clinical overview of the pressure ulcer.

1.1.9 Are pressure ulcers avoidable?

A reasonable assumption that could be made is that 'if pressure ulcers develop in immobilised patients, mobilising them along with meticulous clinical care would prevent pressure ulcer development?'. The answer has not been that simple. Despite current protocols, pressure ulcer incidence remains high and whether or not pressure ulcers are completely preventable remains controversial[56]. The question then becomes 'where does the blame lie?' — is it due to a deficit in nursing care or the inability of the current risk assessment scales and prevention methods to actually prevent pressure ulcers? Once again the answers have not been so clear. Pressure ulcers are often believed to be an indicator of poor patient care that are costly to the individual as well as the public healthcare system[35].

Penalties for poorly managed pressure ulcers are adverse outcomes and high treatment costs, and, increasingly, financial institution-wide penalties specifically for HAPUs. As the old adage goes, prevention is better than cure and this holds true for pressure ulcer care both in terms of cost and patient's quality of life[3,35,37,57–60]. In the UK, the cost of treating a stage 4 pressure ulcer was placed at £10,554 in 2000, compared with an average of £1,064 to treat a stage 1 ulcer[12]. Nonetheless, it has been shown that with conscientious medical management many pressure ulcers that have developed will heal completely without the need for treatment or surgical intervention. At annual consortiums and sandpit events, including the recently formed Medical Device and Vulnerable Skin Network (MDVSN), there is growing interest in emerging biotechnologies that can help evaluate pressure ulcers and that can provide more detailed subsurface information on a developing ulcer as well as in novel biotechnologies that can prevent the first stages of ulcer development before skin deterioration accelerates.

1.2 Fundamental aspects of human skin architecture and structure

1.2.1 The skin — a resilient but breachable barrier

Skin is the largest organ of the human body and is essential for terrestrial life since it carries out a multitude of vital functions. Skin primarily acts as a dynamic barrier that allows us to safely exist within and interact with a harsh external environment. To a great extent, skin protects our internal organs from direct exposure to many external threats including pathogens, parasites, sunlight, toxins and exogenous chemicals. Not only does it help limit entry of these unwanted substances it also prevents what would otherwise be rapid and devastating water loss from our body's interface to the surrounding environment. Skin is also important as a sensory organ and allows the body to respond to changes in heat, cold, touch, pressure and pain through a network of nerves connected to the central nervous system. Temperature control is further

aided through a rich blood supply, fine hair, and sweat glands. It is important to remember, however, that though skin is resilient, it is also vulnerable to injury and its surface can be breached with certain perturbations. Wounds, disturbances to the skin's structural continuity, leave the body vulnerable to infection. Furthermore, deviation from normal skin function and behavior due to acquired or genetic diseases are known to have debilitating consequences, from the relatively common inflammatory skin disorders such as eczema and psoriasis[61] to the rarer skin diseases such as ichthyosis[62].

1.2.2 Function and structure of the skin layers

At its simplest, human skin can be divided into three main 'zones' or layers: the epidermis, the dermis and the subcutis. The epidermis is the thin, avascular outermost layer of skin. The principle cell type here is the keratinocyte which accounts for 95% of all epidermal cells[63]. The epidermis is further sub-divided into five distinct layers: (i) the stratum corneum or SC, (ii) the stratum granulosum, (iii) the stratum lucidum, (iv) the stratum spinosum, and (v) the stratum basale (**Figure 1.5**). The SC is the outermost epidermal layer and is the most important for imparting the barrier properties of the skin which makes it incredibly important when considering the physiological obstacles to transcutaneous delivery[64]. The SC is composed of dead keratinocytes, known as corneocytes, and has a high resistance to changes in temperature and pH[65]. These dead skin cells are constantly being lost from the surface of the SC in a process known as desquamation[66]. Beneath the SC are the remaining layers of the epidermis,

Figure 1.5 — Schematic representation of the epidermal layers and the basement membrane zone [BMZ] that separates the stratum basale from the underlying dermis. Adapted from "Structure and function of the epidermal barrier," by R. R. Wickett l and M. O. Visscher, 2006, American Journal of Infection Control, 34, p. S99.

collectively known as the viable epidermis. This loss of cells from the SC is constantly being balanced by the self-renewing viable epidermis through mitosis and cell growth originating in the stratum basale. Upon leaving the stratum basale, keratinocytes begin to differentiate and migrate through the stratum spinosum and granulosum[66]. During their maturation, keratinocytes undergo a series of changes in their structure and composition synthesising different structural proteins and lipids as they differentiate.

The epidermis is separated from the underlying dermis by the cutaneous basement membrane zone (BMZ) which contains proteins and glycoproteins that ensure adhesion of the two layers[63]. The dermis is a layer of connective tissue that sits below the BMZ and contacts both the epidermis and the subcutis. Unlike the epidermis, the dermis is richly supplied by blood vessels and sensory nerve endings. It also contains lymphatic vessels, sweat glands and hair follicles. Structurally, the dermis is composed of interstitial components including collagen fibres, elastic tissue and ground substance, and cellular components including fibroblasts, mast cells, plasma cells, dermal dendritic cells and histiocytes[63]. Most dermal cells are fibroblasts which are responsible for synthesising and maintaining the tissue's extracellular matrix (ECM)[18]. They secrete collagens, elastic fibres and ground substance, a gelatinous substance composed of proteoglycans and glycoproteins. The dermis is often sub-divided into two sections, the papillary or upper dermis and the reticular or lower dermis[63].

Roughly 70% of the dry weight of the dermis is made up of collagens[67], of which the predominant types are type I and type III. Collagens are proteinaceous structural molecules found throughout the body with at least sixteen different types found in humans[68]. Collagens impart tensile stiffness and strength to the skin. Elastic fibres, on the other hand, form about 5% of the dry weight of the dermis and are responsible for the skin's elasticity. Elastic fibres consist of elastin and elastic microfibrils such as fibrillin. The collagen and elastic fibres are bathed in the ground substance which is important in maintaining the spatial structure of the collagen-elastin network and in supporting the skin's capacity to carry compressive loading[18]. Beneath this network is the subcutis which is composed of lipocytes arranged into fat lobules. Bundles of fibres originating from the dermis percolate into the subcutis, strengthening the connection between the two compartments[63].

1.2.3 Skin vasculature and innervation

While the epidermis is avascular, the dermis has a rich blood supply. The vasculature of the dermis is comprised of two interconnected systems — the superior vascular plexus and the deep vascular plexus. The superficial vascular plexus is located in the papillary dermis and consists of terminal arterioles, arterial and venous capillaries and post capillary venules[69]. Capillaries

arising from the arterioles extend upward into the papillary dermis and then loop back into ventrioles. These structures are known as capillary loops (**Figure 1.6**). The deep vascular plexus is connected to this system by paired ascending arterioles and descending venules. Thermoregulation is, in part, regulated by blood flow through the skin's vasculature by processes known as vasodilation (widening of blood vessels) and vasoconstriction (narrowing of blood vessels). In a stable thermal environment of ambient temperature, skin surface temperature of the torso ranges from 33–37^{o}C while that of the extremities tends to be slightly lower[70]. As well as a role in thermoregulation, the dermis is also well innervated and has an important sensory function. Several branches of the spinal and cranial nerves pass through the subcutaneous space into the dermis and form three plexuses — the papillary, dermal and subcutaneous plexuses[71]. Free nerve endings, sensitive to pain, lie in the dermis with a few extending to the cells of the epidermis. The dermis also contains several additional receptors with larger receptive fields. Important roles include mechanoreception, thermoception and nociception.

1.2.4 Variation of epidermal skin layer thickness

Skin layer thickness varies between different body regions and between individuals based on factors such as age. Epidermal layer thickness typically ranges from 50 to 200 μm while dermal thickness is substantially larger and ranges from 1 to 3 mm. Viable epidermal thickness has been shown to significantly decrease with age[72]. This is in conjunction with a substantial loss in function of aging skin and a dramatic reduction in turnover rate. This is a consequence of cell proliferations rates dropping in the dermis as the skin cells biologically age with the individual. The SC thickness varies considerably with anatomic site and ranges from 5–600 μm thick, though is typically around 20 μm[73]. It has been well documented that the SC is much thicker on the palms and soles of the feet (up to 50 cells thick) compared with the skin on more delicate regions such as the face (around nine cells thick). Considering the frequent interaction with the environment — tactile grasping and gripping with the hands and movement and weight bearing of the feet — these surfaces inevitably require a tough and more resilient SC layer. The SC has also been shown to thicken significantly with hydration[74,75].

1.2.5 Skin barrier function and permeation pathways of molecules

As previously described, the barrier function of the skin is imparted by the epidermis, specifically the SC. The 'bricks and mortar' analogy is commonly used to explain how the SC functions as this barrier. The 'bricks' are the resident corneocytes — elongated, flat cells filled with keratin filaments which have densely cross-linked lipoprotein-containing envelopes, These are surrounded by the 'mortar' — lipid bilayers with hydrophilic regions inbetween[64,76].

The main mechanism of transport of substances into the skin is by passive diffusion. Molecules can pass directly through the lipophilic SC, through either intercellular or transcellular diffusion routes, or indirectly through transappendageal routes, *via* hair follicles, sebaceous glands or sweat ducts (**Figure 1.6**)[77]. The total surface area afforded by the skin appendage openings constitutes only 0.1% of the total skin area however, so their contribution to steady state flux of molecules is considered minimal[77]. Furthermore, permeation is hindered in these routes by natural structures such as hairs[78]. The intercellular route is the most common permeation pathway of drug molecules and involves diffusion of the substance through the lipid matrix occupying the intercellular spaces of the keratinocytes. Due to its hydrophobicity, lipid-soluble molecules will penetrate more readily through the SC than water-soluble molecules.

As the primary skin barrier, the SC is the rate-limiting step to molecular penetration. Diffusion of compounds through the skin is governed by Fick's first and second laws of diffusion[77]. Small lipophilic molecules with lower melting points are of an optimal chemical composition to readily permeate through the SC[79]. A study was carried out by Meinardi and Bos (2000) to define the term 'small' in this context, who proposed the 500 Da rule for the skin penetration of chemical compounds and drugs[76]. The authors reviewed the most commonly used topical drugs in dermotherapy and found, with the exception of two, that they all had a molecular weight of less than 500 Da. They also noted that topical application of an immunosuppressant treatment for inflammatory skin conditions that had a molecular weight of just over 1200 Da was ineffective[80] when compared with its administration by intralesional injections[81]. Though their proposal has been met with several arguments, there is a general consensus amongst researchers that for particularly high molecular weight and hydrophilic molecules disruption of the skin barrier is necessary to allow the compound to efficiently permeate through the SC barrier.

Figure 1.6 — Schematic representation of the human skin and penetration pathways of molecules through the stratum corneum. The three penetration pathways are: (i) the transcellular route, (ii) the intercellular route and, (iii) the transappendageal route. Adapted from "Modelling the human skin barrier — Towards a better understanding of dermal absorption," O.G. Jepps *et al*., 2013, Advanced Drug Delivery Reviews, 2, p. 154.

1.3 Pathophysiological mechanisms behind pressure ulcer development

1.3.1 The normal acute wound healing paradigm

Wound healing is an important homeostatic process which restores the integrity of the skin and its barrier function after it has been breached. Several biological events are involved in the process of wound healing in an orderly and predictable manner. These are hemostasis, inflammation, cell proliferation and skin remodelling and re-epithelisation collectively known as HIPR[82]. These processes are themselves governed by a plethora of coordinated signals between the diverse cell types involved in wound healing including dermal cells, inflammatory cells, enzymes and cytokines[83,84]. The body's hemostatic mechanism is important in preventing

excessive blood loss and in initiating the healing process. Collagen that is exposed during a skin injury activates a clotting cascade pathway which results in platelet aggregation and blood coagulation forming a clot made from collagen, platelets, thrombin, and fibronectin. This fibrin clot acts as temporary wound plug and as a foundation for the laying down of new ECM[85]. The clot also contains a milieu of cytokines and growth factors that initiate wound closure through chemoattractant signals. Prostaglandins cause vasodilation of local blood vessels to increase cellular traffic to the site[86].

Neutrophils are recruited to the wound site within minutes of injury by chemoattractant signals: interleukin-1 (IL-1), tumour necrosis factor-alpha (TNF-α), transforming growth factor-beta (TGF-ß) and platelet factor-4 (PF4)[57]. Neutrophils play an important role in removing bacteria and tissue debris by releasing proteolytic enzymes and through phagocytosis. Next, circulating monocytes are recruited to the wound site where they are stimulated to become activated macrophages. They are responsible for phagocytosing remaining pathogenic material. They also release growth factors and cytokines including collagenases to debride the wound and interleukins and TNF-α to stimulate fibroblasts.

Towards the end of the inflammatory phase, the proliferative phase of wound healing begins. This phase involves re-epithelisation to restore the barrier function of the skin, angiogenesis to supply the growing tissue with the required oxygen and nutrients and granulation tissue formation. Keratinocytes at the wound edge migrate and proliferate to re-epithelise the breach in the skin. This is stimulated by keratinocyte growth factors (KGFs) whose expression, synthesis and secretion are upregulated in fibroblasts in response to IL-1 and TNF-α[57,87]. Angiogenesis involves the development of new blood vessels; endothelial cells release proteolytic enzymes which degrade the basement membrane and allow the formation of primary vessels[85].

Around seven days after the initial injury, the wound site undergoes remodelling[85]. Fibroblasts that have migrated into the wound synthesise collagen types I and III[82]. This occurs at a greater rate than collagen degradation, resulting in net collagen accumulation. Wound contraction begins around the start of collagen synthesis and helps reduce wound size. During scar formation, collagen fibrils become tightly packed. The entire remodelling phase can persist for years after the initial injury. As a normal wound heals, the final process is resolution of the scar. Macrophages, fibroblasts and endothelial cells release collagenases to degrade wound collagen and other matrix proteins, degrading the scar tissue and ultimately healing the wound[85].

1.3.2 Chronic and delayed healing wounds

Chronic wounds do not proceed through the phases of normal wound healing in an orderly or timely manner[3]. There are three major types of chronic wound – pressure ulcers, diabetic ulcers and venous leg ulcers — that develop by different pathophysiological mechanisms but have several similar characteristics. These wounds do not resolve easily, are an immense health and resource burden and reduce the patient's quality of life as they can be painful and debilitating. There is a multitude of factors that contribute to the non-healing characteristic of chronic wounds. These include a combination of environmental factors and certain patient risk factors such as an underlying disease. Chronic wounds exhibit a persistent inflammatory phase and a prolonged influx of inflammatory cells compared with acute wounds. There is excessive expression of certain enzymes and cytokines that leads to cell necrosis and apoptosis. In many cases there is colonisation of the wound by infectious bacteria and, most noticeably, a lack of advancement to the remodelling stage of wound healing.

1.3.3 Effect of pressure on human skin

It is theorised that pressure on the skin can cause damage in multiple ways, especially to the dermis, which constitutes a large structural and functional part of cutaneous tissue. Underlying muscle is also susceptible to pressure-induced injury. The critical threshold for injurious pressure on the body tissues is often referenced as 32 mmHg[35]. This is the capillary closing pressure – the interface pressure at which the capillaries collapse and close completely, thus occluding local blood flow. Prolonged pressure of greater than 32 mmHg for more than two hours at focused regions of the skin is believed to: (i) interrupt the intricate structure of the ECM network causing changes in ECM turnover and potentially leading to ECM degradation[37], (ii) result in compromised lymphatic transport leading to an accumulation of toxic substances in the tissues[18], (iii) lead to direct mechanical insults to cells that cause cellular necrosis[88] and (iv) cause cyclical microvasculature occlusion (if the pressure is intermittently relieved) known as ischemia-reperfusion (IR) injury, ultimately leading to cellular necrosis and apoptosis[89,90].

1.3.4 The role of ischemia-reperfusion injury in pressure ulcer development

Ischemia-reperfusion (IR) injury is a major complication for many clinical conditions including myocardial infarction, stroke and organ transplantation[91]. It is also one of the most widely acknowledged pathophysiological mechanisms behind pressure ulcer development. This has not always been the case, however. Preliminary studies into pressure ulcer formation focused on tissue ischemia as the sole etiological factor[92]. Many of these first studies believed it was ischemia leading to tissue necrosis which drove pressure ulcer development and this was

reflected in the experimental groups and *in vivo* research models used. Over the years, however, many *in vivo* studies have shown a discrepancy between the effect of ischemia alone and the effect of cycles of IR injury[89,93]. In fact, IR injury is believed to be more injurious than ischemia alone, as ischemia alone is unable to account for all the effects seen in pressure ulcers.

IR injury describes the damage to a tissue by not only the initial period of ischemia but also the subsequent reperfusion of blood to that region[94]. When prolonged pressure is applied to the body, the microvasculature in the skin becomes occluded resulting in tissue anoxia and glucose deprivation. If this goes unrelieved for two to six hours, it will lead to local ischemic injury[19]. This total arrest in circulation affects the metabolism of the skin and subcutaneous tissues and will result in cell death and tissue necrosis after six hours of unrelieved pressure[18]. Hyperemic reperfusion represents the reintroduction of blood to the previously ischemic tissue and is believed to play a key role in pressure ulcer development[95]. This is because it not only introduces critically needed oxygen and nutrients back into the tissue, but harmful oxygen radicals as well, including reactive oxygen species (ROS) such as superoxide radicals and hydrogen peroxide[18]. These ROS can lead to oxidative damage and inflammation through the recruitment of leukocytes (macrophages and neutrophils) ultimately resulting in cell apoptosis and further necrosis[51,96]. In addition, toxins are circulated to the area which further contribute to inflammatory damage during reperfusion[90,97,98].

Though IR injury is the most widely supported pathophysiological mechanism behind pressure ulcer development, there have been suggestions of other factors in play. Other mechanisms that are believed to contribute to pressure ulcer development include compromised lymphatic transport leading to an accumulation of toxic substances in the tissues[18] and direct mechanical insults to cells that cause cellular necrosis[88]. For the time being however, IR injury remains at the forefront of pressure ulcer research. For this reason there is speculation about whether the current prevention protocol of intermittently relieving pressure in 'at risk' patients every few hours is contributing to, rather than ameliorating, pressure ulcer development[99,100]. If this is the case current nursing practice may need to be re-assessed. However, it is likely that such intermittent mobilisation is essential in the prevention of life-threatening nosocomial conditions such as thrombosis or chest infection[33]. Furthermore, patients who must remain unmoved due to particular spinal cord injuries also develop pressure ulcers.

1.3.5 The role of matrix metalloproteinases in pressure ulcer chronicity

Among the pathophysiological mechanisms believed to be responsible for pressure ulcer development and other chronic wounds, unregulated degradation of the extracellular matrix (ECM) has been proposed to be key in ulcer chronicity and wound non-healing[88,101–111]. In a

non-healing chronic wound, the wound environment is such that there is prolonged inflammation, unregulated enzymatic activity and a lack of re-epithelialisation resulting in an open wound that is highly susceptible to infection and which reduces a patient's quality of life[112]. It is believed that defective activity in the enzymes responsible for ECM degradation, the matrix metalloproteinase (MMPs), and their inhibitors, tissue inhibitors of metalloproteinases (TIMPS), is a major contributor in potentiating the chronic wound environment[113].

MMPs are a family of zinc-dependent proteases that degrade several components of the skin's ECM including collagen, gelatin, fibrillin and elastin. Twenty-three different MMPs have been identified in humans and include the collagenases, gelatinases, stromelysins and membrane-type MMPs amongst the major types[114]. Importantly, MMPs are required for normal physiological processes such as cell migration, angiogenesis and scar remodeling[110]. However aberrant MMP expression and altered regulation can result in too much or too little MMP activity leading to ulcer formation or other maladies such as tumour metastases or fibrosis[115]. Over the years, observational clinical studies have investigated which MMPs could be responsible for wound development and chronicity by examining the content of tissue exudate and granulation tissue from chronic wounds[102,104–107].

Clinical observational studies combined with evidence from experimental models suggest that elevated MMP levels and aberrant regulation are responsible for the inflammatory component and chronicity of several diseases, pressure ulcers included[102,106,110,113,116]. Despite their deleterious behaviour in these diseases, MMPs have an integral physiological role in maintaining and remodelling extracellular spaces for tasks such as tissue growth and scar repair[114]. What tips the balance in favour of damage has been extensively studied and is believed to result from either MMP overexpression, inadequate MMP inhibition or a combination of both. There is currently no consensus on which MMP or MMPs are responsible for wound severity but patterns in chronic would fluids indicate an increase in several MMP levels, MMPs 2, 8 and 9 and a concurrent increase in the MMP/TIMP ratio[114]. Simultaneously levels of the endogenous MMP inhibitors, TIMPs and alpha2-macroglobulin (α2M) have been shown to be decreased in would fluid contributing to the imbalance that results in ECM degradation[111,117–119].

MMP 9, or gelatinase B, has been suggested as a major protease responsible for ECM degradation in chronic wound fluid. Its persistently elevated state has been observed in pressure ulcers, venous leg ulcers and non-healed burns, with levels dropping as wounds heal[113]. The role of MMP 9 In normal wound healing is to promote inflammation and facilitate migration of

neutrophils. In their murine wound model using 6 mm punch biopsies, Reiss *et al.* (2009) observed that wounds treated with exogenous MMP 9 were significantly larger than control wounds up to twelve days after the initial injury[120]. Their results suggested that MMP 9 could directly delay wound healing through interference with re-epithelialisation and keratinocyte migration. MMP 2, or gelatinase A, has been shown to have increased expression in chronic wounds despite its anti-inflammatory role and role in keratinocyte migration. In one preclinical wound model, MMP 2 was shown not to be essential for wound healing[121] and was shown to be at elevated levels in the wound fluid of chronic leg ulcers[122]. Both MMP 2 and 9 were also shown to be increased in a preclinical model of ischemic stroke[123]. MMP 8, collagenase 2 or neutrophil elastase, has been strongly implicated in the tissue destruction of the inflammatory condition periodontitis, and inhibition of its action has resulted in improvements in wound healing[124,125].

Table 2 — Summary of MMPs that have been implicated in pressure ulcer chronicity in the literature.

MMP	Sub-Family	Alternative name	Principal Substrates
MMP 2	**Gelatinase**	**Gelatinase A**	**Non-fibrillar collagens, types IV and V**
MMP 8	**Collagenase**	**Neutrophil collagenase / Collagenase 2**	**Fibrillar collagens, types I, II, III**
MMP 9	**Gelatinase**	**Gelatinase B**	**Non-fibrillar collagens, types I and IV**

However, it should be noted that, firstly, the composition of chronic wound fluid does not represent the composition of the wound bed. It has in fact been shown that the concentration of MMPs is higher in the fluid than the bed itself[113]. Secondly, MMPs play a crucial role in wound healing and so physiological wound healing would be impaired if their action were fully inhibited. Nonetheless, if administered carefully MMP inhibitors provide a potential treatment for pressure ulcers and other chronic wounds. Thus targeting such MMPs in a precise and controlled way to improve cutaneous wound healing is of great interest. By reducing the time to heal or by preventing ulcer development, this could substantially decrease the healthcare costs as well as alleviate the physical burden on the patient[111]. MMP inhibitors, also known as MMPIs, pose a potential solution to the problem by mimicking endogenous TIMPs. They have gathered great interest in the treatment of late stage cancers as drugs to prevent tumour metastases[126]. Their action could be translated to the prevention and/or treatment of pressure

ulcers[116]. Their role is discussed in the section**:** ***Targeting MMPs to treat pressure ulcers, p. 60***.

1.3.6 The effect of pressure on muscle: superficial versus deep tissue injury

Though degeneration of the skin is the most evident stigmata of pressure ulcer damage the underlying subcutis, especially muscle, is also highly susceptible to the effects of sustained compression[14]. In fact, evidence suggests that this underlying muscle is more susceptible to pressure-induced injury than skin for a given mechanical load[127,128]. Thus, it is believed that superficial ulcers develop in the skin and involve maceration and detachment of the superficial skin layers, while deep ulcers arise in the deeper muscle layers, especially in the skeletal muscle that covers bony prominences susceptible to sustained compression[14]. Hence it should be noted that what is seen clinically may be just the 'tip of the iceberg'[13]. This is to say that the extent of damage to the skin may not reflect the extent of damage to the underlying muscle and subcutaneous tissue which is more susceptible to ulceration[37]. This is important when considering that clinical ulcer staging is achieved through visual inspection and that deep tissue injury of the skin is often not visible for weeks, if at all.

1.3.7 Bacterial colonisation and wound bioburden

In addition to MMP dysregulation, bacterial colonisation of an exposed chronic wound can cause complications[114]. Not only do the bacteria illicit further inflammatory responses, if they are in excess they will firstly delay wound healing and eventually lead to infection. Chronic wounds with a high bacterial load will not heal[38]. Bacteria can form biofilms in the wound which are highly resistant to antibiotics, host antibodies, inflammatory cells and disinfectants[129]. These persistent biofilms can serve as a long-term inflammatory source. As an important co-factor, the proteinaceous exudate from the wound and nonviable tissue acts as a nutrient source, aiding bacterial growth and survival[130]. Additionally, the host immune response to biofilms is deleterious to wound healing. Inflammatory cells secrete ROS and MMPs to counteract the biofilm bacteria which inadvertently destroy the ECM and pro-healing factors in the wound bed, further delaying the wound healing process[114].

1.4 Pharmacological treatment of pressure ulcers

1.4.1 The need for new treatments and improved understanding of pressure ulcer development

Pressure ulcers are not currently at the forefront of medical research and mainly present in an age group that suffers from a range of primary diseases that demand more immediate attention.

However, global shifts in demographics, especially in more economically developed countries, have resulted in aging populations and a corresponding rise in age-related disease and pressure ulcers. With this increasing incidence, there is a need for innovation in pressure ulcer care. Pressure ulcers are important and merit such innovation. Advisory panels and sandpit events such as the Medical Device and Vulnerable Skin Network (MDVSN) have made efforts to unite researchers and clinicians, with the aim of creating devices to efficiently eliminate pressure ulcers and reduce related medical costs.

1.4.2 Targeting MMPs to treat pressure ulcers

Elevated MMP levels can be counteracted in a number of ways including the physical removal of the MMPs or through the use of MMP inhibitors. Promogran, the first MMP-modulating wound dressing, absorbs MMPs from the wound exudate and bed[83,131], and has been shown to improve healing rates of diabetic foot wounds[132] and venous leg ulcers[133]. A large group of MMP inhibitors, which have also been investigated as anti-cancer drugs and which include BB94 (batimastat), GM6001 (ilomastat/galardin) and BB 2516 (marimastat), could also provide effective treatment[126]. These drugs function as potent inhibitors of the MMPs that are responsible for detaching cells from the basement membrane to ultimately prevent cancer spreading throughout the body i.e. inhibiting tumour metastases (though clinical trials for this application were unsuccessful)[134]. However, delivering these drugs in a controlled manner to prevent perturbation of normal physiological function is an important consideration. Doxycycline, an antibiotic and MMP inhibitor used in the treatment of aphthous ulcers (a form of mouth ulcer), has been suggested as a suitable and effective treatment for chronic wounds[116,135], and this suggestion further supports the destructive role the MMPs are believed to play.

The rationale behind choosing doxycycline as the experimental API in this research was based on several factors. Firstly, doxycycline is desirable as it has confirmed MMP inhibitory activity independent of its other pharmacological activity and is already FDA-approved for the treatment of aphthous ulcers based on this attribute[136,137]. For these reasons it also has an established safety and adverse effects profile[138]. Doxycycline has numerous pharmacokinetic advantages over its tetracycline counterparts such as oxytetracycline and tetracycline HCL including improved bioavailability and better penetration into body tissues and fluids[139]. In terms of administration, there are multiple pre-existing formulations of doxycycline (which typically comes in powder form) and this allows for a wide scope of drug delivery methods. Notably, doxycycline had not been experimentally investigated in the treatment of pressure ulcers, or in chronic wounds in general, at the time of its choosing making the concept behind this research novel.

1.4.3 Doxycycline as chronic wound chemotherapy

Doxycycline hyclate is a tetracycline compound that is used as a broad-spectrum antibiotic in the treatment of a wide variety of bacterial infections including *Chlamydia* and gonorrhea[140138]. At sub-antimicrobial doses doxycycline is also a broad-spectrum inhibitor of MMP[141]. MMPs, produced and secreted by a number of dermal cells including fibroblasts, are responsible for the digestion of the structural ECM components, gelatin and collagen. It follows that aberrant or uncontrolled regulation of MMPs resulting in high MMP activity is associated with the chronicity of non-healing wounds due to excessive and unabated tissue degradation[142]. Thus doxycycline, as a matrix metalloproteinase (MMP) inhibitor, is a potential treatment for chronic wounds[116].

Doxycycline comes in three crystal forms: doxycycline hyclate, doxycycline hydrochloride and doxycycline monohydrate[140]. Doxycycline hydrochloride and doxycycline monohydrate can be derived from doxycycline hyclate through several chemical reactions (**Figure 1.7**). Doxycycline hyclate, chemical formula $(C_{22}H_{24}N_2O_8.HCl)_2 \cdot C_2H_6O \cdot H_2O$, is a large hydrophilic molecule with a molecular weight of 1025.89 g/mol (1.03 kDa) and presents as a hygroscopic yellow crystalline powder[140]. It can be readily dissolved in water to form an aqueous solution with a solubility limit of 50 mg/ml[143]. Doxycycline can be delivered orally or intravenously with bioavailability being marginally greater for the latter. It is transported in the bloodstream mostly bound to plasma proteins and is widely distributed in tissue and fluid, with a half-life of 12–24 hours[140]. Clinically, it's the choice treatment over other tetracyclines due to its better absorption and longer half-life.

Doxycycline is sold as a medicament in several formulations including solutions, gels and tablets. Its Periostat® formulation, used to treat aphthous ulcers, is delivered as a mouthwash containing 20 mg doxycycline hyclate for a single oral dose (20 mg twice per day is considered a sub-antimicrobial dose)[144]. Vibromycin® comes as an oral tablet formulation and contains doxycycline powder while Doryx® is an enteric-coated slow release doxycycline-containing pellet[138]. Both are used as antibiotics against multiple types of bacterial infection. Atridox® is a biodegradable *in situ*-forming drug delivery system comprising Atrigel® (the delivery system) and 10% doxycycline[145]. It is used as a locally applied antibiotic as a treatment for periodontitis. The two components are combined together using a dual syringe system immediately prior to application and are injected onto the affected area.

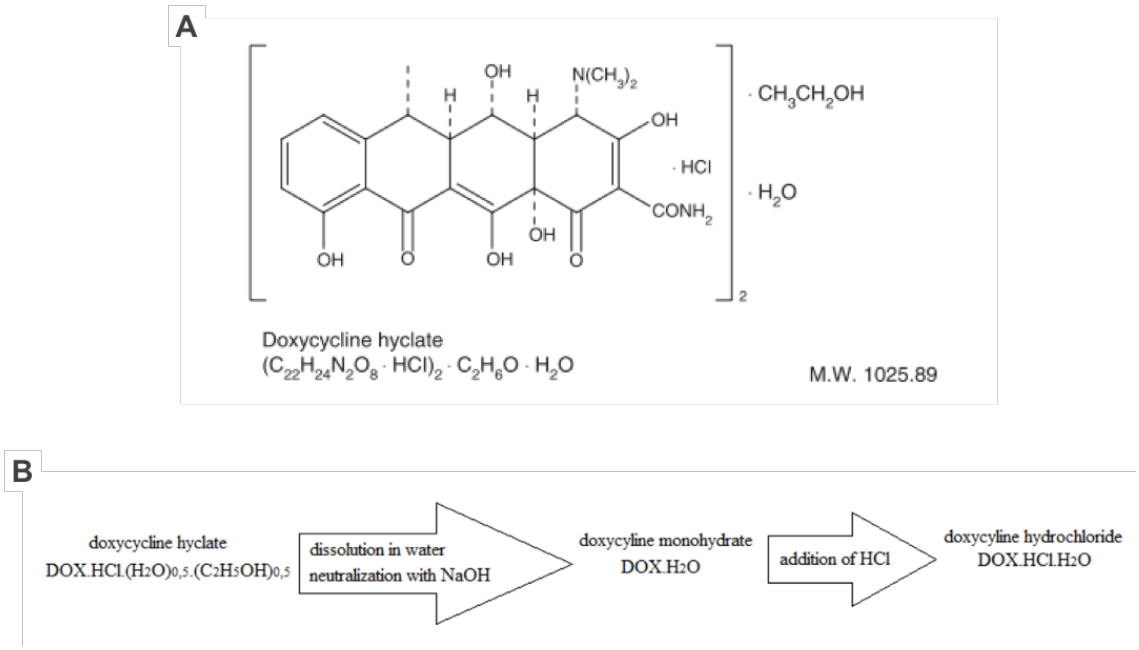

Figure 1.7 — (A) Skeletal and chemical structure of doxycycline (hyclate form). **(B)** Chemical derivation of doxycycline monohydrate and hydrochloride from doxycycline hyclate; from "Doxycycline hyclate: a review of properties, applications and analytical methods," by A.C. Kogawa and H.R.N Salgado, 2012, International Journal of Life Science and Pharma Research, 2, p. 13.

As with all drugs, even those previously approved for other applications, there are safety concerns surrounding doxycycline-based treatment of pressure ulcers. At antimicrobial doses, common allergic reactions with oral doxycycline include hives, shortness of breath and swelling of the face while common systemic reactions include headaches, dizziness, nausea, diarrhea, vomiting, thrush and vaginitis[138]. Oral doxycycline treatment has also been reported to elicit effects on the skin including photosensitivity — sensitivity to UV light — which requires patients to protect their skin from sunlight during the course of the treatment. Skin reactions are rare but include erythema, swelling and blistering rash. These side effects may not be the case with local sub-antimicrobial doses as desired in pressure ulcer treatment but it is important to be aware of potential complications.

As a potential prophylactic treatment for chronic wounds, doxycycline could be delivered intradermally to susceptible skin at the earliest stages of wound development. Later stages of wound development may also benefit from the effects of MMP inhibition but are more likely to require surgical intervention as ultimate treatment. The etiopathogenesis of chronic wounds often begins with MMP-mediated damage occurring below the intact skin. This makes

therapeutic access to the early stages of chronic wounds challenging and requires the skin barrier to be transiently permeabilised to allow for the absorption of larger molecules, like doxycycline, into the dermis to reach the deeper tissue injury.

1.5 Intradermal and transdermal delivery of large drug molecules

1.5.1 Negotiating the epidermal barrier

Transdermal drug delivery (TDD) and intradermal drug delivery (IDD) are indicated when other administrative routes, such as oral administration, are not as effective as desired. TDD describes drug delivery that has a target beyond the dermis (either the underlying tissue or systemic circulation), while IDD typically describes drug delivery where the target is the dermis. There are three major groups of drug that involve skin application: (i) epidermal formulations which are designed to remain active on the surface of the skin such as dermal insect repellents, (ii) endodermal or diadermal formulations which are designed to function in the viable epidermis and dermis but not the systemic circulation, and (iii) formulations that, even though are applied topically, have systemic action[146]. Most proteinaceous drugs are of a large size and are hydrophilic so they cannot permeate passively across the skin due to the stratum corneum which selectively allows the trans- and inter-cellular transport of small lipophilic molecules[147,148]. Tight junctions in the skin epithelium, known as zonae occludentes, may also contribute to the barrier function of the epidermis by inhibiting drug diffusion. To get these larger drugs across the skin the barrier must be temporarily disrupted.

1.5.2 Percutaneous penetration enhancers

Topically treating the skin is often prevented by the skin's natural barrier function and can be especially troublesome if the target lies just beneath the skin's surface. However, delivering drugs through the skin rather than orally provides a range of advantages, mainly by bypassing first-pass metabolism and by increasing local bioavailability. There are many different ways to circumvent the skin barrier, namely percutaneous penetration enhancers, which fall into the two major categories: (i) chemical enhancers and (ii) physical enhancers. Chemical enhancers are compounds, often added with or prior to drug application, that increase drug permeation through biochemical changes to the skin. Examples include alcohol, sulphoxides, surfactants, glycols and pyrrolidines[146,149,150]. Physical enhancers are devices or techniques that mechanically alter the skin to provide channels for drug transit. Common examples include iontophoresis, electroporation and sonophoresis. There are several desirable properties for percutaneous penetration enhancers: the enhancer should not be irritating, allergenic or toxic, its effect should be both predictable and reproducible, it should have no pharmacological effect

within the body, it should have an acceptable sensation or tolerable pain and, once removed, the skin barrier properties should return rapidly and fully[149].

Physical enhancers make use of ultrasound, electric fields, heat and ballistic methods to increase the permeability of the skin[151]. Ultrasound devices have been shown to help deliver high molecular weight medicaments, including proteins, percutaneously[152]. Paliwal *et al.* (2006) showed that the acoustic waves emitted by ultrasound devices made ultrastructural defects in the SC, increasing its permeability[153]. During iontophoretic delivery, low amplitude electrical currents are applied to the skin[154]. This has been shown to enhance percutaneous delivery of drugs, especially charged molecules, by several mechanisms including direct electrophoresis[155]. Iontophoresis has been clinically approved for several drug delivery applications including delivery of lidocaine for local anesthesia[156]. Electroporation utilises electrical fields in a similar manner to iontophoresis. Short, high-voltage pulses (tens to hundreds of volts) are applied to the skin using electric fields for microseconds or milliseconds[157]. This technique is not commercially used in transdermal delivery but has been successful in drug delivery for the treatment of several tumours[158].

High-pressure devices, such as jet injectors, use fluid impact to force drug solutions at high velocities into the skin[151]. Jet injectors have been successfully used in mass immunisation programmes and in the delivery of insulin[159]. Laser heating involves thermal ablation of the SC barrier – it selectively removes the SC without damaging underlying tissues through rapid heating of the skin for a short period of time[151]. Most of the devices and techniques that have been used have a long history in drug delivery across the skin. An emerging technology indicated in an increasing number of TDD and IDD applications are microneedles, another form of physical percutaneous penetration enhancer. These micron-sized needles are able to penetrate through the tough outer layers of skin to deliver a defined amount of drug to a target skin region. Their micron dimensions mean trans-epidermal delivery can be painless, improving patient compliance especially in skin which may already be sensitive and sore.

1.6 Microneedles for intradermal and transdermal drug delivery applications

Microneedles sit at the interface between hypodermic needles and transdermal patches[160]. They are microfabricated arrays filled with micron-sized needles typically ranging from 100–1000 μm in length. Microneedles are considered as an attractive minimally invasive method of delivering drugs across the epidermis and function to increase skin permeability by forming channels that act as conduits for drugs[161,162]. By bypassing oral administration, this approach can avoid degradation of the drug in the gastrointestinal tract and first-pass metabolism by the

liver[162,163]. Microneedles are able to penetrate through the tough outer layers of skin (the SC) to deliver a defined amount of drug to a target skin region. Since they are able to deliver drugs locally, they can avoid distribution to the whole body *via* systemic circulation, decreasing toxicity and reducing side effects[146]. Conversely, they may be used to deliver drugs, such as insulin, and vaccines to the microcapillary system with deep enough penetration if systemic circulation is desired. Microneedles are relatively low-cost and self-application by patients is possible in comparison to other mechanical enhancer techniques, as demonstrated by microneedle rollers that are already commercially available for personal cosmetic applications. Microneedles have improved patient compliance when compared with hypodermic needles and have been shown to deliver drugs painlessly and blood-free[164–166].

Microneedles come in a variety of designs and delivery mechanisms depending on the desired application. They can differ in shaft geometry, tip shape and needle material[162]. These physical parameters govern depth of penetration, rigidity and reusability amongst other factors. Drug formulation, required drug dose and molecular drug size must also be considered when choosing a suitable microneedle array for an application[167]. When choosing the material that the arrays will be made from, several parameters need to be carefully considered including the material's rigidity, hydrophobicity, biocompatibility and toxicity, and costs (both for acquisition and manufacture). Materials currently explored in microneedle manufacture include a range of synthetic and natural polymers, metals, ceramics and biomaterials. For single or smaller dosage amounts, such as with vaccines[168,169] or insulin[170,171], a spot application with a microneedle patch or single microneedle may be sufficient for drug delivery[172]. However, to deliver a drug over a larger surface area, such as a region of skin at risk of chronic wound development, more efficient microneedling techniques for permeabilising skin are required (**Figure 1.8**). Microneedle rollers offer a method for achieving barrier disruption over a large surface area.

Figure 1.8 — Types of microneedle array design: (A) A single hollow microneedle drug infusion unit. Adapted from "Faster pharmacokinetics and increased patient acceptance of intradermal insulin delivery using a single hollow microneedle in children and adolescents with type 1 diabetes," by J.J. Norman *et al*., 2013, Paediatric Diabetes, 14, p. 461. **(B)** A microneedle patch with multiple needles combined with a drug delivery unit that can store liquids. Adapted from "Painless drug delivery through microneedle-based transdermal patches featuring active infusion," by N. Roxhed *et al*., 2008, IEEE Transactions on Biomedical Engineering, 55, p. 1066. **(C)** A set of microneedle rollers of various microneedle lengths. Adapted from "Transdermal delivery of insulin using microneedle rollers in vivo," by C. Zhou *et al*., 2010, International Journal of Pharmaceutics, 392, p. 128.

1.6.1 Mechanisms of microneedle-mediated drug delivery

There are several ways that microneedles can be used to deliver a drug through the skin. To date, there have been five different microneedle-mediated drug delivery modalities reported in the literature. These are: (i) the 'poke and patch' method using solid microneedles, (ii) the 'poke and flow' method — a controlled release method of infusion using hollow microneedles, (iii) the 'coat and poke' method using coated microneedles, (iv) dissolvable or degradable microneedles, and (v) hydrogel-forming microneedles[173,174] (**Figure 1.9**). Solid microneedles are microneedles that do not have an annulus (internal channel) while hollow microneedles have an annulus running their entire length to allow for substance delivery by infusion. Solid microneedles are the most commonly reported microneedles in the literature[175,176]. In the 'poke and patch' approach the solid microneedles are applied to the skin, removed and the drug added on top of the microchannels created in the skin in a two-step process. The drug then enters the skin through these microchannels by passive diffusion. The drug may be stored in a patch acting as a reservoir which is applied onto the skin, or added directly as a solution, gel or nanoparticle formulation. In the 'poke and flow' approach, hollow microneedles are inserted into the skin. The drug (or vaccine) may be stored in a reservoir, such as a cartridge, and is infused through

the microneedles' annuli directly into the skin. The microneedles are removed once the drug has been delivered. This technique is also referred to as 'microinfusion' or 'microinjection'.

In the 'coat and poke' approach, solid microneedles are pre-coated with the active drug on their outer surface. They are then inserted into the skin and the coated drug transferred into the microchannels created during application. The microneedles are then removed from the skin. Dissolvable microneedles are made from soluble or biodegradable material which includes the active drug. Such materials include silk[177], maltose[178], sodium hyaluronate or hyaluronic acid[179,180]. Once inserted into the skin the microneedles either dissolve or degrade into the microchannel spaces they created, releasing their load into the skin. The applicator used to deliver the microneedles may be removed after initial insertion or until the microneedles have sufficiently dissolved. Hydrogel-swelling microneedle arrays are formed from polymeric microneedles combined with a drug reservoir. Once the microneedles are inserted into the skin, the hydrogels expand quickly by absorbing water from the interstitial fluid[174]. The drug diffuses from the reservoir along the swollen microneedles into the skin[181]. Due to the nature of the swelling process, hydrogel-swelling microneedles can be left on the skin securely.

Unpublished data presented during conference proceedings at Microneedles 2016 – The 4th International Conference on Microneedles (London, UK) by A.R Tadros and M.R. Prausnitz (Georgia Institute of Technology, Georgia, USA) introduced a potential sixth microneedle-mediated drug delivery modality. "STAR" particles are single four-pointed (i.e. star-shaped) microneedle units suspended together in an aloe vera gel topical formulation. The microneedles are applied to the skin by gentle rubbing, as would be done with a lotion. They permeabilise the skin in a similar manner to the 'poke and patch' approach, except that the active drug is incorporated into the topical formulation so there is only a single step to the application. One of the major advantages of the "STAR"-microneedle particles approach is that it enables treatment over a large surface area of skin and of anatomic sites that are not so easily accessible with microneedle patches.

1.6.2 Commercially available microneedle systems

Many authors have explored the use of novel and bespoke microneedle arrays, designs and delivery modalities. However, there are already several commercially available

Figure 1.9 — Mechanisms of drug delivery by solid, hollow, coated, dissolvable/degradable and hydrogel-forming microneedles: (A) 'Poke and patch' approach using solid microneedles — the microneedles are used to create micropores and are then removed. The drug to be delivered is immediately applied to the permeabilised region of skin. **(B)** 'Poke and flow' approach using hollow microneedles. **(C)** 'Coat and poke' approach using solid microneedles — the microneedle surfaces are coated with drug. On insertion into the skin, the drug is transferred from the microneedle surface into the skins. **(D)** Dissolvable/degradable microneedles are transferred into the skin during application, with just the array removed. The microneedles degrade over time releasing the drug into the skin. **(E)** Hydrogel-swelling microneedles absorb water from interstitial fluid on insertion into the skin. The drug from the attached drug reservoir diffuses through the swollen microneedles into the skin. Adapted from "*Microneedles: A New frontier in Nanomedicine Delivery*," by E. Lerraneta, 2016, Pharmaceutical Research, 33, p. 1060.

microneedle systems on the market. These CE-marked devices allow for standardised, reliable and consistent microneedle application, requiring only drug loading and positioning of the device by the operator. Some also have integrated display screens that can offer feedback to the operator. The pharmaceutical company, 3M, currently offers two such microneedle devices, their 'Solid Microstructured Transdermal System' and their 'Solid Microstructured Transdermal System' (**Figure 1.10 – A**). The solid microneedle device functions as a 'coat and poke' delivery system for fast bolus delivery of vaccines into the skin. The device inserts the microneedles into the skin, which are delivered as a removable patch. The hollow microneedle device allows for the microinjection delivery of medicaments with a wide range of viscosities and doses from 0.5 – 2 ml into the skin. The solid microneedles are available in various lengths (250, 500 and 700 μm) while the hollow microneedles are available only at a length of 1500 μm.

Several independent or smaller companies have also developed their own microneedle devices, including DebioJect™, DermoPen, DermaJet, DermaFrac and Derma-stamp[182]. These drug delivery systems are typically more expensive than conventional methods since the entire device is not disposable due to integration of digital components. They also typically need to be electrically powered. The DermoPen is a modular microneedling device with an electric handle and disposable needle tip containing twelve microneedles (**Figure 1.10 – B**). The device is also motorised allowing the microneedles tips to oscillate which is claimed to minimise dermal tearing on insertion. DermaJect is a digitalised injection system that allows the operator to set and regulate the exact quantity before injecting (**Figure 1.10 – C**). Detachable and disposable single and multiple microneedle heads are available. DebioJect™ by DermoTech (Lausanne, Switzerland) offer syringe compatible microneedle attachments for microinfusion which come with single or multiple microneedles (**Figure 1.10 – D**).

1.6.3 Microneedle biocompatibility and safety

Material cytotoxicity is an important parameter to consider in microneedle design because the array is to come into contact, at least transiently, with the skin[162]. Skin irritation and exposure to harmful and toxic substances is a valid concern, especially if the area to be treated is already sensitive. Sources of such substances include leachables eluted from the microneedle material when liquid is passed through it or when the microneedles contact with fluids present in the tissue. It is thus important to assess the microneedle material for leachables released on fluid exposure and to be aware of short- and long-term bio-effects of these leachables (i.e. material biocompatibility). Safety of microneedles is discussed further in Chapter 3**: 3.5.3 Microneedle application on injured skin and its effect on cell viability,** ***p.139***.

1.6.4 Medical and cosmeceutical applications of microneedles

Although microneedles have been shown to improve permeation of various dyes and stains, such as methylene blue, trypan blue, bovine serum albumin and calcein-AM[183], across the SC in 'proof-of-concept' studies, they have also been explored successfully in a multitude of medical and cosmeceutical applications[173,184]. These include intradermal and transdermal delivery of drugs and vaccines as well as the use of microneedles in cosmetic purposes to improve the skin appearance. The interest in delivering vaccines using microneedles surrounds the current need to solve current practical issues such as cold chain elimination and reducing sharps waste, as well as a desire to illicit cutaneous immune responses by exposing antigens to the antigen-presenting cells (APCs) in the skin[184,185]. Vrdoljak *et al*. (2012) reported a successful immune response in mice injected with live virus vaccines using coated microneedles, comparable to what had been achieved with traditional needle-and-syringe intradermal immunisation[186]. In their research models, Kommareddy *et al.* (2011) reported immunogenicity against influenza antigens using dissolvable microneedle patches[168] and Edens *et al*. (2013) showed that microneedles coated with measles vaccine resulted in neutralising antibody levels equivalent to those achieved with subcutaneous immunisation at the same dose.

Similar success has been observed with microneedle-mediated insulin delivery[170,171,187]. Current delivery is achieved by daily insulin injection through the abdomen, thigh, arm or buttock using hypodermic needles and syringes or with sub-cutaneous insulin pump catheters. Delivery by microneedles could improve patient compliance and accelerate insulin pharmacokinetics[170]. Delivery of nanoparticles has also been successful[188–190] and has opened up new avenues for microneedle-assisted drug delivery in the field of nanomedicine[174]. There is also much interest in facial administration of microneedles for cosmetic purposes such as facial rejuvenation to reduce the appearance of wrinkles and as a post-acne treatment for skin resurfacing and improvement of the appearance of scarred skin[191]. In recent years there has been development of novel technologies where microneedles are used In combination with other devices[192]. Sonophoresis-enhanced microneedle arrays (SEMA) which use the additive effect of the two established physical enhancers, acoustic waves and microneedles, have been shown to improve upon their individual effects on molecular diffusion rate[193,194]. In the future, microneedles may also be used for fluid removal as well as drug delivery, such as for blood sampling and extraction[195] and as biosensors, especially for glucose[196–199].

Figure 1.10 — A range of commercially available microneedle devices: (A) Hollow and solid structure microneedle systems from 3M. **(B)** DermaPen™ consisting of an electrically-powered adaptor and disposable 12-microneedle head attachment. **(C)** DermaJet consisting of a digital precision injection device adaptable with various microneedles. **(D)** DebioJect™ by Debiotech for single and multiple microneedle microinjections.

1.7 Preclinical research models of the human pressure ulcer

1.7.1 Animal skin models of human skin disease and pressure ulcers

From mice to non-human primates, a range of animals has been used to model human skin disease. The use of non-living (*ex vivo*) animal tissue and other skin substitutes are also widely used. These include skin mimetics such as silicone membranes[200], biosynthetic skin substitutes[201], *in vitro* cellular models of skin and *ex vivo* skin[202], especially human and porcine. However, these models represent the skin in isolation from a fully functioning biological system and this must be taken into account before extrapolating results to living organisms. Animal models provide an excellent alternative and can be used to study wound development and healing in a whole organism. Good ethical research practice should follow the framework of the 3Rs of animal research: replacement, reduction and refinement.

Traditionally the most commonly used animals for *in vivo* skin studies are rodents especially mice, rats and guinea pigs[203]. The advantages of using such small animals are their small size, ease of housing and handling, and relatively low cost. However, larger animals including the pig and non-human primates are believed to make better human skin models due to their similarities to human skin including epithelial architecture, nerve density, vascularity and matrix components[204]. Since the use of primates is highly restricted, the next relevant animal model for human skin is porcine. Pigs have the advantage of anatomic and vascular similarities to humans; the red Duroc pig, in particular, has been extensively validated as a model for human skin pathology and is believed to be the ideal large animal model to study human cutaneous disease[204,205]. However, pigs are large, difficult to house and are expensive, thus the practical use of rodent models cannot be overlooked. As the most recent non-human surgical models of pressure ulcers concentrate on the use of rodents they are the focus of this research.

1.7.2 Fundamental differences between human and rodent skin

Though there are structural and functional similarities between human and rodent skin, there are evident and important discrepancies which need to be considered when using rodents to model a human disease. One of the most evident differences is the hair coverage for the majority of rodents as compared with humans. Rodent skin is typically covered in thick dense hair craniocaudally whilst human hair is much thinner with an androgen-sensitive distribution[206]. This extremely high density of hair follicles is believed to affect percutaneous absorption of molecules so hairy rodent skin is not desirable[203]. Thus, to mimic the hairless nature of human skin, many *in vivo* models remove the dorsal hair of the subject *via* shaving/clipping, hair removal (depilatory) creams or a combination of the two. However, these techniques are

believed to cause cutaneous injury due to abrasion (either mechanical or chemical) to the skin surface. To circumvent the need for hair removal pre-treatment, groups have employed hairless rats or nude mice in their studies, which genetically lack a hair coat and are believed to better mimic human skin than hairy skin[207].

As with human skin, rodent skin is divided into three main layers, the epidermis, the dermis and the subcutis. However, the anatomy and physiology of these layers vary greatly. The thickness of each layer differs with species, with murine skin being much thinner and rat and human skin having more comparable dimensions[203]. Rodent skin lacks rete ridges, epidermal thickenings which extend down through dermal papillae, as well as apocrine sweat glands responsible for secreting several components of sweat[208]. Conversely, rodents contain a subcutaneous muscle layer known as the panniculus carnosus which humans lack[86]. Biomechanically, rodent skin is relatively thin, loose and compliant while human skin is thick, relatively stiff and adherent to underlying tissues[86]. For mice, there also exists a gender difference in skin anatomy and physiology[204]. Females have a thicker epidermis and hypodermis while males have a much thicker dermis that imparts greater strength[209]. This gender discrepancy should be taken into consideration when designing experiments with mixed gender subjects.

As rodent skin is fairly loose and compliant, open wounds can heal by skin contraction whereby normal unwounded skin stretches over the injured area[1]. This process is relatively rapid and sufficient for wound healing and is aided by the presence of the panniculus carnosus. Human wounds, in contrast, do not heal by contraction, which is slow and incomplete, but mainly through the process of re-epithelisation[204]. Humans are also susceptible to chronic wounds whilst most animals do not suffer from them naturally. This is attributed to the lack of truly aged animals as well as the absence of combined hemostatic dysfunction, such as venous insufficiency, neuropathy and chronic debility in animals[1]. Furthermore, chronic wounds in humans tend to occur in regions where skin contraction is relatively poor compared with other sites, such as in the lower leg and feet.

1.7.3 The history of modelling pressure ulcers *in vivo*

To briefly touch on the history of the surgical approaches to modelling *in vivo* pressure ulcers, the very earliest models used large mechanical compression devices on the femoral trochanters in swine or canine models. These devices were cumbersome and required anesthetised subjects. Importantly, from these pioneering studies, it was found that: (i) there existed an inverse relationship between the amount and duration of pressure required to render pathological changes in tissue and (ii) prolonged ischemia alone was insufficient to invoke skin necrosis,

suggesting other critical factors in pressure ulcer aetiopathogenesis[92]. Henceforth, the phenomenon of IR injury has been at the forefront of pressure ulcer modeling and is believed to be an inciting event in pressure ulceration.

The unifying theme amongst the most recent pressure ulcer models is the use of a compact device to generate a compressive force that is able to simulate IR injury. The system generally uses a reversible mechanism whereby mechanical loading by the device causes ischemia which can then be easily and repeatedly unloaded to simulate reperfusion. Due to the simplicity of most of these models the animals are often non-anesthetised during the experiment and do not require long-term immobilisation. Some groups have devised their own novel devices[89,99,100,210], while others have employed previously developed techniques to their particular area of research[59,210]. One of the major challenges these groups face is replicating the pressure exhibited in the human pressure ulcer. The device must be able to provide pressure of a clinically relevant magnitude and for a sufficient duration. Furthermore, to truly mimic the human pressure ulcer, the wound must progress through all clinical stages of ulcer development in order. Two commonly used devices are magnets[59,89,99,100,211,212]and compression chambers[93].

1.7.4 Modelling pressure ulcers using magnetic compression

The use of magnets to create a compressive force appears to be a popular technique and has been utilised by various academic groups throughout the past decade or so. The techniques themselves vary in the procedure (invasive or non-invasive), the properties of the magnet(s) being used, the respective lengths of the compression and release cycles, the location of the magnet(s) as well as the strain of animal being employed, amongst other parameters. Each of these parameters impacts on the severity and stage of the ulcer produced, the types of controls that the experiment requires to validate it and ultimately how well the model reflects the human pressure ulcer.

Surgical procedure

One popular method of mechanically modeling IR injury using magnets is magnet implantation which involves creating an incision in the dorsal tissue and implanting a magnet into the body. This intracorporeal magnet may be placed either beneath the fascia (subcutaneous) or into a muscle layer (sub-muscular). The incision is then sutured and an extracorporeal magnet is placed on top of the implanted magnet (**Figure 1.11 – A, B and D**). In place of an internal magnet, a steel plate may also be used[89,99]. Another surgical method employed by several groups[59,211,212]provides a non-invasive alternative to the implantation procedure. Two magnets are externally loaded onto the skin, pinching the skin between them and leaving a small bridge

of normal tissue (. -). For either method, contralateral skin can act as an intra-individual control.

One of the major and notable disadvantages of the method of magnet implantation is the systemic effect the surgical procedure may have on the animal. Disrupting the skin and implanting a relatively large foreign object into such a small animal may result in inflammatory responses that could affect the interpretation, and thus the validity, of the results. One way to account for the effects of the surgery is to use sham and control animals, which undergo the surgical procedure but which do not form part of the experimental groups. This way differences between the sham and experimental groups can be attributed to the experimental injury. Another way studies have accounted for the effects of the surgical procedure is to allow the animals to recover post-surgery for periods ranging from 18 hours to two weeks. However, the length of time sufficient to completely remove the effects of surgery has not yet been defined. Furthermore, a foreign body (the intracorporeal magnet or plate) will still remain within the body and could continue to provoke responses despite a respite period from surgery. This problem is circumvented by the noninvasive technique of using two external magnets. Removal of the external magnet(s) in either magnet protocol to begin the reperfusion period may cause some local trauma however, as substantial force is required to prise off the magnet.

The location of magnet placement determines the type of wound created; a magnet implanted subcutaneously will develop a different wound from a magnet placed within a muscle. Wassermann *et al.* (2009) suggest their technique of implanting the internal magnet sub-muscularly better represents pressure ulcer pathogenesis as it involves all the relevant tissue layers[99]. This contrasts with the cutaneous pressure ulcer models that target the injurious IR cycles solely at the cutaneous region of the skin. Arguably the Wassermann model of deep tissue injury is the superior technique as it allows pressure ulcer development up to clinical stage 4, resulting in a full-thickness wound whilst the cutaneous models cannot develop past a stage 3 pressure ulcer in a way that could be considered analogous to humans because compression is not being delivered to the subcutaneous tissues.

Anesthesia is an important consideration in surgical models. Anesthesia is required in situations where the surgical procedure is likely to cause significant distress or pain in the subject or subject immobilisation is required for a significant period of time to allow the procedure to take place successfully and safely. Earlier studies that involved large compression devices required anesthesia and subject immobilisation for the entirety of the compression periods[92]. However, the physiological consequences of anesthesia are likely to have confounded the true effects of pressure in the non-anesthetised animal[89]. Due to the simplicity and speed of the procedures,

the recent models do not require anesthesia or prolonged immobilisation. Animals appear to tolerate the procedures well and have been documented to move freely and naturally, despite the extra weight of the magnets

Magnet properties

Magnets can be tailored according to their shape, size and strength. A variety of magnets has been used in pressure ulcer models making direct comparisons between different studies difficult. Circular magnets are the most common, creating wounds of similar shape to pressure ulcers. Several studies have used circular disc magnets in their model whilst others have employed ring magnets[100]. Magnet geometry determines the magnetic field and this, in turn, affects the compressive forces experienced by objects placed between its two magnetic poles. For example, one consideration of using a disc magnet model is that the compression occurs over the entire surface area of skin in contact with the magnetic faces. A ring magnet, in comparison, applies most of its compressive force to the circumferential edge of skin that is in contact with it.

The extent of tissue damage caused by magnets is related to their strength. This is typically measured in Gauss, a measurement of magnetic flux density or magnetic induction. The higher the Gauss value the greater the strength of the magnetic field. Gauss values can be converted to clinically meaningful measurements of pressure, measured in 'mmHg'. Normal human capillary pressure ranges from 16 to 32 mmHg depending on body region[13]. It is believed that external pressures of greater than 32 mmHg are sufficient to cause capillary occlusion, reduce capillary inflow and begin the process of tissue necrosis[13]. Most groups, in fact, use a 50 mmHg pressure to initiate ischemia, enough to cause capillary occlusion in a rodent. A consideration here is whether the compressive pressure is in fact too high for a rodent to be truly analogous to typical injurious pressures seen in the relatively larger human.

The magnet itself must be inert if it is to be implanted in the body or if is to come into contact with tissue for prolonged periods of time. This minimises the risk of (i) magnet corrosion and (ii) the leeching of chemicals into the body which may invoke inflammatory responses. Inert magnet coatings can either be ceramic or gold-plated. The material of surgical tools should also be taken into consideration when choosing equipment which, preferably, should be non-magnetic to minimise interference by the magnets. Housing of animals post-surgery must also be considered carefully. Subjects should be housed singly, if possible, to prevent the magnet from becoming dislodged or wounds being tampered with by other subjects. Caging should be non-magnetic to prevent animals from getting stuck; in this respect the use of stainless steel implants becomes more attractive.

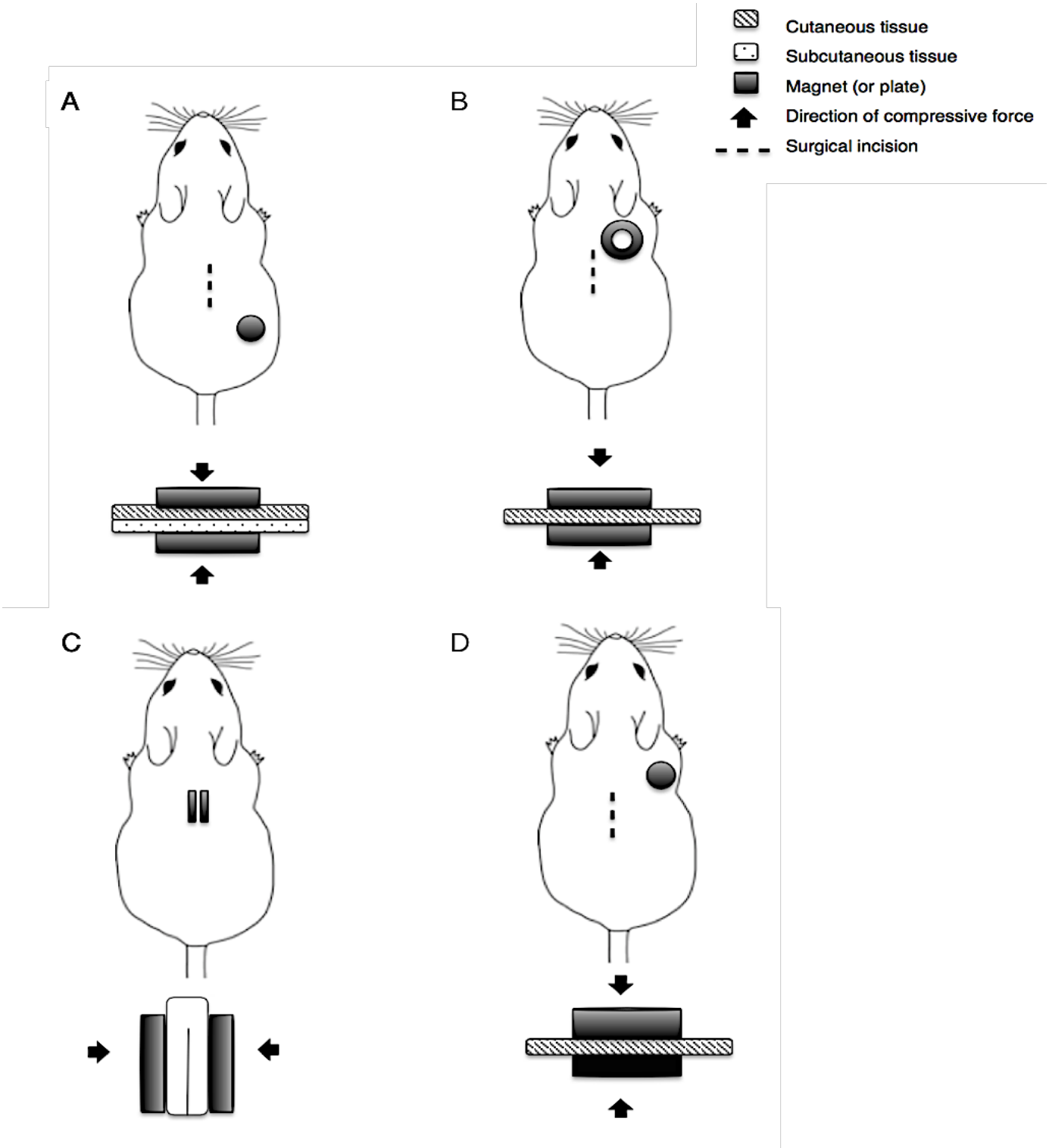

Figure 1.11 — Schematic representation of the recent *in vivo* murine models of pressure ulcers using magnets: (A) Sub-muscular implantation of disc magnets into gluteal muscle. **(B)** Cutaneous implantation of ring magnets. **(C)** External placement of disc magnets to skin. **(D)** Cutaneous implantation of steel magnetic plate and external magnet.

Length and number of compression/release cycles

Studies have altered either (i) the length of the compression and release periods, (ii) the total number of compression-release cycles, or (iii) both. There are no standardised protocols for the length and number of compression-release cycles in order to generate a model pressure ulcer amongst the studies. However, it has been suggested that the current practice of relieving pressure every two hours in afflicted patients contributes to, rather than ameliorates, pressure ulcer progression[99,100]. Therefore several studies have included an experimental group that undergoes a compression period of two hours and a release period of one hour to mimic clinical practice[93,99,100]. Several studies[59,89,100] have also included an 'ischemia alone' experimental group to compare with the 'IR injury' experimental groups, with the aim to assess any additional injurious effect reperfusion may have on top of tissue ischemia.

Modelling pressure ulcers using compression devices

Tsuji *et al.* (2005) forwent the popular magnet model and established a novel cutaneous IR model using a skinfold chamber coupled with an intravital microscope[93]. Their method allows visualization of the *in vivo* microcirculatory response to IR injury which has not been well studied before. Their original chamber is constructed from two aluminum frames held together by four plastic tubes along with several attachments. During the application procedure, an area of dorsal skin on the subject is pulled up and fixed to form a skinfold. A square of skin is then cut away from one of the layers and a coverslip, which is incorporated into one of the frames, covers the underside of the other skin layer. The authors then allow for a 48-hour recovery period post-surgery.

In contrast to the magnet models, compression is provided mechanically *via* the chamber at 500 mmHg using a tension gauge, an articulated manipulator and a compression tip held in place by three holding screws. A fluorophore-conjugated molecule, FITC-dextran, is then injected *via* the tail vein for contrast enhancement while epi-illumination of the compressed tissue is provided by a lamp with a green filter. Images are recorded on video. As previous groups have done, Tsuji *et al.* (2005) divided their subjects into compression only and compression-and-release groups to simulate ischemia only and IR injury respectively[93]. Both groups had a total of eight hours compression: the compression-only group received this in one sitting while the compression-release groups had four cycles of two hours of compression and one-hour release. This once again mimics the time frames reported in clinical practice[31]. Like the magnet models, the skinfold chamber model does not require subject immobilization throughout the entirety of the compression treatments. However, the technique is quite involved and requires specialist equipment that is relatively cumbersome. The procedure is also highly invasive as it requires surgical removal of the skin. However, one of the main advantages of the model is its ability to

visualise the changes in the microcirculation whilst compression is taking place. This has allowed assessment of changes in blood flow associated with IR injury.

Currently, most studies of pressure ulcers in humans are limited to those in patients with pre-existing ulcers. This, in turn, limits the assessment of pressure ulcer development, progression and healing from beginning to end. Animal models represent an alternative avenue to investigate the full pressure ulcer paradigm *in vivo*, bridging the gap between *in vitro* and human studies. However, one must bear in mind inter-species differences as well as the difficulty of fully mimicking pressure ulcer pathogenesis. As described in this review of the literature, there is a spectrum of contributing factors which cannot all be adequately addressed in a single model. Thus the aim of surgical and mechanical animal models is to improve our basic understanding of how pressure ulcers develop and progress. These models have become invaluable tools and, while bearing in mind their limitations, can inform on the biomolecular mechanisms and histological detail of pressure ulcer development in a whole organism. Preclinical surgical models of the human pressure ulcer are further explored in Chapter 5.

Chapter 2 Assessment of Solid Microneedle Rollers to Enhance Transmembrane Delivery of Doxycycline

2.1 Introduction

2.1.1 Doxycycline for the treatment of pressure ulcers

Doxycycline, as a matrix metalloproteinase (MMP) inhibitor, is a potential treatment for chronic wounds[116]. High levels of MMP activity have been widely documented in studies of the chronic wound microenvironment[106,111,113,117,142] and the effect of doxycycline, and other members of the tetracycline family, has been extensively investigated in human diseases that exhibit high MMP activity such as osteoarthritis, rheumatoid arthritis and periodontitis. Doxycycline has also been shown experimentally to reduce tissue degradation[31,58–60]. The MMP inhibitory action of doxycycline is independent of its antimicrobial properties and thus unrelated to its inhibitory effect on bacterial protein synthesis; though the full mechanism has yet to be elucidated, it is believed to inhibit enzymatic MMP activity through the chelation of the zinc molecule[213]. This makes it an attractive treatment for chronic wound care as its antibiotic effects can be clearly distinguished from its MMP inhibitor activity.

Doxycycline's inhibitory activity extends to TNFα-converting enzyme (TACE)[116], a molecule that causes the release of tumour necrosis factor-alpha (TNFα) which is an important inflammatory mediator known to impair wound healing. In all, doxycycline has multiple attributes which make it desirable as a treatment for pressure ulcers; not only does it exhibit MMP inhibitory activity it also is a hydrophilic compound that can be administered as a powder, an aqueous solution or formed into a gel. Furthermore, it is already FDA-approved and has shown pharmacokinetic advantages over its tetracycline counterparts. Thus there has been some interest in doxycycline as a potential treatment for chronic wounds[116].

2.1.2 Microneedle rollers for intradermal doxycycline delivery

The primary barrier to intradermal and transdermal drug delivery (IDD and TDD) is the stratum corneum (SC) which forms the outermost layer of the epidermis[214]. Many drugs, especially proteinaceous drugs, are large and hydrophilic so cannot passively diffuse across the skin due to the SC which selectively allows the intercellular transport of smaller lipophilic molecules, typically up to 500 Da[76,147,148]. Tight junctions in the skin epithelium known as zonulae occludentes also contribute to the barrier function of the epidermis by inhibiting drug diffusion[215–217]. To get larger molecules across the skin, the SC barrier must be temporarily disrupted. There are different ways to achieve this using penetration enhancers which chemically or physically alter the skin to transiently increase its permeability[150]. Microneedles offer a minimally invasive way to achieve this, however patches and arrays only deliver to a relatively small area of skin. To cover larger regions of skin microneedle systems, known as microneedle rollers, can be employed.

Microneedle rollers are solid microneedle systems composed of two main parts – a handle for manual rolling (usually plastic) and a head attachment (sometimes detachable) containing multiple microneedles. The concept behind the use of microneedle rollers is to roll the system against the region of skin where permeabilisation to the active drug is desired. This technique can reach much larger areas much more quickly than repeated applications of microneedle patches. Microneedle rollers come in a multitude of different microneedle lengths while the microneedles themselves are typically made of metal. These systems are commercially available in the public domain and are advertised for personal as well as clinical use. They have become particularly popular in cosmeceutical applications where they can be used alone to stimulate collagen remodelling[84] or to deliver cosmeceuticals such as antioxidant-infused creams and collagen[218,219]. Both approaches have been used to improve the skin appearance after scarring[191,220,221] and as techniques for facial rejuvenation[222–224]. One of the most well-known microneedle roller devices is the Dermoroller® produced by Dermaroller S.a.r.l. (Friesenheim, France) that has been successfully used in the TDD of several drugs[182,225]. The device is composed of 192 metal microneedles (eight circular arrays of 24 microneedles each).

Figure 2.1 — Photographs of different commercially available microneedle roller systems: (A) A microneedle roller with smaller head attachment for application on smaller regions of skin such as the eyelid. **(B)** Microneedle roller system with 540 titanium microneedles. **(C)** The Dermaroller® with 192 metal microneedles**.** From "Microneedling: Advances and widening horizons," by A. Singh and S. Yada, 2016, Indian Dermatology Online Journal, 7, p. 245.

2.1.3 Strat-M™ membrane as a skin substitute for modelling human skin

The use of excised biological tissue (either human or animal in origin) is widely used to model human skin in the investigation of microneedles. However there are multiple disadvantages of these models including high inter-sample heterogeneity, instability of the skin *ex vivo* and significant dissimilarities between human and animal skin when animals are used as a human skin model[203]. Furthermore, bioengineered skin equivalents are costly and have been shown to have higher diffusion rates when compared with human skin[226]. As an alternative, there are a range of synthetic skin substitutes on the market with differing claims on their likeness to human skin permeation properties[227]. Artificial skin membranes hold several advantages over excised skin, including high reproducibility, high stability and being easier to obtain. Strat-M™ (Merck Millipore, Massachusetts, USA), a synthetic non-animal derived human skin mimetic, is marketed as a modified ultrafiltration membrane with human skin-like permeation properties[226]. Structurally it is composed of polyethersulfone and has a pore size of less than 0.1 microns[226]. It has been designed for the screening of active pharmaceutical ingredients

(API) amongst other groups of chemicals such as cosmetics. The manufacturers claim that Strat-M™ is predictive of diffusion of drugs through human skin and that it is also sensitive to enhancers.

2.2 Research outline

This chapter introduces the microneedle roller system used throughout the body of research and investigates the effect of microneedling on Strat-M™ membrane using this roller system and the feasibility of delivering doxycycline hyclate across the skin using this model. Firstly, the materials are analysed in detail. The ultrastructure of the recently marketed Strat-M™ membrane is analysed and compared with the upper layers of human skin. The geometry of the microneedle tips on the roller system is also explored. Micropore entry area is evaluated in detail using high-resolution scanning electron microscopy and the difference between application modes of the roller systems on micropore area is also assessed. *In situ* membrane depth penetration is compared between increasing microneedle lengths (250, 500 and 750 μm) using optical coherence tomography (OCT). To determine the pharmacokinetic diffusion properties, a Franz cell permeation study was used to evaluate the permeability of Strat-M™ to doxycycline hyclate and the effect of microneedle application on drug permeation under infinite dose conditions. Finally, comparison of Strat-M™ and human skin is made by observing the micropores created in each type of surface. Any significant differences may have implications for the suitability of Strat-M™ as a model of the uppermost layers of human skin.

Methods and materials

2.2.1 Microneedle rollers

Commercially available CE-marked microneedle rollers were supplied by Sodacoda™ (Delmenhorst, Germany) in three microneedle lengths: 250, 500 and 750 μm. Rollers were composed of two parts, a detachable head containing the microneedles and a handle for holding and manual insertion (**Figure 2.2 – A).** Each roller head had 540 titanium microneedles arranged as nine discs with 60 microneedles each (**Figure 2.2 – B**).

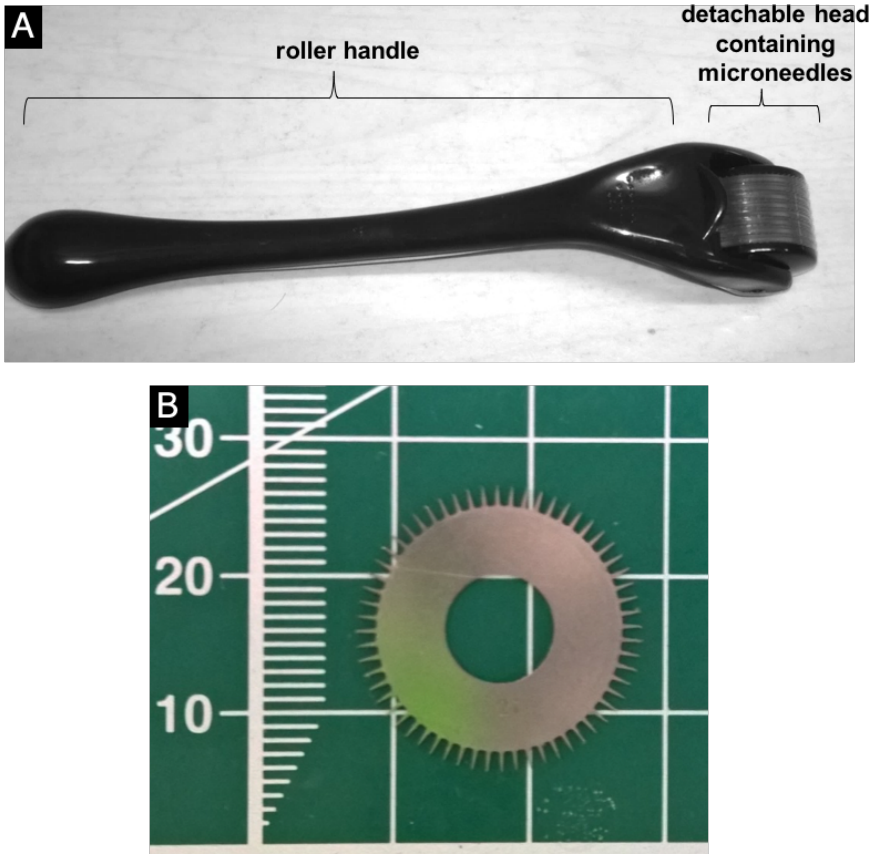

Figure 2.2 — Photographs of the microneedle roller system: (A) The device is made up of two parts, a handle for gripping and rolling and a head containing the microneedle discs. **(B)** Each roller head is made up of nine discs of 60 microneedles (540 microneedles in total).

2.2.2 Franz diffusion cells

Transmembrane drug diffusion was studied quantitatively in synthetic membranes mounted in vertical static Franz diffusion cells (Soham Scientific, Ely, UK). Cells were of modular design and consisted of an upper donor compartment and a lower receptor compartment (**Figure 2.3**). Both chambers had a bore size of 12 mm and could each hold up to 3 ml of fluid. The area of permeation afforded by the cells was 113 mm^2.

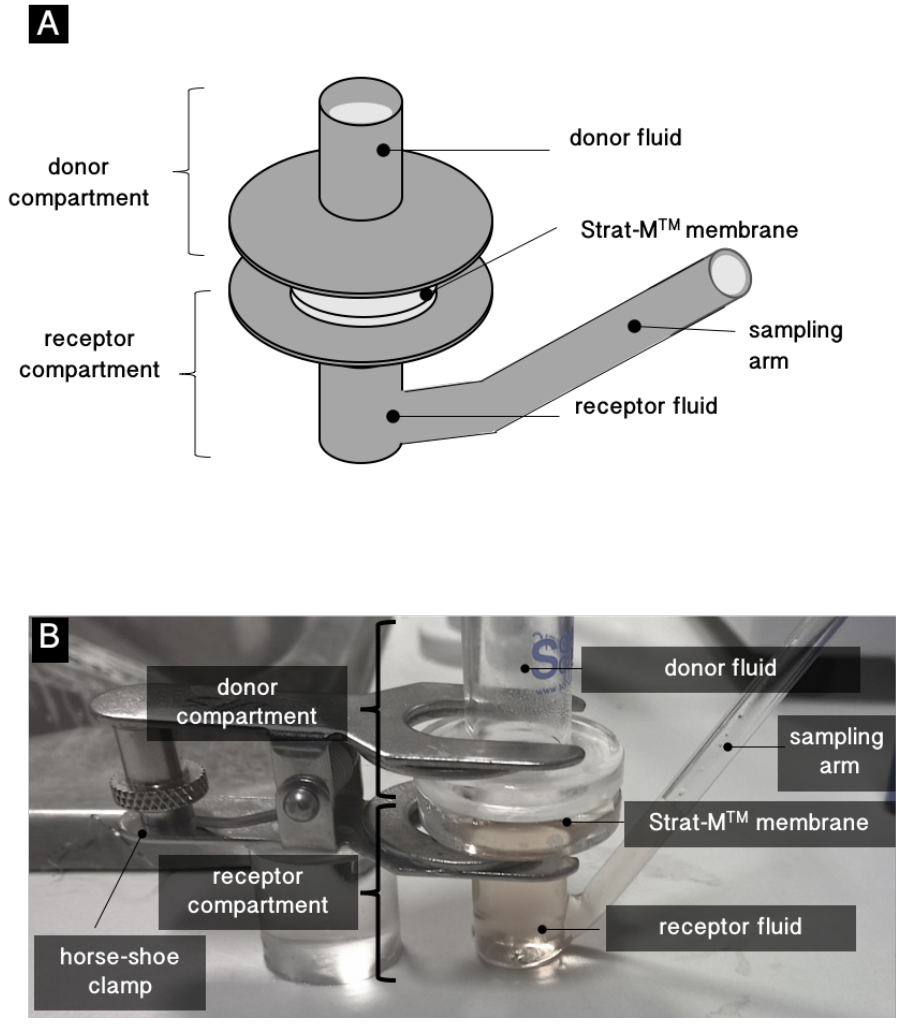

Figure 2.3 — Vertical static Franz cell apparatus: (A) Schematic representation of the apparatus set-up. **(B)** Photograph of the apparatus set-up.

2.2.3 Perforation of Strat-M™ with microneedle rollers

Strat-M™ synthetic membrane was obtained from Merck Millipore (USA). Membranes were cut into circular discs, 23 mm in diameter, and transferred onto a cutting board with tweezers. The discs were mounted onto a support made of silicone elastomer to mimic the compressibility and rigidity of human skin over bony protuberances (**Figure 2.5**). The microneedle roller head (**Figure 2.4 – A**). was placed onto the membrane, secured at the holder base with tack and a 500 g mass added onto the head for 30 seconds (**Figure 2.4 – C**). This provided a downward force on the microneedles of 3.8N. The mass and roller were then removed. In a separate experiment, the rollers were applied to the membranes by manual insertion. The roller was placed onto the membrane and rolled five times bi-directionally along a single axis (**Figure 2.4 – B; Figure 2.5 – B**).

Figure 2.4 — Digital photographs of the microneedle roller system: (A) Microneedle roller head**. (B) The** x and y planes of the microneedle roller head. During manual rolling, the microneedle is rolled along the y plane. **(C)** Application of 500 g mass onto microneedle head providing a vertical force of 3.8N,

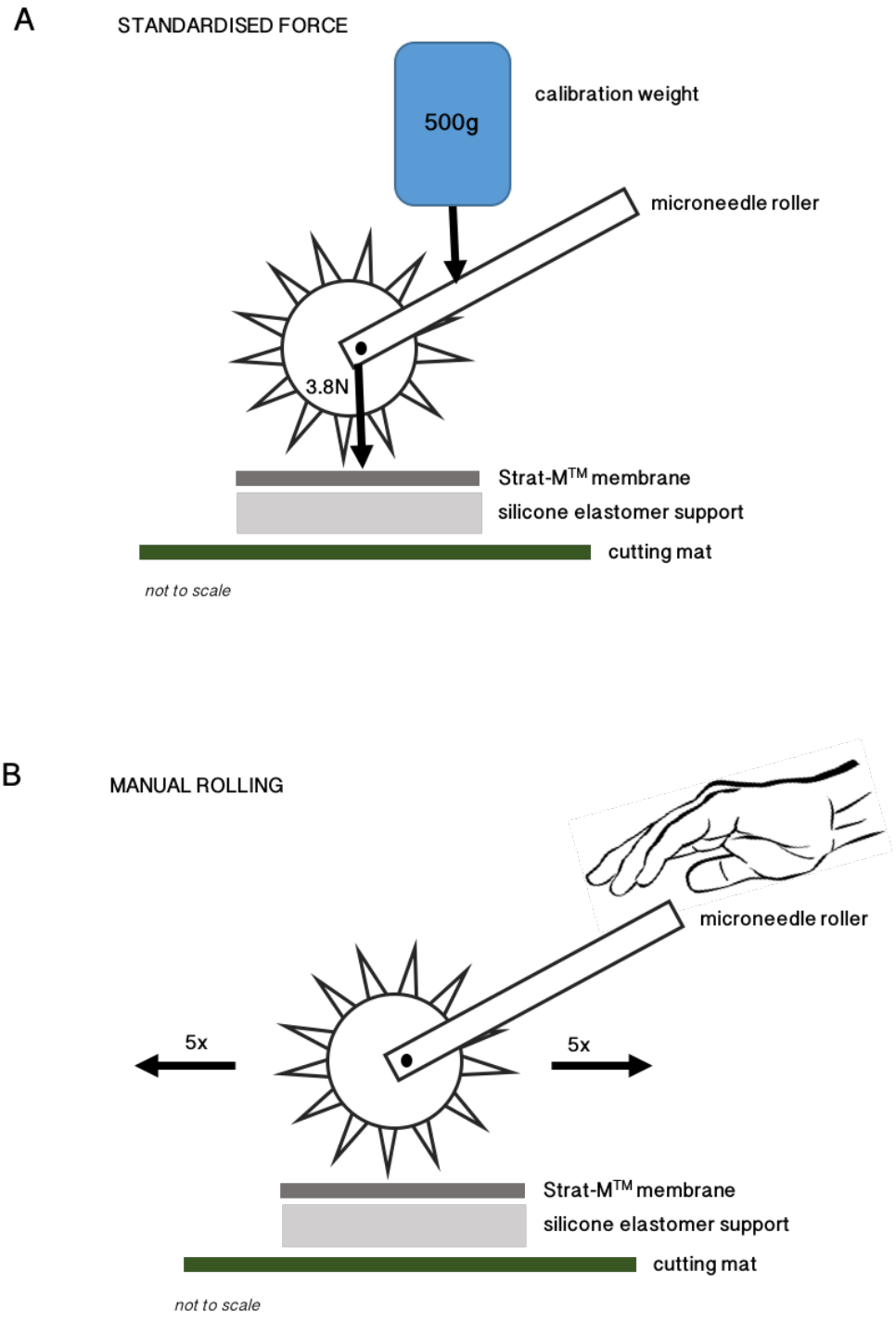

Figure 2.5 — Schematic representation of the two methods of microneedle application onto the Strat-M™ membrane: (A) Static impact insertion of the microneedle roller using a standardised downward force of 3.8N. **(B)** Manual rolling of the microneedle system.

2.2.4 Scanning electron microscopy of Strat-M™ and microneedles (SEM)

Membranes, micropores and microneedles were imaged by scanning electron microscopy (SEM). Strat-M™ membranes were air dried and coated with gold-palladium (SEM coating unit E5000; Polaron Equipment Ltd., Hertfordshire, UK). Microneedle roller heads were dismantled before imaging. Samples were mounted onto metal blocks and placed under vacuum in a scanning electron microscope (XL-30 FEG SEM; Philips Electron Optics, Eindhoven, The Netherlands,). Images were analysed with the Java-based imaging software ImageJ® (National Institutes of Health [NIH], Maryland, USA). Micropore area was calculated using the 'polygon selections' tool to outline the perimeter of the pore and measure the internal area. For each microneedle length, six micropore areas were calculated. Micropores were also visualised by micro-computerised tomography.

2.2.5 Optical coherence tomography (OCT) of Strat-M™

Microneedles inserted into Strat-M™ membrane by applying a mass of 500 g (i.e. a downward force of 3.8N) were imaged using the Michelson Diagnostics EX1301 OCT (Michelson Diagnostics, Kent, UK). The 2D images were analysed in ImageJ®.

2.2.6 Permeation study using Franz diffusion cells

Strat-M™ membranes were cut into discs that overlapped with the edges of the Franz cell compartments to prevent leakage. Membranes were not pre-wetted as per manufacturer's instructions. Membranes were mounted between donor and receptor chambers of individual Franz cells using a horseshoe clamp. High vacuum silicone grease (VWR International, Lutterworth, UK) was applied between the compartments as a water-tight sealant. Temperature equilibrated receptor fluid, 0.01M PBS (NaCl 8 mg/ml, Na_2HPO_4 1.15 mg/ml, KH_2PO_4 0. 2 mg/ml, KCl 0.2 mg/ml; pH 7.4), was sonicated to remove air bubbles that could reduce the surface area of permeation.

Receptor fluid (3 ml) was added to the receptor compartment *via* the sampling arm using a 5 ml syringe and long hypodermic needle (120 mm FineJect® needle, VWR International) ensuring no bubbles were introduced into the chamber; bubbles underneath the membrane would reduce the total area of permeation. A Teflon-coated magnetic stirrer (VWR International) was then added into the receptor compartment. Cells were placed in a temperature-regulated water bath on top of a water-resistant magnetic stirring plate (Thermo Fisher Scientific, Loughborough, UK) and stirred at 400 rpm to maintain receptor solution homogeneity. Distilled water was added to submerge the receptor chamber below the level of

the membrane. The water bath was maintained at 32°C, human skin surface temperature, and an electronic thermometer used to monitor the temperature.

There are two main methods used to investigate drug permeation through membranes: infinite and finite dosing. Infinite dose conditions are achieved when the applied dose of the donor drug formulation is so large that it is essentially unlimited. In this way, drug permeation through the membrane is not restricted by its concentration. This method is used to determine absolute pharmacokinetic parameters and was used in this study for this very reason. This is in comparison to finite dose conditions where a set dosage (i.e. a limited amount of donor formulation) would be applied to the membrane. This is done to mimic the dosages that would be used during real-world *in vivo* application and to monitor the resultant drug permeation properties at that dose[228].

Conditions for infinite dose permeation were met by using a concentration of doxycycline hyclate at 10% of its solubility limit (50 mg/ml) deliverable to the receptor compartment. Doxycycline hyclate solution (10 mg/ml) was made by dissolving 30 mg of doxycycline hyclate powder (Alfa Aesar, Massachusetts, USA) in 3 ml of PBS (pH 7.4) and was pipetted into the donor compartment. Donor and receptor cell compartments were covered with Parafilm™ (Sigma-Aldrich, Poole, UK) to prevent water loss through transpiration. Samples of receptor fluid (200 µl) were taken at pre-determined time intervals — every 10 minutes for the first hour then every hour for the first five hours, and at 24 hours — *via* the sampling arm using a 1 ml syringe and a long needle (120 mm FineJect® Needle; VWR International). Samples were transferred to 1 ml Chromacol™ vials (Thermo Fisher Scientific), wrapped in foil to protect the solutions from light and stored at 4°C for later high-performance liquid chromatography (HPLC) analysis. Temperature-equilibrated PBS was immediately added back into the receptor compartment to replace the volume removed with the sample. This was carried out to maintain thermodynamic equilibrium by keeping the total volume of fluid in the receptor compartment constant.

2.2.7 High-performance liquid chromatography (HPLC) method

An isocratic method for detecting doxycycline hyclate dissolved in aqueous solutions was developed on a modular HPLC system (Agilent HPLC 1200 series; Agilent Technologies, Chesire, UK) using a 15 cm x 4.6 nm, 5 µm, RP-amide column (Sulpeco Analytical, Poole, UK). The mobile phase consisted of 75% (v/v) di-iodinated water (with 0.1% [v/v] trifluoroacetic acid) and 25% (v/v) HPLC-grade acetonitrile (Sigma-Aldrich). System parameters were set with a pump flow-rate of 1.0 ml/min, a sample injection volume of 10 ml, a method stop-time of 10 minutes and a detection wavelength of 273 nm. This method produced

a chromatogram with a major analyte peak corresponding to doxycycline at 6 minutes. A calibration curve was created from serial dilutions of doxycycline solution. This was used to calculate doxycycline concentration from solutions of unknown concentration using the area under the chromatogram peak.

2.2.8 *Ex vivo* human skin

Surgically excised human abdominal skin was obtained from Biopedric International (Saint Grégoire, France). The skin provided contained no stretch marks and had had the adipose tissue removed. Skin was stored at -80^{o}C and used within three months of receipt. Prior to experiments, the skin was thawed for 15 minutes at room temperature in aluminium foil (to prevent dehydration) until soft and flexible. Skin samples measuring approximately 1 cm^2 in area were cut using a surgical scalpel. The skin surface was carefully wiped with cotton buds that had been wetted in sterile PBS buffer.

2.2.9 Perforation of human skin with microneedle rollers

A skin section of 1 cm x 1 cm was transferred onto a cork support where it was fixed into place using hypodermic needles in each corner. Full thickness skin has a strong tendency to shrink once cut, so the needles were placed in such a way that the skin was stretched back to its original size with great care taken to avoid over-stretching. The section was then transferred into 2% glutaraldehyde and fixed for 3 hours at 4^{o}C. The skin was then washed with sterile PBS buffer using a Pasteur pipette to remove the fixative. It was then placed onto a cutting mat and the microneedle roller was placed on top. The microneedle handle was secured with tack and a 500g weight added onto the roller head for 30 seconds. The weight and roller were then removed and the skin transferred back into fresh 2% glutaraldehyde solution for a further 3 hours.

2.2.10 Skin sample preparation for SEM imaging

Samples were dehydrated in graded ethanol solutions of 20, 50, 70 and 90% for 10 minutes each and then 100% ethanol three times for 10 minutes. They were then critically point dried with ≥99% hexmethyldisiazine (HMDS; Sigma-Aldrich) for 5 minutes and sputter-coated with gold-palladium (SEM coating unit E500; Polaron Equipment Ltd.). Samples were mounted onto metal stubs and imaged by SEM (XL-30 FEG SEM; Philips Electron Optics).

2.2.11 Statistical analyses

For each condition there were four replicates (unless otherwise stated) to allow for experimental variation. Where appropriate, data were analysed using a one-way or two-way analysis of variance (ANOVA) with Tukey correction for multiple comparisons. For averages, results are presented as mean ± standard error of the mean. In all instances, $p < 0.05$ denotes a statistically significant difference.

2.3 Results

2.3.1 Strat-M™ membrane structure

Strat-M™ membrane thickness was measured as 300 (± 2.7) µm by SEM analysis. Cross-sectional SEM images showed that Strat-M™ had two main architectural layers — a lipophilic smooth top-most layer that became increasingly porous and had a layer thickness of 108 (± 2.8) µm and a large highly porous bottom layer made up of bundles of thick synthetic fibres with a layer thickness of 192 (± 5.8) µm (**Figure 2.8 – A**).

2.3.2 Microneedle ultrastructure

The ultrastructure of the microneedle tips and shafts of the roller systems were visualised using SEM (**Figure 2.6 – A**–**E**). Two ridges were observed down both sides of the microneedle shafts which joined adjacent needles (**Figure 2.6 – B**). The tips were of an atypical shape for microneedle systems, with two sharp points at the edges and a peak in the centre creating a diamond (**Figure 2.6 – E**). This was reflected in the shape of the micropores.

2.3.3 Micropore area in Strat-M™

Micropores created with all three microneedle lengths were visible by light microscopy. Maximum contact area with the membrane was nine microneedles per row along the x axis, four microneedles per row along the y axis when force was applied perpendicularly and infinite microneedles along the y axis when rolled. SEM allowed the morphology of the micropores created in the Strat-M™ to be examined in greater detail. Due to the tip shape of the microneedles the pores had an atypical modified diamond shape (**Figure 2.7**). Average micropore areas for static impact insertion with standardised force were 11200 (± 1400) μm^2, 14600 (± 2700) μm^2 and 17100 (± 3000) μm^2 for 250, 500 and 750 µm microneedle lengths, respectively (**Figure 2.9 – C**). Though pore size increased with increasing microneedle length, a statistically significant difference in micropore area was only observed between the 250 and

750 µm microneedles ($p < 0.001$) and not between the 250 and 500 µm or 500 and 750 µm microneedles.

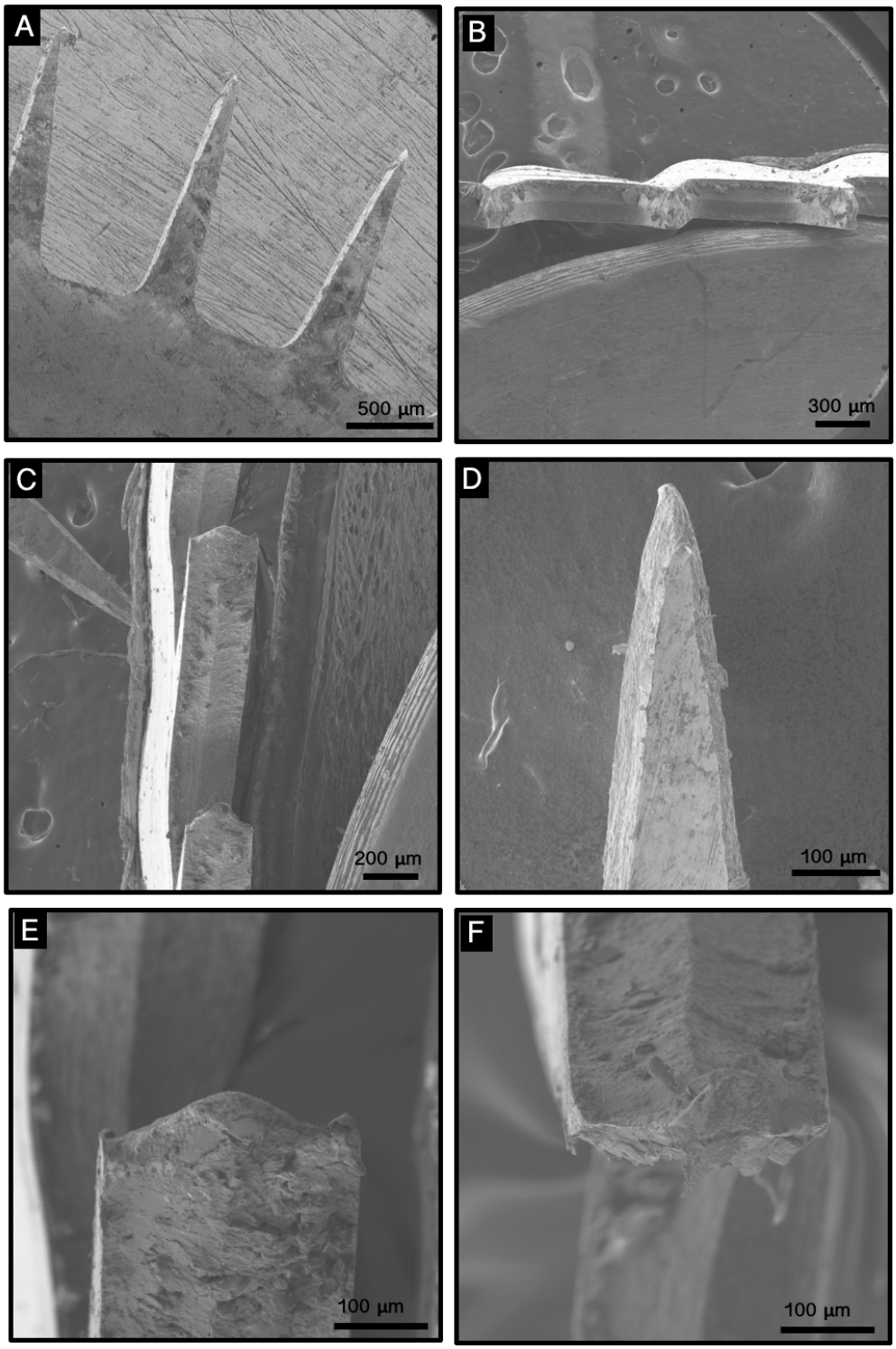

Figure 2.6 — Scanning electron micrographs showing the ultrastructure of the tip and shaft of the 500 µm microneedles, imaged from different angles. The shafts of the microneedles had two ridges on the sides joining adjacent microneedles.

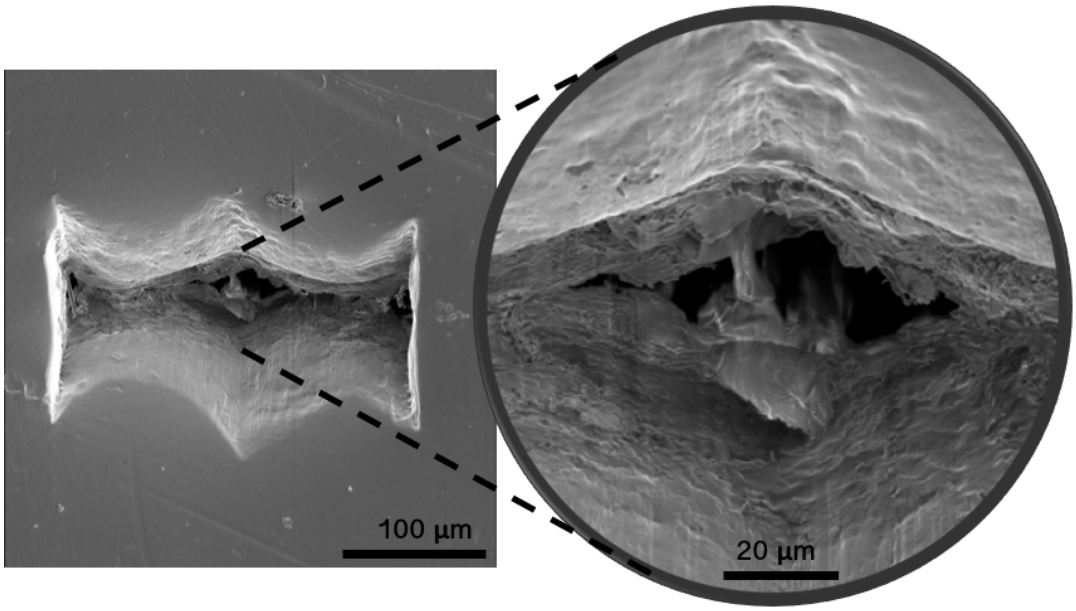

Figure 2.7 — Scanning electron micrograph showing the micropore created in the Strat-M™ apical surface after rolling with a microneedle roller with a microneedle length of 500 µm.

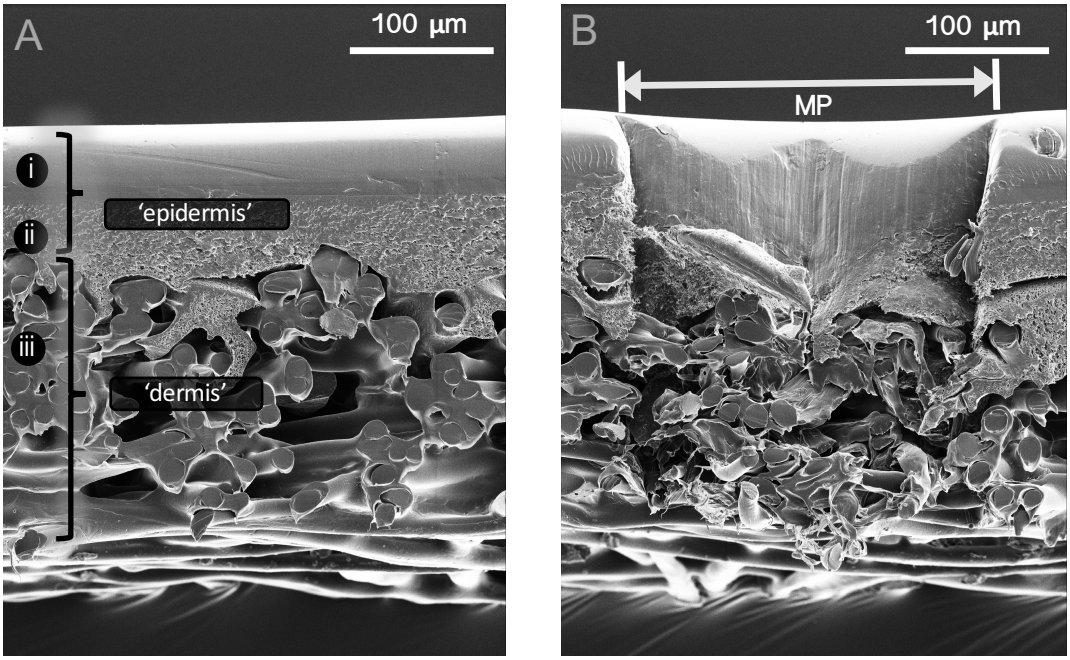

Figure 2.8 — Cross-sectional scanning electron micrographs of Strat-M™ membrane: (A) Untreated Strat-M™ showing its three major architectural layer, which mimic the human epidermis (i-ii) and dermis (iii), respectively**. (B)** Strat-M™ membrane after application with a 500 µm microneedle roller which had created a micropore [MP]. The membrane structure was disrupted by this process.

Table 3 — Effect of microneedle length of the roller systems on micropore area, depth of penetration and drug diffusion in Strat-M™.

	Microneedle shaft length		
	250 µm	500 µm	750 µm
Micropore area in Strat-M™			
500g mass (μm^2)	11190 ± 1358	14580 ± 2685	17100 ± 3012
Manual rolling (μm^2)	26768 ± 1432	29627 ± 1502	36146 ± 1502
Depth penetration in Strat-M™			
Needle tip protrusion (µm)	–	80	170
Unpenetrated needle length (µm)	–	120	280
Drug diffusion parameters			
Mean cumulative drug conc. after 1 h ($mgml^{-1}$)	0.8	1.6	2.2
Mean rate of drug permeation ($mgml^{-1}min^{-1}$)	0.88	1.53	2.3

Results are presented as mean ± standard error of the mean.

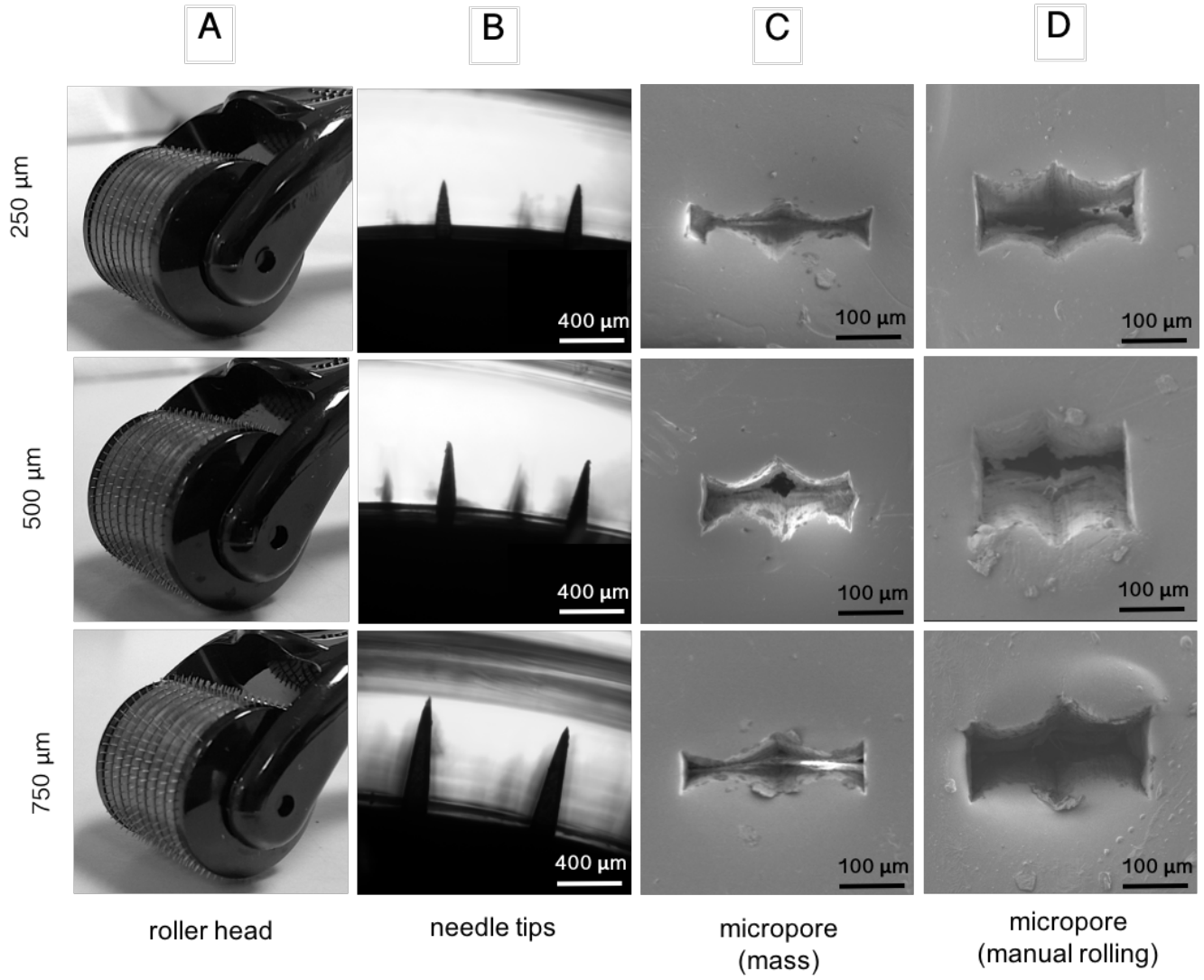

Figure 2.9 — Comparison of 250, 500 and 750 µm microneedle lengths: (A) Digital photographs of the head portion of the roller system containing the microneedles**. (B)** Light microscopy images of the microneedle tips. **(C)** SEM images of micropores in Strat-M^{TM} membrane after application of a 500 g mass onto microneedle rollers providing a downward force of 3.8N. **(D)** SEM images of micropores in Strat-M^{TM} membrane after the bidirectional rolling application method with the microneedle rollers.

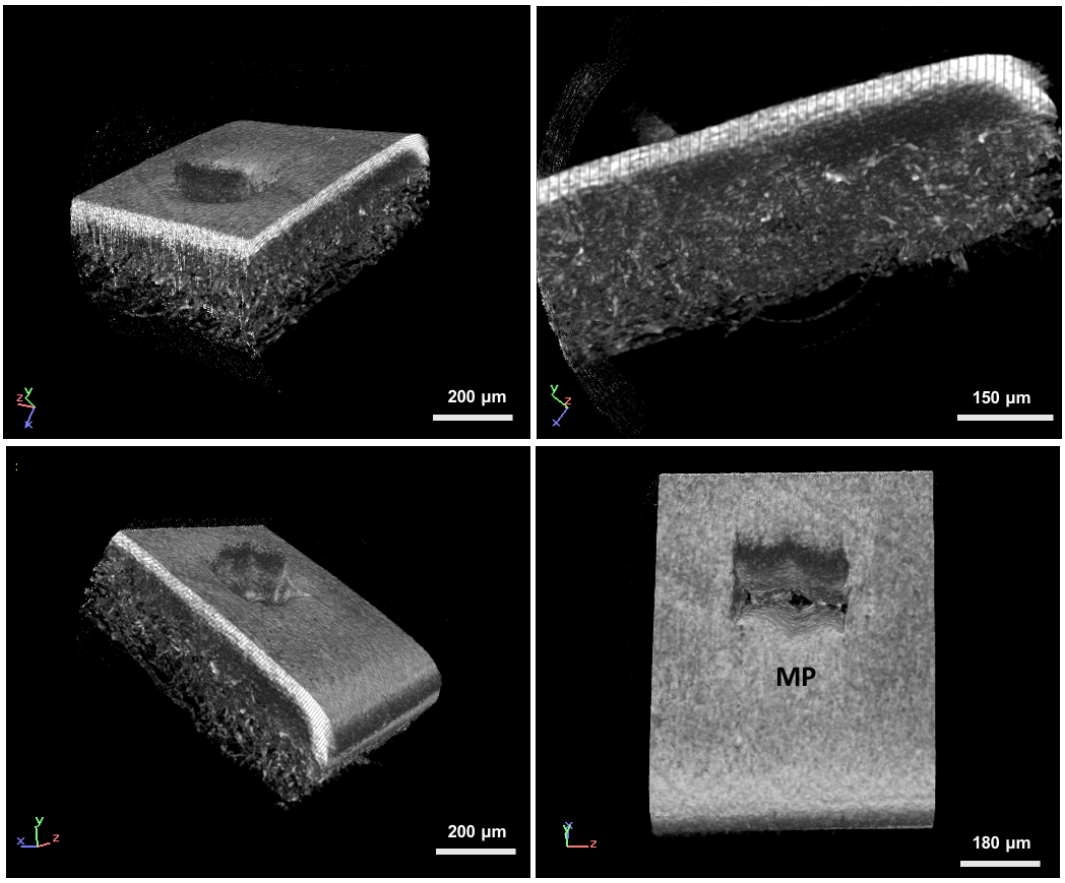

Figure 2.10 — Micro-CT images of a micropore created by manual rolling of the microneedle roller system (500 µm) against the apical surface of Strat-M™ membrane.

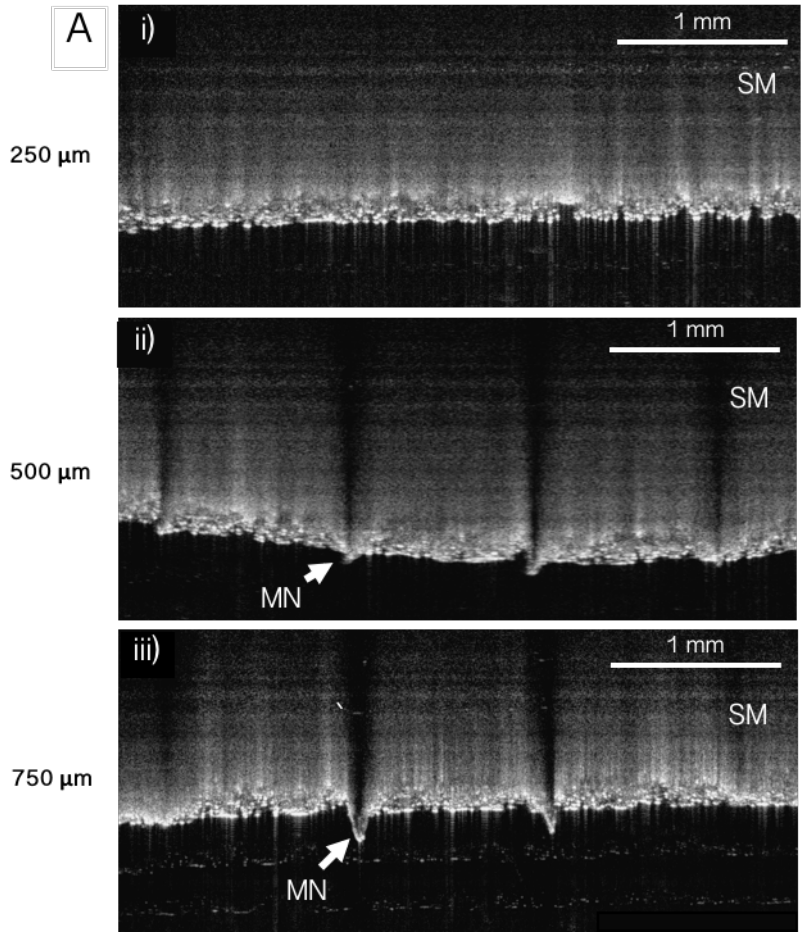

Figure 2.11 — OCT images of the depth penetration of microneedle rollers [MN] in the Strat-M™ membrane [SM]. The 500 µm and 750 µm microneedle rollers penetrate the full-thickness Strat-M™ membrane and protrude from the membrane's basal surface**.** The 250 µm microneedles did not penetrate the basal surface of the membrane. Artefacts are caused by the light casting shadows beyond the microneedle tips.

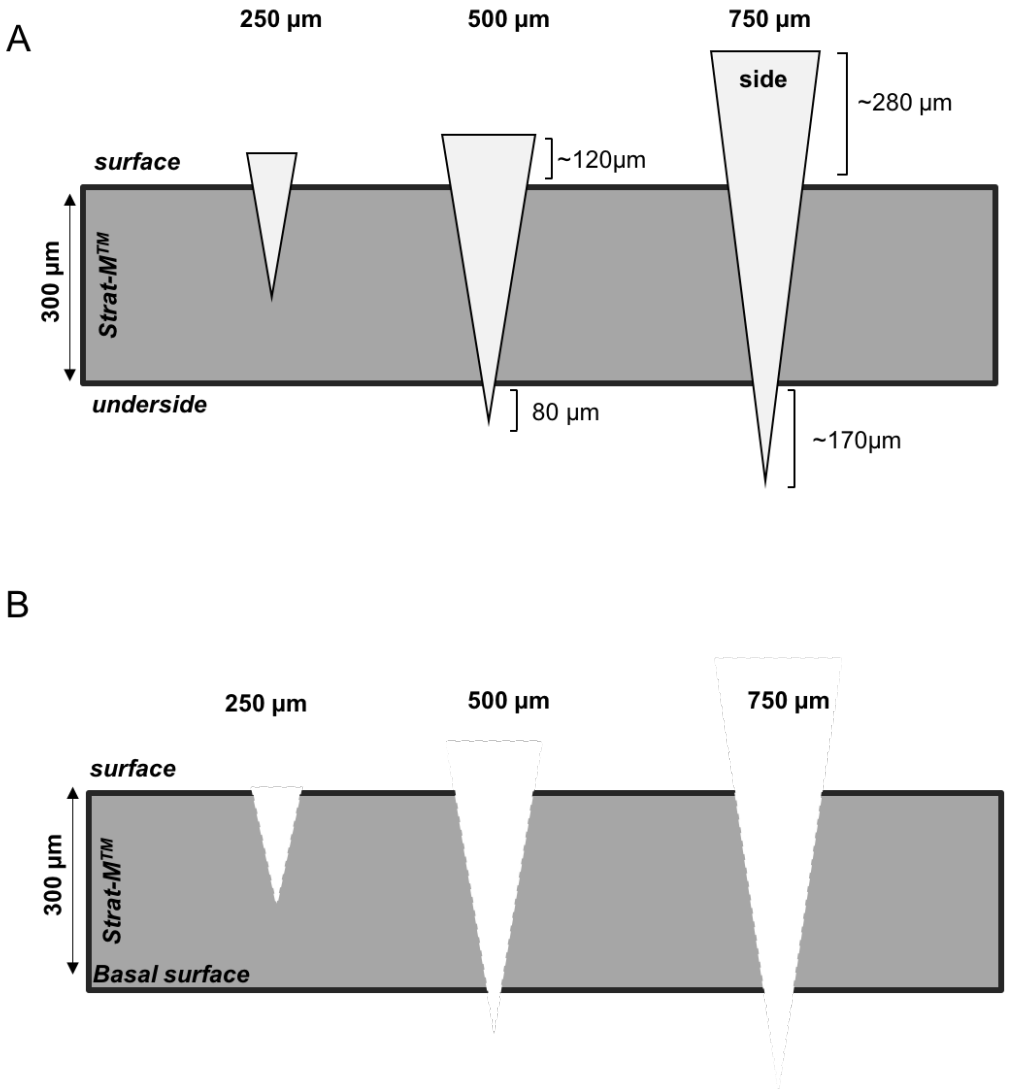

Figure 2.12 — Schematic representation of micropore insertion into the apical surface of the Strat-M™ membrane: (A) Microneedle depth penetration while inserted, as determined from the OCT images. **(B)** Micropores created within the Strat-M™ membrane.

2.3.4 Depth penetration of inserted microneedles in Strat-M™

Depth penetration of the roller tips was investigated using OCT and was used to assess which skin layer the microneedles could theoretically reach. The tomographic images show that the 500 and 750 µm length microneedles completely penetrated the 300 µm-thick Strat-M™ (**Figure 2.9**). The 750 µm microneedles protruded further than the 500 µm microneedles with 170 µm tip protrusion compared with 80 µm, suggesting that 750 µm rollers would reach deeper in full-thickness skin. The 250 µm microneedles were shown to enter the Strat-M™ but to not fully penetrate the membrane.

2.3.5 Manual rolling versus standardised force application

Force was applied to the microneedle rollers in two ways, through manual rolling in a single plane and through application of a 500g mass onto the roller handle. Application of a constant mass is a more standardised way of delivering force to the microneedles in order to penetrate the membrane. However, a more realistic clinical application of the microneedles is to roll them onto the skin by hand. The range of force applied by manual rolling by a single operator was measured as being 2.8-7.8N, while the standardised force was 3.8N. Manual rolling was shown to disrupt the membrane significantly more than a single weighted application demonstrated by greater average micropore areas which were 26800 (± 1400), 29600 (± 1500) and 36100 (±2700) μm^2 corresponding to an average increase in area of 141, 103 and 110% for the 250, 500 and 750 µm microneedle lengths respectively (**Figure 2.9 – D**). Additionally, it was observed under SEM that the manual rolling caused greater damage to the microneedle tip than the standardised force application. Though not all tips were damaged by the application process, those that were more blunted by the rolling than the weighted application (**Figure 2.13**).

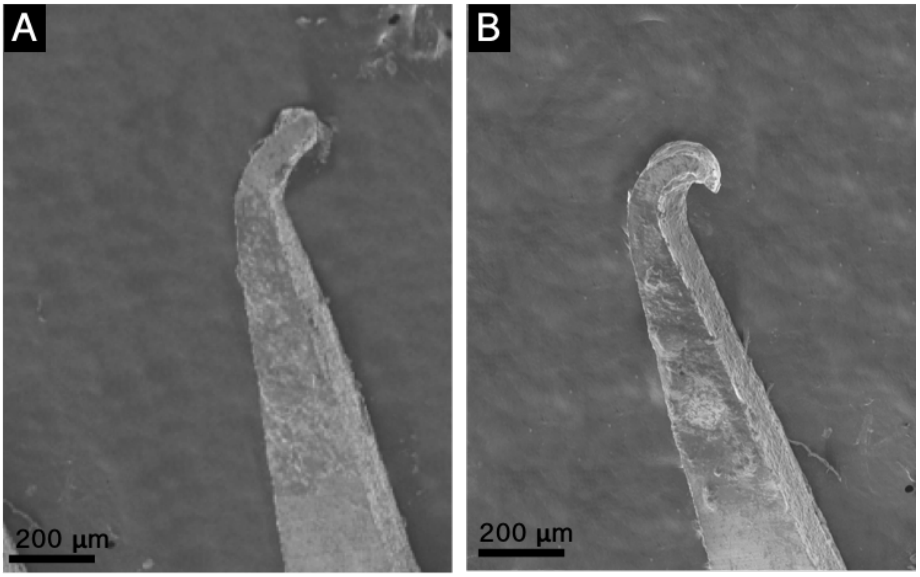

Figure 2.13 — Scanning electron micrographs of the 500 µm microneedles after application onto the Strat-M™ membrane: (A) Microneedle tip after standardised force application of 3.8N. **(B)** Microneedle tip after manual rolling in a single plane five times in each direction.

2.3.6 Transmembrane delivery of doxycycline hyclate

In order to assess the ability of microneedle rollers to enhance intradermal doxycycline delivery, the permeation of doxycycline through untreated and microneedle-treated Strat-M™ was investigated. Disruption of the skin barrier normally results in an increased permeation of small molecules that are already able to traverse the epidermis and allows the transit of larger molecules whose permeation would otherwise be prevented. Microneedles achieve barrier disruption by creating micropores that act as aqueous conduits for drugs to permeate through. Cumulative doxycycline concentration was monitored in the receptor fluid over 24 hours. No doxycycline was detectable in the receptor fluid of untreated membranes, indicating that Strat-M™ alone inhibited doxycycline permeation (**. – A**). Conversely, doxycycline was detectable in the receptor fluid in membranes treated with all microneedle lengths after 10 minutes. Lag time, the time taken for the doxycycline to achieve steady state flux through the membrane, was one hour across all microneedle lengths. Differences in cumulative permeated drug concentration were statistically significant between all microneedle lengths, with 750 µm treated membranes having the greatest rate of drug permeation and 250 µm treated membranes the least. Total doxycycline permeation at steady state flux was 0.8, 1.6 and 2.2 mg/ml and rate of doxycycline permeation during lag time was 0.88, 1.53 and 2.30 mg/ml/min for 250, 500 and 750 µm microneedle lengths respectively (**. – B**). Dose depletion of doxycycline was exhibited up to 24 hours.

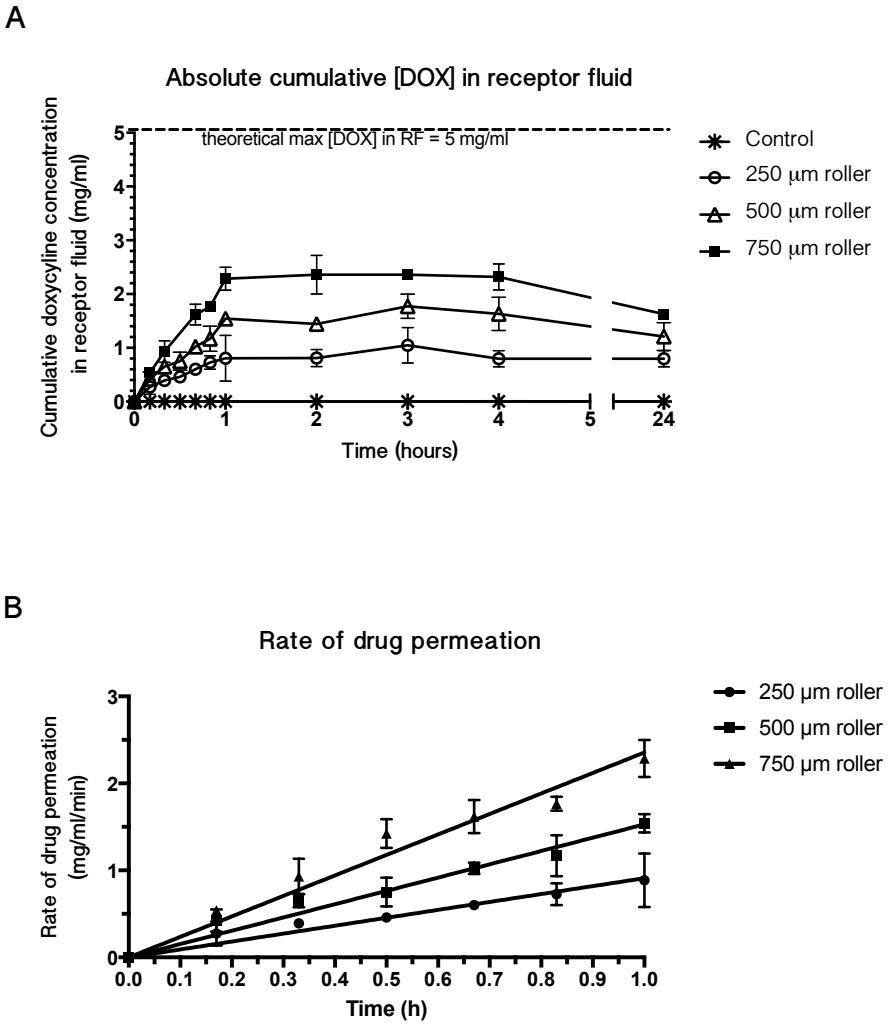

Figure 2.14 — Effect of microneedle application on doxycycline permeation through Strat-M^{TM} membrane (n = 4): (A) Cumulative concentration of doxycycline in receptor compartment fluid after treatment with 250, 500 and 750 µm microneedle lengths. **(B)** Rate of drug permeation from linear regression of cumulative doxycycline concentration during the 1 hour lag period. 'Control' represents the membrane samples which had not been treated with the rollers. *Error bars represent the standard error of the mean.*

2.3.7 Doxycycline retention in and on the Strat-M™ membrane

SEM images and membrane mass measurements indicate that doxycycline was retained within and on the Strat-M™ membrane. Doxycycline crystals were observed partially and completely occluding micropores as well as on the membrane surface (**Figure 2.16 – A**). Mass measurements show that even after desiccation, to account for post-experimental wet mass, there was a statistically significant increase in membrane mass for both treated and untreated membranes (**Figure 2.17**). Doxycycline crystals on the membrane surface were also observable by eye. The total theoretical doxycycline concentration deliverable to the receptor fluid was 5 mg/ml (half of that in the donor fluid), but the maximum concentration reached was 2.2 mg/ml which was through Strat-M™ treated with the 750 µm rollers (**. – A**), indicating drug retention.

.

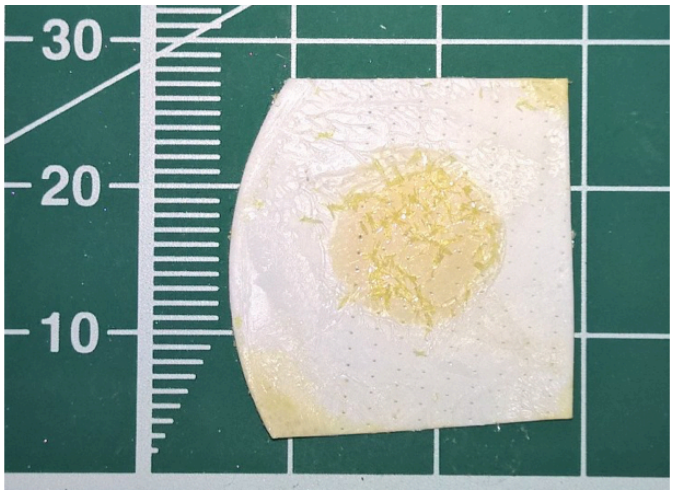

Figure 2.15 — Photograph of yellow crystals that precipitated on the apical surface of the Strat-M™ membrane during the permeation study. Crystals were present on the hydrated tissues and were not a result of drying processes.

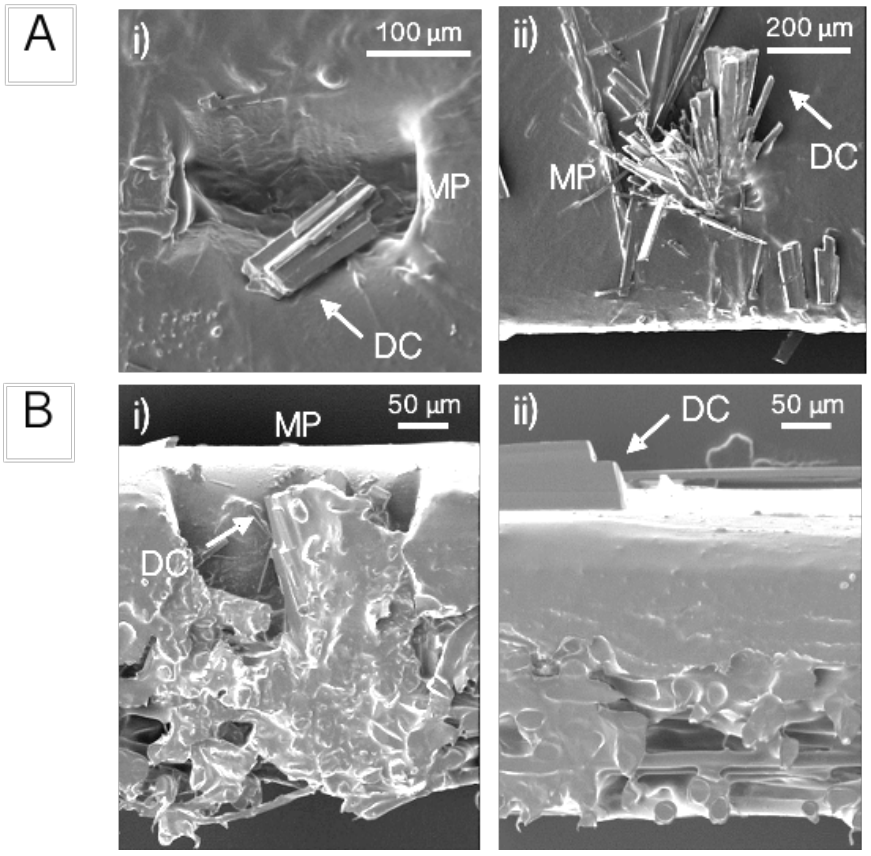

Figure 2.16 — Scanning electron micrographs of doxycycline crystals retained in and on the Strat-M™ membrane: (A) Doxycycline crystals [DC] partially and completely occluding micropores [MP] in Strat-M™ membrane treated with 500 µm rollers. **(B)** Cross-sectional view of micropore occlusion with doxycycline and crystal formation on the membrane surface.

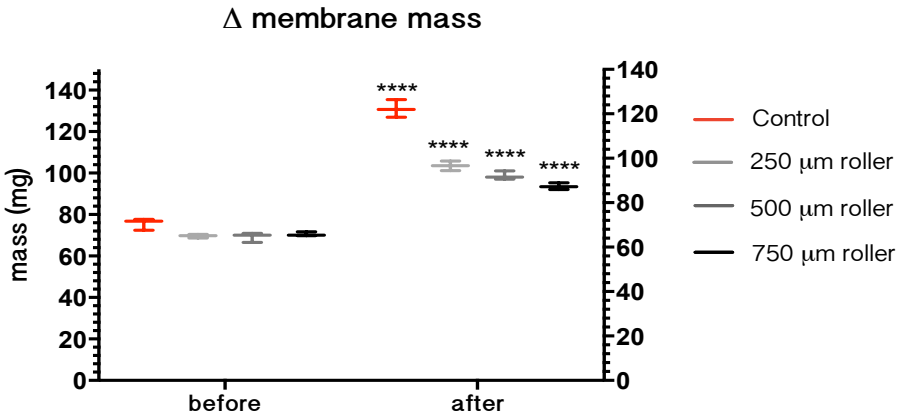

Figure 2.17 — Box and whisker plot comparing the dry mass of the Strat-M™ membrane before the permeation study ['before'] with the mass of the same membrane after the permeation study and post-desiccation ['after'] (n = 4). 'Control' represents the membrane samples which had not been treated with microneedles. The statistical significance shown compares the mass of the same membrane before and after the permeation study. *Error bars represent the standard error of the mean*; **** = $p < 0.0001$.

2.3.8 Microneedling on human skin compared with Strat-M™

Micropores were created on the apical surface of the excised human skin using the microneedle roller systems applied with a standardised static force of 3.8N. The micropores were then visualised by SEM. It was immediately evident that the skin surface greatly differed from that of the synthetic Strat-M™ membrane (**Figure 2.18**). The human skin was covered in striations, pits and grooves with evidence of dead skin sloughing off. There were also several vellus hairs and hair follicles. None of these natural structures were mimicked in the Strat-M™ which had a much smoother, more uniform apical surface. Furthermore, in comparison with micropores created in the Strat-M™, there were fewer micropores distinguishable on the excised human tissue especially since they were less easily demarcated from other structures on the skin surface. When comparing micropore entry area created in the human skin with the those created in the Strat-M, those in the human skin were significantly smaller ($p < 0.001$) across all microneedle lengths (**Figure 2.19**). The 250, 500 and 750 µm microneedles created micropores of 3350 (± 335) µm^2, 5531 (± 695) µm^2 and 8282 (± 1002) µm^2 respectively in the human skin. Consistent with what was observed in the micropores created in the Strat-M™, there was a statistically significant difference in micropore area between the 250 and 750 µm microneedles, but not between the 250 and 500 µm or 500 and 750 µm microneedles.

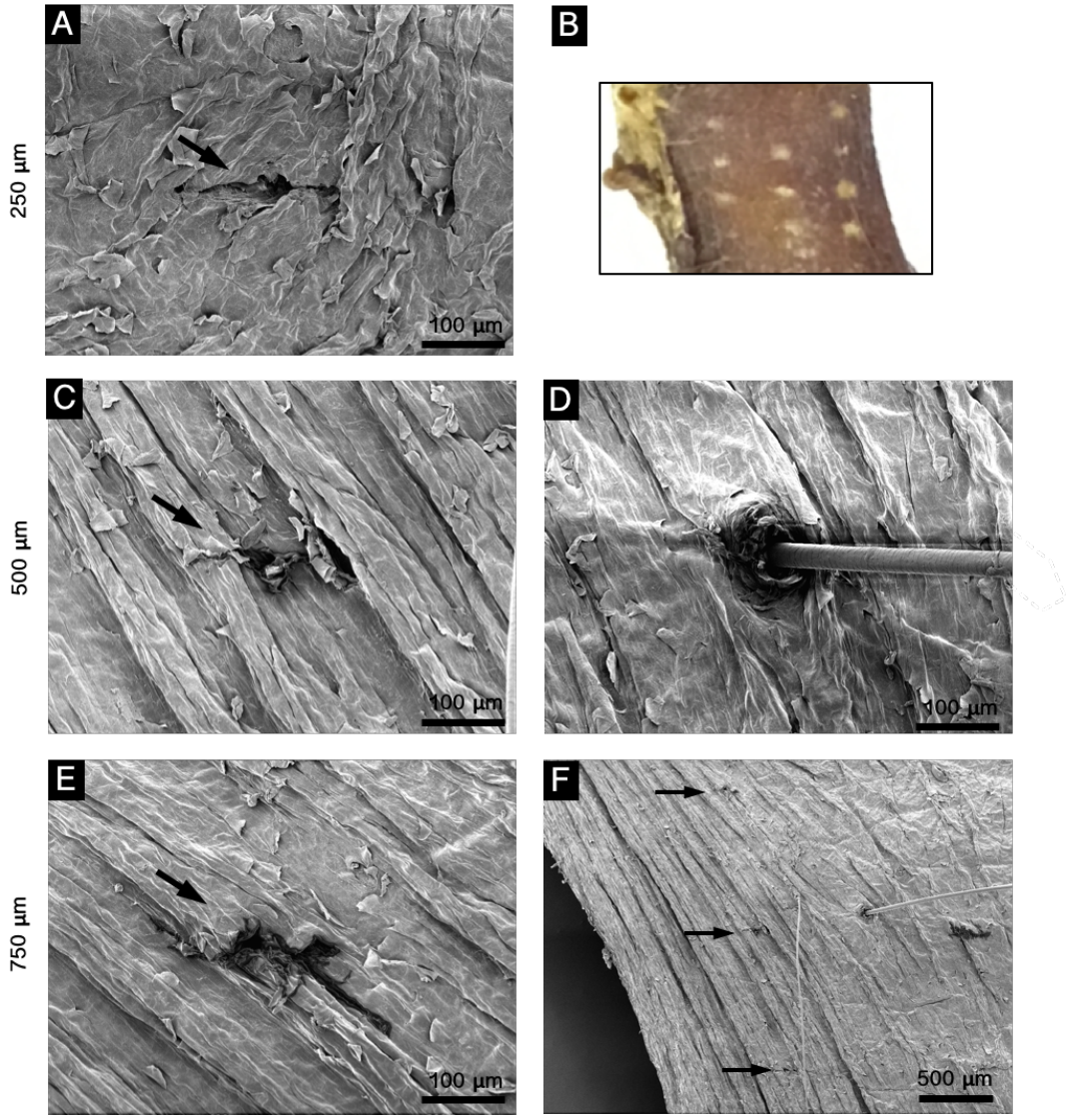

Figure 2.18 — Scanning electron micrographs of micropores created in the apical surface of excised human skin by the microneedle roller systems: (A) Micropore created by a 250 µm microneedle. **(B)** Photograph of a critically point dried and sputtered-coated skin section with micropores created by 500 µm microneedles. **(C)** Micropore created by a 500 µm microneedles. **(D)** A hair follicle containing a hair — a structure which was distinguishable from the micropores **(E)** Micropore created by a 750 µm microneedles. **(F)** A series of micropores created in the skin from a row of 500 µm microneedles.

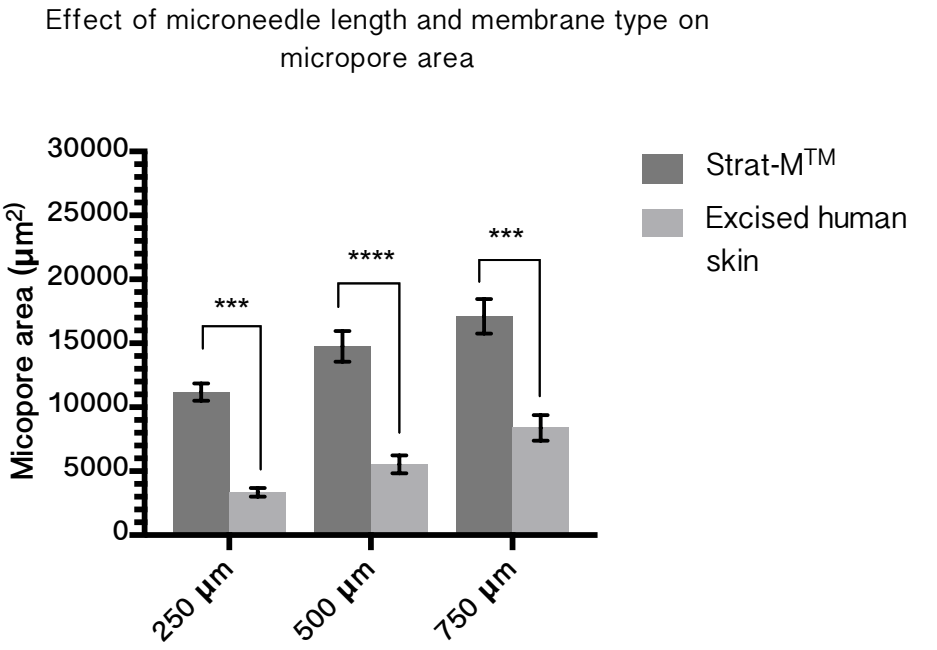

Figure 2.19 — Comparison between micropore areas created in the Strat-M™ and excised human skin by the microneedle roller systems (250, 500 and 750 µm microneedle lengths) (n = 6). A statistically significant difference in micropore area created by the 250, 500 and 750 µm was observed between Strat-M™ membrane and excised human skin. *Error bars represent the standard error of the mean*; *** = $p < 0.001$, **** = $p < 0.0001$.

2.4 Discussion

Doxycycline has multiple attributes which make it a potentially effective treatment for chronic wounds. It not only exhibits MMP inhibitory activity independent of its antibiotic action, but is already FDA-approved for the treatment of ulcers and has several pharmacokinetic advantages over its tetracycline counterparts[138]. The skin offers a large surface area for precise localised drug delivery. However, for intradermal delivery, doxycycline is too large and hydrophilic to passively diffuse across the skin since the acellular keratinised SC is such an efficient barrier against absorption of large exogenous molecules. In this study an *in vitro* model of the skin barrier was investigated using the synthetic membrane Strat-M™, to determine the feasibility of delivering doxycycline intradermally using commercially available microneedle rollers.

2.4.1 Microneedle and micropore ultrastructure

The solid microneedle roller systems used in this study were formed of multiple discs containing microneedles made of titanium. Solid microneedles are typically made of metals including stainless steel, titanium and nickel-iron[160], but are also known to be synthesised from natural polymers[229], plastics and ceramics[230]. This would undoubtedly influence the microneedle's rigidity, durability and minimum impact insertion force. The microneedles used in these experiments had a different geometry to those typically investigated elsewhere in the literature. Firstly the shaft, which had two lateral ridges up to the tip, resulted in an atypical micropore shape (**.**). Microneedles are typically cone-shaped, pyramidal or polygonal and create more circular micropores than what was observed with the SodaCoda^{TM} system (**Figure 2.21)**. Though it has yet to be thoroughly investigated here, or in the published literature, the significance of micropore shape is that it may influence fluid flow, drug crystallisation and precipitation, and pore closure (especially in dynamic tissue). This would impact on several pharmacokinetic parameters including drug delivery rates, however further studies would need to be carried out to assess this.

2.4.2 Strat-M^{TM} as an acellular synthetic epidermal mimetic

Excised animal tissue and other skin substitutes have been widely used to model human skin. No skin model is without its limitations, however, and all models represent the skin in isolation from a fully functioning biological system which must be taken into account before extrapolating results to living organisms. Inevitably human skin provides the best model, but alternative membranes can be used to provide useful data while still being cognisant of their limitations. An important criticism of the Strat-M^{TM} membrane as a skin mimetic is the lack of a dynamic response to mechanical penetration enhancement which is a behaviour exhibited in human skin. It has been widely documented that pore closure is observed in excised human skin that has been treated with microneedles[231]. This process is aided by elastic recoil in the collagenised dermis[231]. This is an important physiological mechanic *in vivo* and is a necessary response of the skin to reduce the risk of infection and prevent water loss by reinstating the skin barrier. Strat-M^{TM} fails to respond to these stimuli which would otherwise have a huge impact on skin permeability as resealing kinetics ultimately reduces drug permeation over time. Furthermore, drying methods (dehydration and desiccation) during sample preparation did not have an effect on the micropores in Strat-M^{TM} but had a huge effect on the excised skin causing tissue shrinkage, collapsing of surface structures and pore closure.

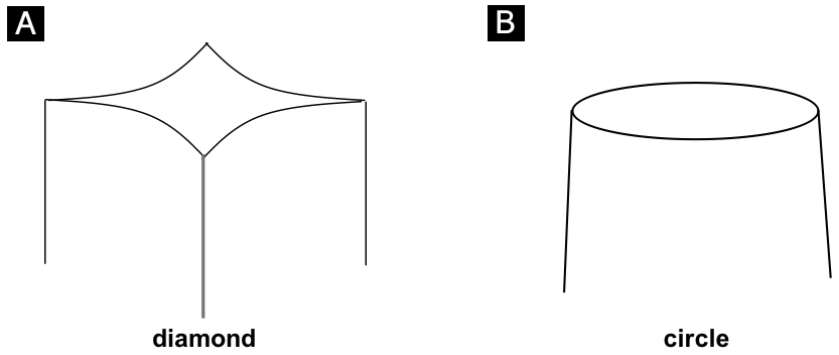

Figure 2.20 — Schematic representation of a cross-section through the shafts of microneedles with different geometries: (A) The suppliers of the microneedle rollers used in this study claimed that the microneedles had a diamond-shaped shaft. This was corroborated by SEM image analysis. **(B)** Microneedle rollers typically have a circular shaft forming a cylindrical needle. Square pyramidal geometries are also commonly used.

Figure 2.21 — Micropores (*above*) created by cone and polygonal-shaped metal microneedles (*below*): (A) Adapted from "Microneedle-mediated intradermal delivery of 5-aminolevulinic acid: Potential for enhanced topical photodynamic therapy," by R. Donnelly *et al*., 2008, Journal of Controlled Resease, 129, pp. 156-157**. (B)** Adapted from "Transdermal delivery of insulin using microneedle rollers in vivo," by C. Zhou *et al*., 2010, International Journal of Pharmaceutics, 392, pp. 128, 130. **(C)** Adapted from "Skin penetration enhancement by a microneedle device (Dermaroller®) *in vitro*: Dependency on needle size and applied formulation" by M.M. Badrana, J. Kuntschea and A. Fahr, 2009, European Journal of Pharmaceutical Sciences, 36, pp. 513, 516.

The permeation properties of Strat-M™ in comparison to human skin have been previously investigated by Uchida *et al.* (2015)[232]. Their study concluded that the diffusion and partition parameters of chemicals between 152–289 Da in Strat-M™ were in good concordance with those seen in excised human skin. However, the molecules investigated were well below the theorised 500 Da molecular weight threshold for passive drug diffusion through healthy human skin and the authors did not explore penetration enhancement of the membrane. Similar studies have compared Strat-M™ to other membranes[233,234], but none have looked at the effect of microneedling on Strat-M™. Doxycycline hyclate has a molecular weight of 1028.56 kDa and will theoretically not naturally diffuse across the human skin. It was observed in this study that native Strat-M™ was also impermeable to doxycycline hyclate solution. Permeabilistion of the apical surface of the Strat-M™ by microneedle application resulted in the creation of micropores that greatly increased drug permeation through the membrane, identifying it as the rate-limiting step of transmembrane diffusion. However, these micropores had a significantly greater entry area than those created in the human skin with microneedles of the same length. This may be an effect of the harsh drying process on the human skin which causes the skin to shrivel and collapse as water is eliminated but may also be a result of the contractile behaviour of the elastic dermis which tends to recoil if the skin is not sufficiently stretched.

Structurally comparing Strat-M™ to human skin, the two membrane layers defined in this study could be considered analogous to two of the major skin layers, the epidermis (including the SC) and the upper portion of the dermis, in terms of layer thickness and porosity. Human skin begins as a tough thin keratinised layer which is highly lipophilic and becomes increasingly porous, fibrous and hydrophilic. This is mirrored in the Strat-M™. However, the surface topology of the Strat-M™ differs greatly from that of human skin. Strat-M™ exhibits a much smoother, more uniform surface while the human skin surface is filled with ridges, pits and hair follicles. These natural structures inevitably affect drug delivery since processes such as drug pooling and retention in the skin's natural contours will impact on its permeation. They also make it much more difficult to distinguish the micropores from other features on the skin. Additionally, resealing of the micropores and contraction of the skin *in vivo* is a biological behaviour that cannot be mimicked by the Strat-M™. In all, Strat-M™ bears many of the advantages and limitations of pre-existing synthetic membranes.

2.4.3 Microneedle application enhances transmembrane drug delivery in a length-dependent manner

The results presented here show that micropore area and depth of penetration into Strat-M™ membrane is determined by microneedle length. The longest microneedles investigated (750 μm) gave the largest micropore entry area and penetrated the Strat-M™ the deepest, followed

by the next longest (500 µm) and then the shortest (250 µm). Since Strat-M™ membrane is impermeable to doxycycline, micropore area afforded by the microneedles act as the sole conduits for its permeation. It follows that the longer the microneedles the larger the micropores, the greater the rate of doxycycline diffusion and the higher the cumulative concentration of doxycycline is in the receptor fluid. Though there were was an increase in micropore area between 250 and 500 µm, and 500 and 750 µm microneedle lengths, these differences were not statistically significant. Thus the significant difference in permeation between these microneedles lengths is most likely accounted for by the increase in depth penetration in addition to the greater micropore area. Studies comparing the effect of differing microneedle roller lengths have also shown a positive correlation between increasing microneedle length and increased drug permeation, Badran *et al.* (2009) between 150, 500 and 1500 µm needle lengths in their excised human skin model[235], and Hyeong *et al.* (2012) between 150, 250 and 500 µm needle lengths in their *in vivo* rat model of Rhodamine B permeation[236].

It is notable that the full lengths of the 500 and 750 µm microneedles did not penetrate the membrane since there was a residual portion of the shaft that never made contact with the membrane. There are several plausible explanations for this, including the inhibitory effect on penetration that neighbouring needles have on one another which prevents maximum depth penetration. This is referred to as the 'bed of nails' effect and confounds the effect of microneedle length on microneedle penetration[173,237,238]. Additionally, the rigid supporting surface underneath the Strat-M™ may interrupt full penetration in a situation where the microneedles are longer than the membrane. A greater force applied to the microneedles may be able to overcome these factors or may simply cause damage to the needle tips. To investigate the confounding effect of needle proximity on maximum needle penetration, a model using a single microneedle would be ideal to look at the effect of shaft length alone[239].

The most desirable microneedle length is the shortest that can deliver doxycycline to the dermal layer with optimal results. However, there is a fine balance between risk of pain and bleeding with the most efficient delivery. Microneedles up to 500 µm in height have been inserted painlessly in some human subjects while lengths up to 1000 µm have shown reduced pain sensation and intensity compared with hypodermic needles[9]. It appears that as well as with length there is a correlation between pain perception and needle diameter[240]. It is important to note that pain sensation and pain perception is highly subjective and may be confounded by those who are nervous of needles in general. Additionally, actual depth penetration is not easily determined by microneedle length, that is to say, a microneedle length of 750 µm does not equal a depth penetration of 750 µm due to the resistance of the material to needle insertion and the inhibitory effect on penetration by the neighbouring microneedles. Furthermore, whether there

is sufficient penetration of needles into dermis will depend on the target body region since SC thickness differs from body site to body site. For example, the heel, a site where several chronic wounds commonly develop, has a notably thicker SC than most body regions and microneedles evaluated on abdominal skin may not be of sufficient to length deliver drugs through heel skin.

2.4.4 Application method of the roller system influences micropore area

Rolling of the microneedles resulted in larger micropores compared with a single application of perpendicular force. Rolling involves shearing forces that disrupt the membrane along the y axis which perpendicular application of force does not. The extent of membrane disruption by manual rolling may be dependent on the number of rolls and the number of planes in which the microneedles are rolled in. In this study the microneedles were rolled bilaterally without removal of the microneedle from the membrane but other studies have used multilateral rolling which creates overlapping micropores[225,241]. Sung-Kyun *et al.* (2010) investigated the effect of the number of rolls in differing numbers of planes on drug permeation and concluded that increasing the number of rolls (from one to nine) increased the drug flux of L-ascorbic acid in their rat model[242]. This suggests that for 'poke and patch' TDD, rolling is a more efficient way of permeabilising skin than impact insertion of an array and that repeated rolls increases drug diffusion rates[235]. However, the force applied with manual rolling is inconsistent and will differ slightly with each application and between individuals, making valid comparisons across and within studies difficult. Furthermore, repeated rolling is likely to reduce the shelf-life of a microneedle roller making it less efficient or more painful by blunting the needle tips and increasing their diameter. It should be noted that, in general, direct comparisons between the work presented here and studies from the published literature are not possible due to substantial differences in: (i) the microneedles and membranes used, (ii) the application methods employed (including both application force and number and direction of rolls), and (iii) the drug being investigated, as a result of a current lack of standardised protocols amongst researchers.

2.4.5 Doxycycline solution is retained in the Stat-M^{TM} membrane in crystal form

A portion of the doxycycline solution was retained within and on the Strat-M^{TM} membrane. Unexpectedly doxycycline formed crystals on the membrane surface of untreated Strat-M^{TM} and also within micropores of microneedle-treated Strat-M^{TM}. These yellow crystals were visible in hydrated membranes immediately after the permeation study, confirming that the presence of crystals was not a result of the drying process. These crystals were also not seen when PBS only was applied onto the membrane. The reason for the crystallisation of doxycycline and its deposition on the membrane is unclear. The donor fluid concentration was a fifth of its solubility limit, so the solution was theoretically unsaturated. Molecules in solution

will crystallise when a nucleation point is reached and it is more energetically favourable to form and deposit crystals than remain dissolved[243].

It is possible that there is an interaction between the Strat-M™ surface and dissolved doxycycline molecules that stimulates this process. The presence of these crystals explains why the theoretical concentration of doxycycline in the receptor fluid is not reached; crystallisation of doxycycline inside micropores would limit further drug permeation and also reduces the available drug to diffuse. A solvent, such as methanol, could be used to improve doxycycline solubility. However, this is likely to interfere with the Strat-M™ structure and integrity, confounding its true permeation properties as it is structurally sensitive to such chemicals. In *in vivo* human skin, drug crystallisation may be overcome through the addition of solubilising agents to the drug. Moreover, concentrations of doxycycline hyclate administered by intradermal delivery would, in reality, be much lower than 10 mg/ml which was used to satisfy infinite dose conditions.

2.4.6 Durability of microneedle roller systems

The microneedle roller systems are commercially available in the public domain. The manufacturers state that they are suitable for repeated individual use. However, it was observed in this study that application of the rollers onto the Strat-M™ membrane resulted in blunting of some of the microneedle tips, most likely the microneedles that made initial contact with the membrane. Moreover, manual rolling caused more damage than application of a vertical standardised force. This suggests that, with repeated use, the microneedles' tips would become more blunted, reducing their efficacy. Further investigations would be needed to determine this however. Furthermore, though disinfection of the roller system is possible, given the nature of the disease that the target patient population typically have, single use would be best clinical practice for hygiene purposes.

2.5 Future work

2.5.1 Drug permeation and micropore resealing kinetics in excised human skin

Further comparisons between the Strat-M™ and membrane excised human skin should be made. For example, differences in microneedle depth penetration observable by OCT and diffusion rates measured by Franz cell permeation studies could be explored. Penetration studies using fluorescently-labelled drugs or dyes with a similar molecular weight to doxycycline could be carried out followed by histological analysis of the micropores created in human skin. Side-by-side comparisons of these sections could then be made with OCT images. The effect of solubilising agents on crystal formation and membrane/skin integrity would be

useful in determining the feasibility of delivering doxycycline *in vivo,* as crystal formation would be undesirable.

The resealing kinetics of micropores created in human skin could be investigated by imaging them at regular time intervals after initial needle application. This would give an indication of the time frame within which doxycycline could be delivered intradermally without the use of drugs to delay micropore closure. The rate of pore closure will be dependent on the elasticity of the skin (age, body site, hydration etc.) and the size of the initial pore created so these factors could also be explored. The effect of the number of microneedle applications and the effect of microneedle application in an increasing number of planes could be investigated along with the effect of different standardised forces on both micropore entry area and depth penetration, and on microneedle blunting.

2.5.2 Controlled-release and gel-based vehicular IDD of doxycycline

One of the next set of experiments of great interest is to investigate the delivery of doxycycline in different formulations. Preliminary experiments have already been carried out to assess controlled-release mechanisms of delivering doxycycline in place of simply adding doxycycline as an aqueous solution onto micropores. To date, these experiments have included: (i) application of a patch impregnated with doxycycline, (**Appendix B — Impregnating various wound dressings with doxycycline solution, *p.242***), (ii) doxycycline delivery in a Granugel vehicle and Atrigel vehicle (Atridox) of varying viscosities, and (iii) development of an *in situ* forming smart gel to be applied into the micropores (Appendix C — Development of an MMP-cleavable protein-based smart gel, ***p.243***).

2.6 Conclusion

The body of work carried out in this chapter has shown, for the first time, how microneedle roller systems are able to enhance the transmembrane delivery of doxycycline hyclate through Strat-M^{TM} membrane. Strat-M^{TM} acts as an effective barrier against the permeation of large molecules like doxycycline, making it a suitable skin mimetic to investigate mechanical penetration enhancement. However, several limitations should be kept in mind when making direct comparisons to human skin including the lack of a dynamic response to mechanical stimuli, specifically micropore closure. In this *in vitro* model increasing microneedle length increased micropore area, depth penetration and ultimately doxycycline permeation through the Strat-M^{TM}. Furthermore, manual rolling disrupted the membrane more than the downward application of a standardised force alone. Evidence of doxycycline retention in the membrane was attributed to interactions with the drug and the membrane surface. It can be concluded that

repurposed microneedle rollers are a promising tool in the treatment of early stage pressure ulcers and the next step is to monitor the biological effects of microneedle-mediated IDD of doxycycline.

Chapter 3 Microneedle-Enhanced Transmembrane Delivery of Doxycycline to a Dermal Tissue Equivalent

3.1 Introduction

Transmembrane delivery of doxycycline in an acellular static system, as outlined in Chapter 2, has provided fundamental permeation data under infinite dose conditions. However, its delivery through the Strat-M™ membrane can also be monitored in cell-based models by directly measuring changes in MMP activity and expression, and indirectly through observing its effects on cell behaviour such as contraction.

3.1.1 Role of dermal fibroblasts in tissue contraction

Dermal fibroblasts are the major cell type found in the human dermis and are integral to tissue remodelling, tissue development and wound repair[244]. Alongside mast, dendritic and plasma cells, they form the cellular component of the skin's extracellular matrix (ECM), while collagens and other proteinaceous molecules form the structural component. The ECM acts as a dynamic structural scaffold for the dermal cells to populate and also functions as a transmitter of mechanical forces originating in their cytoskeleton. Fibroblasts play a fundamental role in the synthesis of the ECM through production of collagens – mainly types I and III in the skin. They are also responsible for secreting and responding to cytokines, chemokines and growth factors for ECM maintenance and remodelling[244].

Forces originating in and transmitted across a population of dermal cells *via* the ECM contribute to tissue contraction, an integral step of several biological processes[245]. When activated, fibroblasts undergo a variety of changes including establishment of a smooth muscle-like contractile apparatus which allows them to generate these transmissible contractile forces[246]. Rapid myosin adenosine triphosphatase (ATPase) directs the arrangement of collagen fibrils into thicker, longer fibres through elimination of water[247]. As a result, the ECM undergoes compaction, becoming a denser matrix with a reduction in volume. Additionally, by a separate

mechanism, physical locomotion of fibroblasts functions to contract collagen[248]. This contractile behaviour can be modelled *in vitro* by emulating the three-dimensional architecture of dermal tissue and its resident cells, allowing factors that may accelerate or inhibit tissue contraction to be investigated.

3.1.2 Tissue equivalent models of the human skin and dermis

Tissue equivalents have been developed to reproduce key structural and functional aspects of human skin. They were originally developed as artificial skin to be used as skin grafts in burns patients, but are now more commonly used as bioengineered research alternatives to excised biological tissue[248]. Tissue equivalents are able to emulate several behaviours exhibited in the *in vivo* tissue by replicating the interaction of the tissues three-dimensional structural environment using its cellular and molecular components. Tissue equivalents provide improved culture systems compared with two-dimensional monolayer cultures since functional studies, such as those based on contraction, can be performed. Collagen substrata for studies on cell behaviour were first described by Elsdale and Bard in 1972[249]. The classic free-floating fibroblast-populated collagen lattice (FPCL) contraction model was first introduced by Bell *et al.* in 1979 and has been replicated and modified ever since[250]. Though their model unfortunately did not translate to successful skin grafts in humans it did provide a robust research model to investigate factors influencing fibroblast-mediated tissue equivalent contraction.

The typical dermal tissue equivalent is composed of collagen gel lattices exclusively populated with dermal fibroblasts. These soft collagen-cell gels are created from three major components: (i) a moderate density of fibroblasts cultured in (ii) serum-enriched culture medium in the presence of (iii) solubilised rat tail type I collagen[247]. *In vitro*, the native collagen spontaneously polymerises into a gel under physiological conditions and the fibroblasts interact with this newly polymerised collagen matrix[247]. Once set, the gel can be detached and become free-floating though gentle agitation or remain attached to the base of the culture plate. Compaction of the collagen fibrils by the resident fibroblasts results in reduction in lattice volume, also referred to as lattice or gel contraction. The FPCL model can be modified to include higher densities of fibroblasts, cell co-cultures or external stressors, each having an effect on the rate and mechanics of gel contraction.

3.1.3 Effect of doxycycline and other MMP inhibitors on FPCL contraction

Upregulation of MMP activity has been linked to fibroblast activation which, in turn, has been linked to augmented tissue contraction. In numerous studies, inhibition of MMPs in FPCL models has resulted in reduced gel contraction, though the exact mechanisms have yet to be

fully elucidated[213]. The effect of MMP expression and activity on gel contraction can be investigated in several ways including culturing fibroblasts lacking expression of particular MMPs[251], transfection of fibroblasts with MMP-specific small interfering RNA (siRNA)[251] or treatment of the FPCLs with MMP inhibitors[213,252]. These methods provide insights into the pathophysiological molecular pathways and thus potential treatments for MMP-mediated disease states.

Of particular interest are non-specific MMP inhibitors which have been shown to reduce gel contraction in FPCLs. The anti-cancer drug and MMP inhibitor GM6001 (also known as ilomastat) initially investigated in the prevention of tumour metastasis, was shown to significantly reduce gel contraction in collagen gels populated with dermal rat fibroblasts[252]. Sub-antimicrobial doses of doxycycline were also reported to reduce gel contraction and inhibit MMP activity in an ocular fibroblast model of human trichiasis containing fibroblasts harvested from affected conjuctiva[213]. Thus, doxycycline is reportedly able to reduce the gel contraction associated with activated fibroblasts and more importantly this acts as an indirect biomarker for its direct inhibition on MMP activity.

3.1.4 Safety of microneedling on injured tissue

The issue of safety of microneedling on skin has been raised[166] and could be especially problematic on injured skin. Though there are no details in the literature of microneedling onto early stage chronic wounds per se, there is evidence to suggest that ischemic tissue more easily propagates apoptotic death signals to neighbouring cells due to an upregulated gap junction function[253–256]. This process may be potentiated by application of microneedles which could further stress tissue. If microneedling does indeed have a deleterious effect on cell viability (which may be length dependent) then a trade-off may need to be made between the initial stress signalling it causes and the effect that delivering the drug has on promoting wound healing and resolution. Additionally, the pain sensation associated with longer microneedles (> 500 μm)[257], may not pose an issue for target patient populations since many of these individuals are paraplegic. Even in these situations, microneedles are advantageous over hypodermic injection as they allow for much more precise dermal delivery.

3.2 Research outline

This chapter outlines a series of experiments that ultimately investigated the delivery of doxycycline to FPCLs through microneedle-treated Strat-M™. The dermal tissue equivalent model used was based on the free-floating FPCL originally described by Bell *et al.* (1979)[250], though human instead of rat fibroblasts were used. Firstly, the effect of doxycycline treatment on the FPCLs was established. Then, in direct continuation of the investigations outlined in

Chapter 2, doxycycline was delivered to the FPCLs through Strat-M™ treated with increasing microneedle lengths on the roller systems. This was carried out to assess the effect of microneedling on enhancing transmembrane doxycycline delivery in a cell-based *in vitro* system. The Strat-M™ was mounted into wells using a cell crown, compartmentalising the upper surface from the FPCL beneath. Doxycycline solutions were then added onto the Strat-M™ surface and gel contraction and MMP activity measured. This group of experiments used fibroblast-mediated gel contraction to produce functional and quantitative data related to doxycycline activity. Gel contraction indirectly reflected the amount of doxycycline that reached the FPCLs — since the more doxycycline that could reach the FPCLs, the greater the reduction in gel contraction mediated by inhibition of MMP activity. MMP activity was also directly assessed by sampling the culture medium that the gels were immersed in.

This chapter aims to corroborate the effect of non-specific MMP inhibitors, specifically the drug of interest, doxycycline, on inhibition of MMP activity and gel contraction (reported in previous studies) in combination with its delivery through microneedle-treated Strat-M™. The set of experiments demonstrated the effect of microneedle application and length on drug permeation through Strat-M™ using established biological markers. Novel aspects of the experiments include: (i) treatment of three-dimensional collagen gels populated with dermal fibroblasts using doxycycline in combination with the assessment of its delivery through microneedled-treated Strat-M™, (ii) monitored through the extent of gel contraction and MMP activity. Additionally, a potentially negative effect of microneedling on cell viability was explored as further physical injury to already wounded tissues raises valid concerns.

3.3 Methods and materials

3.3.1 Human adult dermal fibroblasts

Isolation of fibroblasts

Human adult dermal fibroblasts (also referred to as HDFa cells or fibroblasts) were kindly provided by Dr Maryse Bailly (Institute of Ophthalmology [UCL], London). A 5 mm punch biopsy was harvested from the presternal dermis of a healthy adult donor undergoing blepharoplasty surgery. The biopsy was mechanically dispersed, outgrown from the explant and established as a primary *in vitro* culture[258].

Cell culture

Monolayer cultures of fibroblasts were grown in T75 cm^2 vented flasks in x1 DMEM (D6546; Sigma-Aldrich, Poole, UK) supplemented with 10% (v/v) FBS (Gibco, Paisley, UK), 1% (v/v) L-Glutamine (Sigma-Aldrich) and 1% (v/v) penicillin-streptomycin-amphotericin B (Sigma-

Aldrich). Their environment was maintained at 37^{o}C and 5% CO_2 in a fully-humidified incubator. Cells were used between passages five and 15 and were grown to approximately 80% confluence before passaging. Prior to formation of dermal equivalents in the form of cellularised collagen gels, the cell monolayers were washed once with PBS and detached with trypsin-EDTA (Sigma-Aldrich). The cell-trypsin suspension was neutralised with complete DMEM and cells were pelleted of solution by centrifugation at 1500 rpm for 5 minutes at room temperature. Pellets were then resuspended in complete DMEM and viable cell counts determined using trypan blue staining. For maintenance of cultures, cells were transferred to T75 cm^2 flasks and resuspended in DMEM at a density of 2.5 x 10^5 cells per ml. Cell media was aspirated and replenished 24 hours after passaging and then every three days until cells became confluent.

3.3.2 FPCL contraction assay

Collagen gel synthesis

Concentrated media was made by adding (v/v/v) 73.7% x10 DMEM (Sigma-Aldrich), 7.4 % L-glutamine (Sigma-Aldrich) and 18.9% sodium bicarbonate (Gibco). Concentrated media was added drop wise to 1 ml of Type I Rat Tail Collagen (First Link UK Ltd., Birmingham, UK) and the solution neutralised with 80 µl of 1M sodium hydroxide (Sigma-Aldrich). 100 µl of 1 x10^5 cells resuspended in FBS was added to the collagen solution. The cell-enriched collagen gel solution was cast quickly into the 10 mm microwells of uncoated glass bottomed 24-well plates (P24G-1.5-10-F; MatTek Corp., Massachusetts, USA). The plates were gently tapped to ensure the gels made contact with the microwell edge and to remove any large air bubbles that could affect gel ultrastructure. Gels were allowed to solidify at 37^{o}C for 15–20 minutes to form the FPCLs. FPCLs were monitored under a light microscope. This was useful to assess cell viability when FPCLs were not contracting. Small rounded cells suggested cell death possibly due to on overly acidic environment caused by insufficient neutralization of the concentrated media during FPCL formation.

Figure 3.1 — Photographs of modified cell culture plates supplied by MatTek Corp. containing glass-bottomed microwells [MW] into which cellularised collagen gels were cast: (A) A 24-well glass-bottomed plate (MatTek Corp.) **(B)** A 35 mm glass bottomed dish.

Preparation of doxycycline test solutions

Doxycycline hyclate powder (Alfa Aesar, Massachusetts, USA) was dissolved in sterile water and vortexed to create a 48.7 mM stock solution. A range of sub-antimicrobial concentrations of doxycycline were created (104, 208, 416, and 832 μM) through serial dilutions in complete DMEM. The comparative effect of an alternative doxycycline hyclate powder (Sigma-Aldrich) was also investigated. Once set, gels were gently detached from the edges of the microwell to become free-floating using a sterile pipette tip. DMEM or doxycycline test treatments (1 ml) were added to the gels and plates incubated at 37^{o}C.

Gel contraction analysis

Gel contraction is a qualitative observable effect that occurs when fibroblastic activity causes the surrounding interconnected ECM to contract. The effect can be quantitatively monitored by periodically measuring the size of the gel and comparing it to its original size (**Figure 3.2 – A**). The data can then be used to examine how gel contraction changes over time and the effect of that any treatments added to the gel have. Digital photographs of the FPCLs were taken on days 1, 3, 6 and 7 with a 20MP camera, against a black surface for contrast. Gel areas were measured using the 'elliptical' measuring tool in ImageJ®. Contraction was plotted as a percentage of gel area normalised to the original gel area when cast on day 0 (also equivalent to microwell area).

Gel thickness was not measured by this method, and contraction in the vertical dimension was not assessed. Starting gel thickness was 1.5 mm with a convex meniscus (**Figure 3.2 – B**).

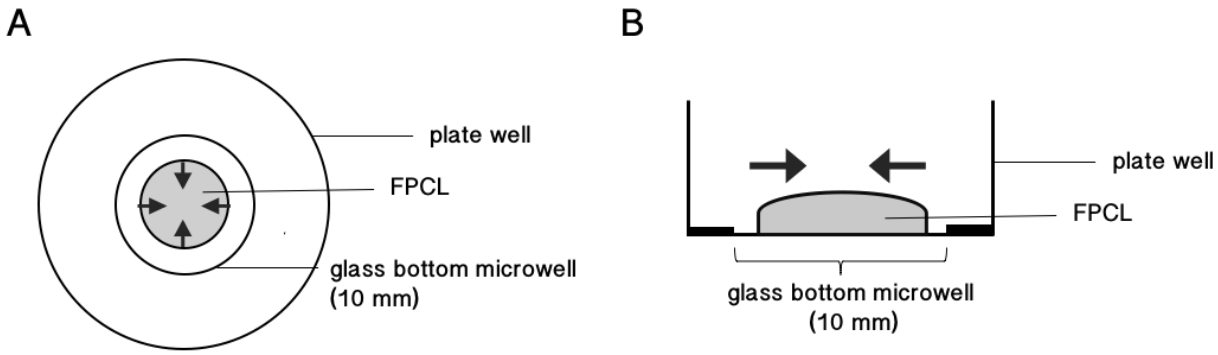

Figure 3.2 — Schematic representation of gel contraction analysis of FPCLs: (A) FPCLs were cast into the 10 mm diameter glass-bottomed microwells of modified tissue culture plates. FPCLs were allowed to set for 20 minutes at 37^{o}C and were gently detached from the microwell to become free-floating by tapping. Percentage gel contraction was calculated by measuring the area of the FPCL compared with that of the microwell from digital photographs. **(B)** Once set, FPCLs had a convex meniscus. Gel contraction was only assessed in the horizontal dimension by this method. Starting gel thickness was approximately 1.5 mm.

3.3.3 Assessing MMP activity

Sample collection

Samples of supernatant (75 µl) were collected 1 hour after initial incubation on day 0 and then on days 3 and 7. Samples were stored at –20^{o}C.

MMP activity assay

The MMP activity assay is a method used to assess and quantify the activity of MMPs in a solution using changes in fluorescent activity. The assay utilises a fluorescence resonance energy transfer (FRET) peptide as an MMP substrate. When this peptide is intact, the fluorescence of the donor portion of the peptide is quenched by another portion known as the 'quencher'. When the FRET peptide is cleaved by MMP activity the two fragments are separated and the fluorescence is recovered. This fluorescence can be detected and measured. The assay broadly distinguishes between MMPs depending on the length of incubation with

substrate solution, for which 3 hours detects the activity of MMPs 1, 2, 7, 8, 9, 11, 12, 13 and 14, inclusive of the MMPs (MMPs 2, 8 and 9) of interest to pressure ulcer pathophysiology.

Total MMP activity was determined using the Abcam FRET-based MMP activity assay kit according to manufacturer's protocol (ab112147; Abcam, Cambridge, UK). Supernatant (25 µl) collected from collagen gel contraction cultures was transferred to 96-well plates (Appleton Woods, Birmingham, UK) and 25 µl of the provided 2 mM p-aminophenylmercuric acetate (AMPA) solution added. Plates were incubated at 37^{o}C for 3 hours. MMP red substrate working solution (50 µl) was added to the samples and the plate incubated at room temperature for 1 hour, protected from light. Fluorescence was measured at Ex/Em 540/590 nm using the FLUOstar Optima plate reader (BMG Labtech, Ortenberg, Germany).

Normalising MMP activity

The fluorescent output readings from the MMP activity assays are relative values that could be affected by signals from background substances and materials. To correct for this effect, the readings for each treatment group were normalised to a background control that contained just the treatments, for each day. This was done by subtracting the background reading from the reading of the sample. This also allowed for meaningful and direct comparisons between treatment groups.

3.3.4 Strat-M^{TM} membrane

Perforation of Strat-M^{TM} by microneedle rollers

Strat-M^{TM} membranes (Merck Millipore, USA) were cut into circular discs, 23 mm in diameter, and transferred onto a cutting board support. Microneedle rollers (Sodacoda, Delmenhorst, Germany) 250, 500 and 750 µm in shaft length were placed onto the membrane and rolled five times bi-directionally along the *y* axis as previously described (**Method 0**, ***p. 85***).

3.3.5 Mounting Strat-M^{TM} membrane into cell crown inserts

Strat-M^{TM} membranes were mounted into cell crowns (Scaffdex, Tampere, Finland). Cell crowns were then inserted into individual wells of the 24-well MatTek plate so that the basal surface of the membrane was in contact with the medium (750 µl) bathing the collagen gels (**Figure 3.3 – A**). Treatment solutions (250 µl) were pipetted onto the apical surface of the Strat-M^{TM} membrane. Supernatant was sampled from around the collagen gel on days 0, 3 and 7 using a fine needle and syringe (**Figure 3.3 – B**) for subsequent MMP activity measurements (**Method 3.3.3, *p. 121***).

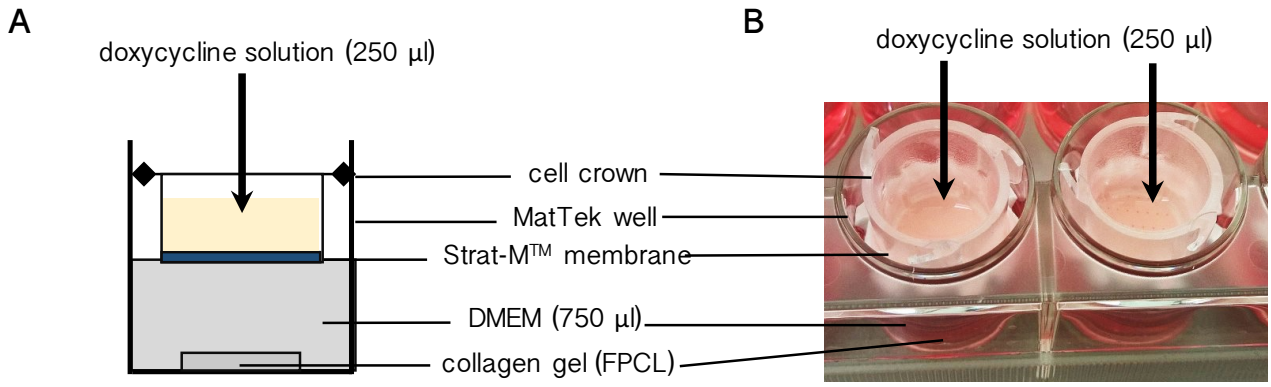

Figure 3.3 — Set-up of the cell crown inserts and Strat-M™ membrane mounted in 24-well plates: (A) Schematic representation of Strat-M™ membrane inserted into a cell crown and mounted into an individual well of a 24-well glass-bottomed plate. The basal surface of the membrane contacted with the DMEM immersing the FPCL. Doxycycline solution was pipetted onto the apical surface of the membrane. (B) Photographs of cell crowns with Strat-M™ membrane inserts mounted into individual wells. Supernatant was sampled from around the cell crown and membrane using a very long, thin needle which could reach the underlying medium without disturbing the experimental apparatus.

3.3.6 Effect of microneedle application on cell viability

Scratch assay

In addition to Strat-M™ perforation, microneedle rollers were applied onto (i) fibroblast monolayers grown on polystyrene tissue culture substrate and (ii) onto the FPCLs. This was investigated to assess the effect of microneedling on cell viability. The volume of collagen gels was scaled up to fit a 35mm diameter glass bottomed MatTek dish (P35G-1.5-14-C; MatTek Corp) — large enough to accommodate the microneedle roller. For the monolayer cultures, fibroblasts were seeded at a density of 1 x 10^6 cells per ml in 6-well plates (Appleton Woods, Birmingham, UK) and incubated for 3 days at 37^{o}C to allow for adhesion and proliferation and for cell density to reach 80% confluence. Microneedles, 250, 500 and 750 µm in length, were applied onto the monolayers and FPCLs by applying a 500 g calibration mass onto the rollers producing a downward force of 3.8N. Cell viability was assessed at 0, 1 and 24 hours. A horizontal scratch wound was applied using a p200 pipette tip and served as a positive control.

Apoptosis/necrosis staining kit

Apoptotic and necrotic activity in the cell monolayers and FPCLs was determined using an apoptosis/necrosis detection kit, a fluorescence-based assay designed to simultaneously monitor apoptotic, necrotic and healthy cells (ab176749; Abcam, Cambridge, UK). The kit contains three different sensors, the Apopxin Deep Red Indicator, DNA Nuclear Green DCS1 Dye and CytoCalcein Violet 450 which distinguish between cells that have undergone apoptosis – active, programmed cell death, necrosis – passive, accidental cell death and healthy live cells, respectively. The Apopxin Deep Red indicator distinguishes apoptotic cells by binding to phosphatidyl serine presented on the cell membranes and producing a red fluorescence. Nuclear Green DCS1 Dye is a membrane-impermeable stain that is able to label the cell nucleus when there is loss of membrane integrity producing a green fluorescence. It stains for late apoptotic and necrotic cells. CytoCalcein Violet 450 is a live cell cytoplasm labelling dye which stains viable cells by producing a blue fluorescence.

For the apoptosis/necrosis assay, media was aspirated from the samples and cells were washed with 100 µl of Assay Buffer. A staining mix consisting of Assay Buffer with 1% (v/v) Apopxin Deep Red Indicator 200x, 0.5% (v/v) Nuclear Green DCS1 Dye 200x and 0.5% (v/v) CytoCalcein Violet 200x was added to the samples. Samples were incubated at room temperature for 1 hour. Cells were washed twice more with Assay Buffer. Samples were imaged under the Leica DM16000 B fluorescent microscope (Leica Microsystems, Wetzlar, Germany) with an N PLAN 10.0 x 0.25 dry objective. Apopxin Deep Red indicator, Nuclear Green DCS1 Dye and CytoCalcein Violet 450 were excited by the 647, 488 and 405 nm wavelength lasers respectively. Bright-field imaging was used to assess physical damage made by the microneedles onto the plate substrates when they were applied to the fibroblast monolayers and FPCLs.

3.3.7 Statistical analyses

For each condition there were six replicates (unless otherwise stated) to allow for experimental variation. A two-way ANOVA with Tukey correction for multiple comparisons was carried out to determine statistical significance of percentage gel contraction and MMP activity between treatment groups for each day. Where appropriate, results are expressed as mean ± standard error of the mean (SEM) and in all instances, $p < 0.05$ denotes a statistically significant difference.

3.4 Results

3.4.1 Effect of doxycycline on collagen gel contraction and MMP activity

Collagen gels cellularised with human dermal fibroblasts (FPCLs) and cultured in FBS-supplemented DMEM exhibited contraction at a decreasing rate over a seven-day period. Collagen gels showed percentage contraction of 59.9 ± 2.2%, 82.3 ± 1.1%, 94.6 ± 0.7%, and 95.7 ± 0.3% on days 1, 3, 6 and 7 respectively. In follow-up studies it was confirmed that percentage gel contraction never reached 100% and would plateau at approximately 98% when allowed to contract over an extended period of time. The presence of sub-antimicrobial concentrations of doxycycline within the culture medium was shown to significantly reduce percentage gel contraction compared with control groups at equivalent time points ($p < 0.0001$), but not to prevent it (**Figure 3.4)**.

A doxycycline concentration of 416 μM was used, as this is a validated concentration in the literature, shown to significantly reduce gel contraction[213,259]. For gels treated with 416 μM doxycycline solution, percentage gel contraction was 29.5 ± 2.4%, 52.6 ± 0.9%, 60.8 ± 2.2% and 63.2 ± 1.9% on days 1, 3, 6 and 7 respectively (**Figure 3.5**). The extent of gel contraction inhibition was shown to be dose dependent between doxycycline concentrations of 104 and 832 μM **(Figure 3.6**). Increasing doxycycline concentration had a statistically significant effect on increasing inhibition of gel contraction compared with control 104 μM ($p < 0.001$), 208 μM ($p < 0.0001$), 416 μM ($p < 0.0001$) and 832 μM ($p < 0.0001$) by day 7). As with the control FPCLs, the rate of gel contraction in all doxycycline-treated FPCLs progressed rapidly up until day 3 then gradually decreased for the remainder the experiment. A dose dependent effect of doxycycline within this concentration range has been also reported in previous studies[259].

MMP activity assays were used to assess the activity of MMPs in the FPCL supernatant throughout the experiment. In control gels, the normalised activity of MMPs was shown to sharply increase over the seven day experiment and effectively doubled between days 0 and 7. Treatment of the FPCLs with 416 μM doxycycline significantly inhibited MMP activity in the gel supernatant compared with control by days 3 and 7, maintaining them at day 0 activity levels ($p < 0.0001$). Inhibition of MMP activity was dose dependent in a range of 104 to 832 μM doxycycline concentrations. The presence of 104 μM doxycycline resulted in statistically significant inhibition of MMP activity. The lower concentrations of 104 and 208 μM reduced the MMP activity compared with control but 416 μM kept them at day 0 levels. The highest concentration assessed of 832 μM resulted in a reduction of MMP activity on days 3 and 7 compared with day 0, consistent with this concentration having the greatest effect on inhibiting gel contraction.

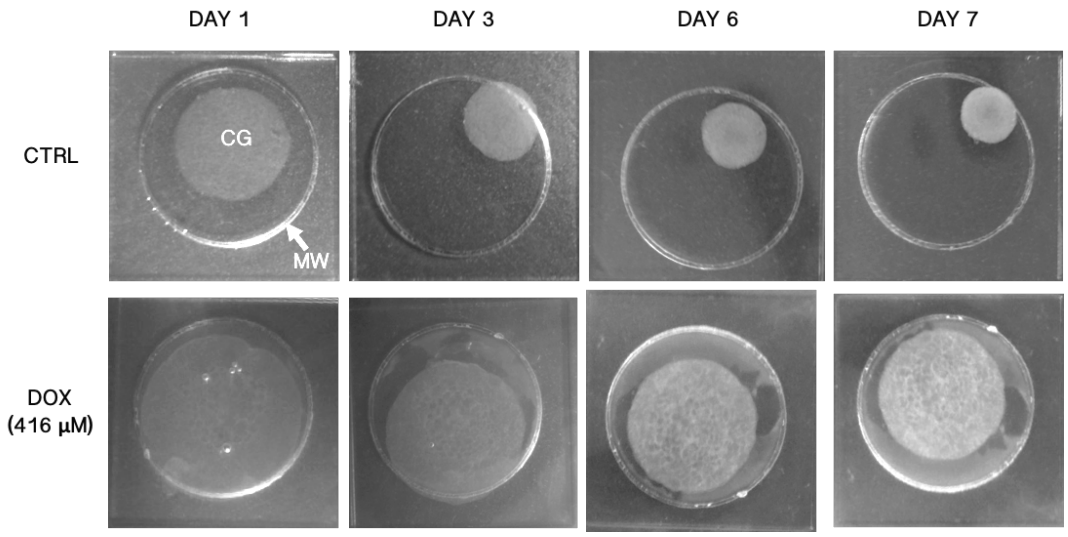

Figure 3.4 — Photographs of gel contraction in FPCLs treated with 416 µM doxycycline and control FPCLs. The collagen gels [CG] were cast into the plate's microwells [MW] on day 0 and photographed on days 1, 3, 6 and 7. Percentage gel contraction was calculated by measuring the area of the collagen gel relative to the microwell. Control gels that were cultured in only complete DMEM, showed rapid contraction between days 1 and 3. Treatment of gels with 416 µM doxycycline significantly reduced total percentage contraction by day 7 ($p < 0.0001$**).**

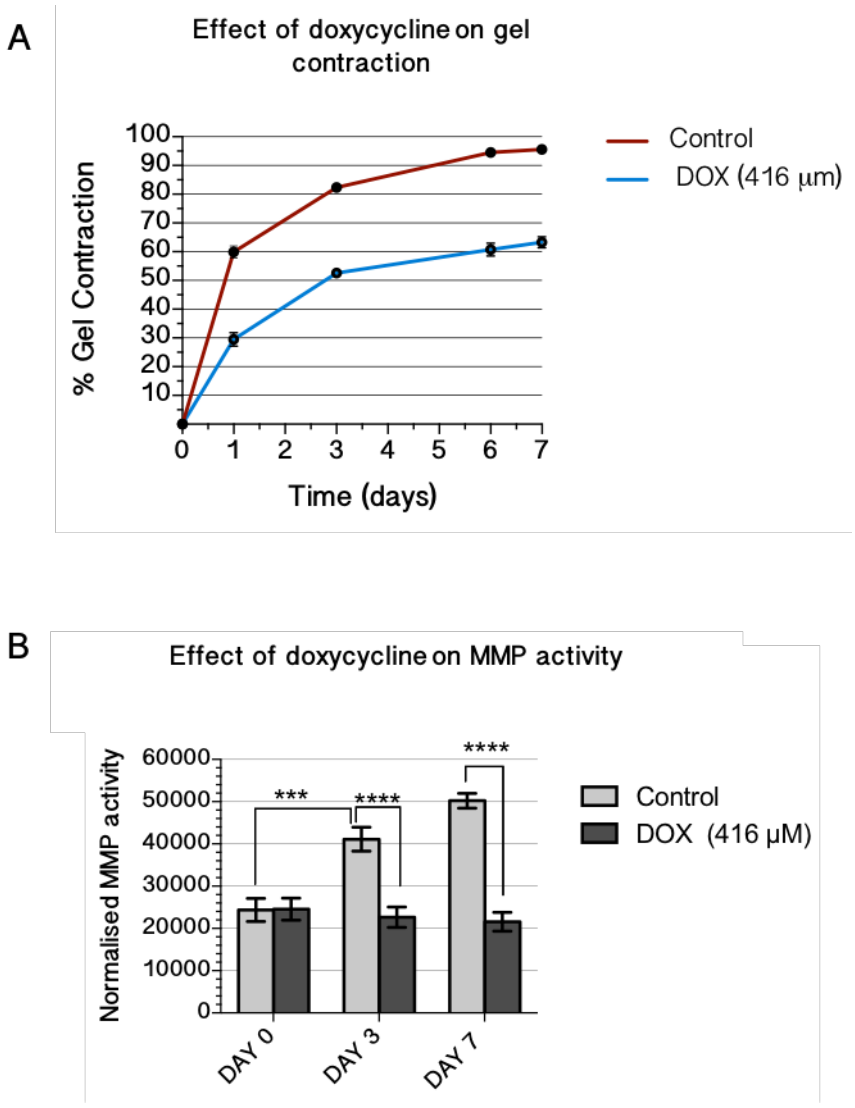

Figure 3.5 — Effect of 416 µM doxycycline concentration on FPCL gel contraction and MMP activity (n = 6): (A) Gel contraction compared between control FPCLs and doxycycline-treated FPCLs. For control gel contraction increased significantly over a seven-day period. A concentration of 416 µM doxycycline significantly reduced gel contraction compared with control on days 1, 3 6 and 7, though gel contraction continued to increase. **(B)** MMP activity compared between control FPCLs and doxycycline-treated FPCLs. For control groups, MMP activity increased over the 7-day experimental period, significantly so between days 0 and 3. For doxycycline-treated FPCLs this increase in MMP activity was significantly inhibited on days 3 and 7. *Error bars represent the standard error of the mean; *** = $p < 0.001$, **** = $p < 0.0001$.*

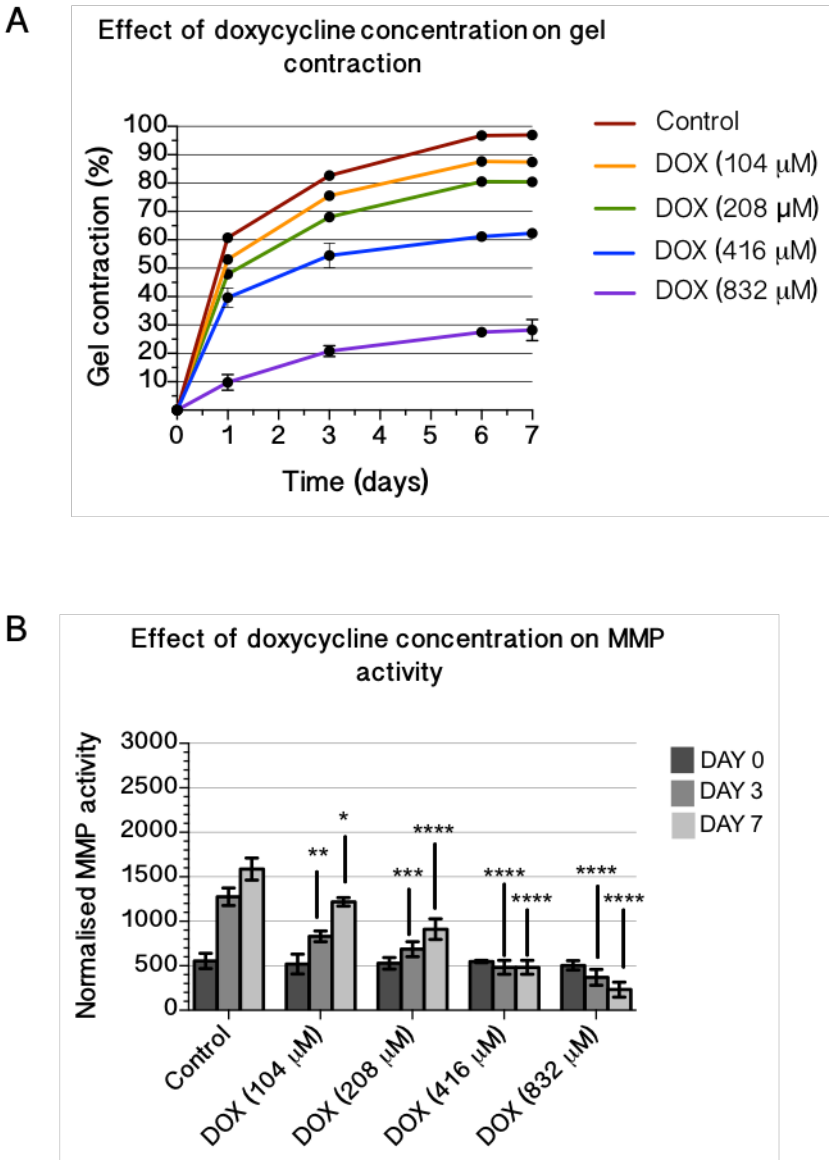

Figure 3.6 — Effect of a range of doxycycline concentrations on FPCL gel contraction and MMP activity (n = 6): (A) The effect of doxycycline concentration on collagen gel contraction. Increasing doxycycline concentration between 104 µM and 832 µM, increased its effect on reducing gel contraction in a dose dependent manner. **(B)** The effect of doxycycline concentration on MMP activity. For a doxycycline concentration range between 104 and 832 µM, MMP activity was significantly reduced compared with control. *Error bars represent the standard error of the mean; * = $p < 0.05$, ** = $p < 0.01$, *** = $p < 0.001$, **** = $p < 0.0001$ and represent a statistically significant difference compared with the day-matched 'Control' value;.*

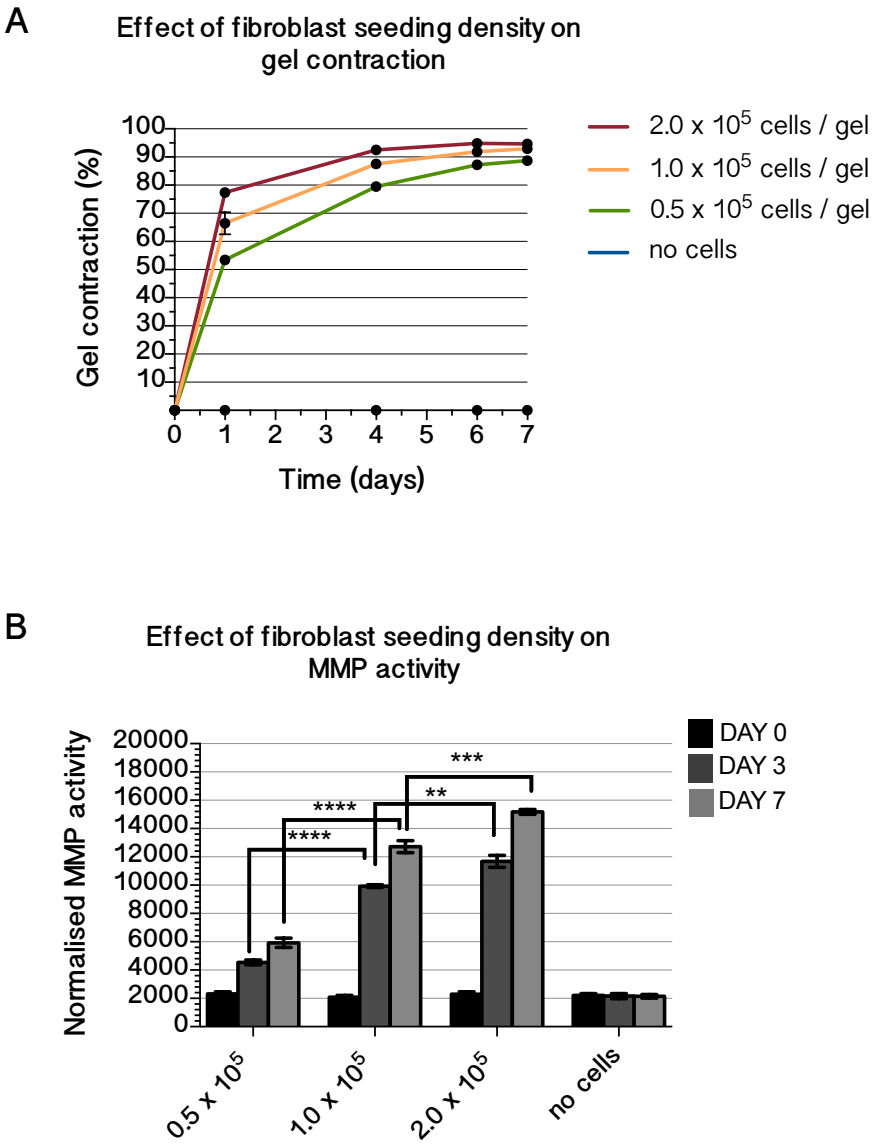

Figure 3.7 — Effect of fibroblast seeding density on FPCL gel contraction and MMP activity (n = 6): (A) Effect of fibroblast seeding density on gel contraction. The rate and extent of gel contraction over the seven-day experimental period was correlated with the initial fibroblast seeding density. FPCLs initially cellularised with 2.0 x10^6 fibroblasts showed a statistically significant increase in percentage gel contraction on days 1, 4 and 6 compared with FPCLs cellularised with 0.5 x 10^6 and 1.0 x 10^6. In the absence of fibroblasts, no FPCL gel contraction was observed. **(B)** MMP activity compared between different FPCL fibroblast seeding densities. Increasing the FPCL seeding density resulted in significantly increased MMP activity between 0.5 x10^6 and 1.0 x10^6 and 1.0 x10^6 and 2.0 x10^6 by days 3 and 7. No increase in basal MMP activity levels was observed in the absence of cells in the collagen gels. *Error bars represent the standard error of the mean; ** = $p < 0.01$, *** = $p < 0.001$, **** = $p < 0.0001$.*

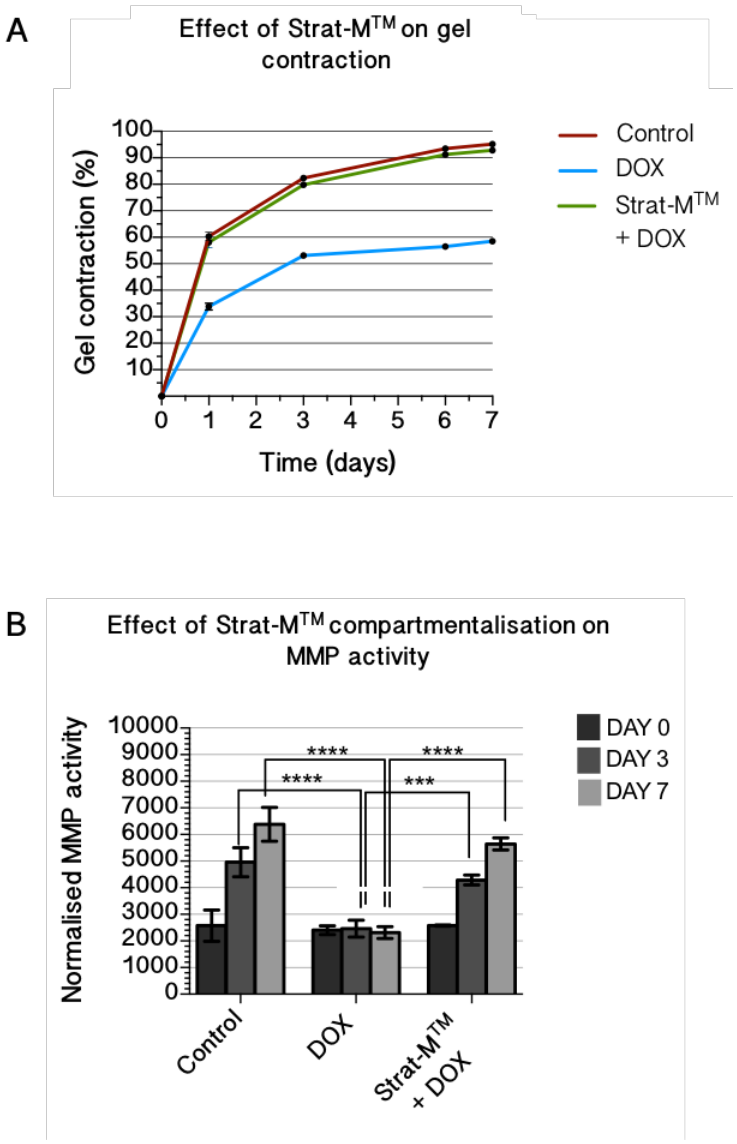

Figure 3.8 — Evaluating the delivery of doxycycline through untreated Strat-M™ membrane (n = 6): (A) The effect of untreated Strat-M™ on gel contraction in comparison with control FPCLs and 416 µM doxycycline treated FPCLs was investigated. Strat-M™ was able to significantly inhibit the delivery of doxycycline to the FPCLs by compartmentalising the doxycycline. There was no significant difference between gel contraction exhibited in control and Strat-M™ groups **(B)** Comparison of MMP activity between control FPCLs, FPCLs compartmentalised from 416 µM doxycycline by the Strat-M™ control and FPCLs treated directly with 416 µM doxycycline. As seen with the gel contraction results, Strat-M™ compartmentalisation of doxycycline did not result in statistically significant difference in MMP activity compared to control, but was statistically different from 'Dox' groups on days 3 and 7. *Error bars represent the standard error of the mean; *** = $p < 0.001$ **** = $p < 0.0001$.*

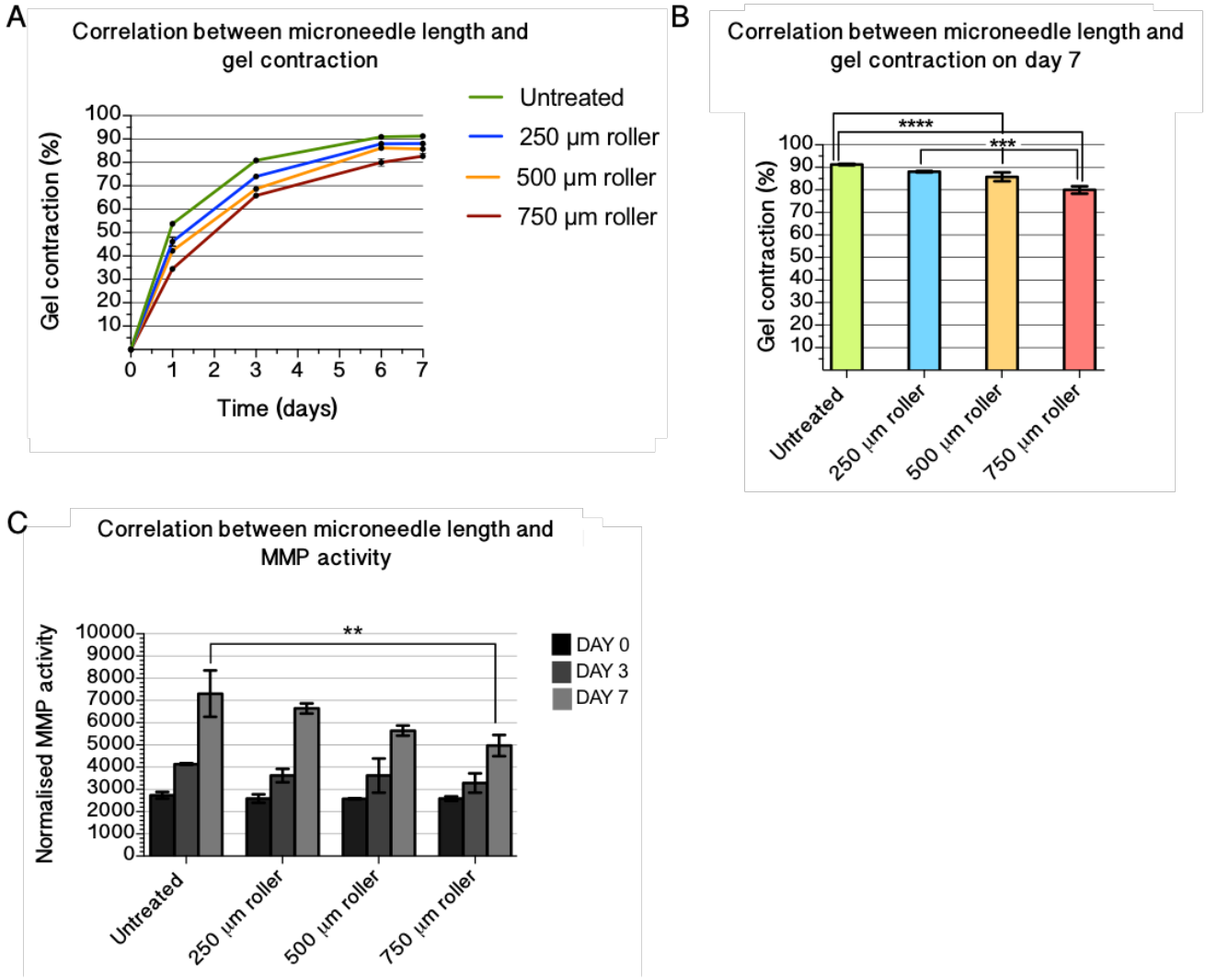

Figure 3.9 — Evaluating the delivery of doxycycline through microneedle-treated Strat-M™ membrane (n = 6): (A) Percentage gel contraction was correlated with the length of the microneedles used to permeabilise the Strat-M™ membrane to the 416 µM doxycycline solution. Permeabilistion of the membrane to doxycycline using the microneedles resulted in reduced gel contraction compared to control, significantly so for 250 µm on days 1 and 3, 500 µm on all days and 750 µm on all days assessed of the seven-day experiment. The magnitude of effect was related to needle length; the 750 µm microneedle-treated membrane resulted in the greatest reduction in gel contraction while the 250 µm resulted in the least. **(B)** A statistically significant difference in gel contraction was observed between both the 500 and 750 µm microneedle groups and control group by day 7. **(C)** Correlation of MMP activity between and Strat-M™ treated with increasing microneedle lengths. A statistically significant difference was only observed between untreated Strat-M™ and 750 µm microneedle-treated Strat-M™ on day 7. *Error bars represent the standard error of the mean; ** $p < 0.01$, *** = $p < 0.001$ **** = $p < 0.0001$.*

3.4.2 Effect of fibroblast number on gel contraction and MMP activity

The presence of fibroblasts in the collagen gels was essential for gel contraction as acellular gels did not exhibit any gel contraction (**Figure 3.7**). The results showed that the rate and extent of gel contraction after 24 hours was dependent on the number of fibroblasts originally seeded into the collagen mix. FPCLs seeded with 2 x 10^5 cells contracted at a significantly greater rate than FPCLs seeded with 1 x 10^5 or 0.5 x 10^5 ($p < 0.0001$) after 24 hours. By day 3, however, the difference in total gel contraction became less marked as the rate of contraction began to plateau across all groups. A limiting effect of cell number on gel contraction was not observed with an initial seeding density of up to 2 x 10^5 cells per ml of gel mix.

3.4.3 Delivery of doxycycline through microneedle-treated Strat-M™

The addition of the Strat-M™ membrane into the cell crown insert compartmentalised the doxycycline solution from the FPCLs. This prevented the doxycycline from reaching the FPCLs and inhibiting gel contraction and MMP activity unlike gels directly treated with doxycycline (**Figure 3.8**). The results suggest that the permeation of doxycycline was significantly inhibited by the Strat-M™ membrane for two reasons – (i) there was no statistical difference in gel contraction or MMP activity between control and Strat-M™ values on any day, and (ii) there was a statistically significant difference in both gel contraction and MMP activity between groups treated with doxycycline and those treated with doxycycline compartmentalised by Strat-M™ on days 1, 3, 6 and 7 ($p < 0.0001$).

To assess the effect of microneedle treatment on enhancing transmembrane diffusion of doxycycline solution, the Strat-M™ membrane was firstly treated with microneedles of 250, 500 or 750 μm in shaft length. Doxycycline solution was then pipetted onto the membrane's apical surface. Since Strat-M™ had been determined to be impermeable to the doxycycline solution, any doxycycline reaching the FPCLs could be attributed to the microneedles permeabilising the membrane. Changes in percentage gel contraction and MMP activity acted as quantitative biomarkers of this effect (**Figure 3.9)**. Treatment of the Strat-M™ with the 250 μm microneedles resulted in a statistically significant difference in gel contraction compared with untreated (control) Strat-M™ on days 1 and 3 ($p < 0.0001$), but not on days 6 and 7. However, increasing microneedle length beyond this corresponded to a significantly reduced total gel contraction for 500 μm ($p < 0.001$) and 750 μm ($p < 0.0001$) microneedles compared with control on days 1, 3, 6 and 7. There was also a significant difference in percentage gel contraction between 250 and 750 μm groups by day 7 ($p < 0.0001$).

3.4.4 Effect of an alternative doxycycline hyclate powder on collagen gel contraction

To confirm that the effect of doxycycline on the FPCLs was consistent across powders from different sources, doxycycline powder from a different supplier (Sigma-Aldrich, Poole, UK) was compared with the originally used powder (Alfa Aesar, Massachusetts, USA). No significant difference in effect on collagen gel contraction or MMP activity was observed between these doxycycline powders from alternative suppliers at varying sub-antimicrobial concentrations over a period of seven days (**Figure 3.10**).

3.4.5 Effect of microneedling on cell viability

A concern with the use of microneedling on wounded skin is the possibility of direct injury to cells at the site of application that may trigger and propagate apoptotic death signals to neighbouring cells. The effect of microneedle application on cell viability (without doxycycline application) was investigated firstly in a cell monolayer of fibroblasts cultured on a rigid polystyrene substrate and then in the FPCLs. A scratch created by a p200 pipette tip acted as a control. In the p200 scratch created in the fibroblast monolayer, cells were found to have been removed and displaced from the site of application (**Figure 3.11**). By 24 hours there was evidence of cell migration into the scratch, alongside an increased number of red fluorescent (apoptotic) signals in the cells neighbouring the scratch margins. Application of the microneedle rollers onto the fibroblast monolayers did not displace the cells as the p200 pipette scratch had done, but instead caused punctures in the polystyrene substrate's surface (**Figure 3.13 – A**).

These punctures matched the tip shape of the microneedle rollers as was observed by the micropores created in Strat-M^{TM} membrane in Chapter 2. Expression of apoptotic and necrotic signals were observed in the centre of the microneedle punctures, but not at the margins or neighbouring cells. (**Figure 3.11**). In the FPCLs, the p200 pipette tip created a different shaped scratch to that made on the fibroblast monolayer (**Figure 3.12**). There was evidence that the gel structure had been displaced but with resistance from the collagen matrix. There was also a significant increase in green fluorescent (necrotic) signals around the margins of the scratch. In contrast, microneedle application on the FPCLs did not create a puncture but most likely transiently displaced the gels due to the elastic recoil of the collagen (**Figure 3.13 – B**). No apoptotic or necrotic signals were observed in microneedle-treated FPCLs 0, 1 or 24 hours after initial microneedle application.

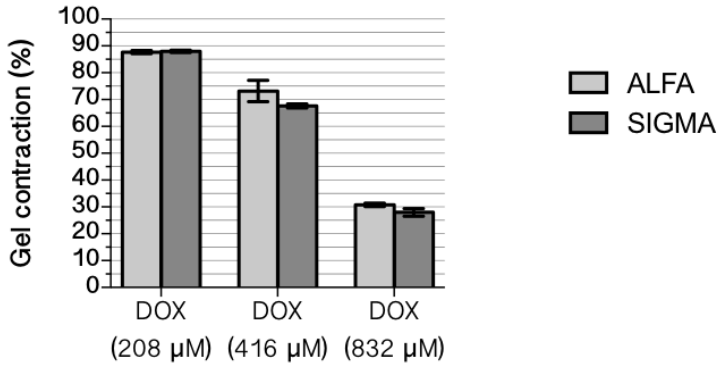

Figure 3.10 — Comparison of FPCL gel contraction between two different commercially available doxycycline powders over a range of sub-antimicrobial concentrations on day 7 (n = 6). No statistically significant difference in gel contraction was observed between the two powders provided by different suppliers (Alfa Aesar and Sigma-Aldrich). *Error bars represent the standard error of the mean.*

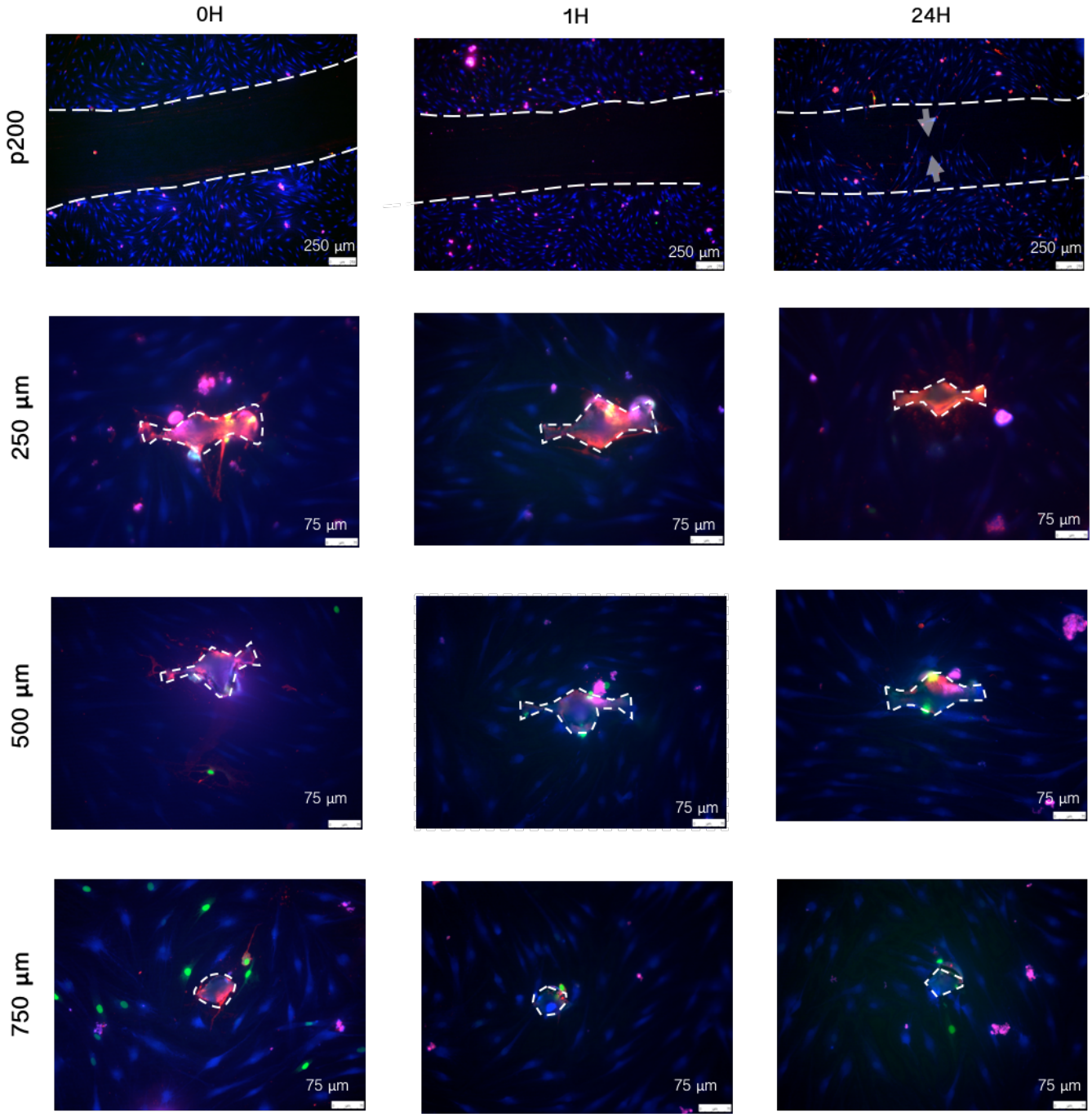

Figure 3.11 — Cell viability staining using the apoptosis/necrosis detection kit on microneedle-treated fibroblast monolayers at 0, 1 and 24 hours. Fibroblast monolayers were grown on a polystyrene substrate for 3 days. After 3 days of culturing, the microneedle rollers (250, 500 or 750 µm) were applied to the monolayers using a standardised vertical force of 3.8N. Monolayers were imaged immediately after microneedle application (*left*) and then at 1 (*centre*) and 24 (*right*) hours after. A scratch wound created by a p200 pipette tip acted as a standard control. Red signals indicate apoptotic cells, green signals indicate necrotic cells and blue signals indicate healthy viable cells. The site of the puncture (physical injury) is outlined in each image.

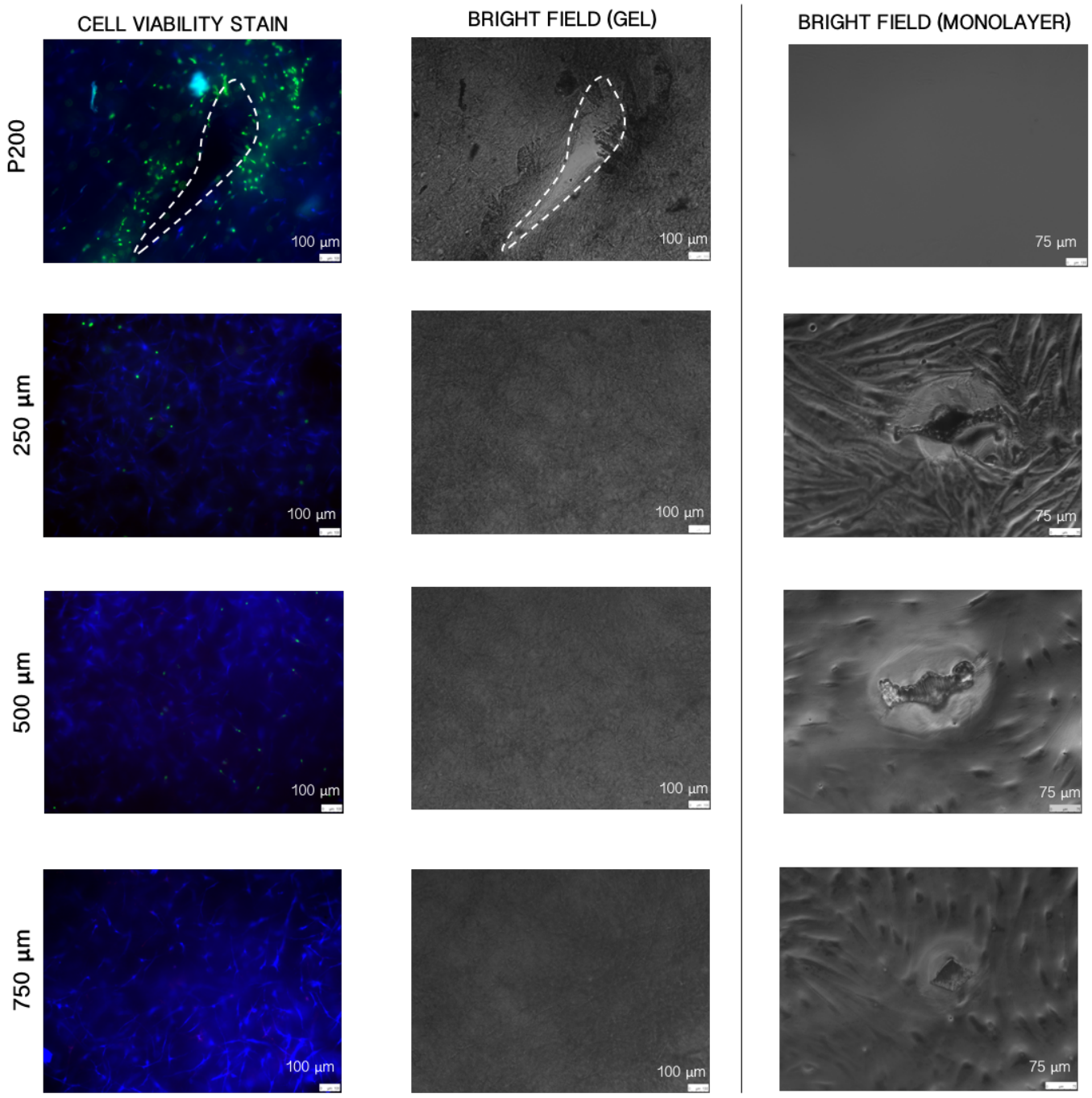

Figure 3.12 — The effect of microneedle application on cell viability on FPCLs. Cell viability staining using an apoptosis/necrosis stain on microneedle-treated FPCLs (*left*). Bright field microscopy of microneedle-treated FPCLs immediately after application (*centre*). Bright field microscopy of microneedle-treated fibroblast monolayers immediately after application (*right*). A p200 pipette tip scratch acted as a standard positive control. Red fluorescence indicates apoptotic cells, green — necrotic cells, and blue — healthy, viable cells.

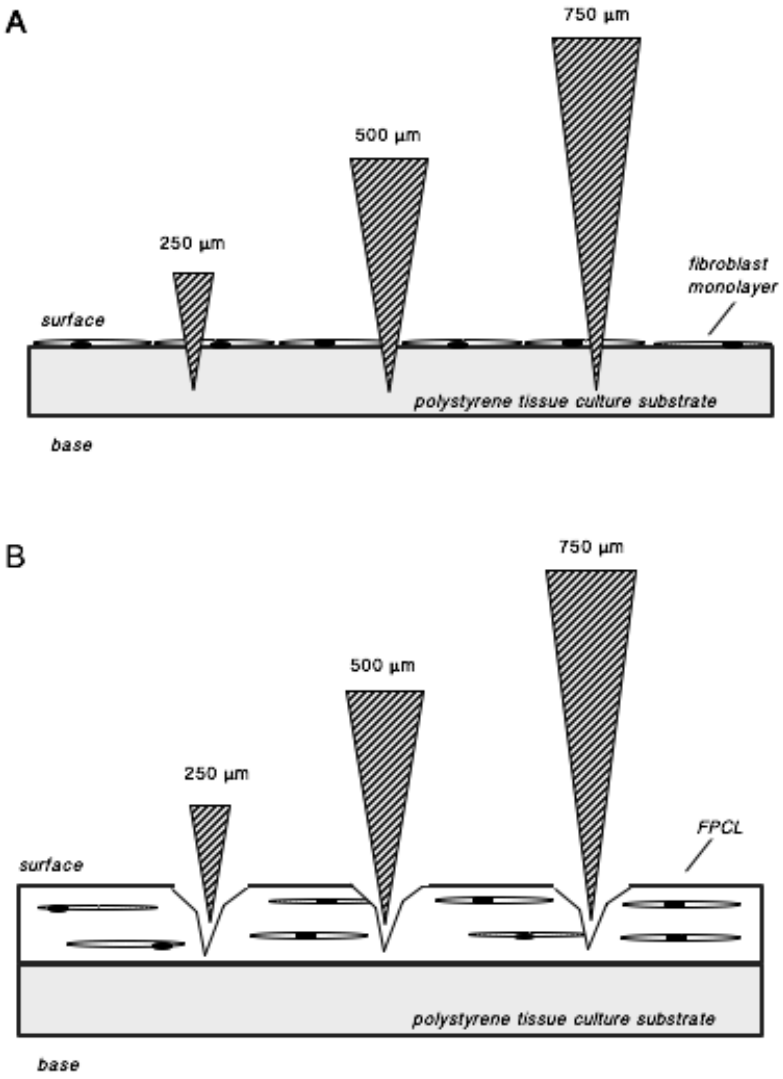

Figure 3.13 — Schematic representation of microneedle application during the cell viability experiments: (A) Microneedles were applied with a downward force of 3.8N using a calibrated 500 g mass onto the dermal fibroblast monolayer that had been cultured on polystyrene substrate until confluent. This created microscopic punctures on the apical surface of the plate**. (B)** The same process was carried out on the FPCLs. No punctures or disturbance to the cells in the FPCLs were microscopically visible**.**

3.5 Discussion

A three-dimensional cell-enriched collagen matrix, the FPCL, was used as a model of the human dermis to investigate the delivery of doxycycline across Strat-M™ membrane using microneedle roller systems. FPCL contraction was used an as indirect marker of MMP activity and doxycycline-mediated inhibition of MMP activity acted as an indirect marker of the doxycycline concentration in the FPCL supernatant.

3.5.1 Inhibition of MMP-mediated gel contraction and MMP activity in FPCL supernatant by doxycycline

The effect of MMP inhibitors on modulating FPCL contraction is well documented[213,252,260,261]. These include compounds being trialled as anti-cancer drugs such as BMS-275291[260], BB94 (batimastat)[261], GM6001 (ilomastat/galardin)[252,261] and the antibiotic doxcycline[213,261,120]. In agreement with previous findings, doxycycline was shown to reduce gel contraction of the FPCLs in a dose-dependent manner over a period of seven days. A concentration of 416 μM doxycycline was chosen based on the work carried out by Franco *et al.* (2006) and Li *et al.* (2014) wherein the authors showed that this sub-antimicrobial concentration significantly reduced contraction in cell-enriched collagen gels by 72 hours and 7 days respectively[258,259]. It has also been reported in numerous studies that removal of the MMP inhibitor from the FPCL supernatant resulted in reversal of its effect with FPCLs continuing to contract. To confirm that the effect of doxycycline on inhibiting gel contraction was correlated with its inhibition of MMP activity, MMP activity was assessed in samples that had been collected from FPCL supernatant. As with its effect on gel contraction, doxycycline inhibited MMP activity in the FPCL culture medium in a dose-dependent manner over a period of seven days.

3.5.2 Microneedle-assisted Strat-M™ membrane permeabilisation monitored by biomarkers in the FPCL model

Initially the FPCL model represented the structural and cellular components of the human dermis by containing fibroblasts, serum and the fundamental ECM component, type I collagen. However, there was no component that mimicked the skin barrier to intradermal drug delivery. Strat-M™ membrane, a non-animal derived synthetic membrane, was selected to act as an epidermal mimetic due to its reported human-like permeability properties and limited evaluations in the literature. From SEM analyses, the Strat-M™ can be structurally subdivided into two major layers — a lipophilic upper layer which replicates the structure and biochemical behaviour of the SC and a hydrophilic underlying layer that replicates the porosity of the upper dermis. When the Strat-M™ membrane was used to compartmentalise the FPCL from the doxycycline treatment, it was able to effectively prevent permeation of doxycycline to the underlying FPCL. This was determined since gel contraction was not inhibited and there was

no statistically significant inhibition of MMP activity compared with control. This corroborated the results reported in Chapter 2, wherein the Franz permeation cell study showed no presence of doxycycline in the receptor fluid when untreated Strat-M™ was placed into the Franz cell.

Once the inhibition of Strat-M™ on DOX permeation to the FPCLs had been ascertained, the effect of microneedle application on permeabilising the membrane was then investigated. Microneedles of 250, 500 and 750 μm in length were applied to the membrane's apical surface using a standardised vertical force of 3.8N. Microneedle application was able to sufficiently permeabilise the membrane, providing conduits for the doxycycline solution to diffuse through. Instead of directly measuring the amount of doxycycline that permeated to the FPCL, this was quantified through doxycycline's biological effect on reducing gel contraction and inhibiting MMP activity. The greater the inhibitory effect, the greater the volume of doxycycline that had reached the FPCL. It followed that for a fixed volume of 416 μM doxycycline solution the 750 μm microneedles permeabilised the Strat-M™ the most to doxycycline over a seven-day period, followed by the 500 μm and then 250 μm microneedles. This is in good concordance with the previous findings which showed that increasing microneedle length correlated with increased total cumulative doxycycline concentration in receptor compartments and an increased rate of drug permeation. The reason for this is likely to be two-fold. Longer microneedles create micropores with a greater entry area on the membranes apical surface. They also are able to penetrate through the entire 300 μm thick Strat-M™ membrane to a greater depth, creating a greater micropore annulus than shorter microneedles that may not fully penetrate the membrane, or do so to a lesser extent.

3.5.3 Microneedle application on injured skin and its effect on cell viability

Undesirable effects such as skin irritation and redness caused by microneedle application are difficult to gauge in *in vitro* systems due to their simplicity compared with the tissues they model such as a lack of blood supply. Safety of microneedle application on *in vivo* human skin has been widely investigated. Studies have reported on the pain sensation associated with microneedling on human subjects especially in comparison to hypodermic needles[166,257]. Localised irritation, redness, bleeding, crusting, oozing and infection and have also been investigated[166,262]. However, there is little reported in the published literature on the effect that microneedle application has on cell viability in *in vitro* systems. The effect of microneedle application on cell viability, especially on injured skin, is indeed an important consideration. Early stage pressure ulcers are at high risk of progression and disturbance of the upper layers may be enough to initiate that transition.

Apoptotic death signals can be propagated to neighbouring cells through connexin gap junctions. Gap junction proteins have an implicated role in various chronic ulcers including human venous leg ulcers and diabetic foot ulcers[253,263]. Gap junctions form hemichannels believed to be important in potentiating the effects of IR injury. IR injury has been hypothesised to cause (i) an up-regulation in the number of hemichannels and (ii) uncontrolled opening of these channels[254]. Through the combination of these effects, cell death can be initiated through cell lysis, metabolite loss, ATP leakage and excessive Na^+ and Ca^{2+} influx and the resultant stress and apoptotic death signals can be propagated to neighbouring cells *via* docked hemichannels[264]. Emerging evidence has suggested novel roles of hemichannels in IR injury. When these cells are communicating strongly in a stressed state these propagating signals will contribute to cell death in that area. If microneedle application stresses the cells and initiates a cascade of apoptotic death signal transduction it could possibly potentiate ulcer development.

The effect of microneedle application on fibroblast viability when applied against different surfaces was investigated in this study. Scratch assays are typically used to monitor cell migration of confluent layer of cells[265], for example, in response to small molecules in search for therapeutics[266]. The first substrate assessed was a confluent fibroblast monolayer grown on a polystyrene tissue culture plate. This acted as a hard rigid surface against which to apply the microneedles. A control scratch, made by scraping a p200 pipette across the monolayer, did not cause a significant loss in cell viability but rather displaced the cells creating a gap within the monolayer. Surrounding viable cells were observed to migrate into the gap within in 24 hours. This migratory behaviour is a standard response of healthy and proliferating cells, as been reported in the literature[265].

With microneedle application against the hard surface, there was very little depth penetration and, instead of displacing cells, a puncture was created in the substrate killing the cells directly contacted. After 24 hours there was no evidence of apoptosis or necrosis beyond the initial injury site. On the soft FPCL surface the control scratch, by the p200 pipette tip, disrupted the collagen matrix, creating a hole with necrotising cells observed around its perimeter. The microneedles, however, did not cause any microscopically observable disruption to the collagen matrix or cells, nor to the underlying polystyrene substrate. It is plausible that during application, the microneedle tips did not pierce through the FPCL meniscus, but rather compressed it. This is most likely due to the compressibility of the FPCL that mimics the structural integrity of the collagen-filled dermis. The results from the scratch wound models suggest that microneedle application in this *in vitro* system does not cause significant cellular damage in the FPCL after 24 hours with a vertical application force of 3.8N and that puncture injury is surface-dependent.

Figure 3.14 — Blood spotting after facial application with a microneedle roller system. From "Microneedling: Advances and widening horizons," by A. Singh and S. Yada, 2016, Indian Dermatology Online Journal, 7, p. 246.

Despite valid concerns surrounding safety, microneedling has been reported to have desirable responses on cell behaviour and ECM structure in sensitive skin[191,262,267]. Positive results with facial skin resurfacing in acne scar treatment have been observed and microneedling has been shown to improve skin appearance and encourage proliferation in previously or persistently inflamed skin, both alone and in conjunction with other therapies. Authors have also reported minimal irritation and redness that subsides[165,166], though bleeding, crusting and oozing after microneedle application on certain skin has been observed (**Figure 3.14**)[262]. This is likely to be highly dependent on microneedle length. Direct comparison between studies is difficult due to differences in the microneedles used, the anatomic site of application and the force of device insertion. One of the major attributes of a good penetration enhancer is that it should be non-irritant, as well as non-toxic and non-allergenic. Though much of the literature suggests that microneedling achieves this, more experiments involving its effect on chronic wounds need to be carried out.

3.5.4 Potential side effects of cutaneous doxycycline treatment

Doxycycline has well-documented side effects which includes skin sensitivity to UV light. As the intended application is cutaneous it is responsible to explore the potential problems this may create. A large proportion of the target patient population for doxycycline-based pressure ulcer

chemotherapy are hospitalised and immobilised so are generally protected from sunlight. Additionally, pressure ulcer sites are typically covered with hospital garments and wound dressings protecting them from the effects of indoor lighting. Notably, local and not systemic doxycycline delivery may prevent generalised photosensitivity. However, side effects can only be speculated and not ascertained at this stage without the appropriate clinical trials.

3.6 Future work

3.6.1 Improving the FPCL model and scratch wound assay

Future work should involve improvements to the FPCL model. The current FPCL model presented here has several limitations. One of its major criticisms is that it represents fibroblasts in a healthy, proliferative state with no external stressors on the cells. Ischemic cells are likely to respond very differently to healthy cells. Thus, the model should better replicate the pressure ulcer microenvironment with the appropriate cells and stimuli. This could be achieved through harvesting dermal fibroblasts from the wound beds or exudate of late stage pressure ulcers, or, through obtaining excision biopsies of tissue from early stage ulcers and out-growing them from the explant. This sort of FPCL model would better reflect the behaviour and secretion profiles exhibited in the chronic wound state.

The scratch wound assay for assessing the effect of microneedling on cell viability also has several limitations. The microneedles are only being applied to the dermal equivalent portion of skin since there is no epidermal component included in the model (i.e. no keratinocytes). Though the Strat-M^{TM} membrane is being used as model for the human epidermis, it itself is acellular. Bi-layered epidermal-dermal equivalents, compatible with the FPCL do exist however, where keratinocytes are seeded at the air interface between the FPCL and the culture medium surface[268]. This could be used to better investigate the effect of microneedling on the epidermal portion of cells.

3.6.2 Creating MMP-specific expression and activity profiles and using MMP-specific inhibitors

The use of MMP and/or TIMP multiplex profiling could be used to determine the exact activity profile and concentration ranges of MMPs already present in the FPCL supernatant and to what extent they are inhibited by doxycycline treatment (though this technique would be best suited in a model that better reflects the ulcer environment). A major assumption of the current model is that all MMPs behave the same, but the activity and/or expression of MMPs may not increase at the same amount and doxycycline has also been shown to inhibit different MMPs to different extents[269]. Preliminary work has been carried out to assess the profile of specific MMPs in the

FPCL model using a technique known as zymography (**Appendix D — MMP zymography of FPCL supernatant, *p. 261***).

Though doxycycline appears to be a suitable active drug in the treatment of pressure ulcers, the fact that it acts as a broad-spectrum MMP inhibitor may prove problematic if only specific MMPs need to be inhibited. One way to achieve this is through the use of MMP-specific inhibitors, especially against the MMPs of most interest in chronic wounds — MMPs 2, 8 and 9. The effect of inhibiting each MMP on different aspects of FPCL behaviour can then be investigated individually.

3.7 Conclusion

This chapter has outlined the development of an *in vitro* model of human dermis, the FPCL, in combination with the Strat-M™ membrane acting as an epidermal barrier to drug permeation. The FPCL is a simple, economical and reproducible model of the human dermis. This is the first study to report enhanced delivery of doxycycline through microneedled Strat-M™ membrane to FPCLs. While Chapter 2 focussed on an absolute permeation profile under infinite dose conditions, this body of work aimed to explore how the permeability of Strat-M™ to doxycycline could be assessed by biological markers of its activity in an *in vitro* system. This should give better indication of how doxycycline treatment may translate into *in vivo* experiments using clinically realistic concentrations and observing a biological response. In all, the current model is suitable as a preliminary *in vitro* drug assay but requires further development to better replicate the pressure ulcer microenvironment.

Chapter 4 Modelling the Pressure Ulcer Microenvironment in an *In Vitro* FPCL system

4.1 Introduction

There are several pathophysiological molecular mechanisms which together drive the onset, development and chronicity of pressure ulcers. These include the molecular effects of ischemia-reperfusion (IR) injury (induced by cycles of blood occlusion), local recruitment of inflammatory cells and the direct mechanical effects of intermittent loading on the skin tissue over prolonged periods of time. These features can be factored into *in vitro* dermal tissue equivalent models to better replicate the pressure ulcer microenvironment and the conditions leading up to their development.

4.1.1 Application of external pressure onto the FPCLs

Intermittent pressure on the skin over prolonged periods of time is a key risk factor in the development of pressure ulcers. The pressure associated with ulcer development is not traumatic — it is not great enough to crush muscle or bones — but it is sufficient to occlude blood flow and cause mechanically-induced damage to the tissue[18]. The pressure required to instigate pressure ulcer development has not been clearly defined but is often linked to the human capillary critical closing pressure (CCP) of 32 mmHg[35]. Application of pressures greater than or equal to 32 mmHg for two hours has been shown to cause local ischemia, with periods of more than six hours leading to tissue necrosis[270]. Capillary CCP is the minimum pressure required to occlude blood flow within the capillaries that supply regional body tissues including the skin. However, the exact pressure exerted at sites where pressure ulcers eventually develop in patients will vary from individual to individual and is also likely to be greater than the capillary CCP threshold. The pressure exerted on the skin is dependent on several factors:- the mass of patient and its distribution, for example whether the mass is concentrated on a single point like over a bony prominence such as the heel or sacrum, and the rigidity of the external support surface such as the mattress or wheelchair[271]. Moreover, the pressure required to potentiate pressure ulcer development may be less than the CCP threshold in particularly

vulnerable patients who have other major risk factors such as very fragile aged skin and co-morbidities such as vascular disease[272].

The effect of mechanical loading on fibroblasts in skin can be simulated by applying external pressure onto the collagen gels. In an *in vitro* fibroblast-populated collagen lattice (FPCL) model using ocular fibroblasts, the pathological pressure associated with Grave's orbitopathy, a disfiguring eye disease, was simulated on collagen gels using a metal insert[273]. This insert had been designed to deliver a pressure onto the gels equivalent to the injurious pressure reported in Grave's orbitopathy of 28 mmHg. The authors reported that this pressure had an effect on the contractile and protein expression profiles of the cellularised collagen gels. Since a pressure of 32 mmHg is enough to incite blood occlusion in human skin it is reasonable to introduce this into the FPCL model to replicate the effect of ulcer-inducing pressure.

4.1.2 Recruitment of inflammatory cells at the wound site

Another component deemed integral in pressure ulcer etiopathogenesis and chronicity is the recruitment and presence of inflammatory cells in the injured tissue[109]. Inflammation is a fundamental step in normal wound healing and the crosstalk between fibroblasts and inflammatory cells including macrophages and neutrophils drives several important processes before the proliferative stage of healing can take place[244]. Neutrophils release proteolytic enzymes responsible for digesting invading bacteria and removing non-viable cellular debris[274]. Macrophages are cytokine-producing immune cells that affect surrounding cells at injured sites, including the resident fibroblasts. Monocytes circulating in the bloodstream are stimulated to differentiate into macrophages by stress signals released from the wound site. Macrophages then migrate into the injured tissue where they release cytokines and enzymes to mediate inflammatory processes. Activated macrophages increase local matrix metalloproteinase (MMP) levels through secretion of collagenases, that help debride the wound, and activation of fibroblasts[83,109,275,276]. They also stimulate fibroplasia and fibroblast-mediated collagen production through secretion of tumour necrosis factor (TNF), interleukins, and synthesis of nitric oxide[57].

Even though inflammation is essential to wound healing, prolonged unabated inflammation with no progression to the proliferative stage is not conducive to healing and, in fact, results in tissue damage. Studies investigating chronic wound fluid composition have reported significantly higher levels of proteolytic and collagenolytic activity compared with healing dermal wounds[102,104,111]. This indicates that high levels of MMP activity are linked to the non-healing characteristic of chronic wounds. In the original FPCL model outlined by Bell *et al. (*1979*),* the collagen gels were exclusively populated with fibroblasts[250]. However, in isolation

from immune and inflammatory cells, fibroblast behaviour is far from what would be exhibited as a pressure ulcer develops. Macrophages can be introduced into collagen gels in co-cultures with fibroblasts to produce fibroblast and macrophage-populated lattices (FMPCLs). The interaction and response of fibroblasts to the presence of macrophages should better simulate the cell behaviour that would be exhibited within a site where a pressure ulcer develops.

4.1.3 Effect of glucose deprivation on pressure ulcer development

Under raised tissue pressure, ischemia induces hypoxia and glucose deprivation leading to compromised cellular function since vital nutrients cannot reach the cells and cellular waste cannot be transported away[90]. The result is cell starvation, necrosis — unprogrammed cell death — and tissue loss[65]. Furthermore, wound healing is an energy-dependent process which requires an adequate supply of adenosine triphosphate (ATP)[57]. The proliferative phase of wound healing in particular requires increased metabolism and protein synthesis for tissue repair. This, in turn, requires a rich blood supply of oxygen and glucose. In the absence of a continual supply of these nutrients, wound healing is impaired[57]. Glucose deprivation can be simulated in the FPCL model by culturing the collagen gels in glucose-free culture medium. The effect on protein expression, collagen biosynthesis, gel contraction and matrix degradation can then be monitored under these conditions[277,278].

4.2 Research outline

In Chapter 3, it was shown how sub-antimicrobial concentrations of doxycycline were able to reduce MMP-mediated gel contraction in the FPCL model. However, the model was comprised of a normal population of fibroblasts that were not exposed to the same external and internal stressors responsible for pressure ulcer etiopathogenesis. To better replicate the pressure ulcer microenvironment these stressors can be introduced to the FPCLs, individually and in combination. This chapter outlines a series of experiments wherein macrophages, glucose deprivation and external pressure were introduced into the model (**Figure 4.1**). It was anticipated that these three processes would have a significant impact on the gel's contractile profile by augmenting MMP activity and by potentially affecting other processes. The ability of doxycycline to counteract any changes was also explored.

Firstly, macrophages were resuspended with fibroblasts to form a fibroblast-macrophage co-culture which was then used to cellularise the gels. The macrophages were derived from monocytes by phorbol myristate acetate (PMA) stimulation. The effect of macrophages on gel contraction and MMP activity was assessed. It was also important to assess the effect of macrophages alone on gel contraction to rule out any contractile behaviour they may have.

Secondly, external pressure was applied to FPCLs using a custom-made metal insert based on the work carried out by Li *et al*. (2014) in their model of Grave's orbitopathy[273]. A pressure of 32 mmHg was applied for 1.5 hours before being removed, equivalent to the period of time reported between patient turning in the hospital setting[3]. The effect of compression on FPCL contraction, MMP activity and cell viability was explored. Finally, FPCLs underwent glucose deprivation by culturing them in glucose-free medium. The effect of pre-conditioning the FPCLs to glucose deprivation was also assessed. In all, the results in this modified FPCL model provided indications on which mechanisms implicated in pressure ulcer development result in significant changes in gel contraction and MMP activity making them most treatable by doxycycline.

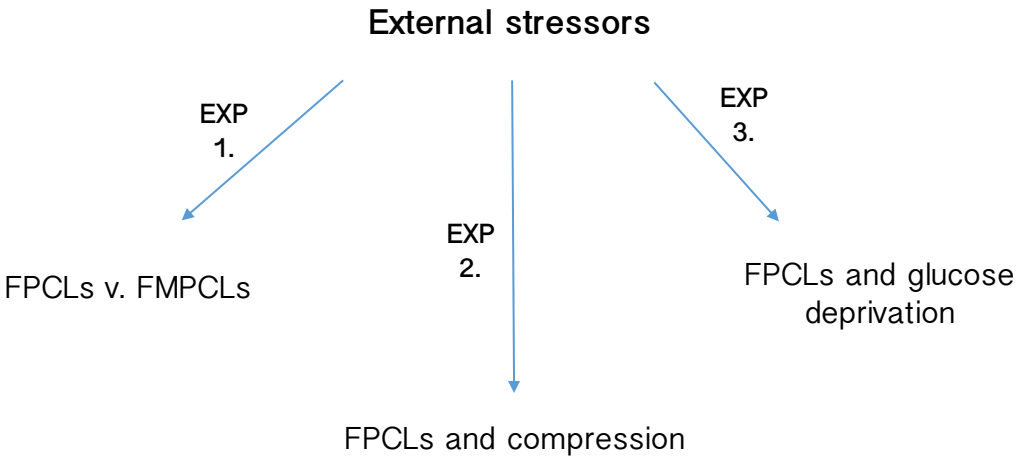

Figure 4.1 — Schematic summarising the three arms of experiments carried out in Chapter 4 which investigate the effect of external stressors on FPCL contractile behaviour and local MMP activity: (i) the effect of introducing macrophages on the FPCLs, **(ii)** the effect of 1.5 hours of external pressure on the FPCLs, and **(iii)** the effect of glucose deprivation on the FPCLs.

4.3 Methods and materials

4.3.1 Human dermal fibroblasts

Please refer to **Method 3.3.1, *p.118*.**

4.3.2 U937 monocytes

Cell culture

U937 monocytes are human monocytes that were originally harvested from the lymphoma of a cancer patient and are routinely used to study the differentiation and behaviour of monocytes. Under specific conditions, U937 monocytes can be stimulated to differentiate into activated macrophages which exhibit a different morphology, cytokine secretion profiles and adherence properties compared with their precursor[279,280]. U937 monocytes (American Type Culture Collection, Vancouver, USA) were grown in suspension in complete Rosswell Park Medical Institute (RPMI)-1640 medium (Sigma-Aldrich, Poole, UK) supplemented with 10% (v/v) FBS (Gibco, Paisley, UK) in vented T75 cm^2 flasks (Thermo Fisher Scientific, Loughborough, UK). Their environment was maintained at 37^oC and 5% CO_2 in a fully-humidified incubator. Cell suspension density was maintained between 1 x 10^5 and 2 x 10^6 cells per ml by regular counting with trypan blue every three days. Excess cells were aspirated and the culture replenished with fresh medium.

Stimulating U937 monocyte differentiation using phorbol myristate acetate (PMA)

Phorbol myristate acetate (PMA) is a compound that can stimulate monocyte differentiation to macrophages by mimicking an activator of protein kinase C (PKC). Activation of PKC initiates a signal transduction pathway which induces adherence, cell cycle arrest and differentiation[281]. PMA powder (Sigma-Aldrich) was dissolved in an aqueous solution to create a 5 mM PMA stock. PMA stock was diluted at 1% (w/v) in RPMI medium to create a 5 µM PMA solution. A final concentration of 150 nM PMA was made by adding the 5 µM PMA solution to RPMI medium containing 2 x 10^6 of monocytes and making up the remaining volume with RMPI medium. Cells were cultured in vented T75 cm^2 flasks (Thermo Fisher Scientific) for 72 hours at 37^oC and 5% CO_2 in a fully-humidified incubator. After 72 hours of differentiation, cell media and floating undifferentiated cells were aseptically aspirated and replenished with fresh medium. Cells were left to differentiate for a further 48 hours. Differentiated cells adhered to the flask and appeared as grape-like clumps. They were detached by washing once with PBS and treatment with trypsin-EDTA solution [0.02 mM trypsin-0.48 mM EDTA 4Na $2H_2O$ solution (Sigma-Aldrich)], followed by removal of remaining cells from the bottom of the flask using a sterile cell scraper (Sigma-Aldrich). The cell-trypsin suspension was neutralised with

complete RPMI medium and viable cell count determined by trypan blue exclusion staining using a hemocytometer.

4.3.3 Co-culture of differentiated monocytes with dermal fibroblasts

Volumes of medium containing 1 x 10^5 human dermal fibroblasts and 1.5 x 10^5 differentiated U937 monocytes were added together in a 30 ml Universal tube. The cells were pelleted by centrifugation at 1500 rpm for 5 minutes at room temperature. The cell pellets were resuspended in 100 µl of FBS or in 100 µl of serum-free DMEM for non-FBS treated groups. Collagen gels were synthesised as previously described (**Method 3.3.2, *p. 119***) using 100 µl of the re-suspended fibroblast-macrophage co-culture in place of 100 µl of fibroblasts. Fibroblast to macrophage ratios of 1:2 and 1:4 were also used.

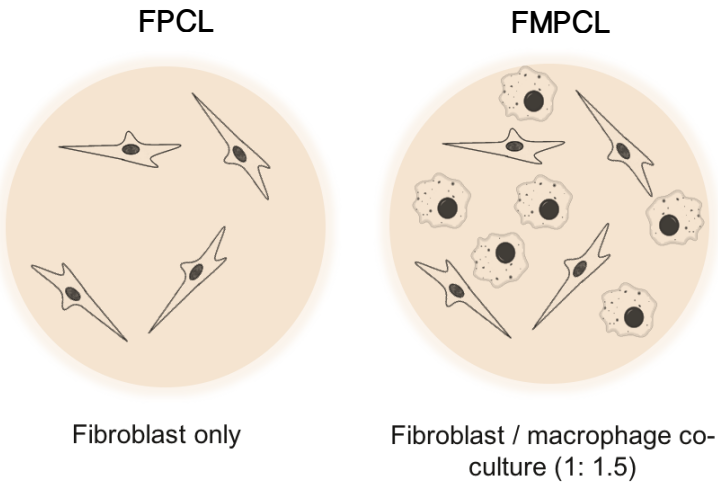

Figure 4.2 — Schematic representation of the two types of collagen gels. Collagen gels populated exclusively with fibroblasts (FPCLs) (*right*) and cellularised with a fibroblast-macrophage co-culture (FMPCLs) at a ratio of 1:1.5 (*left*).

4.3.4 Mechanical loading of FPCLs using a bespoke metal insert

Collagen gels, populated exclusively with fibroblasts (FPCLs) were allowed to polymerise within the microwells of MatTek plates (MatTek Corp., Massachusetts, USA) for 1 hour. External pressure, equivalent to the capillary closing pressure of 32 mmHg, was applied to the gel using a custom-made brass rod as a metal insert. The rod was designed with a 10mm diameter — to match the diameter of the MatTek plate's microwell — and had a mass of 32.4 g to deliver the target pressure based on the rod's density and height.

The rod was applied to the FPCL by firstly laying a fine sterile fabric mesh and a 10 mm diameter coverslip on top of the gel's apical surface, followed by careful placement of the rod on top (**Figure 4.3**). The coverslip and the mesh prevented the gel from sticking to the coverslip. The rod was secured in place by a custom holder to prevent it from moving. One ml of complete DMEM (for untreated FPCLs) or 416 µM doxycycline solution (for treated FPCLs) was pipetted into the well. Wells without FPCLs had the experimental solution and the compression apparatus added to serve as background controls for MMP activity. Due to the height of the rod and the presence of a holder, the experimental apparatus needed to be placed into a vented container to maintain sterility whilst in the incubator. The container with the apparatus inside was incubated at 37^{o}C with 5% CO_2. After 1.5 hours the rods, along with the coverslips and net mesh, were carefully removed from the gels and the plates returned to the incubator for the remainder of the experiment.

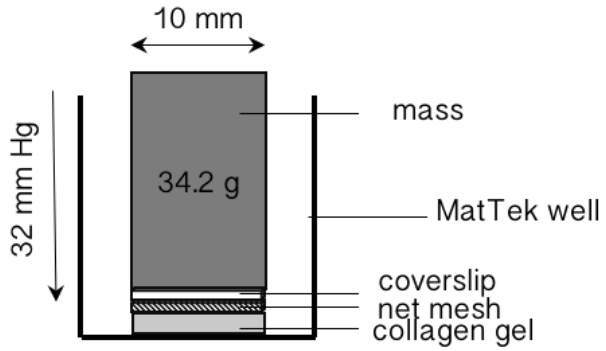

Figure 4.3 — Schematic representation of the compression apparatus used to apply external pressure onto the collagen gel. The custom-made brass rod had a 10 mm diameter to match that of the microwell.

4.3.5 Assessing the effect of mechanical loading on cell viability in FPCLs

Cell death in FPCLs that experienced mechanical loading was quantified using the 'Live/Dead Viability and Cytotoxicity' assay (Molecular Probes^{TM}, Oregon, USA) for mammalian cells, a fluorescence-based kit designed to differentiate between live (viable) and dead (non-viable) cells. Calcein-AM is used to distinguish live cells while ethidium homodimer-1 (Ethd-1) is used to distinguish dead cells. The non-fluorescent calcein-AM is enzymatically converted to the highly fluorescent calcein by intracellular esterase activity and is retained within the live cells. Ethd-1 enters dead cells with damaged membranes becoming fluorescently enhanced by

binding to their nucleic acids but is excluded by the intact plasma membranes of live cells. Together these stains are able to provide superimposable fluorescence signals that identify specific regions of cell death amongst healthy cells.

For the assay, medium was aspirated from the FPCLs, which were then gently washed with sterile phosphate-buffered saline (PBS). A staining mixture consisting of x1 Dulbecco's PBS [10 mM PO_4^{3-}, 137 mM NaCl, 2.7 mM KCl] (Sigma-Aldrich) with 0.2% (v/v) Ethd-1 [2 mM in DMSO/H_2O 1:4 (v/v)] and 0.1% (v/v) Calcein-AM [4 mM in anhydrous DMSO] was added onto the gels and allowed to stain for 1 hour at room temperature protected from light. The staining mixture was then aspirated from the FPCLs and the FPCLs gently washed again with PBS. Stained gels were imaged under a fluorescent microscope (Leica DMI6000 B; Leica Microsystems) with an N PLAN 10.0 x 0.25 dry objective. The fluorescence from these dyes was observed separately. Calcein-AM was excited by a 488 nm (L5 cube) wavelength laser producing a green fluorescent signal in the cell cytoplasm and Ethd-1 by a 647 nm (Y3 cube) wavelength laser producing a red fluorescent signal. Images of the two fluorescent signals were overlaid to determine regions of cell death in the gels and relative proportions of live to dead cells. Six regions of interest (ROIs) of 250 µm x 250 µm were randomly selected from six different composite images of control gels and gels that had been exposed to an external pressure of 32 mmHg. The number of live and dead cells was measured using ImageJ® (National Institutes of Health [NIH], Maryland, USA). The 'colour threshold' and 'analyse particles' tools outlined and counted the cells with thresholds based on fluorescence intensity, size and circularity. The proportion of live and dead cells was then calculated as a percentage of total cells.

4.3.6 Depriving FPCLs of glucose

Glucose deprivation is a consequence of occlusion of blood flow through the capillary networks that supply the skin and can be brought about when high enough pressure is exerted onto the blood vessels. FPCLs were exposed to glucose deprivation by culturing them in glucose-free medium (Gibco). FPCLs were cultured in the usual high-glucose DMEM (4.5mg/ml [25 mM] glucose). All DMEM was supplemented with (v/v) 10% FBS (Gibco) and (v/v) 1% of PSA [10, 00 units/ml penicillin, 10 mg/ml streptomycin, 25 µg amphotericin B] (Sigma-Aldrich) and contained 584 mg/ml [4 mM] L-glutamine. FBS was included in the culture medium since it had already been determined in FPCL models that there was no fibroblast-mediated gel contraction in the absence of FBS[282] and this was corroborated by preliminary results reported here. A separate set of fibroblasts were pre-conditioned to glucose deprivation by sub-culturing them in the absence of glucose for four days prior to the experiment.

4.3.7 Gel contraction analysis

Digital photographs of the gels were taken on days 1, 3, 6 and 7 and analysed for percentage gel contraction as previously described (**Method 3.3.2**, ***p. 119***).

4.3.8 MMP activity assay analysis

Supernatant (75 µl) collected from the samples on days 0, 3 and 7 were analysed by the MMP activity assay as previously described (**Method 3.3.3**, ***p. 121***).

4.3.9 Statistical analyses

For each condition there were six replicates (unless otherwise stated) to allow for experimental variation. Data were analysed using a two-way ANOVA with Tukey correction for multiple comparisons. Averages are represented by the mean ± standard error of the mean (SEM). In all instances, $p < 0.05$ denotes a statistically significant difference.

4.4 Results

4.4.1 Effect of fibroblast-macrophage co-culture on collagen gel behaviour

Monocytes were stimulated to differentiate into activated macrophages using PMA and were then introduced into the collagen gels in co-culture with dermal fibroblasts (**Figure 4.4**). The results show that the presence of macrophages in the co-culture (FMPCLs) significantly increased gel contraction compared with gels populated with fibroblasts alone (FPCLs) ($p < 0.0001$) (**Figure 4.5 – A**). Additionally, macrophages were able to induce gel contraction even in the absence of FBS (the component of culture medium required for gel contraction in the original FPCL model) (**Figure 4.5 – B**). However total gel contraction was significantly reduced compared with serum-treated FMPCLs. In the absence of FBS, FPCLs experienced negligible contraction by day 1 and did not show their typical contractile profile over the seven-day experiment remaining at around 5% gel contraction throughout. A range of fibroblast to macrophage co-culture ratios was used to investigate whether increasing the number of macrophages to fibroblasts augmented gel contraction and MMP activity (**Figure 4.6 – A and B)**. This was shown not to be the case and maximum contraction was observed with a ratio of 1:1.5 fibroblasts to macrophages.

Doxycycline solution (416 µM) was added to the FPCLs and FMPCLs to compare its inhibitory effect on gel contraction between the two gel types. A macrophage to fibroblast ratio of 1:1.5 was chosen for the FMPCLs since it had had the greatest effect on augmenting gel contraction

observed in the FPCLs compared with other ratios. In the FMPCLs, doxycycline significantly inhibited gel contraction over the seven-day experiment ($p < 0.0001$) (**Figure 4.7 – A**). Gel contraction of doxycycline-treated FPCLs was significantly less than doxycycline-treated FMPCLs on days 1, 3 6 and 7 ($p < 0.0001$) (**Figure 4.7 – B**). For MMP activity, doxycycline treatment significantly inhibited the increase in MMP activity observed in the FMPCLs on days 3 and 7 ($p < 0.0001$).

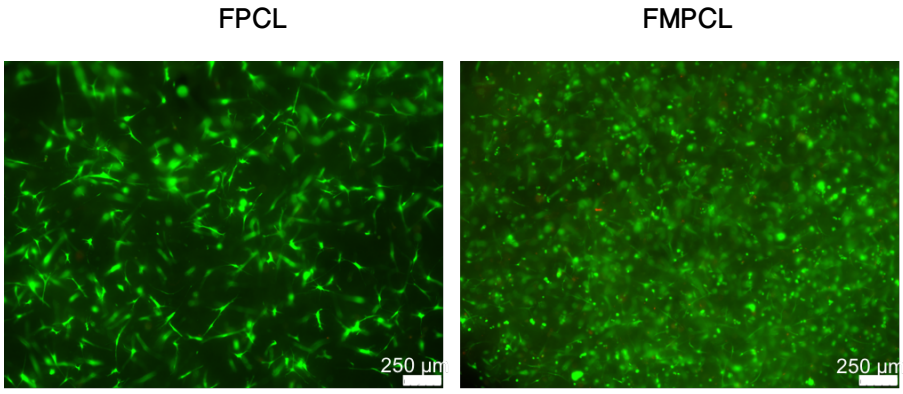

Figure 4.4 — FPCLs and FMPCLs were stained for viable cells with calcein-AM (green fluorescent signal) after 72 hours of incubation: (A) FPCLs are seen with fibroblast of spindle-shaped morphology. **(B)** Collagen gels populated with a co-culture of dermal fibroblasts and macrophages (FMPCLs) at 1:1.5 ratio. Macrophages have a more rounded morphology and are found in grape-like clumps. Due to the co-culture there are considerably more cells in the FMPCLs than the FPCLs. Background signals are caused by auto-fluorescence from the collagen gel.

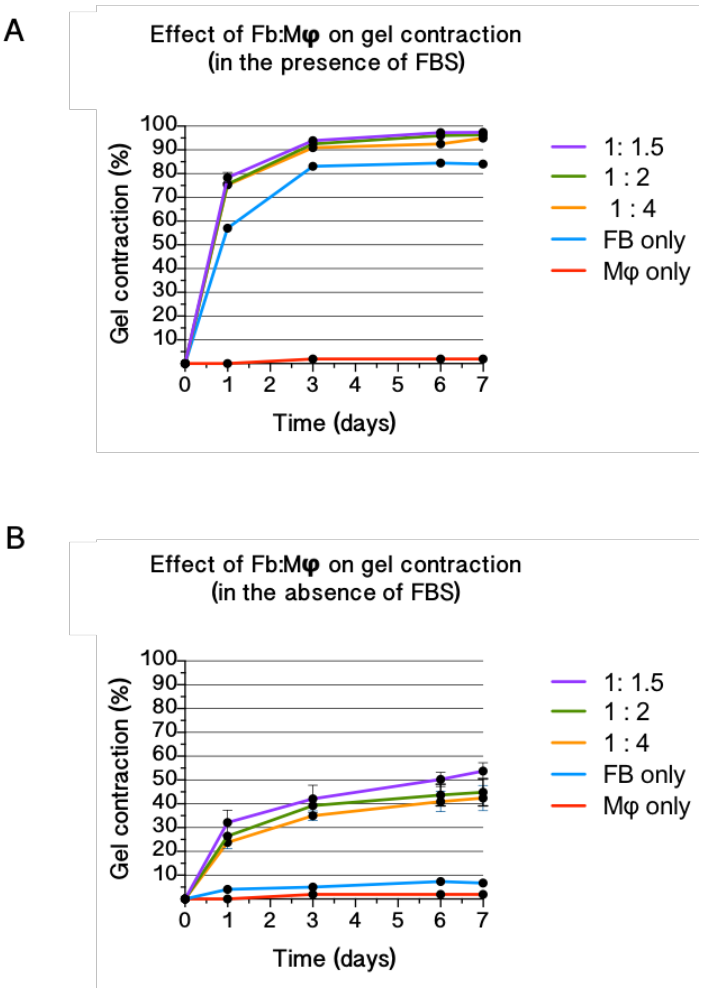

Figure 4.5 — Effect of co-culturing dermal fibroblasts [FB] with macrophages [Mφ] on FPCL gel contraction (n = 6): (A) Co-cultures of fibroblasts and macrophage as FMPCLs at a ratio of 1:1.5, 1:2 and 1:4 incubated in FBS-enriched DMEM resulted in significantly increased gel contraction on days 1, 3, 6 and 7 compared with fibroblast-only gels (FPCLs). Macrophage-only gels did not show any contractile behaviour. **(B)** FMPCLs grown in FBS-free DMEM resulted in significantly reduced contraction compared with those grown in FBS-enriched medium. FPCLs and macrophage-only gels exhibited negligible contraction under serum-free conditions. *Error bars represent the standard error of the mean; ** $p < 0.01$, *** = $p < 0.001$ **** = $p < 0.0001$.*

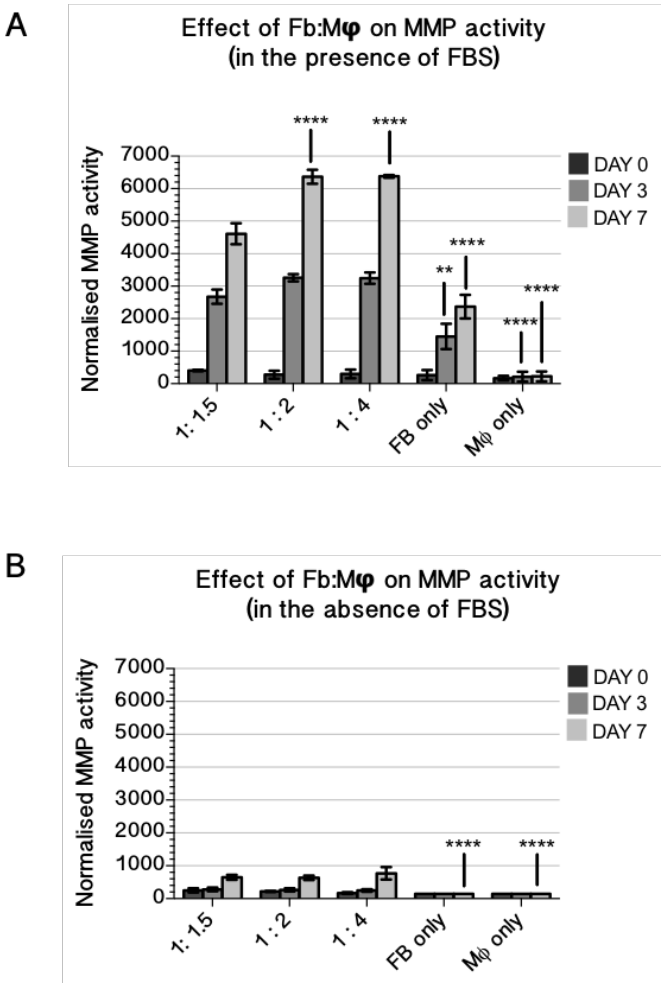

Figure 4.6 — Effect of co-culturing dermal fibroblasts [FB] with macrophages [Mφ] on MMP activity (n = 6): (A) MMP activity profiles of FMPCLs were significantly greater than that of FPCLs. Macrophage-only gels did not show an increase in MMP activity levels. **(B)** For gels grown in FBS-free medium, MMP activity was dramatically reduced for FMPCLs while FPCLs and macrophage-only gels did not show any increase in MMP activity. *Error bars represent the standard error of the mean; ** = $p < 0.01$, **** = $p < 0.0001$ and denotes statistically significance in comparison to fibroblast-only gels (FPCLs).*

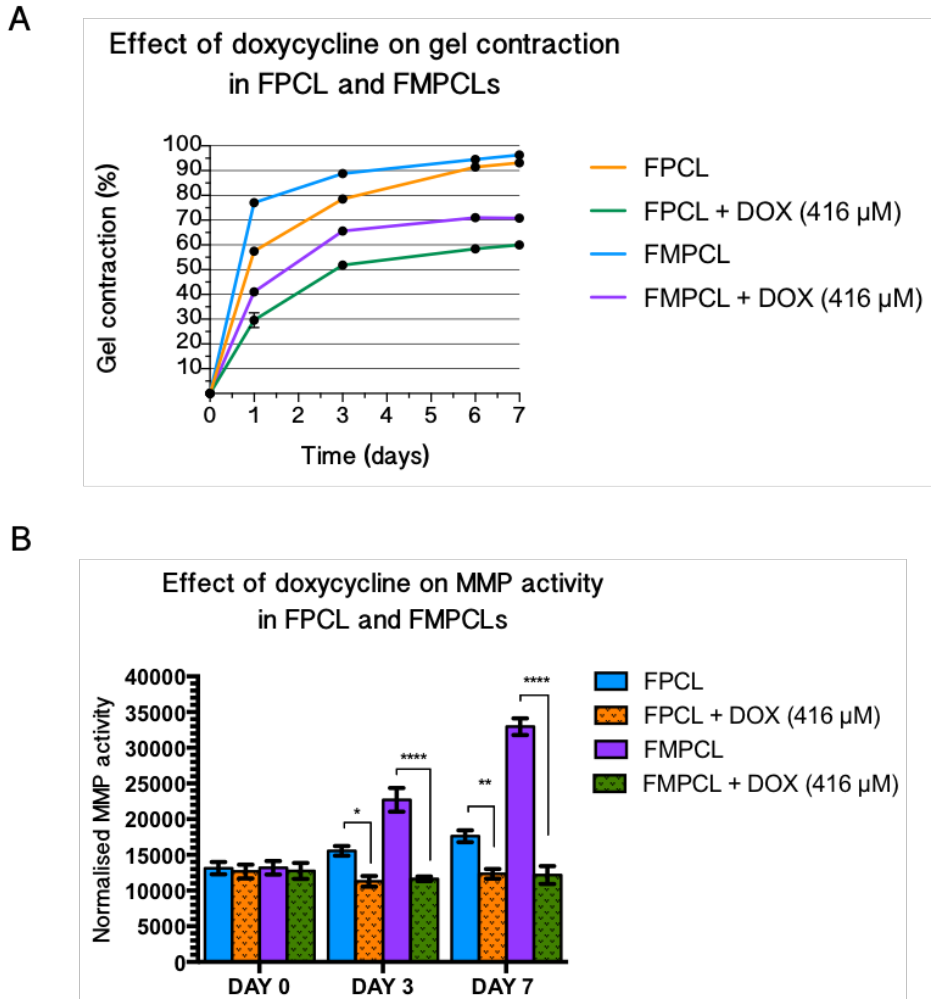

Figure 4.7 — Effect of doxycycline treatment (416 µM) on gel contraction and MMP activity in FPCLs compared with FMPCLs (n = 6): (A) Treatment with 416 µM doxycycline significantly reduced gel contraction in both FPCLs and FMPCLs to a similar extent over the seven-day experiment. **(B)** Doxycycline treatment significantly inhibited the increase in MMP activity measured in the FMPCL supernatant, which was greater compared with the FPCL on days 3 and 7. *Error bars represent the standard error of the mean; * = p <0.05, ** p < 0.01, **** = p < 0.0001.*

4.4.2 Effect of mechanical loading on FPCLs

FPCLs were subjected to external pressure through the application of a custom-made rod onto their apical surface. The rod was designed to deliver a pressure of 32 mmHg onto the FPCLs equivalent to human capillary CCP. The pressure was applied for 1.5 hours, in concordance with the time period between patient turning reported in the literature. Control FPCLs and FPCLs treated with 416 µM doxycycline solution were observed to contract as previously reported (**3.4.1 Results, *p. 125***). However, FPCLs treated with an external pressure of 32 mmHg for 1.5 hours exhibited significantly reduced gel contraction compared with control ($p < 0.05$) with 12.7 ± 1.1%, 22.8 ± 1.4%, 23.0 ± 1.6% and 24.4 ± 0.4% gel contraction on days 1, 3, 6 and 7 respectively (**Figure 4.7**) (**Figure 4.9 – A)**. Treatment with 416 µM doxycycline solution on these gels did not significantly inhibit gel contraction, with 8.48 ± 1.1%, 18.6 ± 1.4%, 18.3 ± 1.6% and 18.6 ± 2.4% gel contraction observed on days 1, 3, 6 and 7 respectively. As with the gel contraction profiles, the control FPCLs and FPCLs treated with 416 µM doxycycline solution exhibited the expected pattern of MMP activity (as previously reported in **Figure 3.6 – B**). Control gels showed an increase in MMP activity from days 0 to 7 while gels treated with doxycycline had MMP activity levels maintained at levels similar to day 0 (**Figure 4.9 – B**). Gels that underwent mechanical loading exhibited a continual reduction in MMP activity between days 0 and 7.

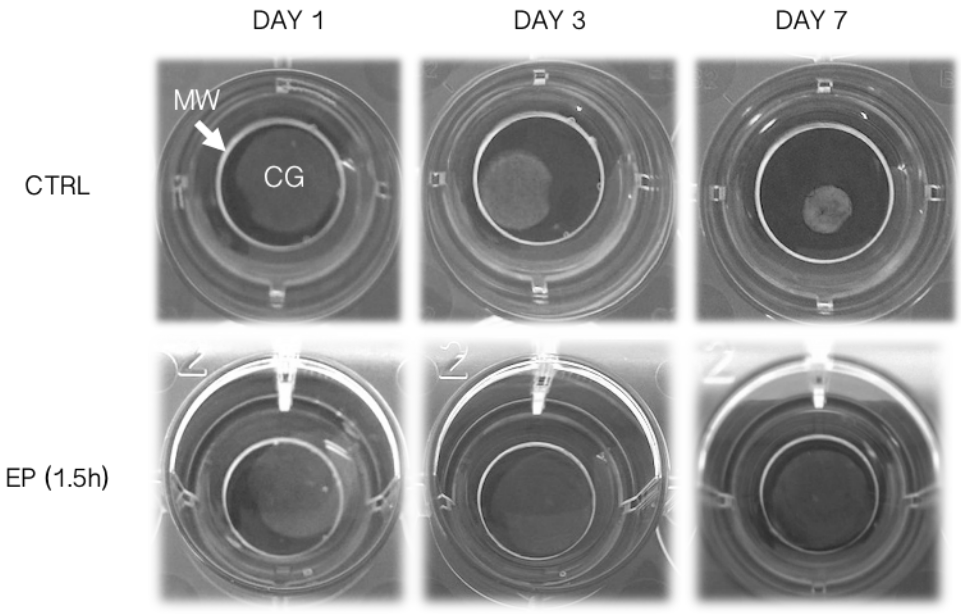

Figure 4.8 — Digital photographs mapping the gel contraction of FPCLs and FPCLS that experienced mechanical loading on days 1, 3 and 7. FPCLs were seeded into microwells [MW] on day 0. Control FPCLs [CTRL] that were not exposed to pressure followed the normal contractile pattern over the seven-day experiment. Compressed FPCLs that were exposed to an external pressure of 32 mmHg for 1.5 hours (EP [1½h]) contracted slightly by day 3 but did not contract any further by day 7.

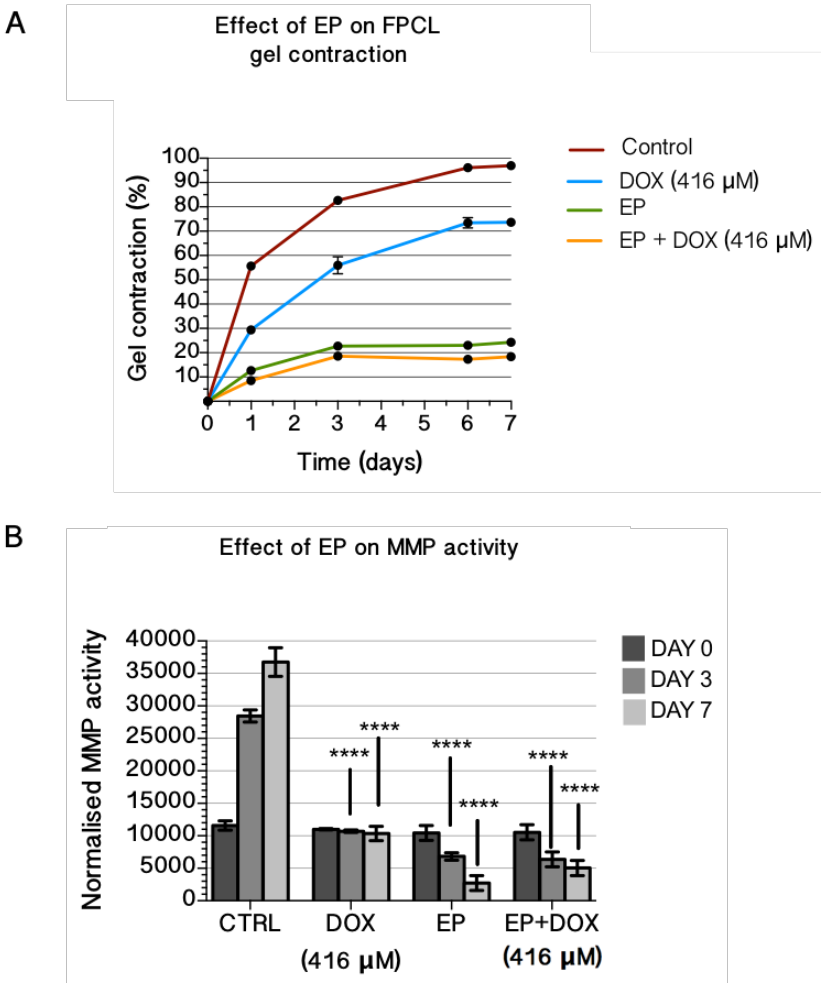

Figure 4.9 — Effect of mechanical loading through application of external pressure [EP] on FPCLs (n = 6): (A) Control FPCLs and FPCLs treated with 416 µM doxycycline solution followed the previously reported contractile pattern. Application of EP (32 mmHg for 1.5 hours) on the FPCLs resulted in significantly reduced gel contraction ($p < 0.0001$) on all days compared with control FPCLs, with no further contraction beyond day 3. FPCLs which experienced mechanical loading and that were then treated with 416 µM doxycycline did not exhibit significantly inhibited gel contraction compared with those that did not receive any doxycycline treatment. **(B)** Treatment with 416 µM doxycycline inhibited the increase of MMP activity in FPCLs on days 3 and 7. FPCLs that had experienced mechanical loading showed a significant drop in MMP activity levels that was not affected by treatment with doxycycline. *Error bars represent the standard error of the mean; **** = $p < 0.0001$ and represents statistical significance compared with control FPCLs [CTRL] .*

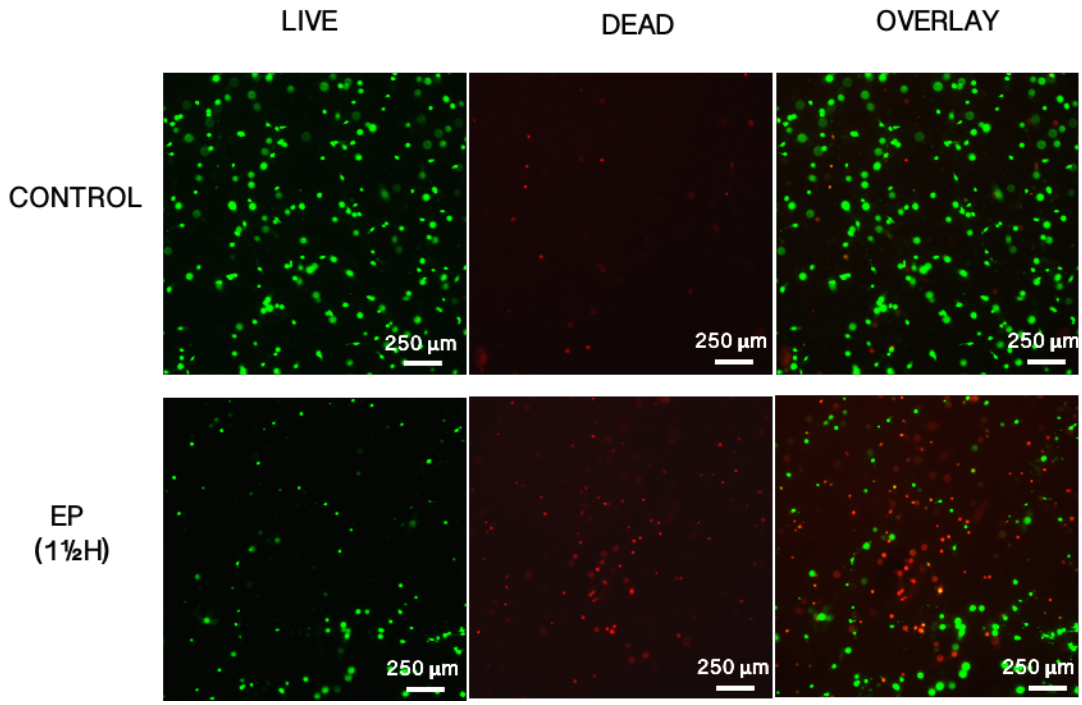

Figure 4.10 — Effect of mechanical loading on cell viability in FPCLs using the live/dead detection staining. An external pressure of 32 mmHg was applied onto the FPCLs for 1.5h followed by a 24-hour incubation period at 37°C. FPCLs were then stained with Ethd-1 and calcein-AM. Green fluorescence signals indicate live cells and red fluorescence signals indicate dead cells.

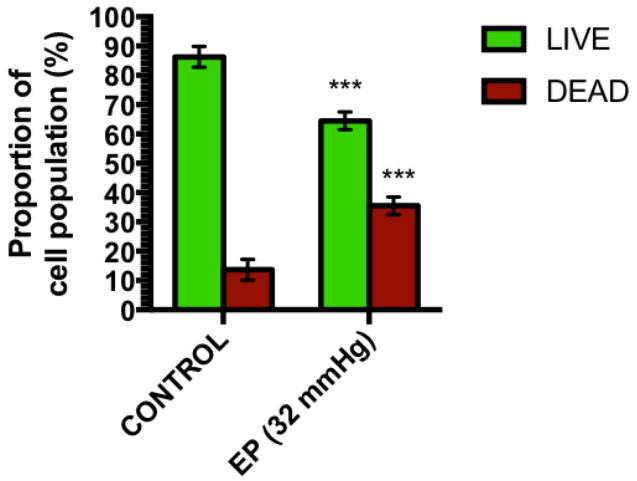

Figure 4.11 — Proportions of the cell population that stained as live or dead in FPCLs after mechanic loading (n = 6). The bar graph shows the comparison between FPCLs that did not experience external pressure (EP) and FPCLs that had experienced an EP of 32 mmHg for 1.5 hours. Mechanical loading resulted in a significantly increased proportion of cells that stained as dead. *Error bars indicate the standard error of the mean; *** = $p < 0.001$ and represents a statistical difference compared with control FPCLs.*

The effect of mechanical loading on cell viability in control gels was assessed using fluorescence staining that distinguished between live and dead cells (**Figure 4.10**). Gels that underwent mechanical loading for 1.5 hours at 32 mmHg had a significantly greater proportion of dead to live cells compared with control gels (**Figure 4.11**). The gels were also notably thinner and flatter compared with control gels when observed microscopically under the same field of view and had a reduced number of planes from the top-most to bottom-most planes at consistent increments.

4.4.3 Effect of glucose deprivation on FPCL contractile behaviour

In the glucose deprivation experiments, FPCLs containing unconditioned or pre-conditioned fibroblasts were cultured in glucose-free medium. No statistical difference was observed between the contraction profiles of high-glucose and glucose-free groups during the seven-day experiment (**Figure 4.12**). There was also no significant difference between the gels containing pre-conditioned and unconditioned cells over this same period.

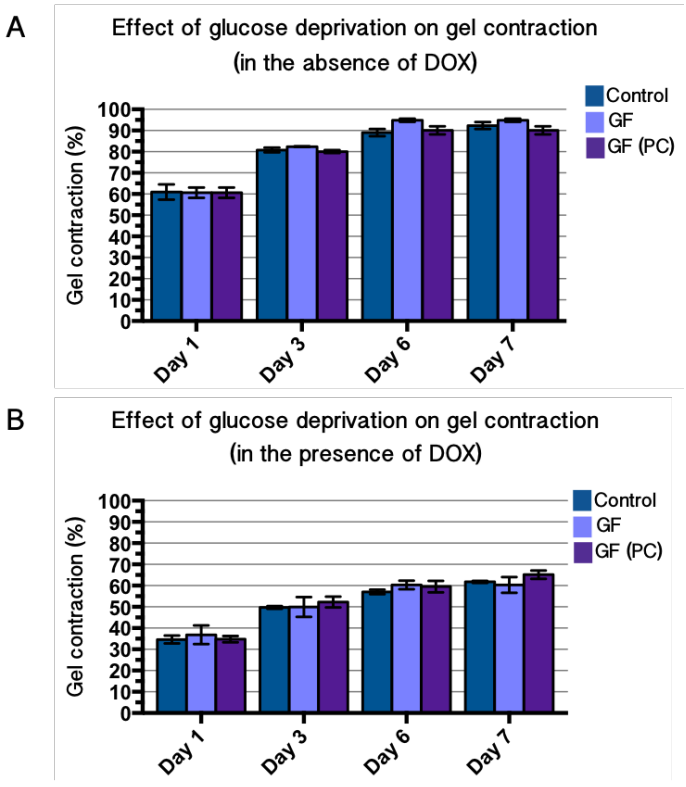

Figure 4.12 — Comparison of gel contraction between FPCLs cultured in glucose-enriched medium (Control), glucose-free medium with unconditioned fibroblasts (GF) and with pre-conditioned fibroblasts [GF(PC)] on days 1, 3 and 7 (n = 6): (A) In untreated FPCLs, no statistically significant difference in gel contraction was observed between the three groups. **(B)** For FPCLs treated with 416 µM doxycycline solution, no statistically significant difference in gel contraction was observed between the three groups. *Error bars indicate the standard error of the mean.*

4.5 Discussion

Pressure ulcers are chronic non-healing wounds characterised in their later stages by large open sores filled with proteolytic exudate. In the earliest stages, pressure ulcer development is instigated by: (i) external stressors, (ii) several normal physiological mechanisms that become aberrant under stress, (iii) in combination with the appropriate patient risk factors. IR injury, which is caused by on-going cyclic mechanical loading on the skin at pressures greater than or equal to capillary CCP, is currently believed to be the main cause of pressure ulcer development[95]. IR injury results in tissue breakdown and prolongs the inflammatory stage of wound healing. Additionally, the mechanical loading responsible for the IR injury is itself reported to cause direct physical damage to cells and tissues[18]. These stressors can be included in tissue equivalent models to better predict the effect that potential therapeutic drugs would have in inhibiting, reversing or resolving the associated pathological mechanisms *in vivo*. In this chapter, mechanical loading, activated macrophages and glucose deprivation were introduced to the FPCLs through modifications to the original model by Bell and colleagues[250].

4.5.1 Macrophage co-culture and FMPCL contractile behaviour

Macrophages significantly augmented the initial rate of contraction of FMPCLs compared with FPCLs. By adding activated macrophages in co-culture with fibroblasts, the rate of gel contraction between days 1 and 3 was greater than that seen with fibroblasts alone ($p < 0.0001$). Additionally, total gel contraction by day 7 was significantly greater in the FMPCLs than the FPCLs. This was as expected, since macrophages are known to bolster MMP levels[85], including collagenases, and this was further corroborated by the MMP activity profiles which showed that the presence of macrophages caused a marked and significant rise in MMP activity ($p < 0.0001$). Notably, macrophages on their own did not exhibit any contractile properties since they lack the contractile apparatus to do so. They also did not significantly increase MMP levels on their own. This suggested that their effects were mediated through their interactions and signalling with the fibroblasts. When a wound is created, macrophages are recruited to the site of tissue injury and communicate with the resident fibroblasts as part of an inflammatory response. Since pressure ulcers are known to be in a persistent inflammatory state, interaction and modulation of behaviour between the activated macrophages and fibroblasts are likely to be significant.

FPCLs were cultured in serum-free media to assess the effect of macrophages on fibroblast behaviour and MMP activity in the absence of FBS. Removal of serum from the culture medium resulted in negligible contraction of FPCLs since FBS is a crucial component of the FPCL model[268,282]. Additionally, MMP activity levels did not significantly increase in FPCL

supernatant in the absence of FBS. For the FMPCLs, however, the macrophages were able to potentiate fibroblast-mediated gel contraction and were able to continuously increase MMP activity between days 0 and 7. Since gel contraction had not plateaued by day 7, a feature that normally occurs in FBS-treated FPCLs, it suggested that the FMPCLs would have continued to contract over an extended experimental time frame.

Even though it was anticipated that a greater density of macrophages would significantly increase initial gel contraction, this was not the case and in serum-free groups the highest ratio of fibroblasts to macrophages, 1:4, significantly reduced gel contraction. This could be because at a 1:1.5 ratio of fibroblasts to macrophages, maximal effect of the macrophages on the fibroblasts has been reached (i.e. the number of fibroblasts is limiting). Additionally, as the number of macrophages increased, the total number of cells in the gel increased, resulting in competition for limited nutrients. This could then act as another limiting factor to the effect of macrophages in the model especially in the absence of FBS. When the effect of cell density in the FPCLs was first explored in Chapter 3, a seeding density of 2×10^5 did not have a negative impact on gel contraction and, in fact, greatly increased it. It had not been ascertained however whether a cell seeding density of 5×10^5 cells, or greater, would have a negative effect on resources or contraction. Higher fibroblast densities are known to more rapidly reduce FPCL and thickness, but the threshold of a limiting or deleterious effect is not clear[268].

Contrary to the results shown here, in their extended blood monocyte-lung fibroblast co-culture model of 21 days, Skold *et al.* (2000) reported that gel contraction was initially attenuated compared with fibroblast-only gels[283]. This was corroborated by Zhu *et al.* (2001), from the same research group, who carried out similar experiments[284]. Their models went on to show augmented tissue contraction from day 15 onwards with the gels being significantly smaller by day 21 than in the fibroblast-only groups. However, direct comparisons between the results reported here and those reported in these studies are confounded by the fact that lung and dermal fibroblasts are distinctly different, for example in terms of the MMPs they express, since they have different developmental origins[285]. Additionally, there was no mention of stimulation of the extracted blood monocytes to macrophages. Activated macrophages and monocytes have distinctly different protein expression profiles and may influence fibroblast-mediated contraction in different ways.

4.5.2 Effect of external pressure and mechanical loading on the FPCLs

Pressure is the main extrinsic risk factor in pressure ulcer etiopathogenesis and development since it leads to blood flow occlusion and acts as a mechanical stressor on cells. It is therefore an important component of any *in vitro* FPCL model attempting to replicate pressure ulcer

development. Since the FPCL model is static, compression on the gels would not be able to mimic the effect of blood occlusion and reperfusion due to the lack of nutrient flow. It would, however, be able to replicate several of the other effects of IR injury, including the effect on cell viability and several aspects of oxygen glucose deprivation (OGD). The results reported here show how an external pressure of 32 mmHg for 1.5 hours on FPCLs resulted in: (i) gel compression and flattening, (ii) prevention of normal contractile behaviour, and (iii) a significant loss of cell viability.

Compression of the FPCL is likely to reduce gas exchange and glucose transport to the cells as well as cause physical damage to the resident fibroblasts, all resulting in cell death. The structural integrity of the collagen fibres is also likely to be compromised, resulting in the observable thinning and flattening of the FPCL. Several *in vivo* models of IR injury that involved compression of animal skin for 1-2 hours reported changes in collagen alignment. This has also been observed during compression of *ex vivo* skin and FPCL models[273]. In the FPCLs, contractile behaviour was slightly regained between days 1 and 3 but this may have been due to recoil of the collagen or locomotion of the remaining viable fibroblasts. Importantly, compression applied in this model could not replicate reperfusion of blood which would not only reintroduce critically needed glucose and oxygen but a milieu of harmful free radicals and toxins that are known to upregulate MMP activity[276].

4.5.3 Effect of glucose deprivation in the FPCL model

Due to the limitations of what compression can replicate in the static FPCL model, several aspects of IR injury must be replicated by alternative means. The effect of glucose deprivation, for example, can be modelled by culturing the collagen gels in glucose-free medium[277,278]. Fibroblasts can also be pre-conditioned to glucose deprivation to minimise the effect of fibroblasts using alternative energy-generating mechanisms in the absence of glucose. This result showed that in the FPCL model, glucose deprivation through removal of glucose from the culture medium` did not have a significant effect on percentage gel contraction within the seven-day experimental period. Gel contraction, as with wound healing, is a highly energy-dependent process requiring energy for fibroblast locomotion and collagen compaction. So it could be theorised that glucose deprivation would reduce gel contraction through the removal of the cell's primary energy source. This was not observed. Alternatively, glucose deprivation could cause stress signals to be released that may bolster MMP activity and augment gel contraction. It is possible that these two opposing effects counteracted each other resulting in a gel contraction profile that was not statistically significant from control.

Several studies have reported that glucose deprivation significantly reduced collagen biosynthesis in their FPCL model[277,278]. However, collagen biosynthesis is not a reported process by which fibroblasts contract gels and is more a function/feature of matrix remodelling. Notably, glucose deprivation only constitutes one arm of the pathological mechanism of IR injury and the second arm, blood reperfusion, is likely to have significant effects. This is corroborated by differences observed between the effects of IR injury and ischemia alone by several authors in *in vivo* models[98–100]. Glucose re-introduction can be investigated by replenishing gels with glucose-enriched medium.

4.6 Future work

4.6.1 Combined effect of external stressors on the FPCLs

The effect of macrophages and compression on FPCLs have been explored and defined in this study but their combined effect may, in fact, be synergistic. Each individual stressor can be combined together in the FPCL to investigate this combined effect. For example, pressure could be applied to the FMPCLs in the absence of glucose and in the presence of macrophages. As previously described, introduction of wound fluid and ischemic fibroblasts in place of complete medium and healthy fibroblasts is likely to improve the overall ability of the model to simulate the pressure ulcer environment. Alternatively, neutrophils along with inflammatory cytokines could be introduced into the model to better replicate the body's inflammatory response. The effects of increasing magnitudes of external pressures applied for different lengths of time could also be explored.

4.6.2 Hypoxic chamber for cyclic oxygen deprivation

The effects of cyclical hypoxia and normoxia can be explored through the transient incubation of gels in a hypoxic chamber[286]. Glucose can also be added and removed from the FPCL supernatant to mimic nutrient depletion as seen in IR injury. Both these methods in combination with exposure of the gels to reactive oxygen species (ROS) and free radicals would better replicate the pressure ulcer microenvironment and may give different results to initially those reported here.

4.7 Conclusion

The pressure ulcer microenvironment is complex and dynamic and there are numerous challenges to fully replicating it *in vitro*. With certain limitations, several aspects of the pressure ulcer microenvironment can be introduced. The results here suggest that the increase in MMP activity levels mediated by macrophage-fibroblast interactions is a reasonable target for

doxycycline treatment. However, since relative cell populations and protein expression for each pressure ulcer stage have not been clearly defined it is difficult to ascertain at what stage doxycycline treatment would be most effective. There is a need for newer evaluative scales based on different, more informative biomarkers (this is explored in Chapter 6). The utility of *in vivo* models in replicating pressure ulcer development is explored next, in Chapter 5.

Chapter 5 An *In Vivo* Preclinical Surgical Model of Early Stage Pressure Ulcers

5.1 Introduction

The main aim of the body of work carried out in this chapter was to establish a pre-existing and peer-reviewed preclinical human pressure ulcer model in our lab that was entirely new (in both terms of materials and methods) to our research group. Once the model had been established the following aim would be to use this model in future explorative experiments to further investigate the effect of microneedle-mediated doxycycline delivery on pressure ulcer development *in vivo*.

5.1.1 Bridging the gap between *in vitro* models and human studies

Despite the utility of our current *in vitro* models, their simplicity means they are limited on what they can inform us. The challenge is to find a model that best mimics pressure ulcers in humans. The model must not only be clinically relevant but also simple, economical and reproducible and should aim to bridge the gap between these *in vitro* studies, which cannot emulate a fully functional biological system and human clinical studies, which are often limited to patients with pre-existing ulcers. Historically, *in vivo* models of pressure ulcers have used cumbersome compression equipment in large animals[21,52], while more recently, compact reversible mechanisms with the ability to mimic IR injury have been employed[13,22,23,28,29,97,98]. These devices are more suitable for small animals such as rodents and do not require subject immobilisation or anesthetisation in most instances. By far the most popular technique of the past decade has been the use of magnets to generate the injurious IR cycles. Rodents are popular choices for preclinical research due to their perceived lower sentience, ease of handling and relatively low cost that makes large scale studies possible[99].

5.1.2 Mechanical loading of pressure ulcers using magnetic compression

The *in vivo* murine model was developed primarily based on the work carried out by Mustoe and colleagues (2004)[29]. The concept was based on mechanically modeling IR injury using magnets that periodically compress the skin to mimic the injurious pressure-release cycles. The aim of the model was to replicate the pressure exhibited in the human pressure ulcer by providing a pressure of a clinically relevant magnitude for a sufficient duration. Furthermore, to truly mimic the human pressure ulcer the wound must progress through all clinical stages of ulcer development, in order. The procedure requires magnet implantation which involves creating an incision in the dorsal tissue of the subject and implanting a magnet into the body. This intracorporeal magnet is placed subcutaneously (beneath the fascia) and the incision is then sutured and an extracorporeal magnet placed on top. The extracorporeal magnet can then be removed and replaced at predetermined intervals and the effects of the cycles monitored by tissue harvesting.

5.2 Research outline

This chapter describes an *in vivo* preclinical surgical model using magnetic compression and release to mimic several of the morphological, histological, cellular and biomolecular changes exhibited in the human pressure ulcer. The main aim was to develop an *in vivo* pressure ulcer model using magnet-based compression-release cycles and to investigate the histological and molecular effects in the dermis. This was carried out using a single ischemia-reperfusion cycle. Injured and non-injured tissue were harvested and assessed for inflammatory, structural and vascular changes in the dermis, in order to have a model to then assess the effect of treatment with doxycycline on.

5.3 Methods and materials

5.3.1 Magnets and magnetic compression

Gold-plated neodymium disc magnets (12 mm x 2 mm, N42 Gold Plated) supplied by Magnet Expert Ltd. (Tuxford, UK) were used to create the compressive force to occlude blood flow in the skin of a pressure ulcer. The magnets provided a pressure of 50 mmHg — greater than the conditions required to develop an ulcer but comparable to surface-tissue interface pressure in at risk patients and enough to effectively occlude blood flow through skin placed between them[29].

5.3.2 Experimental groups

The experiment was split into two groups based on the length of reperfusion. Group A had a 1.5-hour period of ischemia followed by a 4-hour period of reperfusion while group B had a 1.5-hour period of ischemia followed by a 24-hour period of reperfusion (**Table 4**). A 1.5-hour period of ischemia was chosen to replicate the approximate time between patient turning commonly reported in the literature.

Table 4 — Experimental group designation and respective lengths of ischemia and reperfusion.

Group designation	No. of subjects	Ischemia (hours)	Reperfusion (hours)	Total no. of IR cycles
A	5	1.5	4	1
B	5	1.5	24	1

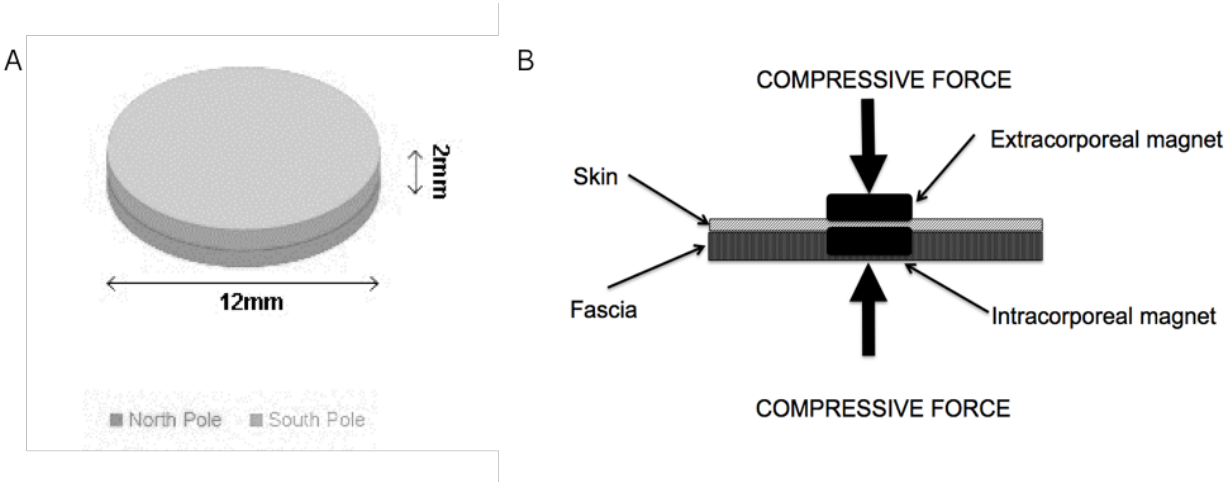

Figure 5.1 — Schematic representation of the magnetic compression apparatus and IR injury procedure: (A) Gold-plated neodymium north and south pole magnets each 12 mm in diameter and 2 mm in height were used to create a compressive force. **(B)** The attraction between the intracorporeal and extracorporeal magnets created a compressive force of 50 mmHg on the skin (shown here in cross-section).

5.3.3 Murine subjects

Six-week old male ICR mice (Harlan Laboratories, Oxon, UK) were used with UK Home Office approval and according to their regulations (PPL number: 70/6778). All subjects were housed singly in non-metal cages during experimental procedures. Immediately prior to the experimental procedure each subject was subcutaneously injected with 0.03 mg/kg buprenorphine (Vetergesic; Recknitt Benckiser Healthcare, Hull, UK). Analgesia lasted for a maximum of 12 hours and the analgesic was reapplied if an animal showed signs of pain or distress. Anesthesia was induced *via* an induction chamber using 4% isoflurane, 2 l/min oxygen and 1 l/min nitrous oxide and was maintained *via* nose cone using 1.5% isoflurane. All subjects were humanely euthanised by cervical dislocation at the end of the experiment.

5.3.4 Implantation procedure

Whilst under anesthesia, subject dorsum was carefully shaved with a razor and the fur removed from a suitably sized area. The subject was transferred to a heating pad and the exposed skin cleaned and sterilised with a sterile gauze and 70% ethanol. A single intracorporeal magnet was inserted sub-dermally into each mouse *via* a single 1-2 cm incision made in the mid-line of the dorsal skin using a scalpel (.). The skin was separated from the underlying fascia using blunt dissection with surgical scissors. The magnet was moved 3–4 cm away from the incision to prevent disruption of stitching with the metal needle and was held in place using a small external rod of metal. Once in place, the extracorporeal magnet was added onto the skin, on top of the implanted magnet. The incision was sutured with interrupted stitches. The area compressed by the magnets was demarcated with a permanent marker.

5.3.5 Cyclic magnetic compression protocol

The period of ischemia was measured from the moment the extracorporeal magnet was added until the moment it was removed. The period of reperfusion was measured from the moment the extracorporeal magnet was removed from the skin until the moment the animal was euthanised. The magnet was removed by hand using a swift sliding motion. For ease, the intracorporeal magnet was left under the skin for the entire experiment and not removed until after euthanisation. After the magnets were applied, subjects were recovered from anesthesia in specially prepared chambers and were returned to individual cages once they were able to move without showing signs of pain or distress.

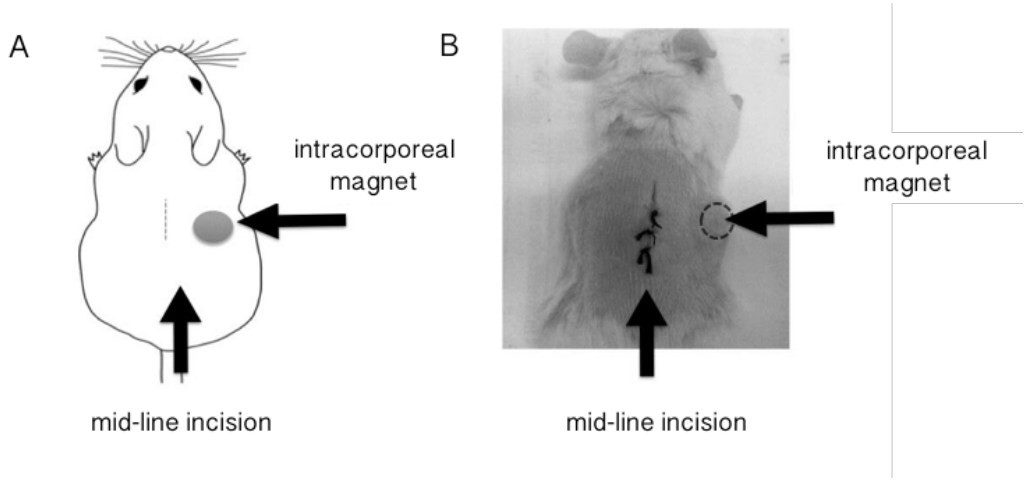

Figure 5.2 — Intracorporeal magnet implantation procedure in murine dorsum: (A) Schematic representation of the IR injury procedure showing the mid-line incision and placement of the magnet to its right**. (B)** Photograph of the IR injury procedure as carried out *in vivo* with the subject under anesthesia. The midline incision was sutured with interrupted stitches.

5.3.6 Tail vein injections of FITC-BSA

Fluorescein isothiocyanate-labelled bovine serum albumin (FITC-BSA) is a fluorophore-conjugated plasma protein which can be used to measure vascular permeability; the FITC fluorophore is bound to BSA protein which accumulates where plasma leaks from blood vessels into the surrounding tissue. The FITC-BSA was formulated as a 1.5% injectable solution using Pluronic gel (Pluronic® F-127; Sigma-Aldrich, Poole, UK). All subjects had tail vein injections of FITC-BSA 20 minutes before their experimental endpoints. Subjects were transferred to heat boxes for 15 minutes to dilate their tail vein to aid the injection process. For the injection, subjects were transferred to tubes to hold them still and prevent needle-stick injuries. FITC-BSA (200 µl) was injected directly into the tail vein of the mouse using a 29G diabetic needle and 1 ml syringe (Becton, Dickinson and Company, New Jersey, USA).

5.3.7 Tissue harvesting

Tissue was harvested on site. An approximately 2 cm x 3 cm section of injury tissue was taken from the right dorsum and an identical section was taken from the contralateral side to act as control tissue. Injury tissue was bisected through the wound. Tissue samples were fixed and stored in 4% (w/v) paraformaldehyde (PFA)-0.1M PBS solution.

5.3.8 Cryosectioning

Tissue samples were washed in 4% PFA-PBS solution (2 x 4 hour washes) and PBS (1 x 24 hour wash) before being transferred to a 20% sucrose (w/v) 0.1M PBS solution containing 0.1% (w/v) sodium azide and left overnight. This was done to prevent ice crystal formation that could damage the tissue during the freezing process. For embedding, large cryomolds (Sakura Finetek, Thatcham, UK) were half-filled with TissueTek 'Optimum Cutting Temperature' (O.C.T.) medium (Sakura Finetek) and the tissue samples added. The remainder of the mold was then filled with O.C.T ensuring that no bubbles were in the medium or surrounding the tissue as this is known to affect sectioning. The cryomolds were placed on a cold stainless steel block on top of dry ice to rapidly freeze down the tissue. Tissue blocks were mounted into a cryostat (Leica CM3050 Cryostat; Leica Biosystems, Nussloch, Germany) and samples were cut into 14 nm sections. Sections were transferred to gelatin-coated glass slides and left to dry for 15 minutes to ensure the tissue had firmly adhered to the slide. Slides were stored at -20^{o}C.

5.3.9 Hemotoxylin and eosin (H&E) histological staining

Hemotoxylin and eosin (H&E) staining was used to stain the structural and cellular components of the skin. The frozen sections were carefully washed in PBS buffer for 5 minutes. They were then stained with 0.1% Mayer's hemotoxylin (MS16, Sigma-Aldrich) for 10 minutes then rinsed with cool running double distilled water (ddH_20) for 5 minutes until the water ran clear. Slides were dipped in 0.5% Eosin (EMD Millipore, Darmstadt, Germany) for 10 minutes and rinsed with ddH_20 by dipping (30 dips). The sections were dipped in graded concentrations of ethanol: 50% (15 dips), 70% (15 dips), 95% (30 seconds) and 100% (60 seconds). The slides were then dipped (15 times) in xylene (Sigma-Aldrich), and a coverslip mounted and fixed with clear nail polish.

5.3.10 Counterstaining for cell nuclei

Frozen slides were thawed for 5 minutes and bathed in PBS for 10 minutes. Slides were placed in cold acetone for 5 minutes to permeabilise the tissue. Slides were removed and counterstained for 5 minutes using Hoechst solution (Hoechst 33258 and Hoechst 33342 dyes each diluted to 1:50,000 in PBS; Sigma-Aldrich). Tissue sections were washed for 2 x 5 minutes in PBS and then mounted and cover-slipped using Citifluor AF1 antifade mountant (Citifluor Ltd., London, UK). Slides were viewed under light and confocal microscopes. Hoechst was excited by the 405 nm wavelength laser.

5.3.11 Histological dermal analysis and leukocyte counts

The dermis in the (i) injury site, (ii) tissue directly surrounding the injury site, and (iii) control tissue in all samples was analysed and imaged under a light microscope. Polymorphonuclear leukoctyes were identified through high power imaging at the injury and control sites in the dermis of each sample. These leukocytes were counted from the histological images in ImageJ® (National Institutes of Health [NIH], Maryland, USA) and the results averaged amongst the subjects ($n = 5$) for both the 4-hour and 24-hour groups.

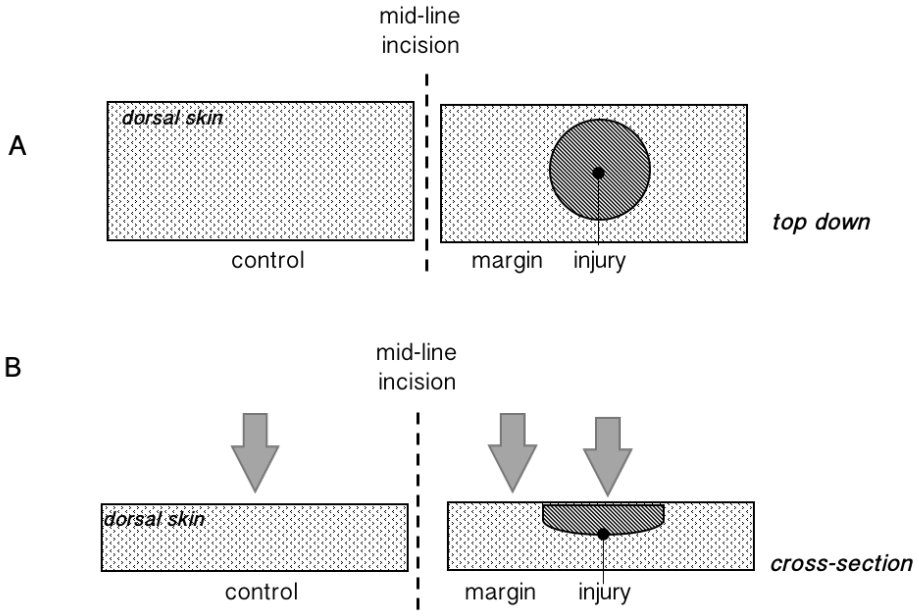

Figure 5.3 — Schematic diagram of regions of interest (ROIs) imaged in the excised dorsal tissue: **(A)** Top down depiction of injury tissue on the right created by the disc-shaped magnets and contralateral skin on the left. **(B)** During confocal microscopy, Z series images were taken through: (i) the injury site (ii) tissue directly surrounding the demarcated injury site i.e. marginal to the injury tissue, and (iii) control tissue collected from contralateral dorsum.

5.3.12 Immunohistochemical dermal analysis using fluorescence confocal microscopy

Immunostained specimens underwent sequential scanning using a Leica SP8 (Leica Biosystems) with a 40x 1.2 numerical aperture (NA) oil objective. Sequential scanning was used to prevent bleed-through of signals. Hoechst was excited by the 405 nm wavelength laser and FITC-BSA by the 488 nm wavelength laser. Images were captured through the Z plane as

a Z series of 1.51 μm slice thickness. For each sample a Z series was taken at the following regions of interest (ROIs): (i) injury site (ii) tissue directly surrounding the injury site, and (iii) control tissue (**Figure 5.3**). Image acquisition settings remained identical between images in order to allow comparisons in image analysis. Images were overlaid and given a maximum projection for visual purposes.

5.3.13 Calculating vascular permeability using image thresholding

Vascular permeability in control tissue, tissue surrounding the injury site and injury tissue was measured using ImageJ®. The Z series for each site were split into the three colour channels (red, blue and green) with the green channel being used to measure vascular permeability. The three middle slices of the Z series acted as triplicates. These were thresholded between 80 and 150. The upper threshold of 150 eliminates the blood vessels and the lower limit of 80 captures the leakage from the blood vessel. The total area covered by the pixels within these two thresholds was calculated using an ImageJ® plug-in. The mean vascular permeability for: (i) IR injury tissue (ii) tissue directly surrounding the injury site (transition tissue), and (iii) control tissue was calculated per group. As there was most likely a discrepancy between the exact amount of FITC-BSA injected into each animal, each animal was normalised to its own control and the vascular permeability for the transition and injury tissue expressed as a fold-change. The results were analysed by a two-way ANOVA with Tukey correction for multiple comparisons and were represented as a column graph.

5.3.14 OCT of magnetic compression in *ex vivo* murine skin

A skin section of 3 cm x 2 cm was excised from the dorsum of a young male ICR mouse. The skin was shaven and treated with a depilatory cream to remove as much fur as possible. The gold-plated N42 neodymium magnets (**Method 1.1.1, *p. 167***) were applied to the apical and basal surfaces of the skin. The magnets were applied to the skin at room temperature for five minutes. Optical coherence tomography (OCT) was used to examine the effect of compression on the skin's subsurface structure up to a depth of 1mm. Images were taken of the skin before and after magnet application at the centre and boundary using the EX1301 OCT scanner (Michelson Diagnostics, Kent, UK).

5.3.15 Statistical analyses

For each condition there were five subject replicates (unless otherwise stated) to allow for experimental variation. Where appropriate results were analysed by a two-way ANOVA with Tukey correction for multiple comparisons and were represented as a column graph. Averages

are represented by the mean ± standard error of the mean. In all instances $p < 0.05$ denotes a statistically significant difference.

5.4 Results

5.4.1 Macroscopic images of the magnet loading site

Photographs taken of the injury sites during harvesting show how magnetic compression affected the skin macroscopically. After a reperfusion period of 24 hours, the skin showed evidence of erythema and localised damage, with the area compressed by the magnet being raised above surrounding tissue. This corresponds to the NPUAP description of a stage 1 pressure ulcer (**Figure 5.4**). No deep tissue injury was observable since, in this model, compression was only provided to the cutaneous tissue.

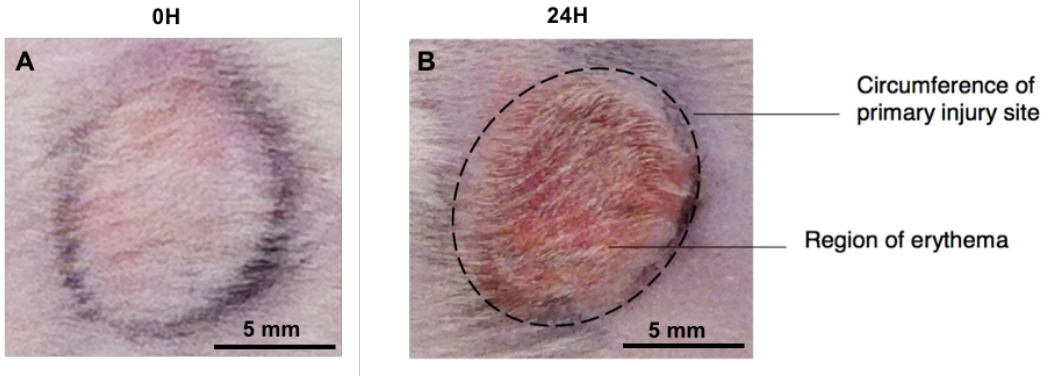

Figure 5.4 — Photographs of the primary injury site after a 1.5-hour period of ischemia induced by magnetic compression of cutaneous tissue: (A) The injury site immediately after the extracorporeal magnet was removed**. (B)** Injury site after a 24-hour period of reperfusion.

5.4.2 Histological analyses

Qualitative histological observations in the dermis

H&E stained specimens were analysed under a light microscope to observe structural and cellular changes in the dermis. Injured tissue demonstrated changes in cellularity, leukocyte count, the structure of the ECM and cell morphology when compared with the control tissue (**Table 5**). The eosin-staining of the proteinaceous components of the ECM such as collagen

was much darker and more histologically 'normal' in control tissue than seen in injury tissue (**Figure 5.5**) where collagen fibrils were densely packed. In injury tissue the ECM appears to have lost its regular structure, with bundles of protein much more weakly stained (i.e. less pink) and less densely packed. Furthermore, there was a marked difference in cellular morphology in injured tissue when compared with control tissue, with fibroblasts appearing to have lost their stellate appearance in the injury tissue. Another clear feature of damaged tissue areas were blood vessels packed with erythrocytes and extravasating leukocytes — a feature not seen in control tissues (**Figure 5.6 – A, B and C**). In the 24-hour but not 4-hour injured tissues there is also evidence of dead cells and cellular debris scattered throughout the dermis (**Figure 5.6 – D**). Leukocyte recruitment was seen in all injured tissues; however, recruitment was greater in tissue after a 24-hour period of reperfusion than after a 4-hour period of reperfusion.

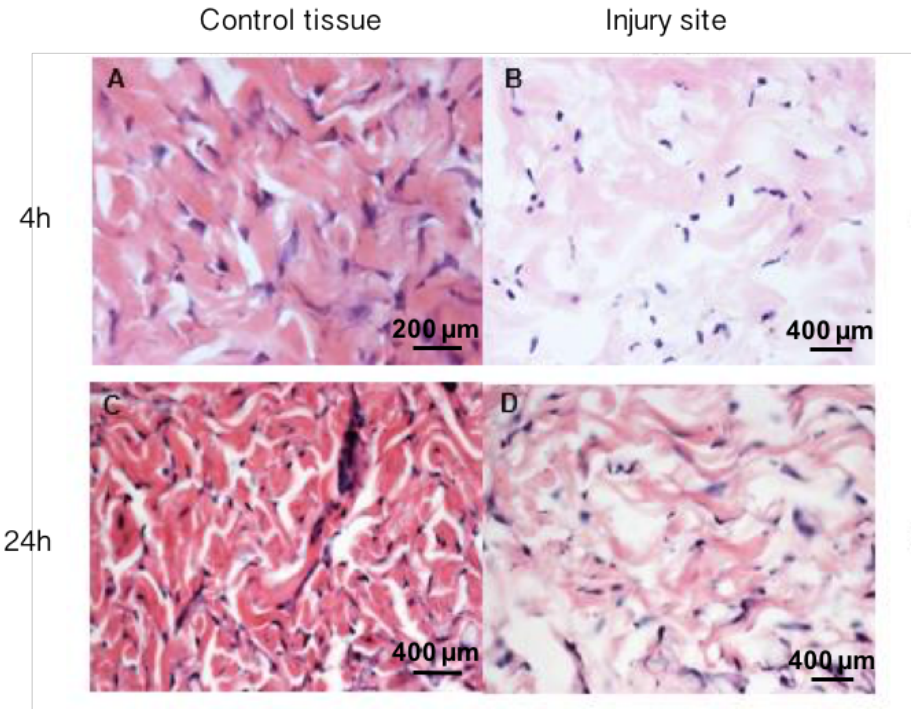

Figure 5.5 — H&E stained histological sections of control and injury cutaneous tissue. Skin samples after a 4-hour period of reperfusion **(A-B)** and skin samples after a 24-hour period of reperfusion . The figure compares control tissue (contralateral to the IR injury site) to tissue from the injury site. Differences in the ECM staining are evident between the two sites at both 4 and 24 hours, suggesting changes in the collagen and/or elastin composition of the ECM as a result of the IR injury. *Paired images were taken with the same exposure and were white balance corrected where necessary*.

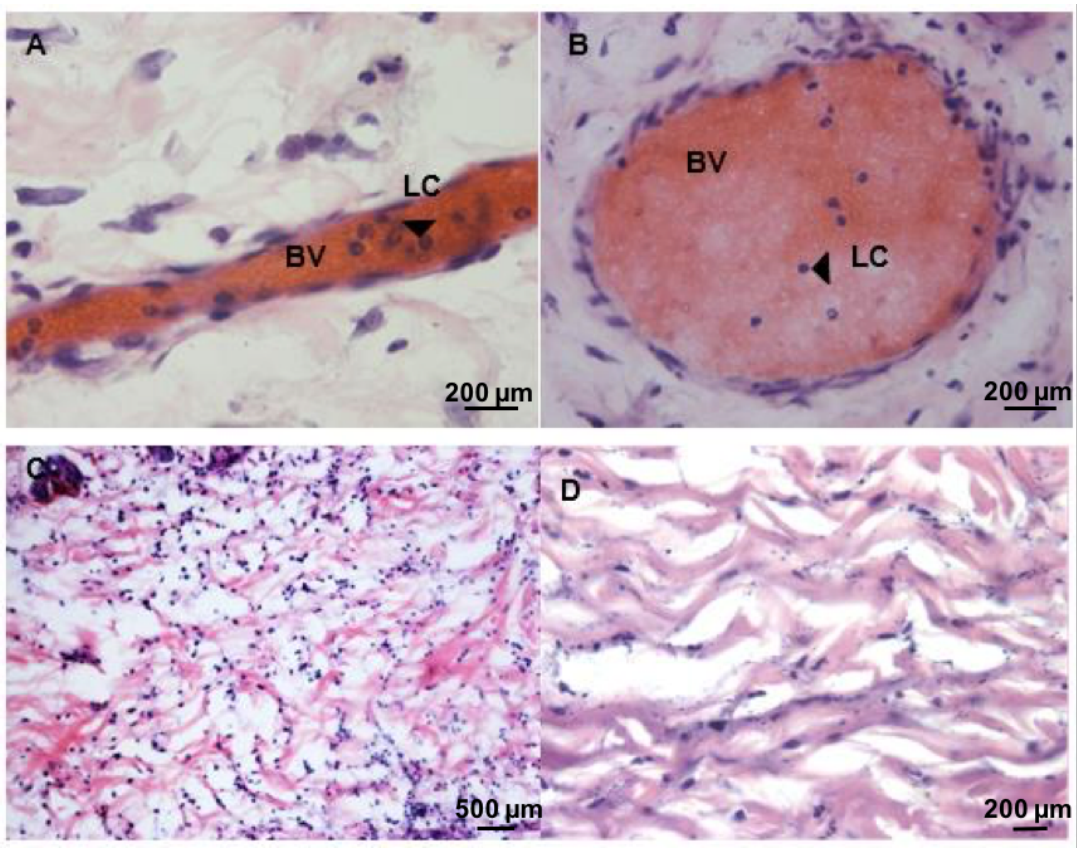

Figure 5.6 — H&E-stained dermis showing histological features of magnetic compression: (A) Injury tissue after 4 hours of reperfusion with extravasating leukocytes [LC] migrating from blood vessels [BV]. **(B)** Injury tissue after 24 hours of reperfusion with evidence of leukocyte recruitment**. (C)** injury tissue after 24 hours of reperfusion filled with recruited leukocytes in the lower dermis. **(D)** Injury tissue after 24 hours of reperfusion shown to contain post-apoptotic cells, cellular debris and nuclear blebs**.**

Table 5 — Comparison of the histological features in control (non-injured) and injured tissue

Histological Feature	Control tissue		Injury tissue	
	4h	**24h**	4h	24h
ECM structure	Normal	Normal	Abnormal	Abnormal
Cell death	None	None	No evidence of cell death	Evidence of cell death
Leukocyte recruitment	None	None	Recruitment	Recruitment
Fibroblast morphology	Stellate	Stellate	Rounded	Rounded

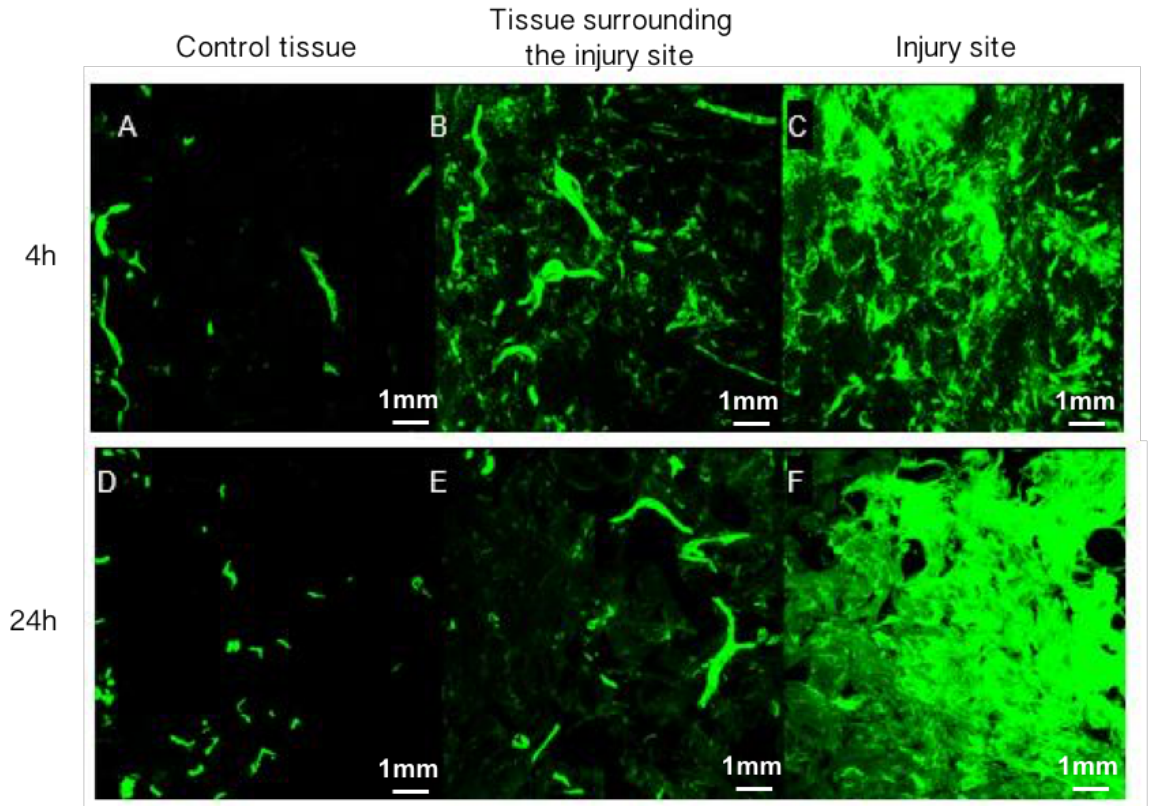

Figure 5.7 — Maximum projections of FITC-BSA stained dermal tissue showing the effect of magnetic compression on blood vessel permeability in control tissue, tissue surrounding the injury site and injury tissue: (A-C) Vascular permeability in dermal tissue after 4 hours of reperfusion. Local vascular permeability was increased in injured dermis and tissue surrounding the injury site compared with control dermis. **(D-F)** Vascular permeability in dermal tissue after 24 hours of reperfusion. Local vascular permeability was increased in injured dermis and tissue surrounding the injury site compared with control dermis. Green fluorescent signals indicate FITC-BSA staining. Image acquisition settings remained identical between images.

5.4.3 Vascular permeability

Effect of magnetic compression on vascular permeability in dermal tissue

FITC-BSA was used to assess the effect of IR injury on blood vessel permeability after a 4-hour and 24-hour reperfusion period between injury, margin and control tissue. Of the five subjects in each group, only three were successfully intravenously injected with FITC-BSA due to the difficulty of the procedure. The FITC-BSA dye fluoresces green when excited by the 488 nm laser. So when injected into the tail vein, the lumen of blood vessels become filled with dye and appear as bright green circumscribed bands. If a blood vessel becomes leaky, the FITC-BSA can diffuse into the surrounding tissues. The greater the permeability of the blood vessel, the greater the amount of dye that leaks out leading to a more intense green staining.

After a 4-hour period of reperfusion there was a statistically significant increase in blood vessel permeability at the injury site compared with control tissue (**Figure 5.7 – A and C**). In addition there was evidence that there was a spread vessel permeability beyond the injury site into surrounding tissue, though this was not statistically significant (**Figure 5.7 – B**). There was a statistically significant difference in vascular permeability between the transition and injury tissue ($p < 0.05$), with a five-fold increase in leakiness at the injury site compared with the surrounding tissue (**Figure 5.8 – A**). After a 24-hour period of reperfusion, there continued to be a pattern of increasing vascular permeability from control to transition to injured tissue (**Figure 5.7 – D, E and F**). There also was a highly significant increase in the fold change of vascular permeability between transition and injury tissue ($p < 0.0001$) (**Figure 5.8 – B**). No statistically significant difference between the control and transition tissue was observed.

5.4.4 Leukocyte count

Effect of magnetic compression on leukocyte recruitment to the dermis

The leukocyte count in the dermis gives an indication of the inflammatory response within the skin after a particular insult. After a 4-hour period of reperfusion there was a significant increase in the average leukocyte count at the injury tissue compared with the control tissue ($p < 0.001$) (**Figure 5.9**). After a 24-hour period of reperfusion there was a significant increase in the average leukocyte counts in injury tissue when compared with control tissue with a much greater increase in fold change compared with what was observed after the hour reperfusion period ($p < 0.001$).

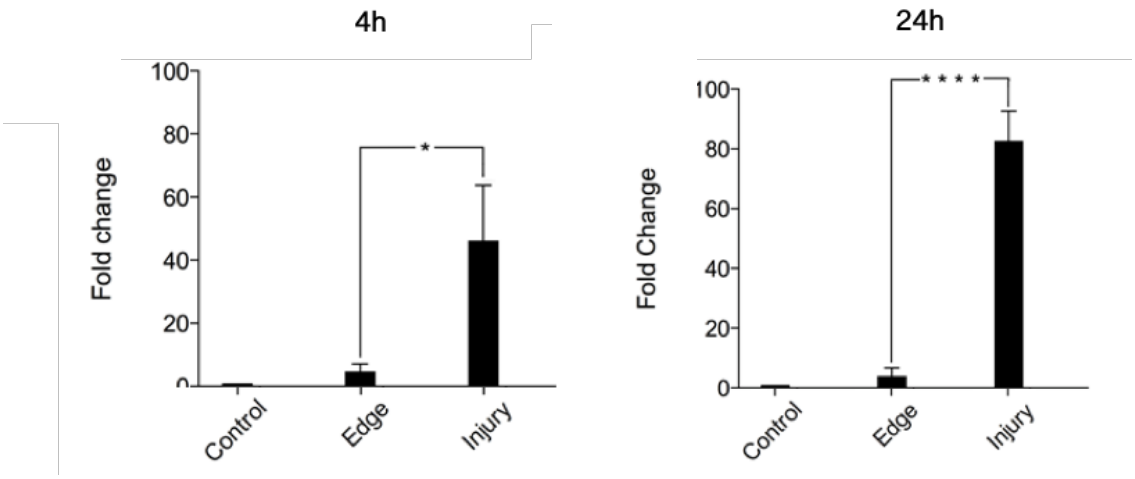

Figure 5.8 — Fold change in vascular permeability in tissue after 4 and 24 hours of reperfusion (n = 3): Vascular permeability was significantly increased in injury tissue compared with transition [edge] and control tissue. No significant difference was observed between control and transition tissue, though fold change in vascular permeability in control tissue was numerically higher. Transition and injury tissue values were normalised to the corresponding control. *Error bars represent the standard error of the mean; * = $p < 0.05$, **** = $p < 0.0001$.*

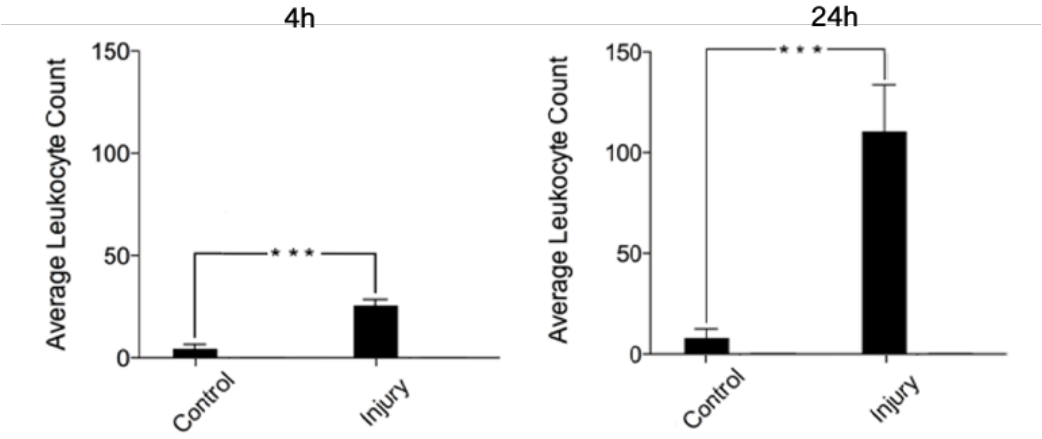

Figure 5.9 — Average leukocyte count in control and injury dermal tissue after 4 and 24 hours of reperfusion (n = 5). Average leukocyte count was significantly increased in injury tissue compared with control tissue after both 4 and 24 hours of reperfusion. *Error bars represent the standard error of the mean; *** = $p < 0.001$.*

5.4.5 OCT images

OCT images of magnetic compression in excised murine dorsum

Cross-sectional subsurface images were taken of excised murine dorsum using optical coherence tomography (OCT). This non-invasive, non-contact method of imaging provided subsurface details not visible by eye without causing morphological changes to the tissue. In control tissue, subsurface striations were observed (**Figure 5.10 – A**). In dorsal tissue that had been compressed on its apical and basal surface with the 12 m x 2 mm 2000 Gauss magnets, compression of the striations at the centre of the injury was observed (**Figure 5.10 – B**). At the boundary where the magnets were applied to the skin there was evidence that the tissue there had experienced greater pressure (**Figure 5.10 – C**).

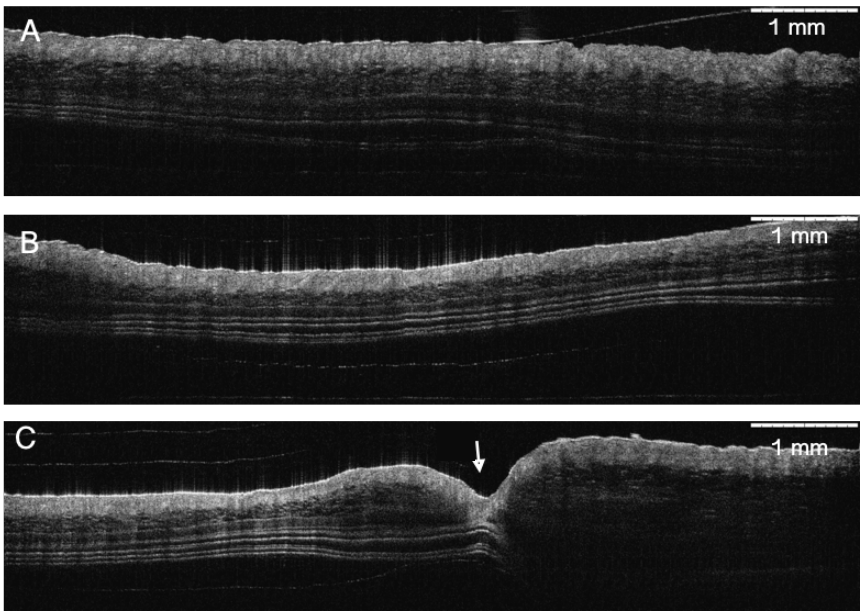

Figure 5.10 — OCT images demonstrating the effect of magnetic compression on excised murine dorsum: (A) Depilated control skin showing subsurface striations. **(B)** Skin after percutaneous application of magnets for five minutes. Striations are noticeably compressed. **(C)** Skin after the application of magnets at boundary (*arrow*). Skin has been significantly deformed at the boundary.

5.5 Discussion

In vitro models, though useful, represent the skin in isolation from a fully functioning biological system and this must be taken into account before extrapolating results to living organisms.

Animal models have provided an excellent alternative to *in vitro* systems to study wound development and healing in a whole organism. In the *in vivo* surgical model reported here, pressure-related injury was simulated by compressing the epidermal and dermal layers of the skin between two attracting magnets that provided a pressure of 50 mmHg. The effects on histological features, vascular permeability and leucocyte count were assessed after reperfusion periods of 4 and 24 hours.

5.5.1 IR injury caused significant histological changes in the dermis

IR injury that included a 1 hour period of ischemia followed by a 4-hour or 24-hour period of reperfusion was shown to cause significant histological changes in the dermis. The results showed that IR injury in this model invoked changes in cellularity, the acute inflammatory response, vascular permeability, ECM structure and fibroblast morphology in the dermis. The histological observations also corroborated the results of the FITC-BSA imaging of vascular permeability and leukocyte count analysis. Control tissue appeared histologically normal, with a well-structured densely-packed ECM, few or no leukocytes and normal cell morphology. Injury tissue, on the other hand, showed signs of a large degree of morphological damage which had spread into the surrounding transition tissue.

The transition tissue found at the margins of the primary injury site showed intermediate traits of control and injury tissue. Injury tissue had lost the regular structure of the ECM and the normal cell morphology of fibroblasts; blood vessels were filled with erythrocytes, while neutrophils and other leukocytes could be seen being recruited into the area. It is important to note that significant differences between the 4-hour and 24-hour reperfusion periods could not be observed through the qualitative histological observations alone and called for more detailed and quantitative analyses through histological leukocyte counts and assessment of vascular permeability. OCT imaging of compressed murine skin provided indications that there were significant structural changes in the dermis and underlying fascia due to the compaction of striations.

5.5.2 Acute inflammatory response to IR injury in the dermis

There is evidence of an acute inflammatory response to IR injury in the dermis. The average leukocyte counts of polymorphonuclear cells were used to assess the acute inflammatory responses in the dermis to IR injury. During the initial phase of a normal inflammatory response, neutrophils are attracted and recruited to an injured area through the release of cytokines. A cascade of pro-inflammatory cytokines released from the neutrophils themselves then follows, resulting in the recruitment of more and more neutrophils and circulating

leukocytes including macrophages. The results presented here show that there is an initial influx of neutrophils into the dermis of injury tissue after 4 hours of reperfusion. As expected, the number of neutrophils greatly increased after a 24-period of reperfusion.

These results corroborate the theory that IR injury causes an acute inflammatory response in cutaneous tissue. During reperfusion the production of reactive oxygen species (ROS) leads to oxidative stress in the tissue and encourages the recruitment of leukocytes ultimately leading to a pro-inflammatory response and damage to the region. The neutrophil is deemed to be the critical cellular mediator of this response. In their study, Mustoe *et al.* (2004) showed a significant increase in leukocytic infiltrates in groups that had been cyclically compressed for 24 hours[100], consistent with the results presented here. The authors also showed that infiltration of neutrophils was not only found in skin bearing necrosis but also in pre-necrotic skin, suggesting that the infiltration of neutrophils could be seen as a cause, and not an effect, of injury. Peirce and colleagues (2000), who were looking at average leukocyte extravasation in their rat model of IR injury[89], showed a significant increase in leukocyte extravasation between control tissue (i.e. no IR injury) and tissue that had undergone 5 cycles of IR injury — 2 hours of ischemia and ½ hour reperfusion — in a 24-hour period.

5.5.3 IR injury increased vascular permeability

IR injury significantly increased vascular permeability at the primary injury site. The quantitative results from the vascular permeability studies are in good concordance with the initial histological observations. Together the results suggest that IR injury greatly increased vascular permeability at the site where the magnet was loaded 4 hours after the initial ischemic insult and continued to have this effect up to 24 hours later. Furthermore, this effect was not limited to the injury site alone, but appears to have spread to surrounding tissue according to the FITC-BSA images, though not significantly according to quantitative image analysis. Implications of this are that apoptotic death and stress signals could be more easily spread to neighbouring cells *via* connexin gap junctions — a mechanism by which stress is known to spread during ischemic injury[254,264,287–289].

5.5.4 Discussion of the validity of recent surgical murine models of IR injury

The seminal studies modeling pressure ulcers regarded ischemia to be the principal inciting factor in ulcer development[92]. In these experiments, single applications of high pressures (greater than 100 mmHg) were applied to the animal models[92,127]. Not only were the pressures too high to be of clinical relevance in humans, the single applications of pressure-induced ischemia were an inadequate explanation of pressure ulcer pathogenesis. This was still the case

even when lower pressures were applied[92]. The model needed to be advanced from the simplistic ischemic insult model to a more sophisticated model that incorporated the significant role of reperfusion. This has led to the current model designs of cyclical IR injury.

IR injury versus ischemia alone

Though there are still no standardised *in vivo* models for pressure ulcers, studies in the published literature, though differing in protocol, appear to show similar trends. Firstly, as anticipated, ischemia alone is not as injurious as IR injury (with the same total compression time). This has been indicated amongst the range of studies. Peirce *et al.* (2004) showed a relative increase in the necrotic area and leukocyte extravasation in the IR-injury group (2 hours ischemia, ½ hour reperfusion, 5 cycles) when compared with the ischemia-alone group (10 hours ischemia, 1 cycle) [89]. Tsuji *et al.* (2005), using their compression chamber model, demonstrated that microcirculatory injury caused by compression-release cycles (2 hours ischemia, 1 hour reperfusion, 4 cycles) was significantly more severe compared with prolonged compression alone (8 hours ischemia, 1 cycle), indicated by analysis of the functional capillary density visualised through their compression chamber device[93].

Secondly, it appears that an increasing (total) number of IR cycles leads to a greater degree of tissue damage. Wassermann *et al.* (2009) demonstrated a strong association ($r^2 = 0.949$) between the NPUAP stage of generated pressure ulcers and the number of applied compression cycle, and reported creating a stage 1, 2, 3 and 4 pressure ulcer after 4, 6, 8 and 10 cycles of compression-release respectively[99]. Reid *et al.* (2004) reported in their study that the magnitude of necrosis appeared to be cycle responsive because a consistent daily progression was observed[100]. Similarly, Peirce *et al.* (2000) showed significant differences in tissue damage between experimental groups that had received 5, 10 or 15 cycles of ischemia-reperfusion[89]. In groups that had received more IR cycles there was evidence of an increased area of tissue necrosis at the magnet application site and increased leukocyte extravasation, as determined by histological analysis. Furthermore, there was a significant reduction in both blood flow and tissue oxygen between groups that had received 5 and 10 cycles.

Thirdly post-injury necrosis, which was used amongst studies as an indicator of the ability of the model to mimic a chronic wound, was observed in experimental groups that had undergone compression-release cycling. Post-injury necrosis describes continuing tissue death days after the experimental procedure has ended. This is key, as one major concern of a rodent model is its ability to successfully produce a wound that is considered analogous to a chronic wound in humans. Reid *et al.* (2004) observed the natural history of the compressed skin after the IR cycles were completed[100]. Their results indicated that necrosis was sustained over time with

lesions reaching their worst by day 10 (1 hour ischemia, ½ hour reperfusion, 5 cycles). Furthermore, for longer periods of ischemia (2 hours), the worse the post-ischemic skin survival exhibited. Similarly Stadler *et al.* (2004), reported that lesions reached their maximum extent 10 days post-injury with continuing evidence of tissue necrosis and inflammatory exudate in the wound days after the end of the IR cycles[212].

Pressure exerted by magnetic compression

The reported pressure generated in the magnet models has been fairly consistent across the recent studies, with most indicating a pressure of 50 mmHg being delivered by the magnets[59,89,99,100], theoretically enough to occlude blood flow in a human and thus a rodent. All groups managed to achieve a substantial reduction in blood flow to the occluded area at this pressure, with Peirce *et al*. (2000) reporting an 80% reduction in flow[89]. The main disparities amongst the magnet studies have been (i) the location of the magnet and (ii) magnet geometry. The cutaneous models, which applied pressure to skin only, were able to emulate a stage 1 pressure ulcer, with evidence of unblanchable erythema during macroscopic analysis, and production of a stage 2 pressure ulcer, evidenced by breakage of the skin and exposure of the dermis. However, these models were unable to mimic full pressure ulcer development as the wounds generated were 'superficial' (they did not develop from within the subcutaneous tissues such as muscle). This meant the ulcers failed to progress through to the most severe stage, stage 4. In contrast, Wassermann and colleagues' sub-muscular model was able to produce the full range of pressure ulcers in progressive order and demonstrated the production of a stage 4 ulcer after ten applications of compression-release cycling[99]. The wound showed evidence of necrosis not only in the epidermis and dermis but in the subcutaneous tissue and muscle as well.

5.5.5 Compression versus crushing

The aim of magnet application is to mimic the pressure conditions required to develop a pressure ulcer. However, the wound generated by the disc magnet model, like the one used in this chapter, could overlap with a closely related clinical condition known as crush syndrome due to the compression of the entire skin surface between the magnet faces. Clinically, crush syndrome results from direct pressure or crushing resulting in muscle cell damage with associated symptoms arising from the systemic manifestations of both IR injury and rhabdomyolysis[290,291]. It is possible that other physiological consequences of crushing, other than IR injury, are attributable to the tissue damage exhibited in the models using disc magnets. One study addresses this issue, reporting a lack of evidence of crush injury in their results, although without detailed explanation[89]. The use of ring magnets could circumvent this problem as, hypothetically, they should be able to induce tissue ischemia by occluding blood flow to the area without compressing tissue at the centre.

Thus, even though the use of disc magnets runs the risk of simulating crush syndrome, the use of ring magnets runs the risk of not sufficiently occluding the central area of tissue from blood, therefore not truly simulating ischemia. However, in their cutaneous ring magnet model, Reid *et al.* (2004) reported that necrosis occurred in the central portion of skin (in the middle of the ring) where no compression was occurring[100]. This suggests that ring magnets are sufficient to provide occlusion. However, without the appropriate technique to visualise the hemodynamic effect of the system, the distribution of pressure cannot be characterised. It is possible, however, that using two ring magnets provides sufficient magnet-magnet interactions that enhance uniformity of the pressure distribution[100].

Murine subjects

The animal subjects employed differed amongst studies. Different rodent species and strains having particular strengths and weaknesses for modeling human skin. Rats have the advantage of having similar skin dimensions to humans as compared with mice[203], while mice have a wider range of genetic variation allowing for a catalogue of knock-out studies[292]. For example, Saito *et al*. (2009) used a knock-out mouse model to investigate the role of monochemoattractant protein-1 (MCP-1) in their IR injury experiment[59]. Furthermore, rats tend to be more expensive to employ in studies due to their larger size, however they may tolerate surgical implantation and the extra weight of magnets better than mice. Both species come in hairless variations which eliminates the need for hair removal and the subsequent abrasion it causes to the skin. For this reason, Wassermann *et al.* (2009) employed a nude rat in their chronic pressure ulcer model[99].

In vivo modeling is limited by practicality and costs. Practical and budgetary considerations include the feasibility, ease and reproducibility of the surgical procedure, the costs of the animal subjects (purchasing, housing, maintenance etc.), the interference of magnets with surgical equipment and caging and the interference of co-housed animals with the wounds. In addition to this, there are confounding factors that may compromise the validity of the study. These include the trauma induced by the surgery, foreign body reactions of implanted materials, irritation to the skin by external magnets, induction of a different clinical syndrome and the systemic effects of anesthesia. Studies have accounted for many of these factors by using controls[89,99,100]. Peirce *et al.* (2000) included a control group that underwent their implantation procedure but which did not receive any IR cycles[89]. The sham group demonstrated significant differences in the area of tissue necrosis, leukocyte extravasation, tissue oxygen and skin blood flow compared with the group which received the minimum five compression-release cycles. Similarly, in the study by Reid *et al*. (2004), the authors noted that the histological features of tissue injury seen in the groups receiving IR injury, such as hyperchromatism, nuclear pyknosis,

vascular congestion and endothelial cell swelling were not present in the sham controls[100]. Furthermore, leukocyte counts were significantly lower in the control skin than skin taken from a group that had received IR injury.

5.5.6 Towards better surgical preclinical models

Taking the culmination of work into consideration, it is evident that there is value of mechanical and surgical preclinical rodent models in pressure ulcer research. Based on these observations, an optimal model might consist of the following: (i) a nude rodent subject; (ii) compression provided sub-muscularly, (iii) an implanted intracorporeal steel plate; and (iv) an external ring magnet. The reasoning behind this is (i) to mimic human skin to the greatest possible extent, (ii) to deliver compression to subcutaneous tissues including muscle, (iii) to minimize implant interference with surgical equipment and caging due to magnetism, and (iv) to circumvent the simulation of crush syndrome. Any implanted materials would be coated with inert material, such as gold plating, to minimise the possibility of invoking a foreign body reaction. Furthermore, to prevent the stresses caused to the body by the surgical implantation procedure clouding the interpretation and validity of the results and to prevent misleading conclusions, there should be a long recovery period post-surgery along with the relevant controls (both sham and intra-individual).

The evolution of the *in vivo* pressure ulcer model is on-going. No single *in vivo* model will ever be able to fully represent the complexity of pressure ulcer development in humans. The models addressed here focus mainly on IR injury but, as detailed, there are other factors that have contributing roles. Factors that have not been extensively studied in conjunction with pressure in these models include friction, moisture, and the effect of aged skin, though studies have looked at them in the past[293]. Despite this, the expected pattern of development of human pressure ulcers (i.e. progressive skin and subcutis degeneration) has been seen in these *in vivo* models. Even though the different protocols used by different groups makes direct comparisons difficult, the results from the studies are in good concordance and can inform on potential biomarkers of disease and on which preventative measures and treatments may be successful in humans.

5.6 Future work

Having gathered data from this preliminary experiment strongly implicating a role of IR injury in initial pressure ulcer development, the next step is to further develop the model to better represent the human pressure ulcer and to investigate, in more detail, other potentially important biomarkers of injury, in particular MMPs and their local levels of activity. The study presented

here shows how IR injury impacted several components of the skin up to 24 hours after the initial ischemic insult both at the primary tissue site and surrounding tissue. What has not been determined is whether the damage caused by the injury ameliorates or worsens beyond this time frame. Furthermore, a better representation of pressure ulcer development would be a model with repeated cycles of IR injury insult since some biomarkers of pressure-related injury may be cycle responsive. Future experiments would include assessing the treatment and prophylaxis of these model ulcers using doxycycline formulations and IDD/TDD with microneedles.

5.6.1 MMP activity assays and zymography to assess the activity of MMPs in IR injury tissue after homogenisation

As previously outlined, an up-regulation of MMP activity and/or expression is believed to be responsible for the ECM degradation seen in IR injury tissue. One method for assessing the effect of MMP on the ECM at an injury site is zymography, which is used for the detection of enzyme activity alongside the MMP activity. Excised tissue that has undergone IR injury can be liquefied and homogenised and the supernatant used to determine levels of MMPs present in the tissue. Data from these analyses could be used to determine how the activity and/or expression of MMPs correlates with ECM degradation. In this vein, other biomarkers of IR injury could be explored. For example, a validated marker of IR injury is inducible nitric oxide synthase (NOS)[97]. PCR analysis can be used to assess iNOS mRNA expression in IR injury tissue. If the model shows an up-regulation of iNOS at the injury site, it strengthens the argument that we are truly demonstrating IR injury in the model.

5.6.2 Alternative methods to histology for determining ECM deformation and leukocyte counts

It is evident that the ECM in IR injury tissue is being damaged and degraded, but exactly which component of the ECM is being affected is not quite clear. Elastin, collagen or both are potential contenders. One way of detecting collagen is second-harmonic generation imaging (SHG) which is a better method of collagen detections compared with the use collagen stains. SHG is a multi-photon technique that can be used on unstained tissue sections which contain non-centrosymmetric structures such as collagens I and III. Elastin, on the other hand, can be stained for using the Verhoeff-Van Gieson (VVG) elastin stain. A less subjective way of assessing neutrophil counts than through counting cells under high power field is to use alpha-neutrophil elastase antibodies which can be used against murine neutrophils and can detect their recruitment as part of an acute inflammatory response.

5.6.3 Imaging techniques to monitor and confirm ischemia and reperfusion

Ischemia and reperfusion can be visualised *in situ* using several techniques to confirm blood occlusion and reperfusion to the areas being compressed. This can achieved in real-time through several imaging modalities including laser Doppler imaging[294], OCT microangiography[295] or visualisation aided by a light compression chamber[93].

5.7 Conclusion

This chapter has shown the role that IR injury plays in pressure ulcer formation using an established *in vivo* murine model. It was demonstrated that IR injury is a multifactorial process which involves many structural, functional and inflammatory changes in the dermis. The experimental outcomes of this were the successful development and implementation of the preclinical *in vivo* IR injury model using magnets, the demonstrated macroscopic effects of IR injury analogous to those seen in early stage human pressure ulcers and confirming the ability of IR injury in the model to increase local vascular permeability, stimulate leukocyte recruitment to injured tissue and alter the histological structure of the ECM.

Chapter 6 Optical Coherence Tomography for the Non-Invasive Evaluation of Pressure Ulcers

6.1 Introduction

New methods of pressure ulcer evaluation are needed to complement the microneedle technology that this research has focussed on. The current methods are not able to inform on the subsurface changes that could be indicative of pressure ulcer development and this could be overcome by repurposing existing *in vivo, in situ* imaging modalities. Such modalities could also help precisely guide microneedles during intradermal drug delivery (IDD) and monitor the pharmacologic action of the administered active drug over time. Specifically, during my research, it was noted that insertion of microneedles into excised skin resulted in compression of the skin's striations as visualised by OCT and implicated that OCT imaging, as an alternative imaging modality, may have diagnostic value in evaluating the pressure ulcer condition. For these reasons the use of OCT in subsurface imaging for microneedle-assisted drug delivery and pressure ulcer evaluation purposes was investigated.

6.1.1 Traditional pressure ulcer evaluation systems

Traditionally pressure ulcer evaluation at the bedside has been achieved through clinical scoring and classification systems such as the staging system outlined by the National Pressure Ulcer Advisory Panel (NPUAP). These systems categorise pressure ulcers on a scale of increasing severity, based on the presence of unblanchable erythema, extent of skin loss and exposure or damage to underlying tissues[296]. These scales, however, are heavily limited by the subjectivity associated with visual assessment of the skin that results in inter- and intra-observer variation. Importantly, miscategorisation at the clinical diagnosis level can result in incorrectly projecting patient prognosis thus impacting on preventative measures or treatments put in place for that patient. Furthermore, the assumption that the surface of the skin reflects the extent of internal damage has been widely disputed, with many studies suggesting that deep-tissue injury (DTI), not readily detectable at the skin surface, is responsible for rapid pressure ulcer development, leading to an 'ice-berg' effect[14,37,297–299].

This phenomena has also been referred to as the 'bottom-up' theory which theorises that a subset of pressure ulcers develop and worsen in subcutaneous fat and/or muscle tissue under intact skin with minimal surface indication of the underlying necrosis at first and without raising immediate medical concern[300]. Discussion amongst clinicians, researchers and educators on the issue of pressure-related DTI encouraged the introduction of a separate stage in the NPUAP classification system in 2007 known as the DTI stage[296]. As with the previous stages, this classification does not provide any information on the extent or severity of the underlying injury or whether or not the ulcer is likely to heal by secondary intention or if it requires surgical intervention methods. There is definitely a need for an improved standardised and universal method of evaluating pressure ulcers and this is corroborated by researchers repurposing existing medical devices or developing new tools for the evaluation of pressure ulcers and pressure-related injuries.

6.1.2 Clinical applications of OCT imaging

Optical coherence tomography (OCT) is a clinically-used imaging modality that can provide subsurface cross-sectional images of opaque structures such as the skin. Originally designed to image into the eye, OCT imaging has crossed over into the medical fields of cardiology, gastroenterology and dermatological diseases. This includes both cancerous and non-cancerous skins conditions such as skin melanomas, non-melanoma skin cancers, dermatitis and psoriasis. Even though OCT is not the standard technique for dermatological investigations, there has been much interest in recent years in repurposing this existing imaging modality for the diagnosis and monitoring of skin diseases. OCT imaging of skin diseases has shown correlation with the morphological changes observed in histopathological investigation of blistering disease, tumour tissue and inflammatory conditions including psoriasis and contact dermatitis as well as with markers of acute wound healing[61,301,302]. With this success, OCT devices have become better adapted for dermatological applications with development of light-weight and handheld scanners, such as the VivoSight scanner, which is marketed as the next generation imaging modality in the diagnosis of non-melanoma skin cancers by Michelson Diagnostics (Maidestone, USA).

6.1.3 Technical aspects of OCT in dermatology

OCT uses light to image into structures with micron resolution, employing a methodology analogous to ultrasound. However, unlike ultrasound which employs acoustic waves, OCT uses infra-red light with a wavelength of approximately 840 nm to provide depth-resolved tissue structure information[303]. This information is encoded in the magnitude and delay of the back-scattered light and is based on the principle of Michelson interferometry[304,305]. Light from a single source is split into two paths — a sample path and a reference path. The light in the

sample path interacts with the tissue being imaged; some of this light is reflected while some is scattered. Meanwhile the light in the reference path is reflected back to recombine with the light returning from the sample path[306]. Optical interference only occurs when the distance travelled by the light in both paths matches with the coherence length of the source light[307]. At its simplest, the greater the backscattering of light from a region of tissue, the greater the intensity of the incoming signal. For grey-scale image acquisition this results in a brighter area on the generated image, while regions of low-back-scattering result in lower intensity signals leading to darker areas on the image. The back-scattering properties of tissues can thus be used to identify particular structures and demarcate different regions.

The resulting 'optical biopsy' is achieved through non-invasive, non-contact, *in situ* and real-time bedside imaging that rivals the gold standard, histology, in terms of ease and practicality. OCT imaging is able to provide information on discrete layers of skin including the stratum corneum, the viable epidermis and the upper (papillary) dermis due to a lateral resolution as low as 5-10 μm[71,79,80]. Furthermore OCT imaging offers different scans and image types. The simplest OCT scan is the A-scan, a one-dimensional scan that plots axial depth against scattering intensity at a particular point in a tissue[305]. When information from neighbouring A-scans is collated a B-scan is generated — a two-dimensional grey-scale image with both width and depth[308] (**Figure 6.1**). OCT B-scans across a tissue can be amalgamated to produce a three-dimensional scan; this technique is known as 3D-OCT[309]. Depending on the scattering properties of the skin, which can vary from skin condition to skin condition and from site to site, depth penetration of cutaneous OCT imaging can reach up to 2 mm[303].

6.1.4 Non-invasive, *in situ* and *in vivo* imaging alternatives to visual-based assessment scales

Though pressure ulcers are traditionally evaluated and scored by visual assessment scales, the gold standard for morphological investigations of the skin is excision biopsy and subsequent histological analysis[308]. Skin specimens are excised from the diseased tissue, then prepared, stained and analysed by microscopy. Histology has a very high resolution and provides a great amount of detail on the cellular and structural changes in tissues. This includes the presence of cell infiltrate as a result of inflammation, changes in extracellular matrix (ECM) density and collagen alignment and changes in cell morphology which is especially important in the grading of cancers. The skin layers are also well demarcated in histological sections and highly accurate measurements can be made. However, despite being an invaluable technique, histology presents a lot of disadvantages mainly surrounding its practicality. Specimen collection by excision biopsy is highly invasive and is injurious to damaged or diseased skin often creating a second iatrogenic wound[72]. The biopsy cannot be repeated at the same site and may alter the tissue's original morphology[301]. Additionally, it takes time to prepare the samples so there is no real-

time (immediate) feedback but rather a snapshot of the wound in time and analysis requires highly trained specialists.

Due to the setbacks of visual-based scoring scales and the practicality issues surrounding histology, numerous studies have investigated the ability of a range of *in vivo* imaging modalities to image skin conditions. These modalities include ultrasound, scanning laser confocal microscopy, epiluminescence microscopy (also known as dermoscopy) and OCT. Of these techniques, ultrasound has the most in common with OCT. It is a widely used non-invasive imaging modality that uses the reflectance of acoustic waves from internal structures to generate cross-sectional images through tissues. Due to its low associated health risk and deep tissue penetration, ultrasound is the most commonly used pre-natal imaging technique and has a range of other clinical applications. However, unlike OCT, ultrasound requires direct contact with the skin and the application of a gel at the site of contact to improve image

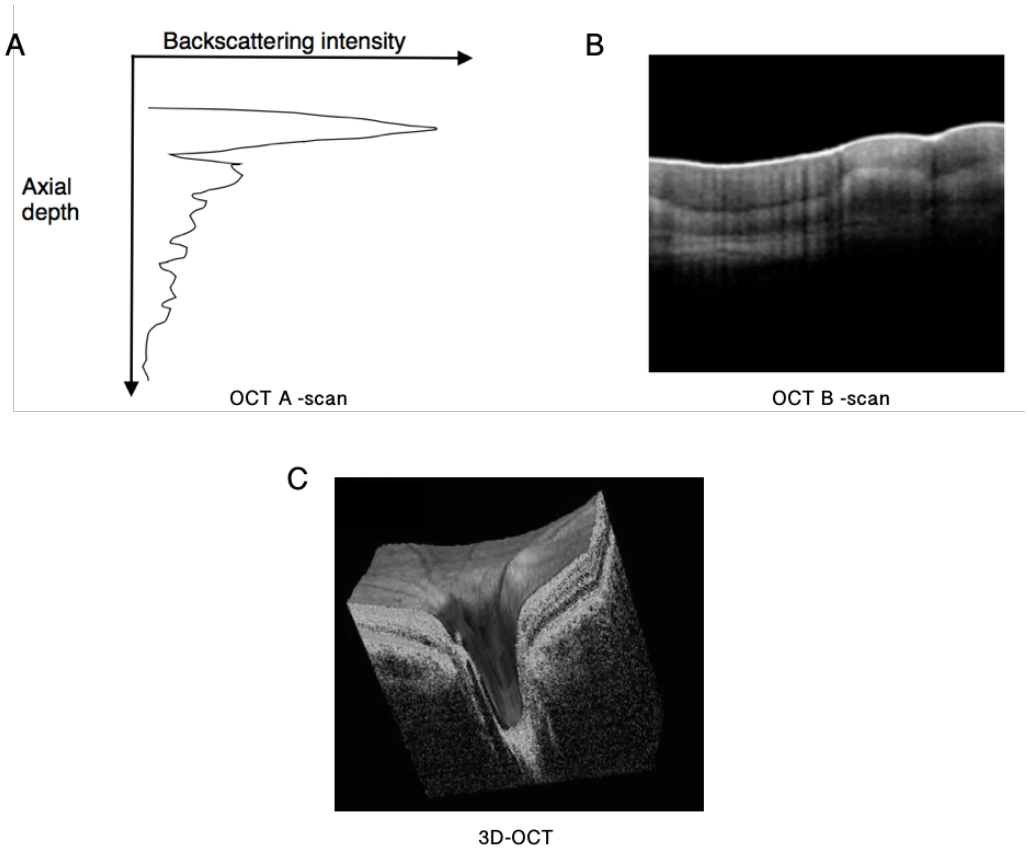

Figure 6.1 — Different types of OCT scan: (A) The OCT A-scan gathers information on backscattering intensity relative to depth at a particular point in a tissue. **(B)** When a series of A-scans are collected from a tissue, an OCT B-scan is generated which provides a two-dimensional cross-sectional image through the tissue. **(C)** 3D OCT is an amalgamation of OCT scans across a tissue; *adapted from "Optovue iSeries OCT Systems" by Optovue, Incorporated, 2016 (http://www.optovue.com/products/ivue-ifusion/).*

acquisition. This could pose a problem for assessing cavitied ulcers or broken skin when imaging pressure ulcers. Furthermore, even though high-frequency ultrasound has very good depth penetration and can image deep into structures, soft tissues and organs, it is at a cost to its resolution which is poorer than that of OCT (**Table 6**) .

In vivo CSLM uses laser microscopy to image into the skin and provides high-resolution images approaching the level of cellular and sub-cellular detail seen with histology[310]. In contrast to ultrasound, CSLM offers excellent resolution in favour of depth penetration (**Table 6**). It has been used in the assessment of age-related effects in the skin[311] and pigmented skin lesions[310]. Epiluminescence microscopy, also known as dermoscopy, is essentially a magnification technique that enhances the morphological features of the skin that are not visible to the naked eye. This makes it particularly good for assessing pigmentation disorders and for accurately demarcating skin lesions. However, unlike the previous imaging methods, epiluminescence microscopy does not provide subsurface detail of intact skin. This makes it harder to make evaluations of skin lesions on darker, more heavily pigmented skin which poses a problem for all visual-based assessments. Overall, in comparison to other available techniques, OCT is arguably the superior imaging modality for this application since it provides a non-invasive alternative to histology, provides superior resolution of architectural components of the skin compared with ultrasound, allows for greater depth penetration than laser confocal microscopy and can provide subsurface images of intact skin unlike epiluminescence microscopy.

Table 6 — Typical axial and lateral resolutions and depth penetration in soft tissues of different *in vivo* non-invasive imaging modalities.

Imaging modality	Resolution	Tissue depth penetration	Examples of traditional clinical/medical application(s)
OCT	≥ 5 µm	≥ 2 mm	Ophthalmology — retinal/corneal scans
Ultrasound (high frequency 50 hz)	≥ 20 µm TBC	> 10 mm	Pre-natal scanning
CLSM	≥ 2 µm	≥ 500 µm	Diagnoses of skin disorder
Epiluminescence microscopy	- -	none	Diagnosis of depigmentation disorders Demarcation of skin lesions

OCT = optical coherence tomography, CLSM = confocal laser scanning microscopy.

Figure 6.2 — Images of various skin diseases, disorders and conditions using different imaging modalities: (A-B) From "Optical coherence tomography in contact dermatitis and psoriasis" by J. Wlezel et al., 2003, Arch Dermatol Res, 295, p. 52. **(C-D)** From "In vivo confocal scanning laser microscopy in dermatology" by A. L. Branzan et al., 2007, Laser Med Sci, 22, pp. 76-77. **(E)** From "Dermatoscopy in the diagnosis of pigmented skin lesions: a new semiology for the dermatologist" by P. Carli et al., 2000, European Academy of Dermatology and Venereology, 14, p. 355. **(F)** From Ultrasound Assessment of Deep Tissue Injury in Pressure Ulcers: Possible Prediction of Pressure" by A. Noriyoki et al., 2009, American Society of Plastic Surgeons, 124, p. 546.

6.2 Research outline

This chapter outlines an observational audit carried out by myself designed to investigate the potential application of OCT imaging in the assessment of pressure ulcer development and the evaluation of pre-and post-ulcerous skin. The ability of OCT to detect changes in skin layers that had undergone compression was demonstrated in Chapter 5, when magnets were applied to excised murine tissue. It was anticipated that these results could be extrapolated to human skin, whereby the effect of pressure on skins layers would be detectable in *in vivo* OCT scans. This chapter explores the ability of OCT to predict sites of pressure ulcer formation by imaging the skin before the ulcer is surface-detectable and to differentiate between ambiguous pressure ulcer stages based on internal subsurface biomarkers, such as changes in skin layer thickness and the presence/absence of particular structures. OCT can provide both standardised qualitative and quantitative data through B-scans and A-scans respectively and could potentially provide information on pressure-related injury on a continuous scale rather than in discrete categories. In this way, OCT scanning could help improve clinical diagnosis and help reduce the number of pressure ulcers that develop in hospital setting by providing information that is more indicative of the severity and nature of subsurface skin damage. Furthermore, its use could be combined with algorithms that could determine when and where the application microneedling should be applied to the greatest effect and could also be used to monitor the pharmacologic action of therapeutics delivered by microneedles.

The main aims of the audit were to investigate whether OCT could improve the evaluation of early stage pressure ulcers at the bedside over traditional scoring scales. Secondary to this was whether OCT could predict if an existing pressure sore was likely to resolve or worsen (which could impact on treatment) and if it could identify where a pressure sore was likely to occur. The final aim was to investigate whether OCT could distinguish between early stage pressure ulcers and other skin diseases. To achieve these aims, the objectives of the observational audit were to acquire OCT images from subjects with:

- pressure ulcers at differing NPUAP stages,
- resolved pressure ulcers (resolved either through secondary intention or surgical intervention),
- areas predicted by the ward staff to be at risk of pressure ulcer development,
- any other existing skin conditions in the areas of the body at high risk of pressure ulcer development.

6.3 Methods and materials

6.3.1 Subject selection

The observational audit was carried out by myself in the Osborne 2 ward of the Spinal Cord Injuries and Neurorehabilitation Unit of the Northern General Hospital, Sheffield, UK. Osborne 2 accommodates twenty-two subjects and admission into the ward is based on the primary criterion that the individual has a pressure ulcer that needs surgical intervention or close clinical care. Subject participation in this study was granted by verbal consent and a total of six volunteers consented to participate in the audit. Of the six participants four were male and two were female. There were no exclusion criteria based on age, gender, body mass index (BMI) or co-morbidities. To be included in the study the subject must either have a pressure ulcer of any stage or have previously had a pressure ulcer of any stage which resolved through surgical intervention or by secondary intention. Subjects with a dermatological condition at an anatomical site where pressure ulcers typically develop, such as the sacrum, were also included.

6.3.2 Equipment

This evaluative study used non-contact image acquisition of pressure ulcers, skin margins and healthy skin using a portable OCT scanning workstation. The workstation was supplied by Grafton Optics (Watford, UK) and was comprised of a central processing unit, a monitor and the lightweight and modular iVue® spectral-domain OCT ocular scanner (Optovue, California, USA). The iVue® scanner was originally designed for ophthalmological applications including retinal and corneal assessments of medical eye problems, but was employed in this study as the resolution was far superior to the available OCT skin-scanning alternative. The scanner had a special iCam® lens attachment required to take corneal scans. Corneal scans were chosen to image the skin instead of retinal scans since retinal scans modify image acquisition algorithms to account for the refraction of light as it passes through the eye's viscous humour. The iVue® scanner produced 26,000 A-scans per second with a scan beam wavelength of 840 nm (± 10 nm) and a subject interface working distance of approximately 2 cm. It offered a depth resolution of as low as 5 μm.

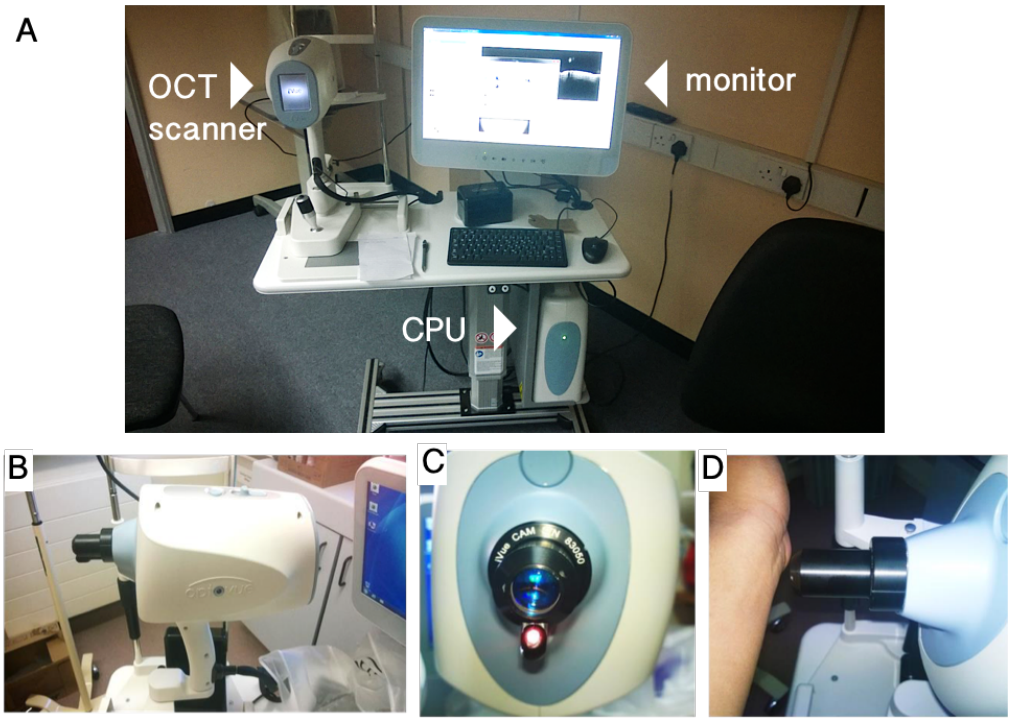

Figure 6.3 — Photographs of the OCT scanner and workstation supplied by Grafton Optics, Watford: (A) The OCT workstation consisted of the iVue® Optovue OCT scanner, a computer monitor and a central processing unit [CPU] on a portable table. **(B)** Side view of the OCT scanner. **(C)** Front view of the OCT scanner with the iCam® lens attachment. **(D)** Demonstration of non-contact imaging of wrist skin with a working distance of approximately 2 cm.

6.3.3 Image acquisition

The OCT workstation was moved to the subject's bedside on a portable table and was powered by mains electricity available by each bed. The skin was not cleaned prior to imaging but any wound dressings were removed. The working distance of the scanner was 2 cm, so the scanning head was held approximately this distance from the skin until the skin surface and a suitable portion of the subsurface were displayed. The images were displayed simultaneously on the computer monitor and on an in-built screen at the back of the OCT scanner. Image acquisition was manually controlled by the computer mouse and through foot pedals. Images were taken in grey-scale format and saved electronically for later analysis by imaging software. The scanning software provided immediate feedback on scan quality, prompting the operator to repeat the scan were the quality was below standard. A 5MP camera just below the lens also took digital images of the skin.

Each subject constituted an individual case study and data on their basic profile and medical history were collected with informed consent. Sites where images were taken depended on the location of the subjects' pressure ulcer(s). Where possible, scans of contralateral or unaffected wrist skin were also taken. Subjects were asked to remain as still as possible during scans to aid the acquisition of high quality images. Multiple scans of the same region were achieved through stay-on modus replicates. Each set of subject scans took roughly ten to fifteen minutes including set-up of the OCT scanning equipment. The best quality scans were selected for analysis. To minimise cross-contamination between subjects the iCam® lens was cleaned and sterilised with antiseptic wipes and alcohol rub between different subjects. This was a precautionary measure advised by the nurses even though the OCT scan was a non-contact method.

6.3.4 Image analysis

The OCT images were saved during scanning and analysed afterwards using ImageJ® software by the operator (myself). Of the six subjects scanned, only one subject had insufficient scan quality as indicated by low quality scan score and their scans were excluded from the study. ImageJ® was used to make scaled measurements of the thickness of skin layers. Maximum subsurface penetration depth averaged around 600 μm across all scans. As the OCT images provided subsurface cross-sections through the skin, different architectural characteristics could be compared across different skin states and ulcer stages. OCT images were also taken from a healthy individual (who was not a patient in the ward) to act as a control. When analysing the images, the operator was not blinded to the patient or the NPUAP stage of the pressure ulcer due to the preliminary nature of the audit. Structures in the OCT images of the pressure ulcers were compared to the corresponding NPUAP description to help identify them. A '+' score was assigned when a structure had been positively identified and '++' when there was a strong presence of that structure. When a structure was not present in an image a score of '–' was assigned. Quantitative data had also been collected for each image through the iVue® scanning system.

6.4 Cases studies

Subject case studies are presented as a brief medical background of the subject followed by their pressure ulcer history and their OCT scans. For confidentiality, subjects are referred to by number.

6.4.1 Subject 1

Subject 1 was a 63 year-old Caucasian male with a normal BMI who had been paraplegic for 30 years. The subject had a surgically debrided and sutured stage 4 sacral pressure ulcer that

had been treated one week prior to the OCT scan and was the cause of ward admission (**Figure 6.4 – B**). The subject also had a stage 1 pressure ulcer on the right ischium, previously stage 2, that had healed by secondary intention prior to ward admission (**Figure 6.4 – C**) and a stage 1 pressure ulcer on their knee which was reported by the clinical staff to heal transiently (**Figure 6.4 – D-E**). OCT scans where compared with healthy ipsilateral skin on the trochanter (**Figure 6.4 – A**).

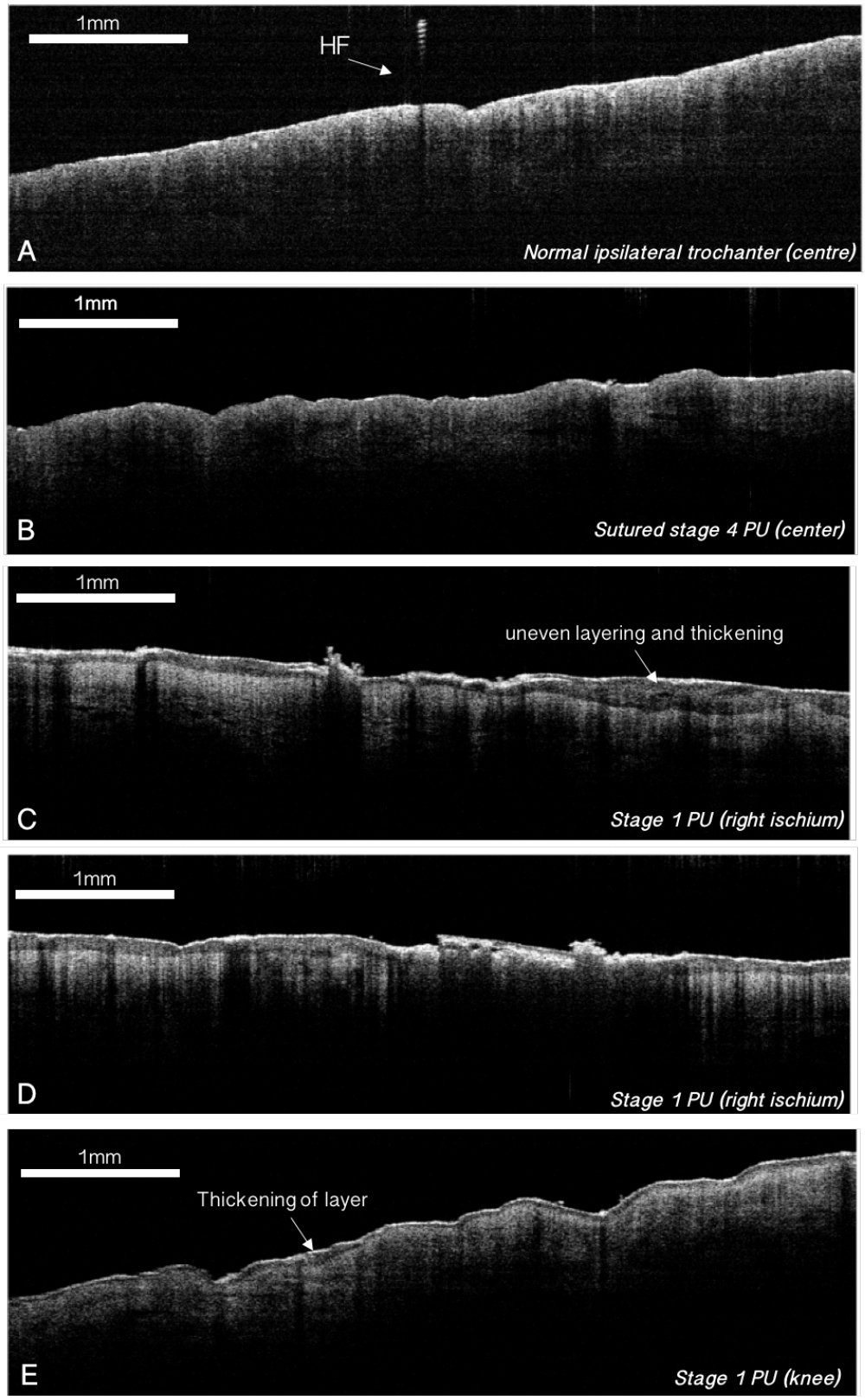

Figure 6.4 — OCT scans from subject 1: (A) Scan of the centre of normal ipsilateral trochanter. **(B)** Centre of a surgically treated and sutured stage 4 pressure ulcer on the right ischium. **(C-D)** uneven layering and thickening of the upper skin layers observed in a stage 1 pressure ulcer on the subject's right ischium. **(E)** Thickening in upper epidermal layers observed in the OCT scans of a stage 1 pressure ulcer on the subject's knee; [PU = pressure ulcer; HF = hair follicle].

6.4.2 Subject 2

Subject 2 was a 75 year-old Caucasian female subject and T12 paraplegic The subject had a surgically debrided and cavitied stage 4 pressure ulcer on their right trochanter.

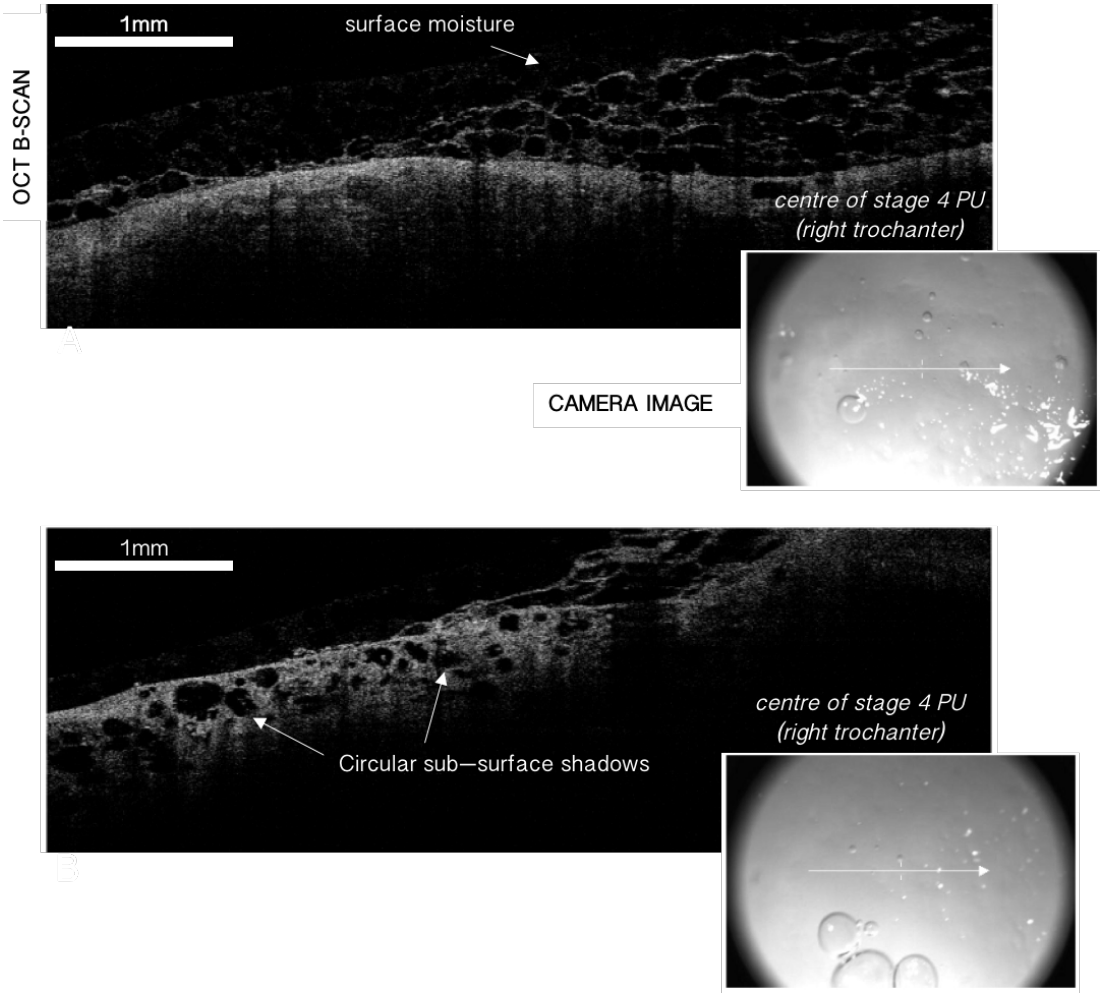

Figure 6.5 — OCT scans and camera images from subject 2: (A) Scan taken from the centre of a stage 4 pressure ulcer on the subject's right trochanter. Wound exudate and surface moisture can be seen in both the camera image (*inset*) and the scan. **(B)** Circular subsurface shadows observed in the centre of the same stage 4 pressure ulcer; [PU = pressure ulcer].

6.4.3 Subject 3

Subject 3 was an 80-year-old Caucasian male subject with a notably high BMI (> 25) and was a T10 paraplegic. The subject had a surgically debrided stage 4 sacral pressure ulcer treated one week prior to the OCT scan which had been the cause of admission to the ward.

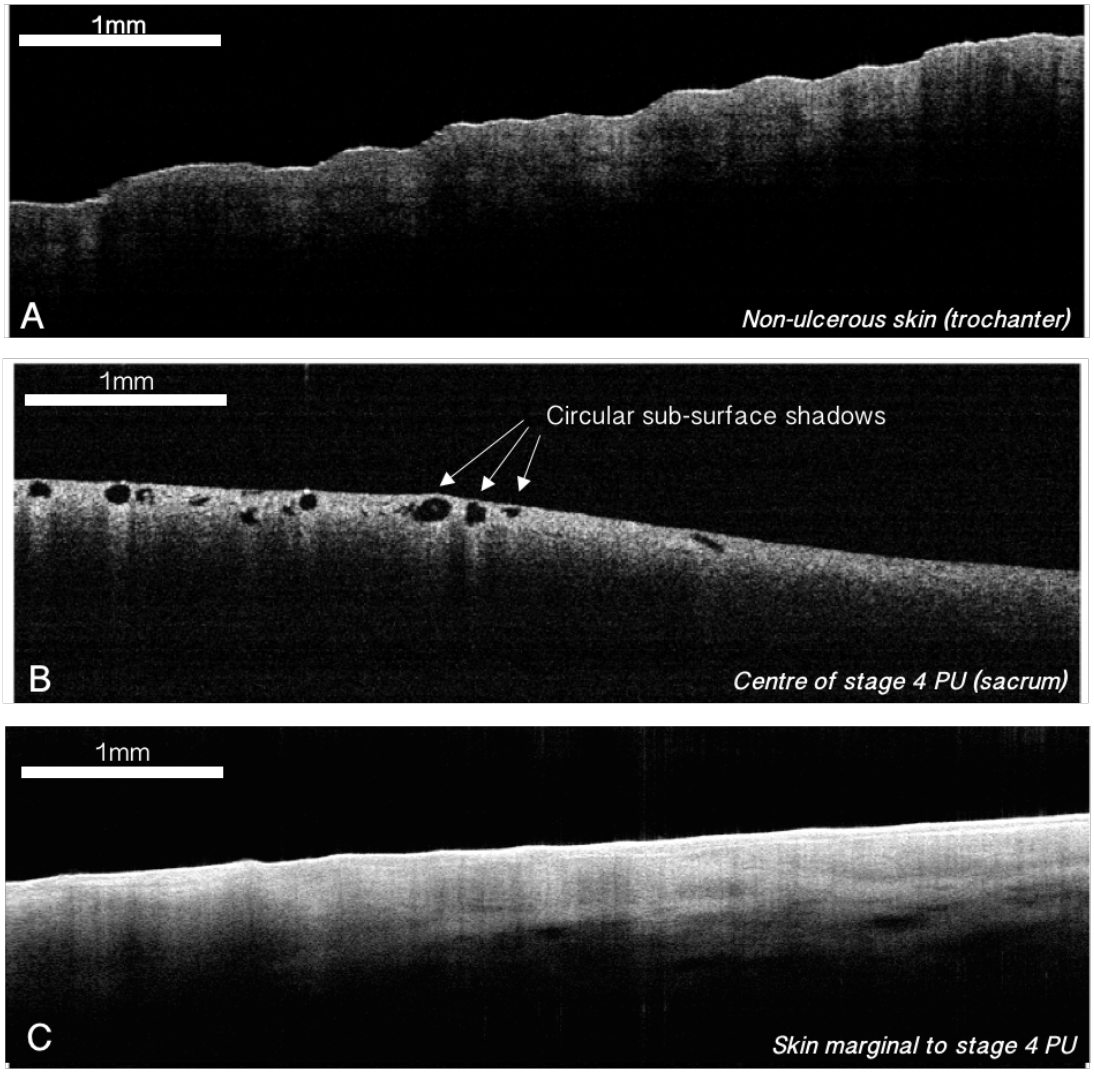

Figure 6.6 — OCT scans from subject 3: (A) Scan of non-ulcerous skin taken from the subject's trochanter. **(B)** Circular subsurface regions observed at the centre of the subject's stage 4 sacral pressure ulcer. **(C)** Scan of skin marginal to the stage 4 pressure ulcer; [PU = pressure ulcer].

6.4.4 Subject 4

Subject 4 was a 54-year-old Black-British male and a T10 paraplegic. The subject had a surgically debrided and sutured stage 4 pressure ulcer on their right ischium. New breakage of the skin (exposure of dermis) along the anterior portion of the suture line was observed.

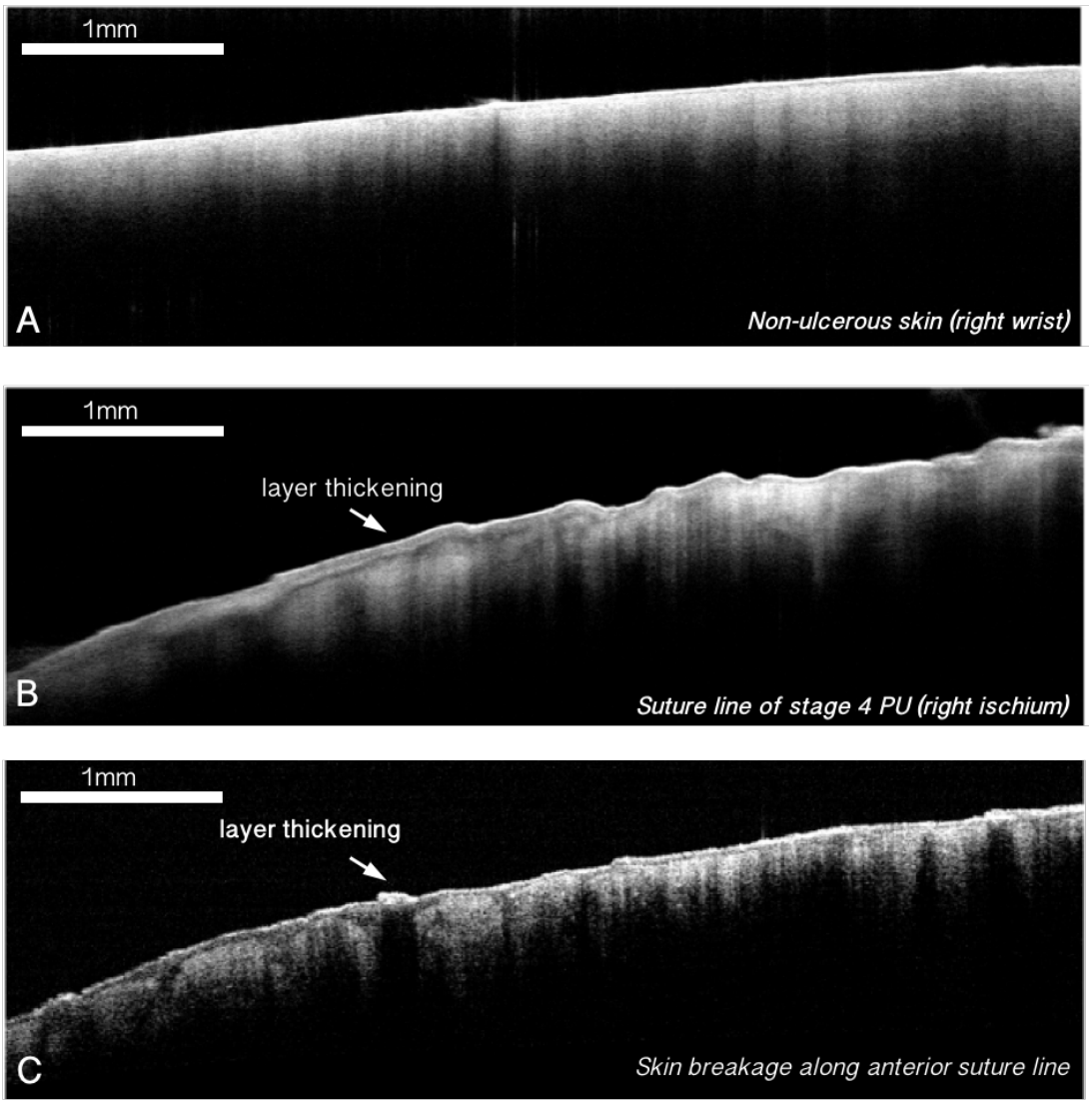

Figure 6.7 — OCT scans from subject 4: (A) Scan of non-ulcerous skin taken from the subject's right wrist**. (B)** Scan from the suture line of a surgically debrided and sutured stage 4 pressure ulcer on the subject's right ischium with evidence of thickening of the upper skin layers. **(C)** Scan of skin breakdown along the anterior aspect of the suture line layer showing evidence of layer thickening**; [**PU = pressure ulcer].

6.4.5 Subject 5

Subject 5 was a 74-year-old Caucasian female and a T6 paraplegic. The subject had no current detected pressure ulcers but had large areas of chronic dermatitis on their groin, genitalia, perianal region and buttocks.

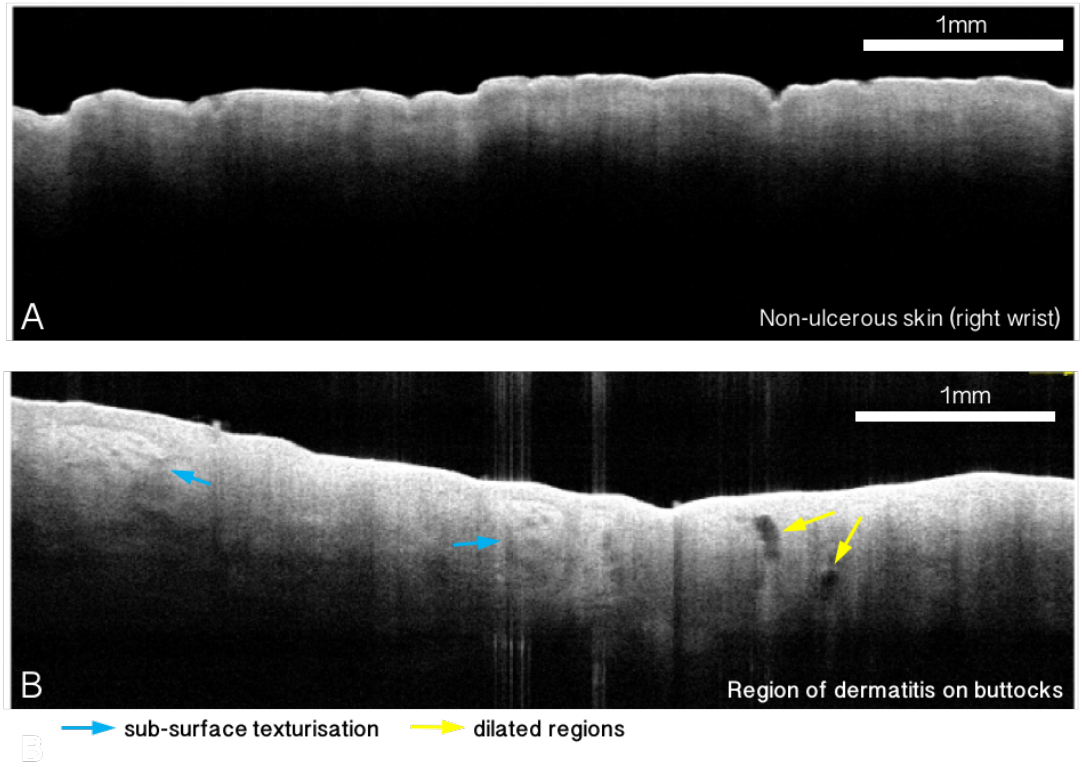

Figure 6.8 — OCT scan of subject 5 suffering from chronic dermatitis on their buttocks: (A) Non-ulcerous skin from the subject's right wrist. **(B)** A region of dermatitis on the buttocks with evidence of subsurface texturisation and dilated area as indicated.

6.5 Results

6.5.1 iVue® OCT scans

The typical penetration depth of OCT scanning ranges from several hundred microns to several millimetres depending on the exact frequency of light being used and the scattering properties of the tissue being imaged. For the iVue® scanner, skin penetration depth in the observation audit was on average 600 µm (with up to 800 µm in some scans) and this provided enough depth to image into the upper dermis. The iVue® OCT scans were also able to differentiate between the discrete structural layers of the upper skin namely the stratum corneum, epidermis and papillary dermis as well as being able to resolve hair follicles. It is important to note that

the relative thicknesses of these layers from the case studies were dependent on several factors including body region and the subject's age. For example, the stratum corneum is thicker on the palms of the hands compared with the dorsal aspect of the forearm[312]. Additionally, older subjects may have thinner skin as the epidermis is known to thin with age[72]. Measurements from the OCT scans of healthy human skin from an individual with no prior history of pressure ulcers was in good concordance with previously reported values for the age-range and gender of the individual (**Figure 6.9**).

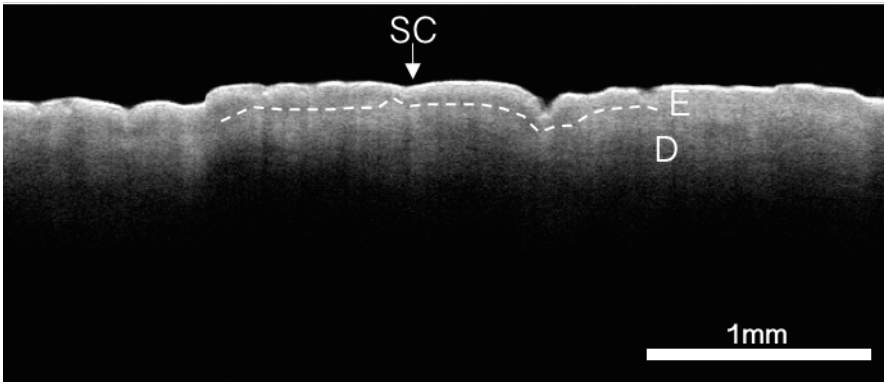

Figure 6.9 — OCT scan of healthy forearm skin from an individual with no prior history of pressure ulcers. The OCT image is able to distinguish between three skin layers the stratum corneum [SC], epidermis [E] and dermis [D] which have been demarcated. A photograph taken on the the iVue® scanner's in-built 5MP camera of the same region is inset.

6.5.2 Subject case studies

Subjects had to be imaged lying down — all were paraplegic so body positions for imaging were highly limited or required assistance from a second person that needed to be a trained member of medical staff. Pressure ulcer distribution amongst the subjects indicated that the supine and lateral positions were the most common positions for bed-ridden subjects in the ward (**Figure 6.10**). Pressure ulcers were typically seen around the lower back, sacrum, ischium and trochanter. Despite current turning protocols reported in the literature, nurses commented that subjects in Osborne 2 were turned every 4–6 hours. All subjects in the study were paraplegic either due to congenital illness or paralysis acquired during their life-time. Of the five subjects included in the study, three presented with a surgically debrided stage 4 pressure ulcer, two with a surgically sutured stage 4 pressure ulcer, one with a stage 2 pressure ulcer and one without any pressure ulcers but with chronic dermatitis in a region vulnerable to ulcer development. Only one subject (subject 1) had two concurrent unresolved pressure ulcers.

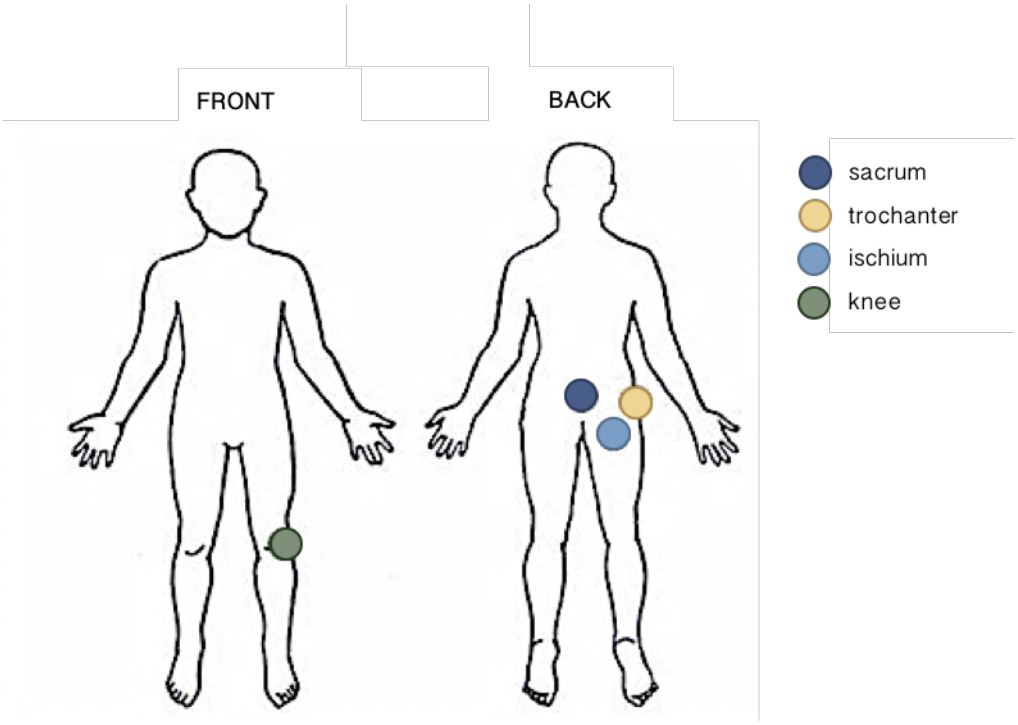

Figure 6.10 — Anatomical positions showing the distribution of exisiting or resolved pressure ulcers amongst all five subjects successfully scanned in Osborne 2.

Table 7 — NPUAP staging and corresponding OCT findings for the five subjects with current or healed pressure ulcer injury or a dermatological condition at typical pressure ulcer development sites.

			OCT Finding		
Subject	**NPUAP stage or condition**	**Location**	*Uneven layer thickening*	*Subsurface shadowing*	*Subsurface texturisation*
1	1	ischium	++	–	–
	1	knee	+	–	–
	4 healed (sutured)	sacrum	–	–	–
2	4	trochanter	–	++	–
3	4	sacrum	–	+	–
4	4 healed (sutured)	ischium	+	–	–
5	dermatitis	buttocks	–	–	+

NPUAP = National Pressure Ulcer Advisory Panel. ++ strongly positive, + positive, – negative.

Both subjects scanned with unsutured, surgically debrided stage 4 pressure ulcers (subjects 2 and 3), showed circular subsurface shadowing indicative either of potential artefacts caused by surface moisture, deteriorated subsurface regions or subcutaneous fat. Two pressure ulcers on the same subject (subject 1), currently classed as stage 1, showed uneven thickening within the epidermal layer, not seen as prominently in healthy skin or ulcers at higher stages in other subjects. This uneven subsurface thickening was also observed at the breakage of a suture line of a surgically treated stage 4 ulcer (subject 4). Subsurface skin texturisation and very strong back-scattering signals could be indicative of underlying inflammation. What appears to be subsurface texturisation is present in the dermis of a subject suffering from chronic dermatitis of the buttocks (subject 5). Compared with healthy control skin, this area exhibited strong signal reflectance which is consistent over a series of images taken in that area.

6.6 Discussion

This first-of-its-kind observational audit was carried out to evaluate the ability of cutaneous OCT scanning to assess pre-ulcerous, ulcerous and post-ulcerous skin and to ascertain whether there was congruity between current clinical staging scales and the subsurface characteristics observed in the scans. OCT B-scans in cutaneous imaging have already been shown to be excellent for obtaining qualitative results on the subsurface skin architecture and quantitative measurements of individual skin layers[59,71,98–100]. Authors have reported accurate *in vivo* measurements of epidermal thickness across different genders, ages and body regions using OCT scanning[72,312–314]. OCT scanning has also been used to diagnose and evaluate a range of skin conditions and has been repurposed from its original clinical application of monitoring

medical eye conditions, for example in the non-invasive diagnosis of non-melanoma skin cancer and monitoring of inflammation in inflammatory skin conditions.

During the audit, there were four subsurface structures that were flagged as potentially representing abnormal tissue damage. These were uneven thickening of the uppermost skin layers, circular subsurface shadows, subsurface texturisation and dilated low back-scattering regions. Uneven thickening of the uppermost skin layers was seen in early stage ulcers of several subjects as well as at suture scars of surgically treated stage 4 ulcers. The epidermal layers appeared to thicken but without blistering and could be indicative of necrosis or inflammatory changes. This uneven thickening of subsurface layers in pre-ulcerous, early ulcerous and post-ulcerous skin could also be indicative of future skin deterioration. Circular subsurface shadows were present in all the open stage 4 pressure ulcers that were imaged and could be indicative of underlying necrotic damage, an artefact of wound exudate on the skin surface or the backscattering pattern of subcutaneous fat. Similar structures have been identified in OCT images of skin in the inflammatory phase of acute wound healing[301]. The authors identified honeycomb shadows caused by the presence of subcutaneous fat in a healthy subject that had been given a 5 mm punch biopsy (**Figure 6.11 – B**).

Subsurface skin texturisation with very strong signalling could be indicative of underlying inflammation that may be a result of a dermatological condition other than pressure-related injury such as contact dermatitis. These structures have been previously identified as collagen misalignment in the dermis[298]. A participant in the audit with contact dermatitis and no current pressure ulcers exhibited these signals in the OCT scans of their buttocks. Dermatitis in this region is related to urinary and/or faecal incontinence, whereby moisture and changes in pH result in an inflammatory response due to prolonged excretory product contact with the skin. The OCT scans of this subject also contained regions of relatively low backscattering in the dermis. Similar structures have been reported in psoriatic skin and have been identified as dilated blood vessels[61]. This is in good concordance with tissue in a highly inflammatory state. Though dermal inflammation is not specific to dermatitis, presence of these markers may be able to differentiate between contact dermatitis and pressure-related injuries.

OCT scanning could be also useful in scar assessment of subjects with surgically treated pressure ulcers. Skin scarred from surgical treatment of a severe pressure ulcer often has a very different physical appearance and texture to normal skin due to the remodelling of the ECM during post-wound closure. These scars should be closely monitored in subjects as they occur in places already identified as high risk for pressure ulcer development and are vulnerable to deterioration. OCT scans could be used to monitor such scars for signs of skin or suture line deterioration, especially in recurrently or consistently immobilised individuals. The scans may

be able to identify and differentiate between wounds that have healed successfully and those that are likely to worsen without the appropriate preventative measures. From the OCT images on subject 4 it may be inferred that this subject is at risk of re-developing an ulcer at that site since the subsurface markers are similar to those seen with stage 1 ulcers, though a subject follow-up would be required to determine the exact outcome. For confirmation of what the observed structures represent, the OCT scans need to be compared with histological sections. Alternatively, to avoid highly invasive biopsies, a prospective aspect to the audit would assess whether predictions made from the subsurface biomarkers observed in the OCT scans were accurate.

Table 8 — Summary of the possible relationship between OCT findings and the pressure ulcer stage or dermatological condition they were observed in; [PU = pressure ulcer].

OCT finding	Possible biomarker of:	PU stage or condition observed in
Upper layer thickening	Epidermal changes potentially indicative of skin deterioration	• Stage 1 PU • Suture line breakage
Circular subsurface shadows	Exposed subcutaneous fat *or* Artefacts from surface moisture *or* Underlying necrotic damage	Stage 4 PU
Subsurface texturisation	Collagen misallighnment in dermis	Dermatitis (chronic inflammation)
Dilated regions	Dilated blood vessels in dermis	Dermatitis (chronic inflammation)

Figure 6.11 — Images of different skin conditions using optical coherence tomography or ultrasound: (A) OCT scan of inflammation in psoriatic skin showing dilated blood vessels in the dermis. Adapted from "Optical coherence tomography in contact dermatitis and psoriasis," by J. Wlezel et al., 2003, Arch Dermatol Res, 295, p. 52. **(B)** OCT scan of skin in the process of acute wound healing. Adapted from "Optical coherence tomography: a reliable alternative to invasive histological assessment of acute wound healing in human skin?" by N.S Greaves et al., 2014, The British Journal of Dermatology. 170, p. 846. **(C)** Ultrasound scans showing hypoechoic regions (*left*) and collagen misalignment (*right*). Adapted from "Ultrasound Assessment of Deep Tissue Injury in Pressure Ulcers: Possible Prediction of Pressure," by A. Noriyoki et al., 2009, American Society of Plastic Surgeons, 124, p. 546.

6.6.1 Limitations of the OCT scanning system

During the observational audit there were several notable limitations of the OCT scanning system. Firstly, to acquire high quality scans the subject needed to remain completely still and the hand of the operator needed to be steady. Poor quality scans were typically a result of subject body movement (**Figure 6.12 – A**). With repeated measurements at the same site, scan quality typically became poorer as any unnatural positions the subject was placed in became more difficult to maintain. Secondly, undulating or jutting structures were difficult to image such as those around the knee or uneven wound surfaces (**Figure 6.12 – B**). Similarly, imaging into ulcerated cavities, such as the unsutured stage 4 pressure ulcers proved difficult since the scanning head had to be very carefully guided into the ulcer without any part of the lens or scanning head touching the sides of the wound bed. In these instances, imaging at the margins of the pressure ulcer was an easier option. Furthermore, artefacts in the images — namely the circular subsurface shadows seen in the stage 4 pressure ulcer scans — may have be caused by slough, debris and wound exudate on the skin which were not removed prior to scanning.

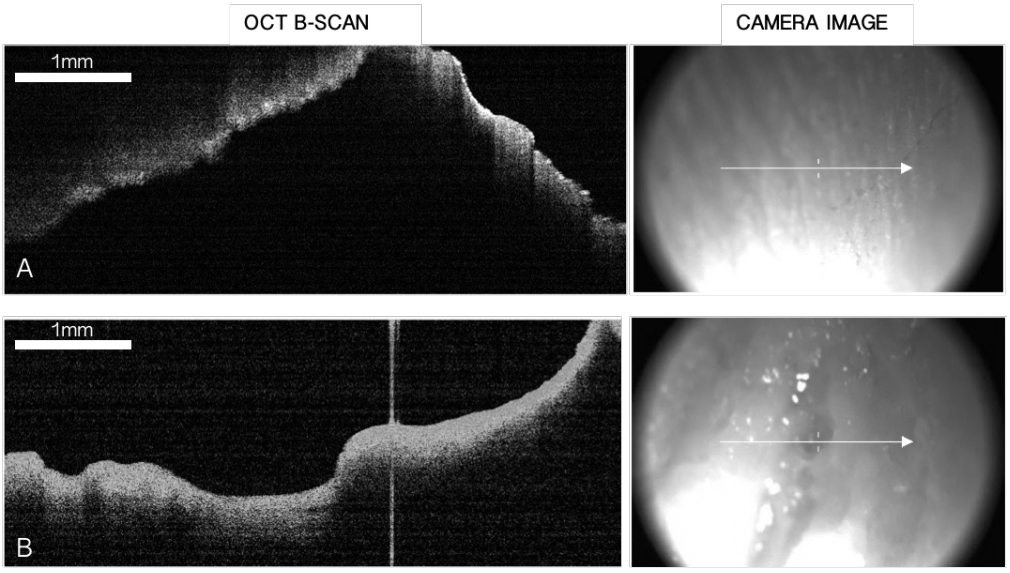

Figure 6.12 — Examples of poor quality OCT scans and their corresponding digital photographs taking during the observational audit: (A) OCT scan taken across a stage 4 pressure ulcer**. (B)** An OCT scan taken during subject movement.

6.6.2 Novel pressure ulcer evaluation and early pressure ulcer detection techniques

There have been two major approaches to the imaging of pressure ulcers that have emerged over the past twenty years. These are the repurposing of existing imaging tools and the development of new medical devices. Each approach has its own advantages and limitations. The rationale behind the repurposing of existing imaging modalities is to reduce costs associated with device development, extensive clinical trials and product manufacture. Well-documented protocols and safety profiles already exist for the equipment, there are cohorts of staff already trained to operate the systems and the technology is often readily available in the clinic. The major disadvantage is that the technology is not specific to the disease in question. Furthermore, any biomarkers identified in one dermatological disease may in fact be seen in other diseases and thus not provide enough diagnostic detail. It is likely that the repurposed devices need adaptations to better suit their novel application, such as being made more portable or having adjustments made to image acquisition parameters. Examples of repurposed imaging modalities include magnetic resonance imaging (MRI), computerised tomography (CT), and ultrasound which have all been investigated in pressure ulcer evaluation[210,298,315]. Of particular interest, in comparison to OCT, is ultrasound due to its very low risk, highly portable, *in vivo* imaging capabilities.

Ultrasonographic evaluation of pressure ulcers has identified potential bio-structural markers indicative of underlying DTI. In their clinical study, Aoi *et al.* (2009) investigated the ability of ultrasound assessment to predict pressure ulcer progression in pressure ulcers with DTI[298]. The authors noted four structures in their prospective study that were consistent with abnormal signs of DTI. These were unclear layered structures, discontinuous fascia, hypo-echoic lesions and heterogeneous hypo-echoic areas. Their results suggested that of the four structures observed only two, discontinuous fascia and a heterogeneous hypoechoic area, were reliable predictors of a negative outcome i.e. advancement of pressure ulcer staging, and were reported as being indicative of deep tissue necrotic changes. In comparison with OCT, high-frequency ultrasound does not resolve structures or skin architecture as well as OCT but is able to image much deeper into the tissue. This can be clearly seen when comparing OCT and ultrasound scans of similar regions.

As aforementioned, one of the major setbacks of repurposing existing imaging tools designed for a particular medical application is that the device is often not completely adapted or specific to the new purpose. In contrast, there have been several medical devices designed for use by healthcare providers for implementation as part of pressure ulcer prevention programmes. Objective biophysical markers such as tissue bioimpedance and sub-epidermal moisture have been identified as useful indicators of pressure ulcer-related subsurface injury[316]. Sub-

epidermal moisture reflects changes in the interstitial fluid as a result of inflammatory and necrotic activity in the epidermal and dermal layers of the skin which also have an effect on the electrical properties — or bioimpedance — of the tissue[316]. The handheld SEM (sub-epidermal moisture) Scanner™ produced by Bruin Biometrics (California, USA) was designed as a biosensor for changes in pressure ulcer injury[317]. The developers suggest that sub-epidermal moisture representing localised oedema can differentiate between healthy skin and skin with current or imminent pressure-induced tissue damage which has been corroborated by numerous studies[318–322]. When pressed against the skin the SEM Scanner™ displays a digital reading which acts as a comparative measure of sub-epidermal moisture relative to adjacent tissues[317]. The device offers the operator simple feedback, providing an objective value with minimal interpretation needed. However, there is no visual feedback from the scanner of the regions being imaged. Pilot month-long trials have been undertaken to assess the predictive capacity and reliability of the SEM scanner™ in pressure ulcer assessment[317].

6.6.3 A role for OCT at the bedside?

OCT for early stage pressure ulcer evaluation

One of the main aims of pressure ulcer evaluation should be to reduce avoidable harm through early pressure ulcer detection. Pre-ulcerous skin or pressure ulcers at the earliest stages of development are most likely the best targets for OCT imaging evaluation since, at later stages, the extent of damage is already evident and the main intervention methods would be currently limited to surgical debridement and suturing. OCT may also be able to assess pressure ulcers marked as unstageable and provide insight to the extent of underlying non-visible damage to confirm clinical suspicion. A less subjective method of pressure ulcer categorisation could also improve consensus among medical staff. Despite its limitations, OCT offers a reasonable alternative to traditional bedside scoring systems and competitor devices.

OCT for monitoring microneedle-assisted drug delivery

In addition to its evaluative capacity, OCT could also be used to observe the effect of treatments at an injury site. OCT is able to image and guide microneedle-mediated drug delivery for example. Microneedle insertion has been successfully visualised by OCT scanning *in vivo*[239,323], wherein microneedle dissolution[177,323,324] and rate of micropore closure[325,326] were observed. In Chapter 2, depth penetration of the microneedle was observed in the Strat-M™ synthetic membrane. In this vein, OCT could also be used to monitor the pharmacologic action of the delivered active pharmaceutical ingredient (API), such as doxycycline, and could help determine whether an intact ulcer is resolving or worsening through the observation of informative subsurface markers. OCT microangiography may also be useful in monitoring ischemia and reperfusion of tissue in response to external pressure at the bedside[295,327].

Preliminary experiments have begun to explore the application of OCT in facilitating intradermal drug delivery (**see**

***Appendix E — OCT images of drug delivery through a hollow microneedle array, p.265*)**.

6.7 Future work

Future studies would require a larger subject cohort, preferably with a broader range of skin pigmentation and pressure ulcer stages and a prospective aspect to the study to follow-up the pressure ulcers over time. In this way the predicative ability of OCT in evaluating pressure ulcer development can be assessed and can also be compared with existing risk assessment scales including the Norton, Waterlow and Braden scales. Furthermore, quantitative analysis of the OCT scans such as the mean grey value or peak values from A-scans could allow for an algorithm between scan and skin status to be developed. A high-resolution hand-held dermatological OCT scanner, rather than a portable ophthalmological OCT scanner could improve the scanning and image acquisition experience for the operator. Inclusion of two or more operators within the study would help determine whether inter-operator image acquisition and interpretation is in good concordance.

6.8 Conclusion

Here it has been demonstrated, with preliminary scans, a potential correlation between subsurface markers imaged by OCT and traditional clinical staging systems for pressure ulcer classification. It has been shown that OCT may offer additional useful information on top of these scales, such as prediction of normal skin areas likely to become ulcerous or predictions of that an existing sore will soon worsen, which could immensely improve clinical care and intervention strategies for the subject implicating a role for OCT at the bedside. Further still, scar assessment could be achieved through OCT scanning and allow for monitoring of high risk, previously deteriorated and ulcerous regions. A hypothesised congruity between current staging scales and architectural changes in OCT scans is outlined in **Figure 6.14** .

Figure 6.13 — The use of OCT in the literature to visualise microneedle insertion and monitor dissolution: (A) OCT images over time of dissolving microneedles applied to rat skin. From "Influence of skin model on *in vitro* performance of drug-loaded soluble microneedle arrays": by M. J. Gardland *et al.,* 2012, International Journal of Pharmaceutics, 434, p 86. **(B)** Dissolution of 2 mm silk microneedles in murine skin as visualised by OCT. From "*In vivo* and *in situ* imaging of controlled-release dissolving silk microneedles into the skin by optical coherence tomography," by R. Lie, M. Zhang and C. Jin, 2016, Journal of Biophotonics, 8, p. 7.

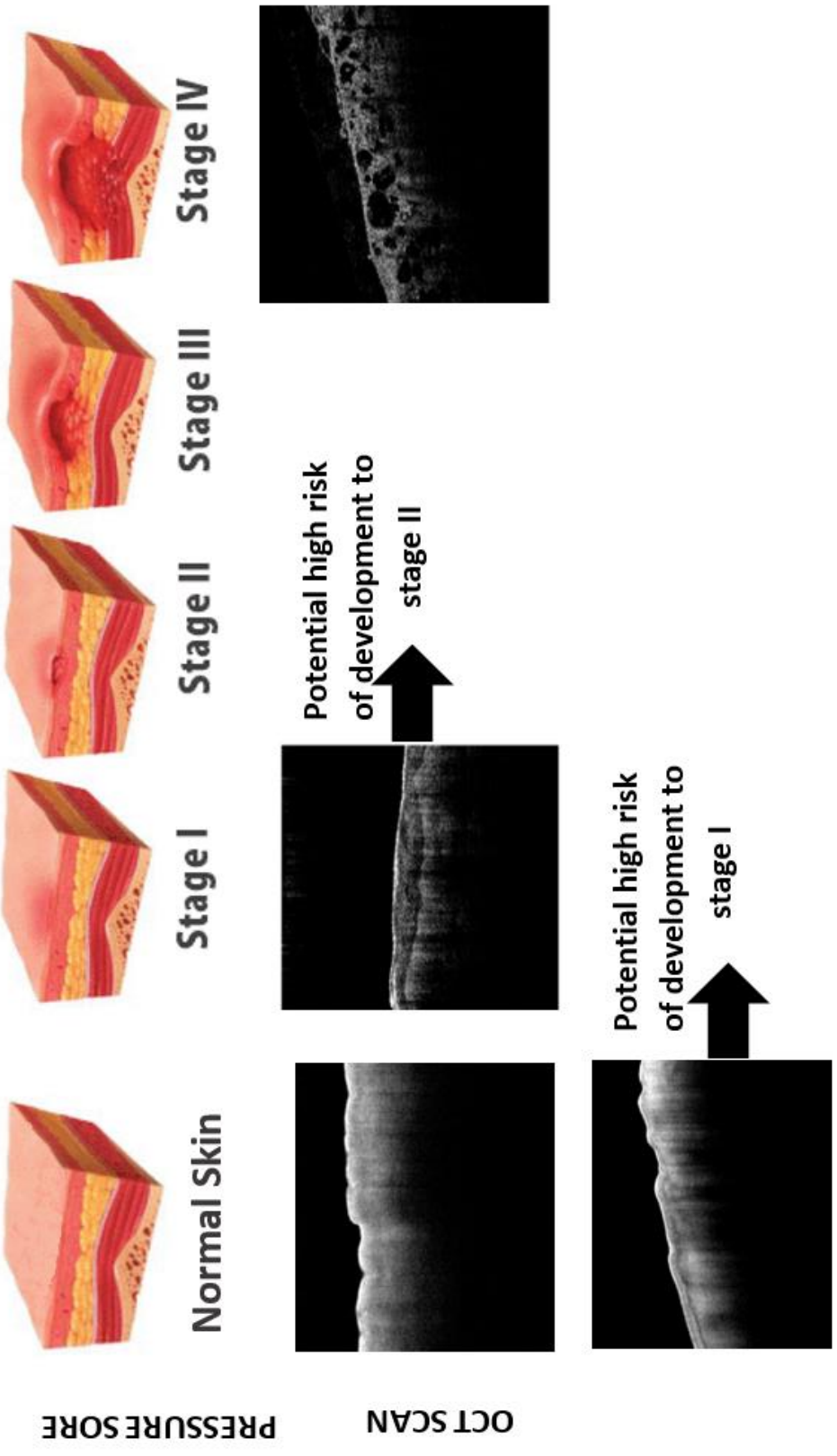

Figure 6.14 — Schematic representation of potential congruity between subsurface markers imaged by OCT and traditional clinical staging systems for pressure sore classification

Overall Discussion

Research summary

The research hypothesis outlined at the beginning of this thesis was as follows:

"Intradermal delivery of doxycycline by microneedles is a promising tool for treating and preventing the development of early stage pressure ulcers."

This hypothesis was tested by: (i) showing how doxycycline inhibits MMP activity *in vitro*, (ii) showing how doxycycline can be efficiently delivered across the skin barrier using an epidermal mimetic, (iii) refining a preclinical model of pressure ulcer formation to simulate stage 1 ulcers, (iv) establishing a non-invasive *in vivo* imaging tool to identify changes in the skin in the *in vivo* and preclinical models (and validating the technical feasibility of this approach in humans), and (v) evaluating pressure ulcer formation in the preclinical model (MMP expression, histological and vascular changes etc.) which could be used to assess the effect of treatment with doxycycline delivered by microneedles. From the culmination of research reported in this thesis, microneedles have been shown to enhance intradermal permeation of doxycycline and doxycycline has several attributes of an active drug suitable for the treatment and prevention of pressure ulcers. However, further confirmatory experiments and most likely clinical trials would be required to test the latter portion of the hypothesis.

Contribution to knowledge

This body of work has introduced several concepts that have not previously been published in the literature. Firstly, microneedles have been suggested specifically in the treatment of pressure ulcers and this research has provided a background to how and why this is feasible, which, to my knowledge, has not been done before. Secondly, it has been shown for the first time how the newly launched synthetic epidermal mimetic Strat-M^{TM} could be permeabilised to large, hydrophilic molecules through the application of microneedles. This offers a useful basis on which other similarly-sized drugs could also be tested. Thirdly, it was shown how the delivery of doxycycline through microneedle-treated Strat-M^{TM} could be monitored through its effect on existing and validated tissue equivalent models.

Furthermore, these existing *in vitro* models have been better adapted in this research to reflect the external stressors associated with the pressure ulcer microenvironment. This included introducing clinically relevant pressure (that results in tissue breakdown *in vivo*) by exposing the model to a pressure of 32 mmHg (equivalent to capillary closing pressure [CCP]). From this work, the effect of doxycycline and its microneedle-mediated delivery could be further explored in the preclinical model using magnetic compression to simulate CCP. Importantly, this research also began to explore a potentially negative effect of microneedling on cell viability in injured and stressed tissue, though further investigation is required to draw valid conclusions. Finally, the concluding research chapter detailed the first known evaluative study to use OCT to image into both intact and open pressure ulcers. This novel approach provided a basis for the repurposing of existing imaging tools in clinical pressure ulcer care and management.

From bench to bedside — potential real world applications

There is great potential for the clinical use of microneedle rollers in the chronic wound management of pressure ulcers, specifically to deliver an active drug in a timely manner to prevent pressure ulcer development and to treat existing tissue damage. There are several ways this can be achieved. The microneedle rollers could be used to permeabilise the skin surface of an intact stage 1 pressure ulcer, or DTI, using their high mobility and ability to cover large surface areas. A drug-infused patch or wound dressing could then be applied onto the skin to promote wound healing (**Figure 7.1 – A**). In the case of early stage open ulcers (i.e. stage 2 pressure ulcers), the microneedle rollers can be used in a circumferential manner, by rolling the device around the perimeter of the wound. This process should itself promote re-epithelisation[84], but also permeabilises the surrounding skin to active drugs in order to help reduce the spread of damage into the surrounding tissue (**Figure 7.1 — B**).

For very large cavitied ulcers, the traditional treatment options are indicated. In these instances, doxycycline treatment could be used as an adjunctive chemotherapy to help reduce elevated MMP levels. This could be achieved through the administration of a doxycycline-containing gel into the wound cavity or lavage of the wound bed surface, essentially rinsing, with doxycycline solution (**Figure 7.1 – C**). Although doxycycline is the current drug of interest, it need not be the only drug delivered in pressure ulcer treatment — its role is interchangeable with other large hydrophilic drugs with a potential therapeutic effect in pressure ulcers. In a similar vein, microneedle-enhanced drug delivery could also be applied to other chronic wounds including diabetic ulcers and venous leg ulcers.

Hollow microneedles may be able to replace the solid microneedles in some instances, for example in the infusion of less viscous, fluid drug formulations. Sufficient dosaging by infusion may be problematic however. The development of a single hollow microneedle was explored during the research in collaboration with a materials scientist and is discussed further in:

Appendix A — Development of a single custom-made hollow microneedle in combination with a Hamilton syringe, *p. 240*. A potential drug delivery vehicle that could be used in combination with the hollow microneedles is a specialised gel that was developed in collaboration with a protein chemist. This MMP-cleavable smart gel encapsulates doxycycline and only forms when the components are combined during dual microinjection. This novel smart gel is discussed in detail in:

Appendix C — Development of an MMP-cleavable protein-based smart gel, *p. 243*.

The maximum length of microneedles that were investigated in this research were 750 µm. However, microneedles, contrary to their name, can reach up to 3 mm. Due to the variety of different lengths, different microneedles could be used at different anatomic sites for intradermal drug delivery, seeing as skin layer thickness is not consistent throughout the body. Numbing cream may be applied if the patient is capable of pain sensation in the region of application (pressure ulcer patients are typically paralysed) and if the microneedles penetrate sufficiently deep as to stimulate dermal nerves. Clinically-used microneedle roller systems should be single-use devices for hygiene purposes and due to the likelihood of blunting of the needle tops which would reduce efficacy. The use of drug 'delayers' could help slow micropore-resealing kinetics to increase the length of time in which the drug can permeate[328,329].

Achieving the goals of the BBSRC LIDo programme

The major goal of the LIDo programme is to answer research questions through inter-disciplinary, multi-institution research. This has been demonstrated in this research through collaborations across several disparate, but complementary, fields. These have included pharmaceutics for the monitoring of microneedle-mediated drug delivery, cell and molecular biology for the development of a dermal tissue equivalent model, material sciences for the fabrication of microneedles, molecular biophysics and protein chemistry for the development of smart gels and clinical imaging, in a research and a hospital setting, for the evaluation of OCT in a novel application.

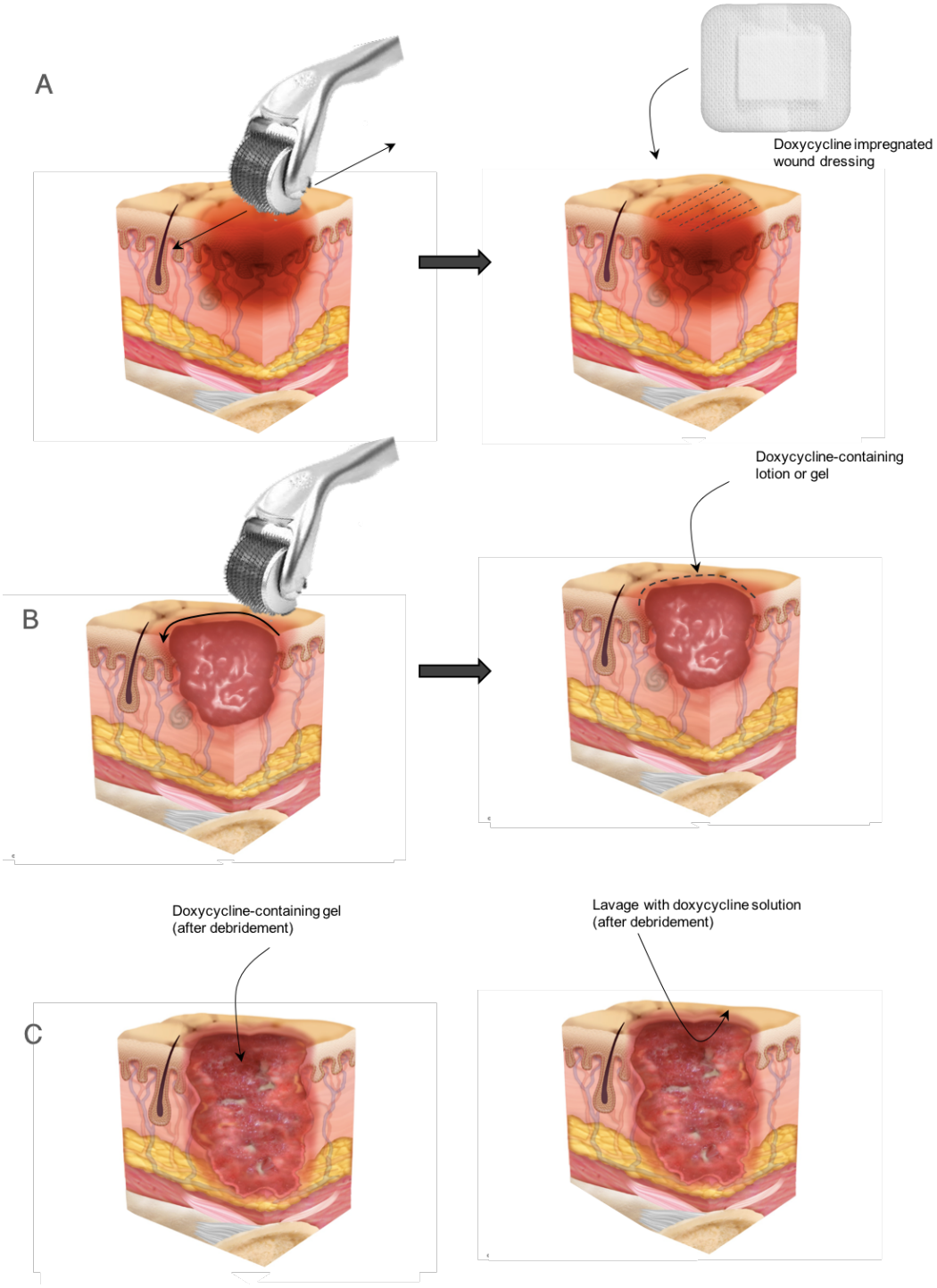

Figure 7.1 — Potential approaches to microneedle-mediated doxycycline delivery to various pressure ulcer stages: (A) Microneedle-mediated permeabilisation of a stage 1 ulcer, followed by application of a wound dressing, gel or lotion containing doxycycline or another suitable API. **(B)** Circumferential application of the microneedles around the perimeter of the open ulcer, followed by direct application of a drug-infused gel or lotion. **(C)** Direct delivery of doxycycline into a cavitied late stage ulcer in the form of a gel (*left*) or lavage (*right*) with doxycycline solution.

Bibliography

1. Mustoe, T. Understanding chronic wounds: a unifying hypothesis on their pathogenesis and implications for therapy. *Am. J. Surg.* **187,** 65S–70S (2004).

2. Coleman, S. *et al.* Patient risk factors for pressure ulcer development: Systematic review. *Int. J. Nurs. Stud.* **50,** 974–1003 (2013).

3. Thomas, D. R. Prevention and treatment of pressure ulcers: what works? what doesn't? *Cleve. Clin. J. Med.* **68,** 704–7, 710–14, 717–22 (2001).

4. (2014a)., N. C. G. C. *Pressure Ulcer Prevention: The Prevention and Management of Pressure Ulcers in Primary and Secondary Care. CG179.* (2014).

5. Schindler, C. A. *et al.* Under pressure: Preventing pressure ulcers in critically ill infants. *J. Spec. Pediatr. Nurs.* **18,** 329–341 (2013).

6. Shahin, E. S. M., Dassen, T. & Halfens, R. J. G. Incidence, prevention and treatment of pressure ulcers in intensive care patients: a longitudinal study. *Int. J. Nurs. Stud.* **46,** 413–21 (2009).

7. Keller, B. P. J. A. & Ramshorst, B. Van. Pressure ulcers in intensive care patients : a review of risks and prevention. *Intensive Care Med* **28,** 1379–1388 (2002).

8. Peterson, N. & Bittmann, S. The epidemiology of pressure sores. *Scand. J. Plast. Reconstr. Surg.* **5,** 62–66 (1970).

9. Barbenel, J., Jordan, M. & Nicol, S. Incidence of pressure sore in the greater Glasgow health board area. *Lancet* **2,** 548–550. (1977).

10. Versluysen, M. Pressure sores in elderly patients. The epidemiology related to hip operations. *J. Bone Jt. Surg.* **67,** 10–13 (1985).

11. Marsden, G. *et al.* A cost-effectiveness analysis of two different repositioning strategies for the prevention of pressure ulcers. *J. Adv. Nurs.* 1–7 (2015). doi:10.1111/jan.12753

12. Bennett, G., Dealey, C. & Posnett, J. The cost of pressure ulcers in the UK. *Age Ageing* **33,** 230–5 (2004).

13. Agrawal, K. & Chauhan, N. Pressure ulcers: Back to basics. *Indian J. Plast. Surg.* **45,** 244–254 (2012).

14. Bouten, C. V, Oomens, C. W., Baaijens, F. P. & Bader, D. L. The etiology of pressure ulcers: skin deep or muscle bound? *Arch. Phys. Med. Rehabil.* **84,** 616–9 (2003).

15. Bouton, V. C. B. *Etiology and pathology of pressure sores: a literature review. WFW report 96.015* (1996).

16. Baranoski, S. Raising awareness of pressure ulcer prevention and treatment. *Adv. Skin Wound Care* **19,** 398-405–7 (2006).

17. Meehan, M. National pressure ulcer prevalence survey. *Adv Wound Care* **7,** 27–37 (1994).

18. Mak, A. F. T., Zhang, M. & Tam, E. W. C. Biomechanics of pressure ulcer in body tissues

interacting with external forces during locomotion. *Annu. Rev. Biomed. Eng.* **12,** 29–53 (2010).

19. Walton-Geer, P. S. Prevention of pressure ulcers in the surgical patient. *AORN J.* **89,** 538-48-51 (2009).

20. Campbell, C. & Parish, L. C. The decubitus ulcer: facts and controversies. *Clin. Dermatol.* **28,** 527–32 (2010).

21. Alvarez, O. Pressure ulcers - critical considerations in prevention and management. *Clin Mater* **8,** 209–222 (1991).

22. Levi, B. & Rees, R. Diagnosis and management of pressure ulcers. *Clin Plast Surg* **34,** 735–248 (2007).

23. Serpa, L. F., Santos, V. L. C. G., Peres, G. R. P., Cavicchioli, M. G. S. & Hermida, M. M. Validity of the Braden and Waterlow subscales in predicting pressure ulcer risk in hospitalized patients. *Appl. Nurs. Res.* **24,** e23-8 (2011).

24. Anthony, D., Papanikolaou, P., Parboteeah, S. & Saleh, M. Do risk assessment scales for pressure ulcers work? *J. Tissue Viability* **19,** 132–6 (2010).

25. Waterlow. Pressure sores: A risk assessment card. *Nurs. Times* **81,** 49–55 (19865).

26. Braden, B. & Bergstrom, N. A conceptual schema for the study of the etiology of pressure sores. *Rehabil. Nurs.* **12,** 8–12 (1987).

27. Kottner, J. & Dassen, T. Pressure ulcer risk assessment in critical care: interrater reliability and validity studies of the Braden and Waterlow scales and subjective ratings in two intensive care units. *Int. J. Nurs. Stud.* **47,** 671–7 (2010).

28. Mallah, Z., Nassar, N. & Kurdahi Badr, L. The effectiveness of a pressure ulcer intervention program on the prevalence of hospital acquired pressure ulcers: controlled before and after study. *Appl. Nurs. Res.* **28,** 106–113 (2014).

29. Pressure ulcers. *NHS choices* (2012). Available at: http://www.nhs.uk/Conditions/Pressure-ulcers/Pages/Introduction.aspx.

30. Sugarman, B. *et al.* Osteomyelitis beneath pressure sores. *JAMA* **143,** 683–688 (1983).

31. Hagisawa, S. & Ferguson-pell, M. Evidence supporting the use of two-hourly turning for pressure ulcer prevention. *J. Tissue Viability* **17,** 76–81 (2008).

32. Ã, K. V., Grypdonck, M. & Defloor, T. Alternating pressure air mattresses as prevention for pressure ulcers : A literature review. **45,** 784–801 (2008).

33. Mcinnes, E., Sem, B., Jc, D. & Cullum, N. Support surfaces for pressure ulcer prevention (Review). *Cochrane Libr.* 1–130 (2011).

34. Yusuf, S. *et al.* Microclimate and development of pressure ulcers and superficial skin changes. *Int. Wound J. ISSN* **12,** 1–7 (2015).

35. Thomas, D. R. Prevention and treatment of pressure ulcers. *J. Am. Med. Dir. Assoc.* **7,** 46–59 (2006).

36. Whitney, J. *et al.* Guidelines for the treatment of pressure ulcers. *Wound Repair Regen.* **14,** 663–679 (1999).

37. Kuffler, D. P. Techniques for wound healing with a focus on pressure ulcers elimination. *Open Circ. Vasc. J.* **3,** 72–84 (2010).

38. Menke, M. N., Menke, N. B., Boardman, C. H. & Diegelmann, R. F. Biologic therapeutics

and molecular profiling to optimize wound healing. *Gynecol. Oncol.* **111,** S87-91 (2008).

39. Cornell, R. S., Meyr, A. J., Steinberg, J. S. & Attinger, C. E. Debridement of the noninfected wound. *J. Vasc. Surg.* **52,** S31–S36 (2010).

40. Sherman, R. . Maggot therapy for foot and leg wounds. *Int J Low Extrem Wounds* **1,** 135–142 (2002).

41. Thomson, P. D. & Smith, D. J. What is infection? *Am. J. Surg.* **167,** 7–11 (1994).

42. Daltrey, D., Rhodes, B. & Chattwood, J. Investigation into the microbial flora of healing and non-healing decubitus ulcers. *J Clin Pathol* **34,** 701–705 (1981).

43. Seiler, W., Stahelin, H. & Sonnabend, W. Effect of aerobic and anaerobic germs on the healing of decubitus ulcers. *Schweiz Med Wochenschr* **109,** 1594–1599 (1979).

44. Black, J. M. *et al.* Pressure ulcers: avoidable or unavoidable? Results of the National Pressure Ulcer Panel consensus conference. *Ostomy Wound Manag.* **57,** 24–37 (2011).

45. Lazzara, D. & Buschmann, M. Lazzara DJ, Buschmann MT. Prevention of pressure ulcers in elderly nursing home residents: Are special support surfaces the answer? *Decubitus* **4,** 42–49 (1991).

46. Whitney, J., Fellows, B. & Larson, E. Do mattresses make a difference? *J Gerontol Nurs* **10,** 2025 (1984).

47. Krouskop, T., Williams, R. & Krebs, M. Effectiveness of mattress over- lays in reducing interface pressures during recumbency. *J Rehabil Res* **22,** 7–10 (1985).

48. Daechsel, D. & Connine, T. Special mattresses: effectiveness in preventing decubitus ulcers in chronic neurologic patients. *Arch Phys Med Rehabil* **66,** 246–248 (1985).

49. Bourdel-Marchasson, I Barateau, M. & Sourgen, C. Prospective audits of quality of PEM recognition and nutritional support in critically ill elderly patients. *Clin Nutr* **18,** 233–240 (1999).

50. Bourdel-Marchasson, I., Barateau, M. & Rondeau, V. A multi-center trial of the effects of oral nutritional supplementation in critically ill older inpatients. GAGE Group. Groupe Aquitain Geriatrique d'Evaluation. Nutrition ; 16:1–5. **16,** 1–5 (2000).

51. Tandara, A. a & Mustoe, T. a. Oxygen in wound healing--more than a nutrient. *World J. Surg.* **28,** 294–300 (2004).

52. Braddock, M., D, P., Campbell, C. J. & Zuder, D. Current therapies for wound healing : electrical stimulation , biological therapeutics , and the potential for gene therapy. *Int. J. Dermatol.* **38,** 808–817 (1999).

53. Chen, S., Ward, S. & Oluyinka, O. Ability of chronic wound fluids to degrade peptide growth factors is associated with increased levels of elastase activity and diminished levels of proteinase inhibitors. *Wound Repair Regen* **30,** 23–32 (1997).

54. Gregory, S., Boyle, J., Rennison, T. & Cullen, B. An ORC/ Collagen Matrix containing silver preserves wound healing growth factors from host and bacterial proteolytic degradation. *Wound Repair Regen.* **13,** A23-33 (2005).

55. Wlaschek, M., Peus, D. & Achterberg, V. Protease inhibitors protect growth factor activity in chronic wounds. *Br J Dermatol* **137,** 646–476 (1997).

56. Thomas, D. R. Are all pressure ulcers avoidable? *J. Am. Med. Dir. Assoc.* **2,** 297–301 (2003).

57. Broughton, G., Janis, J. E. & Attinger, C. E. Wound healing: an overview. *Plast. Reconstr. Surg.* **117,** 1e-S–32e-S (2006).

58. Stechmiller, J. K. *et al.* Guidelines for the prevention of pressure ulcers. *Wound Repair Regen.* **16,** 151–168 (2008).

59. Saito, Y. *et al.* The loss of MCP-1 attenuates cutaneous ischemia-reperfusion injury in a mouse model of pressure ulcer. *J. Invest. Dermatol.* **128,** 1838–51 (2008).

60. Ramundo, J. & Gray, M. Collagenase for enzymatic debridement - a systematic review. *J. Wound Ostomy Cont.* **36,** S4–S11 (2009).

61. Welzel, J., Bruhns, M. & Wolff, H. H. Optical coherence tomography in contact dermatitis and psoriasis. *Arch. Dermatol. Res.* **295,** 50–5 (2003).

62. Levin, J. & Maibach, H. The correlation between transepidermal water loss and percutaneous absorption: an overview. *J. Control. Release* **103,** 291–299 (2005).

63. Lai-Cheong, J. E. & McGrath, J. a. Structure and function of skin, hair and nails. *Medicine (Baltimore).* **37,** 223–226 (2009).

64. Wickett, R. R. & Visscher, M. O. Structure and function of the epidermal barrier. *Am. J. Infect. Control* **34,** S98–S110 (2006).

65. Salcido, R., Popescu, A. & Ahn, C. Animal models in pressure ulcer research. *J Spinal Cord Med.* **30,** 107–116 (2007).

66. Bouwstra, J. A. & Ponec, M. The skin barrier in healthy and diseased state. *Biochim. Biophys. Acta 1758* **1758,** 2080–95 (2006).

67. Gniadecka, M. & Jemec, G. B. Quantitative evaluation of chronological ageing and photoageing in vivo: studies on skin echogenicity and thickness. *Br. J. Dermatol.* **139,** 815–21 (1998).

68. Lodish, H., Berk, A. & Zipursky, S. in *Molecular Cell Biology. 4th edition.* Section 22.3 (W. H. Freeman;, 2000).

69. Liao, F., Burns, S. & Jan, Y.-K. Skin blood flow dynamics and its role in pressure ulcers. *J. Tissue Viability* **22,** 25–36 (2013).

70. Bierman, W. The temperature of the skin surface. *Jour. A. M. A* **106,** 1158–1162 (1936).

71. JA., K. *Barr's the Human Nervous System: an Anatomical Viewpoint.* (Lippincott, Williams and Wilkins, 2009).

72. Gambichler, T., Matip, R., Moussa, G., Altmeyer, P. & Hoffmann, K. In vivo data of epidermal thickness evaluated by optical coherence tomography: effects of age, gender, skin type, and anatomic site. *J. Dermatol. Sci.* **44,** 145–52 (2006).

73. Sandby-Møller, J., Poulsen, T. & Wulf, H. C. Epidermal thickness at different body sites: relationship to age, gender, pigmentation, blood content, skin type and smoking habits. *Acta Derm. Venereol.* **83,** 410–3 (2003).

74. Schwindt, D. A., Wilhelm, K. P. & Maibach, H. I. Water diffusion characteristics of human stratum corneum at different anatomical sites in vivo. *J. Invest. Dermatol.* **111,** 385–9 (1998).

75. Farage, M. A., Miller, K. W., Elsner, P. & Maibach, H. I. Characteristics of the aging skin. *Adv. wound care* **2,** 5–10 (2013).

76. Bos, J. D. & Meinardi, M. M. The 500 Dalton rule for the skin penetration of chemical compounds and drugs. *Exp. Dermatol.* **9,** 165–9 (2000).

77. Benson, H. Transdermal drug delivery: penetration enhancement techniques. *Curr. Drug Deliv.* **2,** 23–33 (2005).

78. Marwah, H. *et al.* Permeation enhancer strategies in transdermal drug delivery. *Drug Deliv* **23,** 564–578 (2016).

79. Hadgraft, J. & Pugh, W. J. The selection and design of topical and transdermal agents: a review. *The journal of investigative dermatology* **3,** 131–135 (1998).

80. De Rie, M., Meinardi, M. & Bos, J. Lack of efficacy of topical cyclosporin A in atopic dermatitis and allergic contact dermatitis. *Acta Derm Venereol.* **71,** 452–454 (1991).

81. Powles, A. V *et al.* Intralesional injection of cyclosporin in psoriasis. *Lancet* **331,** 537 (1988).

82. Diegelmann, R. F. & Evans, M. C. Wound healing: an overview of acute, fibrotic and delayed healing. *Front. Biosci.* **9,** 283–289 (2004).

83. Toriseva, M. & Kähäri, V.-M. Proteinases in cutaneous wound healing. *Cell. Mol. Life Sci.* **66,** 203–24 (2009).

84. Liebl, H. & Kloth, L. C. Skin cell proliferation stimulated by microneedles. *J. Am. Coll. Clin. Wound Spec.* **4,** 2–6 (2012).

85. Xue, M., Le, N. T. V & Jackson, C. J. Targeting matrix metalloproteases to improve cutaneous wound healing. *Expert Opin. Ther. Targets* **10,** 143–55 (2006).

86. Dorsett-Martin, W. A. Rat models of skin wound healing: a review. *Wound Repair Regen.* **12,** 591–9 (2004).

87. Mirastschijski, U., Impola, U., Karsdal, M. A., Saarialho-Kere, U. & Agren, M. S. Matrix metalloproteinase inhibitor BB-3103 unlike the serine proteinase inhibitor aprotinin abrogates epidermal healing of human skin wounds ex vivo. *J. Invest. Dermatol.* **118,** 55–64 (2002).

88. Sanders, J. E., Mitchell, S. B., Wang, Y.-N. & Wu, K. An explant model for the investigation of skin adaptation to mechanical stress. *IEEE Trans. Biomed. Eng.* **49,** 1626–31 (2002).

89. Peirce, S. M., Skalak, T. C. & Rodeheaver, G. T. Ischemia-reperfusion injury in chronic pressure ulcer formation: a skin model in the rat. *Wound Repair Regen.* **8,** 68–76 (2000).

90. Groot, H. De & Rauen, U. Ischemia-reperfusion injury: in pathogenic networks: a review. **484,** 481–484 (2007).

91. Weiskopf, R. B., Collard, C. D., Gelman, S. & Ph, D. Prevention of ischemia-reperfusion injury. **94,** 1133–1138 (2001).

92. Kosiak, M. Etiology and Pathology of ischemic ulcers. *Arch. Phys. Med. Rehabil.* **40,** 19–29 (1959).

93. Tsuji, S., Ichioka, S., Sekiya, N. & Nakatsuka, T. Analysis of ischemia-reperfusion injury in a microcirculatory model of pressure ulcers. *Wound Repair Regen.* **13,** 209–215 (2005).

94. Woolfson, R. G., Millar, C. G. & Neild, G. H. Ischaemia and reperfusion injury in the kidney: current status and future direction. *Nephrol. Dial. Transplant* **9,** 1529–31 (1994).

95. Herrman, E. C., Knapp, C. F., Donofrio, J. C. & Salcido, R. Skin perfusion responses to surface pressure-induced ischemia: implication for the developing pressure ulcer. *J. Rehabil. Res. Dev.* **36,** 109–20 (1999).

96. Wang, W. Z., Baynosa, R. C. & Zamboni, W. A. Update on ischemia-reperfusion injury for the plastic surgeon: 2011. *Plast. Reconstr. Surg.* **128,** 685–92 (2011).

97. Anaya-Prado, R. The molecular events underlying ischemia/reperfusion injiury. *Transplant. Proc.* **34,** 2518–2519 (2002).

98. Kalogeris, T., Baines, C. P., Krenz, M. & Korthuis, R. J. *Cell Biology of Ischemia/Reperfusion Injury*. *International Review Of Cell and Molecular Biology* **298,** (Elsevier Inc., 2012).

99. Wassermann, E. *et al.* A chronic pressure ulcer model in the nude mouse. *Wound Repair Regen.* **17,** 480–4 (2009).

100. Reid, R. R., Sull, A. C., Mogford, J. E., Roy, N. & Mustoe, T. a. A novel murine model of cyclical cutaneous ischemia-reperfusion injury. *Journal of Surgical Research* **116,** 172–180 (2004).

101. Pilcher, B. K. *et al.* Role of matrix metalloproteinases and their inhibition in cutaneous wound healing and allergic contact hypersensitivity. *Ann. N. Y. Acad. Sci.* **878,** 12–24 (1999).

102. Weckroth, M., Vaheri, a, Lauharanta, J., Sorsa, T. & Konttinen, Y. T. Matrix metalloproteinases, gelatinase and collagenase, in chronic leg ulcers. *The Journal of investigative dermatology* **106,** 1119–24 (1996).

103. Witte, M. B. *et al.* Metalloproteinase inhibitors and wound healing: a novel enhancer of wound strength. *Surgery* **124,** 464–70 (1998).

104. Rogers, A. A., Burnett, S., Moore, J. C., Shakespeare, P. G. & Chen, W. Y. Involvement of proteolytic enzymes--plasminogen activators and matrix metalloproteinases--in the pathophysiology of pressure ulcers. *Wound Repair Regen.* **3,** 273–83 (1995).

105. Wysoci, A., Stiano-Coico, L. & Grinnell, F. Wound fluid from chronic leg ulcers contain elevated levels of MMP-2 and MMP-9. *J Invest Dermatol* **101,** 64–68 (1993).

106. Nwomeh, B. C., Liang, H., Cohen, I. K., Yager, D. R. & Ph, D. MMP-8 is predominant collagenase in healing wound and nonhealing ulcers. *J. Surg. Res.* **195,** 189–195 (1999).

107. Yager, D., Zhang, L., Liang, H.-X., Diegelmann, R. F. & Cohen, I. K. Wound Fluid from Human Pressure Ulcers Contain Elevated Matrix Metalloproteinase Levels and Activity Compared to Surgical Wound Fluids. *J Invest Dermatol* 734–748 (1996).

108. Madlener, M. Differential expression of matrix metalloproteinases and their physiological inhibitors in acute murine skin wounds. *Arch. Dermatol. Res.* **290 Suppl,** S24-9 (1998).

109. Rayment, E. A. & Upton, Z. Finding the culprit: a review of the influences of proteases on the chronic wound environment. *Int. J. Low. Extrem. Wounds* **8,** 19–27 (2009).

110. Saarialho-Kere, U. K. Patterns of matrix metalloproteinase and TIMP expression in chronic ulcers. *Arch. Dermatol. Res.* **290 Suppl,** S47-54 (1998).

111. Moor, A. N., Vachon, D. J. & Gould, L. J. Proteolytic activity in wound fluids and tissues derived from chronic venous leg ulcers. *Wound Repair Regen.* **17,** 832–9 (2009).

112. Naidoo, C., A, H. G., J, H. P. & Gp, H. C. Matrix metalloproteinase inhibition and antibiotics in the treatment of chronic wounds. *Wound Heal. South. Africa* **2,** 71–73 (2009).

113. Widgerow, A. D. Chronic wound fluid--thinking outside the box. *Wound Repair Regen.* **19,** 287–91 (2011).

114. Gibson, D., Cullen, B., Legerstee, R., Hardina, K. & Schultz, G. MMPs made easy. *Wounds Int.* **1,** 1–6 (2009).

115. Mutsaers, S. E., Bishop, J. E., McGrouther, G. & Laurent, G. J. Mechanisms of tissue repair: from wound healing to fibrosis. *Int. J. Biochem. Cell Biol.* **29,** 5–17 (1997).

116. Stechmiller, J., Cowan, L. & Schultz, G. The role of doxycycline as a matrix metalloproteinase inhibitor for the treatment of chronic wounds. *Biol. Res. Nurs.* **11,** 336–

44 (2010).

117. Trengove, N. J. *et al.* Analysis of the acute and chronic wound environments : the role of proteases and their inhibitors. *Wound Repair Regen* **7,** 442–452 (1999).

118. Ladwig, G. P. *et al.* Ratios of activated matrix metalloproteinase-9 to tissue inhibitor of matrix metalloproteinase-1 in wound fluids are inversely correlated with healing of pressure ulcers. *Wound Repair Regen.* **10,** 26–37 (2002).

119. Tarnuzzer, R. W. & Schultz, G. S. Biochemical analysis of acute and chronic wound environments. *Wound Repair Regen.* **4,** 321–325 (1996).

120. Reiss, M. J., Han, Y., Garcia, E., Goldberg, M. & Yu, H. Matrix metalloproteinase-9 delays wound healing in a murine wound model. *Surgery* **147,** 295–302 (1994).

121. Frøssing, S., Rønø, B., Hald, A., Rømer, J. & Lund, L. R. Skin wound healing in MMP2-deficient and MMP2 / plasminogen double-deficient mice. *Exp. Dermatol.* **19,** e234-40 (2010).

122. Wysocki, A. B. Evaluating and managing open skin wounds: colonization versus infection. *AACN Clin. Issues* **13,** 382–97 (2002).

123. Machado, L. S. *et al.* Delayed minocycline inhibits ischemia-activated matrix metalloproteinases 2 and 9 after experimental stroke. *BMC Neurosci.* **7,** 56 (2006).

124. Gendron, R., Grenier, D., Sorsa, T. & Mayrand, D. Inhibition of the activities of matrix metalloproteinases 2, 8, and 9 by chlorhexidine. *Clin. Diagn. Lab. Immunol.* **6,** 437–9 (1999).

125. Kiili, M. *et al.* Collagenase-2 (MMP-8) and collagenase-3 (MMP-13) in adult periodontitis: molecular forms and levels in gingival crevicular fluid and immunolocalisation in gingival tissue. *J. Clin. Periodontol.* **29,** 224–32 (2002).

126. Ramnath, N. & Creaven, P. J. Matrix metalloproteinase inhibitors. *Curr. Oncol. Rep.* **6,** 96–102 (2004).

127. Daniel, R., Priest, D. & DC, W. Etiologic factors in pressure sores: an experimental model. *Arch. Phys. Med. Rehabil.* **62,** 492–8 (1981).

128. Nola, G. & Vistines, L. Differential response of skin and muscle in the experimental production of pressure sores. *Plast. Reconstr. Surg.* **66,** 728–33 (1980).

129. Boyce, S. T. & Warden, G. D. Principles and practices for treatment of cutaneous wounds with cultured skin substitutes. *Am. J. Surg.* **183,** 445–56 (2002).

130. Kirketerp-møller, K., Zulkowski, K. & James, G. in *Biofilm Infections* (eds. Bjarnsholt, T., Jensen, P. Ø., Moser, C. & Høiby, N.) 11–25 (Springer New York, 2011). doi:10.1007/978-1-4419-6084-9

131. Sv, M., Min, D. & Dk, Y. Matrix metalloproteinases and their roles in poor wound healing in diabetes. *Wound Pract. Res.* **16,** 116–121 (2008).

132. Cullen, B., Smith, R., McCulloch, E., Silcock, D. & Morrison, L. Mechanism of action of Promogran, a protease modulating matrix, for the treatment of diabetic foot ulcers. *Wound Repair Regen.* **10,** 16–25 (2002).

133. Vin, F., Teot, L. & Meaume, S. The healing properties of Promogran in venous leg ulcers. *J. Wound Care* **11,** 335– 341 (2002).

134. Vandenbroucke, R. E. & Libert, C. Is there new hope for therapeutic matrix metalloproteinase inhibition? *Nat. Rev. Drug Discov.* **13,** 904–927 (2014).

135. Scimeca, C. L., Bharara, M., Fisher, T. K., Giovinco, N. & Armstrong, D. G. Novel use of doxycycline in continuous-instillation negative pressure wound therapy as 'wound chemotherapy'. *Foot Ankle Spec.* **3,** 190–193 (2010).

136. Skúlason, S., Ingólfsson, E. & Kristmundsdóttir, T. Development of a simple HPLC method for separation of doxycycline and its degradation products. *J. Pharm. Biomed. Anal.* **33,** 667–672 (2003).

137. Skulason, S., Holbrook, W. P. & Kristmundsdottir, T. Clinical assessment of the effect of a matrix metalloproteinase inhibitor on aphthous ulcers. *Acta Odontol. Scand.* **67,** 25–9 (2009).

138. Sloan, B. & Scheinfeld, N. The use and safety of doxycycline hyclate and other second-generation tetracyclines. *Expert Opin. Drug Saf.* **7,** 571–577 (2008).

139. Giovagnoli, S., Tsai, T. & DeLuca, P. P. Formulation and release behavior of doxycycline-alginate hydrogel microparticles embedded into pluronic F127 thermogels as a potential new vehicle for doxycycline intradermal sustained delivery. *AAPS PharmSciTech* **11,** 212–220 (2010).

140. Kogawa, A. C. & Salgado, H. R. N. Doxycycline hyclate: A review of properties, applications and analytical methods. *Int. J. Life Sci. Pharma Res.* **2,** 11–25 (2012).

141. Manning, M. W., Cassis, L. A. & Daugherty, A. Differential effects of doxycycline, a broad-spectrum matrix metalloproteinase inhibitor, on angiotensin II-induced atherosclerosis and abdominal aortic aneurysms. *Arterioscler. Thromb. Vasc. Biol.* **23,** 483–8 (2003).

142. Yager, D. R. & Nwomeh, B. C. The proteolytic environment of chronic wounds. *Wound Repair Regen.* **7,** 433–41 (1999).

143. *Doxycycline Hyclate: Product Information*. (Sigma-Aldrich, 1993).

144. Peridontics: Trade News Focus - Periostat (doxycycline 20 mg). *British Dental Journal* **200,** 115 (2006).

145. Javali, M. A. & Vandana, K. L. A comparative evaluation of atrigel delivery system (10% doxycycline hyclate) Atridox with scaling and root planing and combination therapy in treatment of periodontitis: A clinical study. *J. Indian Soc. Periodontol.* **16,** 43–8 (2012).

146. Trommer, H. & Neubert, R. H. H. Overcoming the stratum corneum: the modulation of skin penetration. A review. *Skin Pharmacol. Physiol.* **19,** 106–21 (2006).

147. Gill, H. S. & Prausnitz, M. R. Pocketed microneedles for drug delivery to the skin. *J. Phys. Chem. Solids* **69,** 1537–1541 (2008).

148. Prausnitz, M. R. & Langer, R. Transdermal drug delivery. *Nat. Biotechnol.* **26,** 1261–1268 (2009).

149. Williams, A. C. & Barry, B. W. Penetration enhancers. *Adv. Drug Deliv. Rev.* **56,** 603–618 (2004).

150. Pathan, I. B. & Setty, C. M. Chemical penetration enhancers for transdermal drug delivery systems. *Trop. J. Pharm. Res.* **8,** 173–179 (2009).

151. Mitragotri, S. Devices for overcoming biological barriers: the use of physical forces to disrupt the barriers. *Adv. Drug Deliv. Rev.* **65,** 100–3 (2013).

152. Mitragotri, S., Blankschtein, D. & Langer, R. Ultrasound-mediated transdermal protein delivery. *Science* **269,** 850–853 (1995).

153. Paliwal, S., Menon, G. K. & Mitragotri, S. Low-frequency sonophoresis: ultrastructural basis for stratum corneum permeability assessed using quantum dots. *J. Invest. Dermatol.*

126, 1095–1101 (2006).

154. Kalia, Y. N., Naik, A., Garrison, J. & Guy, R. H. Iontophoretic drug delivery. *Adv. Drug Deliv. Rev.* **56,** 619–658 (2004).

155. Guy, R. H. *et al.* Iontophoresis: Electrorepulsion and electroosmosis. *J. Control. Release* **64,** 129–132 (2000).

156. Spierings, E. L. H., Brevard, J. A. & Katz, N. P. Two-minute skin anesthesia through ultrasound pretreatment and iontophoretic delivery of a topical anesthetic: A feasibility study. *Pain Med.* **9,** 55–59 (2008).

157. Prausnitz, M. R., Bose, V. G., Langer, R. & Weaver, J. C. Electroporation of mammalian skin: a mechanism to enhance transdermal drug delivery. *Proc. Natl. Acad. Sci. U. S. A.* **90,** 10504–10508 (1993).

158. Heller, L., Ugen, K. & Heller, R. Electroporation for targeted gene transfer. *Expert Opin. Drug Deliv.* **2,** 255–68 (2005).

159. Mitragotri, S. Immunization without needles. *Nat. Rev. Immunol.* **5,** 905–16 (2005).

160. Nava-Arzaluz, M. G., Calderon-Lojero, I., Quintanar-Guerrero, D., Villalobos-Garcia, R. & Ganem-Quintanar, a. Microneedles as transdermal delivery systems: combination with other enhancing strategies. *Curr. Drug Deliv.* **9,** 57–73 (2012).

161. Henry, S., McAllister, D., Allen, M. & Prausnitz, M. Microfabricated microneedles: A novel approach to transdermal drug delivery. *J. Pharm. Sci.* **88,** 948 (1999).

162. Wu, Y., Qiu, Y., Zhang, S., Qin, G. & Gao, Y. Microneedle-based drug delivery: studies on delivery parameters and biocompatibility. *Biomed. Microdevices* **10,** 601–10 (2008).

163. Davis, S. P., Landis, B. J., Adams, Z. H., Allen, M. G. & Prausnitz, M. R. Insertion of microneedles into skin: measurement and prediction of insertion force and needle fracture force. *J. Biomech.* **37,** 1155–63 (2004).

164. Kaushik, S. *et al.* Lack of pain associated with microfabricated microneedles. *Anesth. Analg.* **92,** 502–4 (2001).

165. Gupta, J., Park, S. S., Bondy, B., Felner, E. I. & Prausnitz, M. R. Infusion pressure and pain during microneedle injection into skin of human subjects. *Biomaterials* **32,** 6823–31 (2011).

166. Bal, S. M., Caussin, J., Pavel, S. & Bouwstra, J. A. In vivo assessment of safety of microneedle arrays in human skin. *Eur. J. Pharm. Sci.* **35,** 193–202 (2008).

167. Park, J.-H., Allen, M. G. & Prausnitz, M. R. Polymer microneedles for controlled-release drug delivery. *Pharm. Res.* **23,** 1008–1019 (2006).

168. Kommareddy, S., Baudner, B. C., Oh, S., Kwon, S. & Singh, M. Dissolvable microneedle patches for the delivery of cell-culture-derived influenza vaccine antigens. *J. Pharm. Sci.* **101,** 1021–1027 (2012).

169. Edens, C., Collins, M. L., Ayers, J., Rota, P. A. & Prausnitz, M. R. Measles vaccination using a microneedle patch. *Vaccine* **31,** 3403–3409 (2013).

170. Jj, N., Na, R., Faster, F. E. I., Brown, R. & Nicholas, A. Faster pharmacokinetics and increased patient acceptance of intradermal insulin delivery using a single hollow microneedle in children and adolescents with type 1 diabetes. *Pediatr. Diabetes* **14,** 459–465 (2013).

171. Gupta, J., Felner, E. I., Prausnitz, M. R. & Ph, D. Minimally invasive insuling delivery in subjects with type 1 diabetes using hollow microneedles. *Diabetes Technol. Ther.* **11,** 329–337 (2009).

172. Prausnitz, M. R. Engineering microneedle patches for vaccination and drug delivery to the skin. *Annu. Rev. Chem .Biomol. Eng.* **8,** 1–24 (2017).

173. van der Maaden, K., Jiskoot, W. & Bouwstra, J. Microneedle technologies for (trans)dermal drug and vaccine delivery. *J. Control. Release* **161,** 645–55 (2012).

174. Larrañeta, E., McCrudden, M. T. C., Courtenay, A. J. & Donnelly, R. F. Microneedles: A New Frontier in Nanomedicine Delivery. *Pharm. Res.* **33,** 1055–1073 (2016).

175. Ita, K. Transdermal delivery of drugs with microneedles—potential and challenges. *Pharmaceutics* **7,** 90–105 (2015).

176. McAllister, D. V *et al.* Microneedles for transdermal delivery of macromolecules. in *[Engineering in Medicine and Biology, 1999. 21st Annual Conference and the 1999 Annual Fall Meetring of the Biomedical Engineering Society] BMES/EMBS Conference, 1999. Proceedings of the First Joint* **2,** 836 (IEEE, 1999).

177. Liu, R., Zhang, M. & Jin, C. In vivo and in situ imaging of controlled-release dissolving silk microneedles into the skin by optical coherence tomography. *J. Biophotonics* **8,** 1–8 (2016).

178. Li, G., Badkar, A., Nema, S., Kolli, C. S. & Banga, A. K. In vitro transdermal delivery of therapeutic antibodies using maltose microneedles. *Int. J. Pharm.* **368,** 109–15 (2009).

179. Liu, S. *et al.* Transdermal delivery of relatively high molecular weight drugs using novel self-dissolving microneedle arrays fabricated from hyaluronic acid and their characteristics and safety after application to the skin. *Eur. J. Pharm. Biopharm.* **86,** 267–276 (2014).

180. Liu, S. *et al.* The development and characteristics of novel microneedle arrays fabricated from hyaluronic acid, and their application in the transdermal delivery of insulin. *J. Control. Release* **161,** 933–941 (2012).

181. Kim, M., Jung, B. & Park, J.-H. Hydrogel swelling as a trigger to release biodegradable polymer microneedles in skin. *Biomaterials* **33,** 668–78 (2012).

182. Singh, A. & Yadav, S. Microneedling: Advances and widening horizons. *Indian Dermatol. Online J.* **7,** 244 (2016).

183. Oh, J.-H. *et al.* Influence of the delivery systems using a microneedle array on the permeation of a hydrophilic molecule, calcein. *Eur. J. Pharm. Biopharm.* **69,** 1040–5 (2008).

184. Kim, Y.-C., Park, J.-H. & Prausnitz, M. R. Microneedles for drug and vaccine delivery. *Adv. Drug Deliv. Rev.* **64,** 1547–1568 (2012).

185. Raphael, A. P. *et al.* Formulations for microprojection / microneedle vaccine delivery : Structure , strength and release pro fi les. *J. Control. Release* **225,** 40–52 (2016).

186. Vrdoljak, A. *et al.* Coated microneedle arrays for transcutaneous delivery of live virus vaccines. *J. Control. Release* **159,** 34–42 (2012).

187. Davis, S. P., Martanto, W., Allen, M. G., Member, S. & Prausnitz, M. R. Hollow metal microneedles for insulin delivery to diabetic rats. *IEEE Trans. Biomed. Eng.* **52,** 909–915 (2005).

188. Zhang, W. *et al.* Penetration and distribution of PLGA nanoparticles in the human skin treated with microneedles. *Int. J. Pharm.* **402,** 205–12 (2010).

189. Kumar, A. *et al.* Permeation of antigen protein-conjugated nanoparticles and live bacteria through microneedle-treated mouse skin. *Int. J. Nanomedicine* **6,** 1253–64 (2011).

190. Kim, C. S. *et al.* Efficient and facile delivery of gold nanoparticles in vivo using dissolvable microneedles for contrast-enhanced optical coherence tomography. *Biomed. Opt. Express*

1, 106–113 (2010).

191. Fabbrocini, G., Fardella, N., Monfrecola, a, Proietti, I. & Innocenzi, D. Acne scarring treatment using skin needling. *Clin. Exp. Dermatol.* **34,** 874–9 (2009).

192. Bariya, S. H., Gohel, M. C., Mehta, T. a & Sharma, O. P. Microneedles: an emerging transdermal drug delivery system. *J. Pharm. Pharmacol.* **64,** 11–29 (2012).

193. Chen, B., Wei, J. & Iliescu, C. Sonophoretic enhanced microneedles array (SEMA)-Improving the efficiency of transdermal drug delivery. *Sensors Actuators, B Chem.* **145,** 54–60 (2010).

194. Han, T. & Das, D. B. Permeability enhancement for transdermal delivery of large moelcule using low-frequency sonophoresis combined with microneedles. *J. Pharm. Sci.* **102,** 3614–22 (2013).

195. Li, C. G., Lee, C. Y., Lee, K. & Jung, H. An optimized hollow microneedle for minimally invasive blood extraction. *Biomed. Microdevices* **15,** 17–25 (2013).

196. Strambini, L. M. *et al.* Self-powered microneedle-based biosensors for pain-free high-accuracy measurement of glycaemia in interstitial fluid. *Biosens. Bioelectron.* **66,** 162–168 (2015).

197. Valdés-Ramírez, G. *et al.* Microneedle-based self-powered glucose sensor. *Electrochem. commun.* **47,** 58–62 (2014).

198. Hwa, K. Y., Subramani, B., Chang, P. W., Chien, M. & Huang, J. T. Transdermal microneedle array-based sensor for real time continuous glucose monitoring. *Int. J. Electrochem. Sci.* **10,** 2455–2466 (2015).

199. Jina, A. *et al.* Design, development, and evaluation of a novel microneedle array-based continuous glucose monitor. *J. Diabetes Sci. Technol.* **8,** 483–7 (2014).

200. Cunningham, J. J., Nikolovski, J., Lindernab, J. J. & Mooney, D. J. Quantification of fibronectin adsorption to silicone-rubber cell culture substrates. *Biotechniques* **32,** 876–887 (2002).

201. Netzlaff, F., Lehr, C.-M., Wertz, P. W. & Schaefer, U. F. The human epidermis models EpiSkin, SkinEthic and EpiDerm: an evaluation of morphology and their suitability for testing phototoxicity, irritancy, corrosivity, and substance transport. *Eur. J. Pharm. Biopharm.* **60,** 167–78 (2005).

202. Xu, W. *et al.* Application of a partial-thickness human ex vivo skin culture model in cutaneous wound healing study. *Lab. Invest.* **92,** 584–99 (2012).

203. Godin, B. & Touitou, E. Transdermal skin delivery: predictions for humans from in vivo, ex vivo and animal models. *Adv. Drug Deliv. Rev.* **59,** 1152–61 (2007).

204. Wong, V. W., Sorkin, M., Glotzbach, J. P., Longaker, M. T. & Gurtner, G. C. Surgical approaches to create murine models of human wound healing. *J. Biomed. Biotechnol.* 1–8 (2011). doi:10.1155/2011/969618

205. Xie, Y. *et al.* The microvasculature in cutaneous wound healing in the female red Duroc pig is similar to that in human hypertrophic scars and different from that in the female Yorkshire pig. *J. Burn Care Res.* **28,** 500–6 (1976).

206. Porter, R. M. Mouse models for human hair loss disorders. *J. Anat.* **202,** 125–31 (2003).

207. Simon, G. a & Maibach, H. I. Relevance of hairless mouse as an experimental model of percutaneous penetration in man. *Skin Pharmacol. Appl. Skin Physiol.* **11,** 80–6 (1998).

208. Walker, J. M. *Mouse models for drug discovery: methods and protocols*. (Humana Press,

2012).

209. Azzi, L., El-Alfy, M., Martel, C. & Labrie, F. Gender differences in mouse skin morphology and specific effects of sex steroids and dehydroepiandrosterone. *J. Invest. Dermatol.* **124,** 22–7 (2005).

210. Stekelenburg, A. *et al.* Role of ischemia and deformation in the onset of compression-induced deep tissue injury: MRI-based studies in a rat model. *J. Appl. Physiol.* **102,** 2002–11 (2007).

211. Lanzafame, R. J. *et al.* Reciprocity of exposure time and irradiance on energy density during photoradiation on wound healing in a murine pressure ulcer model. *Lasers Surg. Med.* **542,** 534–542 (2007).

212. Stadler, I., Zhang, R.-Y., Oskoui, P., Whittaker, M. S. & Lanzafame, R. J. Development of a simple, noninvasive, clinically relevant model of pressure ulcers in the mouse. *J. Invest. Surg.* **17,** 221–7 (2004).

213. Li, H., Ezra, D. G., Burton, M. J. & Bailly, M. Doxycycline prevents matrix remodeling and contraction by trichiasis-derived conjunctival fibroblasts. *Invest. Ophthalmol. Vis. Sci.* **54,** 4675–82 (2013).

214. Vandervoort, J. & Ludwig, A. Microneedles for transdermal drug delivery: a minireview. *Front. Biosci. a J. virtual Libr.* **13,** 1711–1715 (2008).

215. Scott, C. a & Kelsell, D. P. Key functions for gap junctions in skin and hearing. *Biochem. J.* **438,** 245–54 (2011).

216. Scott, C. a, Tattersall, D., O'Toole, E. a & Kelsell, D. P. Connexins in epidermal homeostasis and skin disease. *Biochim. Biophys. Acta* **1818,** 1952–61 (2012).

217. Dbouk, H. a, Mroue, R. M., El-Sabban, M. E. & Talhouk, R. S. Connexins: a myriad of functions extending beyond assembly of gap junction channels. *Cell Commun. Signal.* **7,** 4 (2009).

218. Sun, W. *et al.* Transdermal delivery of functional collagen vial polyvinylpyrrolidone microneedles. *Ann. Biomed. Eng.* **43,** 2978–2990 (2015).

219. Mohammed, Y. H. *et al.* Microneedle enhanced delivery of cosmeceutically relevant peptides in human skin. *PLoS One* **9,** 1–9 (2014).

220. Pudukadan, D. Treatment of acne scars on darker skin types using noninsulated smooth motion, electronically controlled radiofrequency microneedles treatment system. *Dermatologic Surg.* **43,** S64–S69 (2017).

221. Wang, R. *et al.* Oxygen-glucose deprivation induced glial scar-like change in astrocytes. *PLoS One* **7,** e37574 (2012).

222. Mccrudden, M. T. C. *et al.* Microneedle applications in improving skin appearance. *Exp. Dermatol.* **24,** 561–566 (2015).

223. Kim, M., Yang, H., Jung, H. & Jung, H. Novel cosmetic patches for wrinkle improvement: retinyl retinoate- and ascorbic acid-loaded dissolving microneedles. *Int. J. Cosmet. Sci.* **36,** 207–12 (2014).

224. Lee, C. *et al.* Evaluation of the anti-wrinkle effect of an ascorbic acid-loaded dissolving microneedle patch via a double-blind, placebo-controlled clinical study. *Int. J. Cosmet. Sci.* **38,** 375–381 (2016).

225. Badran, M. M., Kuntsche, J. & Fahr, A. Skin penetration enhancement by a microneedle device (Dermaroller) in vitro: Dependency on needle size and applied formulation. *Eur. J. Pharm. Sci.* **36,** 511–523 (2009).

226. Chernokalskaya, E., Vivek, J., Kavonian, M. & Brewster, D. Polymeric membranes with human skin-like permeabiltiy properties and uses thereof (US 8,765,254 B2). (2014).

227. Balasubramani, M., Kumar, T. R. & Babu, M. Skin substitutes: a review. *Burns* **27,** 534–44 (2001).

228. Selzer, D., Abdel-Mottaleb, M. M. A., Hahn, T., Schaefer, U. F. & Neumann, D. Finite and infinite dosing: Difficulties in measurements, evaluations and predictions. *Adv. Drug Deliv. Rev.* **65,** 278–294 (2013).

229. Justin, R. & Chen, B. Strong and conductive chitosan-reduced graphene oxide nanocomposites for transdermal drug delivery. *J. Mater. Chem. B* **2,** 3759–3770 (2014).

230. Boks, M. A. *et al.* Controlled release of a model vaccine by nanoporous ceramic microneedle arrays. *Int. J. Pharm.* **491,** 375–383 (2015).

231. Kalluri, H., Kolli, C. S. & Banga, A. K. Characterization of microchannels created by metal microneedles: formation and closure. *AAPS J.* **13,** 473–481 (2011).

232. Uchida, T. *et al.* Prediction of skin permeation by chemical compounds using the artificial membrane, Strat-M. *Eur. J. Pharm. Sci.* **67,** 113–118 (2015).

233. Karadzovska, D. & Riviere, J. E. Assessing vehicle effects on skin absorption using artificial membrane assays. *Eur. J. Pharm. Sci.* **50,** 569–76 (2013).

234. Simon, A., Amaro, M. I., Healy, A. M., Cabral, L. M. & de Sousa, V. P. Comparative evaluation of rivastigmine permeation from a transdermal system in the Franz cell using synthetic membranes and pig ear skin with in vivo-in vitro correlation. *Int. J. Pharm.* **512,** 234–241 (2016).

235. Park, J., Choi, S., Seo, S., Bin, Y. & Prausnitz, M. R. A microneedle roller for transdermal drug delivery. *Eur. J. Pharm. Biopharm.* **76,** 282–289 (2010).

236. Kim, H. M., Lim, Y. Y., An, J. H., Kim, M. N. & Kim, B. J. Transdermal drug delivery using disk microneedle rollers in a hairless rat model. *Int. J. Dermatol.* **51,** 859–863 (2012).

237. Banga, A. K. Microporation applications for enhancing drug delivery. *Expert Opin. Drug Deliv.* **6,** 343–354 (2009).

238. Birchall, J. *et al.* Cutaneous DNA delivery and gene expression in ex vivo human skin explants via wet-etch micro-fabricated micro-needles. *J. Drug Target.* **13,** 415–21 (2005).

239. Ashraf, M. W. *et al.* Design, fabrication and analysis of silicon hollow microneedles for transdermal drug delivery system for treatment of hemodynamic dysfunctions. *Cardiovasc. Eng.* **10,** 91–108 (2010).

240. Arendt-Nielsen, L., Egekvist, H. & Bjerring, P. Pain following controlled cutaneous insertion of needles with different diameters. *Somatosens. Mot. Res.* **23,** 37–43 (2006).

241. Zhou, C., Liu, Y., Wang, H., Zhang, P. & Zhang, J. Transdermal delivery of insulin using microneedle rollers in vivo. *Int. J. Pharm.* **392,** 127–133 (2010).

242. You, S.-K. *et al.* Effect of applying modes of the polymer microneedle-roller on the permeation of L-ascorbic acid in rats. *J. Drug Target.* **18,** 15–20 (2010).

243. Markov, I. *Crystal Growth for Beginners: Fundamentals of Nucleation, Crystal Growth and Epitaxy*. (World Scientific Publishing Co Pte Ltd, 2003).

244. Van Linthout, S., Miteva, K. & Tschope, C. Crosstalk between fibroblasts and inflammatory cells. *Cardiovasc. Res.* **102,** 258–269 (2014).

245. Ehrlich, H. P. Wound closure: evidence of cooperation between fibroblasts and collagen

matrix. *Eye* **2,** 149–57 (1988).

246. Phillips, J. a, Vacanti, C. A. & Bonassar, L. J. Fibroblasts regulate contractile force independent of MMP activity in 3D-collagen. *Biochem. Biophys. Res. Commun.* **312,** 725–732 (2003).

247. Ehrlich, H. P. & Hunt, T. K. Collagen organization critical role in wound contraction. *Adv. Wound Care* **1,** 3–9 (2012).

248. Dallon, J. C. & Ehrlich, H. P. A review of fibroblast-populated collagen lattices. *Wound Repair Regen.* **16,** 472–479 (2008).

249. Elsdale, T. & Bard, J. Collagen substrata for studies on cell behaviour. *J. Cell Biol.* **54,** 626–637 (1972).

250. Bell, E., Ivarsson, B. & Merrill, C. Production of a tissue-like structure by contraction of collagen lattices by human fibroblasts of different proliferative potential in vitro. *Proc. Natl. Acad. Sci. U. S. A.* **76,** 1274–8 (1979).

251. Kobayashi, T. *et al.* Matrix metalloproteinase-9 activates TGF-β and stimulates fibroblast contraction of collagen gels. *Am. J. Physiol. - Lung Cell. Mol. Physiol.* **306,** L1006–L1015 (2014).

252. Martin-Martin, B., Tovell, V., Dahlmann-Noor, A. H., Khaw, P. T. & Bailly, M. The effect of MMP inhibitor GM6001 on early fibroblast-mediated collagen matrix contraction is correlated to a decrease in cell protrusive activity. *Eur. J. Cell Biol.* **90,** 26–36 (2011).

253. Becker, D. L., Thrasivoulou, C. & Phillips, A. R. J. Connexins in wound healing; perspectives in diabetic patients. *Biochim. Biophys. Acta* **1818,** 2068–75 (2012).

254. Wang, N. *et al.* Selective inhibition of Cx43 hemichannels by Gap19 and its impact on myocardial ischemia/reperfusion injury. *Basic Res. Cardiol.* **108,** 309 (2013).

255. Evans, W. H., De Vuyst, E. & Leybaert, L. The gap junction cellular internet: connexin hemichannels enter the signalling limelight. *Biochem. J.* **397,** 1–14 (2006).

256. Evans, W. H. & Martin, P. E. M. Gap junctions: structure and function (Review). *Mol. Membr. Biol.* **19,** 121–36 (2002).

257. Haq, M. I. *et al.* Clinical administration of microneedles: skin puncture, pain and sensation. *Biomed. Microdevices* **11,** 35–47 (2009).

258. Li, H., Roos, J. C. P., Rose, G. E., Bailly, M. & Ezra, D. G. Eyelid and sternum fibroblasts differ in their contraction potential and responses to inflammatory cytokines. *Plast. Reconstr. Surg.* **3,** e448 (2015).

259. Franco, C. *et al.* Doxycycline alters vascular smooth muscle cell adhesion, migration and reorganization of fibrillar collagen matrices. *Am. J. Pathol.* **168,** 1697–1709 (2006).

260. Daniels, J. T. *et al.* Matrix metalloproteinase inhibition modulates fibroblast-mediated matrix and collagen production in vitro. *Invest. Ophthalmol. Vis. Sci.* **44,** 1104–1110 (2003).

261. Bildt, M. M., Bloemen, M., Kuijpers-Jagtman, a M. & Von den Hoff, J. W. Matrix metalloproteinase inhibitors reduce collagen gel contraction and alpha-smooth muscle actin expression by periodontal ligament cells. *J. Periodontal Res.* **44,** 266–74 (2009).

262. Lee, S. J. *et al.* Use of fractionated microneedle radiofrequency for the treatment of inflammatory acne vulgaris in 18 Korean patients. *Dermatol. Surg.* **38,** 400–5 (2012).

263. Mendoza-Naranjo, A. *et al.* Targeting Cx43 and N-cadherin, which are abnormally upregulated in venous leg ulcers, influences migration, adhesion and activation of Rho GTPases. *PLoS One* **7,** e37374 (2012).

264. Sáez, J. C. *et al.* Cell membrane permeabilization via connexin hemichannels in living and dying cells. *Exp. Cell Res.* **316,** 2377–89 (2010).

265. Liang, C.-C., Park, A. Y. & Guan, J.-L. In vitro scratch assay: a convenient and inexpensive method for analysis of cell migration in vitro. *Nat. Protoc.* **2,** 329–33 (2007).

266. Yarrow, J. C., Perlman, Z. E., Westwood, N. J. & Mitchison, T. J. A high-throughput cell migration assay using scratch wound healing, a comparison of image-based readout methods. *BMC Biotechnol.* **4,** 21 (2004).

267. Cho, S. I. *et al.* Evaluation of the clinical efficacy of fractional radiofrequency microneedle treatment in acne scars and large facial pores. *Dermatol. Surg.* **38,** 1017–24 (2012).

268. Ehrlich, H. P. & Moyer, K. E. in *Wound Regeneration and Repair: Methods and Protocols, Methods in Molecular Biology* **1037,** 45–58 (Springer Science+Business Media New York, 2013).

269. Smith, G. N., Mickler, E. a, Hasty, K. a & Brandt, K. D. Specificity of inhibition of matrix metalloproteinase activity by doxycycline. *Arthritis Rheum.* **42,** 1140–6 (1999).

270. Pieper, B. in *Acute & Chronic Wounds: Current Management Concepts* 205–234 (Mosby Elsevier, 2007).

271. Defloor, T. The effect of position and mattress on interface pressure. *Appl. Nurs. Res.* **13,** 2–11 (2000).

272. Manorama, A., Meyer, R., Wiseman, R. & Bush, T. R. Quantifying the effects of external shear loads on arterial and venous blood flow: implications for pressure ulcer development. *Clin. Biomech.* **28,** 574–8 (2013).

273. Li, H. *et al.* Independent adipogenic and contractile properties of fibroblasts in graves' orbitopathy: an in vitro model for the evaluation of treatments. *PLoS One* **9,** e95586 (2014).

274. Martin, P. & Leibovich, S. J. Inflammatory cells during wound repair: the good, the bad and the ugly. *Trends Cell Biol.* **15,** 599–607 (2005).

275. McKleroy, W., Lee, T.-H. & Atabai, K. Always cleave up your mess: targeting collagen degradation to treat tissue fibrosis. *Am. J. Physiol. Lung Cell. Mol. Physiol.* **304,** L709-21 (2013).

276. Mandal, M., Mandal, A., Das, S., Chakraborti, T. & Sajal, C. Clinical implications of matrix metalloproteinases. *Mol. Cell. Biochem.* **252,** 305–29 (2003).

277. Cechowska-Pasko, M., Pałka, J. & Bańkowski, E. Glucose-depleted medium reduces the collagen content of human skin fibroblast cultures. *Mol. Cell. Biochem.* **305,** 79–85 (2007).

278. Cechowska-Pasko, M., Surazyński, A. & Bańkowski, E. The effect of glucose deprivation on collagen synthesis in fibroblast cultures. *Mol. Cell. Biochem.* **327,** 211–8 (2009).

279. Passmore, J. S., Lukey, P. T. & Ress, S. R. The human macrophage cell line U937 as an in vitro model for selective evaluation of mycobacterial antigen-specific cytotoxic T-cell function. *Immunology* **102,** 146–156 (2001).

280. Ishikawa, M. *et al.* A Novel Assay System for Macrophage-activating Factor Activity Using a Human U937 Cell Line. **4582,** 4577–4581 (2014).

281. Castrillo, A. *et al.* Protein kinase C is required for macrophage activation and defense against bacterial infection. *J. Exp. Med.* **194,** 1231–1242 (2001).

282. Tomasek, J. J., Haaksma, C. J., Eddy, R. J. & Vaughan, M. B. Fibroblast contraction occurs on release of tension in attached collagen lattices: dependency on an organized actin cytoskeleton and serum. *Anat. Rec.* **232,** 359–368 (1992).

283. Skold, C. M. *et al.* Blood monocytes attenuate lung fibroblast contraction of three-dimensional collagen gels in coculture. *Am J Physiol Lung Cell Mol Physiol* **279,** L667–L674 (2000).

284. Zhu, Y. *et al.* Fibroblasts and monocyte macrophages contract and degrade three-dimensional collagen gels in extended co-culture. (2001).

285. Lindner, D. *et al.* Differential Expression of Matrix Metalloproteases in Human Fibroblasts with Different Origins. **2012,** (2012).

286. Choi, W. Combined oxygen and glucose deprivation in cortical cell culture: calcium-dependent and calcium independent mechanisms of neuronal injury. *J. Neurosci.* **13 (8),** 3510–3524 (1993).

287. Wang, X. *et al.* The role of connexin 43 and hemichannels correlated with the astrocytic death following ischemia/reperfusion insult. *Cell. Mol. Neurobiol.* **33,** 401–10 (2013).

288. Cronin, M., Anderson, P. N., Cook, J. E., Green, C. R. & Becker, D. L. Blocking connexin43 expression reduces inflammation and improves functional recovery after spinal cord injury. *Mol. Cell. Neurosci.* **39,** 152–60 (2008).

289. Chanson, M. *et al.* Gap junctional communication in tissue inflammation and repair. *Biochim. Biophys. Acta* **1711,** 197–207 (2005).

290. Gillani, S., Cao, J., Suzuki, T. & Hak, D. J. The effect of ischemia reperfusion injury on skeletal muscle. *Injury* **43,** 670–5 (2012).

291. Jagodzinski, N. A., Weerasinghe, C. & Porter, K. Crush injuries and crush syndrome - a review. Part 1: the systemic injury. *Trauma* **12,** 69–88 (2010).

292. Reid, R. R., Said, H. K., Mogford, J. E. & Mustoe, T. a. The future of wound healing: pursuing surgical models in transgenic and knockout mice. *J. Am. Coll. Surg.* **199,** 578–85 (2004).

293. Dinsdale, S. Decubitus ulcers: role of pressure and friction in causation. *Arch. Phys. Med. Rehabil.* **55,** 147–52 (1974).

294. Tew, G. A., Klonizakis, M., Crank, H., Briers, J. D. & Hodges, G. J. Comparison of laser speckle contrast imaging with laser doppler for assessing microvascular function. *Microvasc. Res.* **82,** 326–332 (2011).

295. Choi, W. J., Wang, H. & Wang, R. K. Optical coherence tomography microangiography for monitoring the response of vascular perfusion to external pressure on human skin tissue. *J. Biomed. Opt.* **19,** 56003 (2014).

296. Black, J., Dorner, B. & Ratliff, C. National Pressure Ulcer Advisory Panel's updated pressure ulcer staging system. *Adv Ski. Wound Care* **20,** 269–274 (2007).

297. Stojadinovic, O. *et al.* Deep tissue injury in development of pressure ulcers: a decrease of inflammasome activation and changes in human skin morphology in response to aging and mechanical load. *PLoS One* **8,** e69223 (2013).

298. Aoi, N. *et al.* Ultrasound assessment of deep tissue injury in pressure ulcers: possible prediction of pressure ulcer progression. *Plast. Reconstr. Surg.* **124,** 540–50 (2009).

299. Donnelly, J. Should we include deep tissue injury in pressure ulcer staging systems? The NPUAP debate. *J. Wound Care* **14,** 207–10 (2005).

300. Berlowitz, D. R. & Brienza, D. M. Are all pressure ulcers the result of deep tissue injury? A review of the literature. *Ostomy Wound Manag.* **53,** 34–8 (2007).

301. Greaves, N. S. *et al.* Optical coherence tomography: a reliable alternative to invasive

histological assessment of acute wound healing in human skin? *Br. J. Dermatol.* **170,** 840–850 (2013).

302. Mogensen, M., Thrane, L., Jørgensen, T. M., Andersen, P. E. & Jemec, G. B. E. OCT imaging of skin cancer and other dermatological diseases. *J. Biophotonics* **2,** 442–51 (2009).

303. Fujimoto, J. G. Optical coherence tomography for ultrahigh resolution in vivo imaging. *Nat. Biotechnol.* **21,** 1361–7 (2003).

304. Baris, H. N., Cohen, I. J. & Mistry, P. K. Gaucher disease: The metabolic defect, pathophysiology, phenotypes and natural history. *Pediatr. Endocrinol. Rev.* **12,** 72–81 (2014).

305. Schmitt, J. M. Optical coherence tomography (OCT): a review. *IEEE J. Sel. Top. Quantum Electron.* **5,** 1205–1215 (1999).

306. Sainter, A. W., King, T. A. & Dickinson, M. R. Effect of target biological tissue and choice of light source on penetration depth and resolution in optical coherence tomography. *J. Med. Opt.* **9,** 193–199 (2004).

307. Gambichler, T. *et al.* Applications of optical coherence tomography in dermatology. *J. Dermatol. Sci.* **40,** 85–94 (2005).

308. Gambichler, T., Jaedicke, V. & Terras, S. Optical coherence tomography in dermatology: technical and clinical aspects. *Arch. Dermatol. Res.* **303,** 457–73 (2011).

309. Adegun, O. K. *et al.* Quantitative analysis of optical coherence tomography and histopathology images of normal and dysplastic oral mucosal tissues. *Lasers Med. Sci.* **27,** 795–804 (2012).

310. Branzan, A. L., Landthaler, M. & Szeimies, R.-M. In vivo confocal scanning laser microscopy in dermatology. *Lasers Med. Sci.* **22,** 73–82 (2007).

311. Neerken, S., Lucassen, G. W., Bisschop, M. a, Lenderink, E. & Nuijs, T. a M. Characterization of age-related effects in human skin: A comparative study that applies confocal laser scanning microscopy and optical coherence tomography. *J. Biomed. Opt.* **9,** 274–81 (2004).

312. Gambichler, T. *et al.* Epidermal thickness assessed by optical coherence tomography and routine histology: preliminary results of method comparison. *J. Eur. Acad. Dermatol. Venereol.* **20,** 791–5 (2006).

313. Mogensen, M., Morsy, H. a, Thrane, L. & Jemec, G. B. E. Morphology and epidermal thickness of normal skin imaged by optical coherence tomography. *Dermatology* **217,** 14–20 (2008).

314. Weissman, J., Hancewicz, T. & Kaplan, P. Optical coherence tomography of skin for measurement of epidermal thickness by shapelet-based image analysis. *Opt. Express* **12,** 5760–9 (2004).

315. Stekelenburg, A., Oomens, C. W. J., Strijkers, G. J., Nicolay, K. & Bader, D. L. Compression-induced deep tissue injury examined with magnetic resonance imaging and histology. 1946–1954 (2006). doi:10.1152/japplphysiol.00889.2005.

316. Moore, Z., Patton, D., Rhodes, S. L. & O'Connor, T. Subepidermal moisture (SEM) and bioimpedance: A literature review of a novel method for early detection of pressure-induced tissue damage (pressure ulcers). *Int. Wound J.* (2016). doi:10.1111/iwj.12604

317. Clendenin, M., Jaradeh, K., Shamirian, A. & Rhodes, S. L. Inter-operator and inter-device agreement and reliability of the SEM Scanner. *J. Tissue Viability* **24,** 17–23 (2015).

318. Bates-Jensen, B. M., McCreath, H. E., Kono, A., Apeles, N. C. R. & Alessi, C. Subepidermal

moisture predicts erythema and Stage 1 pressure ulcers in nursing home residents: A pilot study. *J. Am. Geriatr. Soc.* **55,** 1199–1205 (2007).

319. Bates-Jensen, B. M., McCreath, H. E., Pongquan, V. & Apeles, N. C. R. Subepidermal moisture differentiates erythema and stage I pressure ulcers in nursing home residents. *Wound Repair Regen.* **16,** 189–197 (2008).

320. Harrow, J. J. & Mayrovitz, H. N. Subepidermal moisture surrounding pressure ulcers in persons with a spinal cord injury: a pilot study. *J. Spinal Cord Med.* **37,** 719–28 (2014).

321. Guihan, M. *et al.* Assessing the feasibility of subepidermal moisture to predict erythema and stage 1 pressure ulcers in persons with spinal cord injury: a pilot study. *J. Spinal Cord Med.* **35,** 46–52 (2012).

322. Ching, C. T.-S. *et al.* Tissue electrical properties monitoring for the prevention of pressure sore. *Prosthet. Orthot. Int.* **35,** 386–94 (2011).

323. Coulman, S. A. *et al.* In vivo, in situ imaging of microneedle insertion into the skin of human volunteers usint optical coherence tomography. *Pharm. Res.* **28,** 66–81 (2011).

324. Larrañeta, E. *et al.* A proposed model membrane and test method for microneedle insertion studies. *Int. J. Pharm.* **472,** 65–73 (2014).

325. Enfield, J., Connell, M. O., Lawlor, K. & Leahy, M. In-vivo dynamic characterization of microneedle skin penetration using optical coherence tomography. *J. Biomed. Opt.* **15,** 1–7 (2013).

326. Thakur, R. R. S., Fallows, S. J., McMillan, H. L., Donnelly, R. F. & Jones, D. S. Microneedle-mediated intrascleral delivery of in situ forming thermoresponsive implants for sustained ocular drug delivery. *J. Pharm. Pharmacol.* **66,** 584–585 (2014).

327. Guo, L. *et al.* Optical coherence tomography angiography offers comprehensive evaluation of skin optical clearing in vivo by quantifying optical properties and blood flow imaging simultaneously. *J. Biomed. Opt.* **21,** 81202 (2016).

328. Brogden, N. K. *et al.* Diclofenac delays micropore closure following microneedle treatment in human subjects. *J. Control. Release* **163,** 220–229 (2012).

329. Brogden, N. K., Banks, S. L., Crofford, L. J. & Stinchcomb, A. L. Diclofenac Enables Unprecedented Week-Long Microneedle- Enhanced Delivery of a Skin Impermeable Medication in Humans. 1947–1955 (2013). doi:10.1007/s11095-013-1036-1

330. Grove, T. Z., Osuji, C. O., Forster, J. D., Dufresne, E. R. & Regan, L. Stimuli-responsive smart gels realized via modular protein design. *J. Am. Chem. Soc.* **132,** 14024–6 (2010).

331. Grove, T. Z., Forster, J., Pimienta, G., Dufresne, E. & Regan, L. A modular approach to the design of protein-based smart gels. *Biopolymers* **97,** 508–17 (2012).

332. Turk, B. E., Huang, L. L., Piro, E. T. & Cantley, L. C. Determination of protease cleavage site motifs using mixture-based oriented peptide libraries. *Nat. Biotechnol.* **19,** 661–7 (2001).

333. Zhang, M., Desai, T. & Ferrari, M. Proteins and cells on PEG immobilized silicon surfaces. *Biomaterials* **19,** 953–60 (1998).

334. Zakeri, B. & Howarth, M. Spontaneous intermolecular amide bond formation between side chails for irreversible peptide targeting. *Am. Chem. Soc.* **132,** 4526–4527 (2010).

335. Zhang, W.-B., Sun, F., Tirrell, D. a & Arnold, F. H. Controlling macromolecular topology with genetically encoded SpyTag-SpyCatcher chemistry. *J. Am. Chem. Soc.* **135,** 13988–97 (2013).

Appendices

Appendix A — Development of a single custom-made hollow microneedle in combination with a Hamilton syringe

An alternative to solid microneedles for doxycycline delivery is the use of hollow microneedle for the infusion of doxycycline solutions or *in situ*-forming gels. To begin the process of developing a bespoke hollow microneedle for intradermal delivery of doxycycline, an existing system that could already provide precise delivery in a controlled way was adapted. Hamilton needles are needles with a modular design that allows its individual components to be tailored by volume and needle gauge to suit particular applications (**Figure 8.1 – A**). The Hamilton syringe used was a Hamilton #702 N 25 µl syringe (Hamilton Company, Nevada, USA). The aim was to first create an adaptor upon which microneedles of differing length and geometry could be integrated (**Figure 8.1 – B**).

The measurements of the annulus and height of the tip of the syringe body were calculated and used to produce a design which was brought to fruition by the team at the Joint Department of Biomedical Engineering (University of North State University, Georgia, USA) who produced the small urethane dimethacrylate (UDMA)-based adaptor (**Figure 8.1 – C**). The measurements of the Hamilton syringe were determined using calipers and manufacturer's references. The adaptor module was designed to fit onto the opening of the syringe to be as seal-tight as possible. The annulus of the adaptor on the opposite end had to be of a greater enough width as to avoid backpressure of liquid when needling. The production of the adaptor alone proved successful and thus the single microneedle-adaptor module has been designed and is in production.

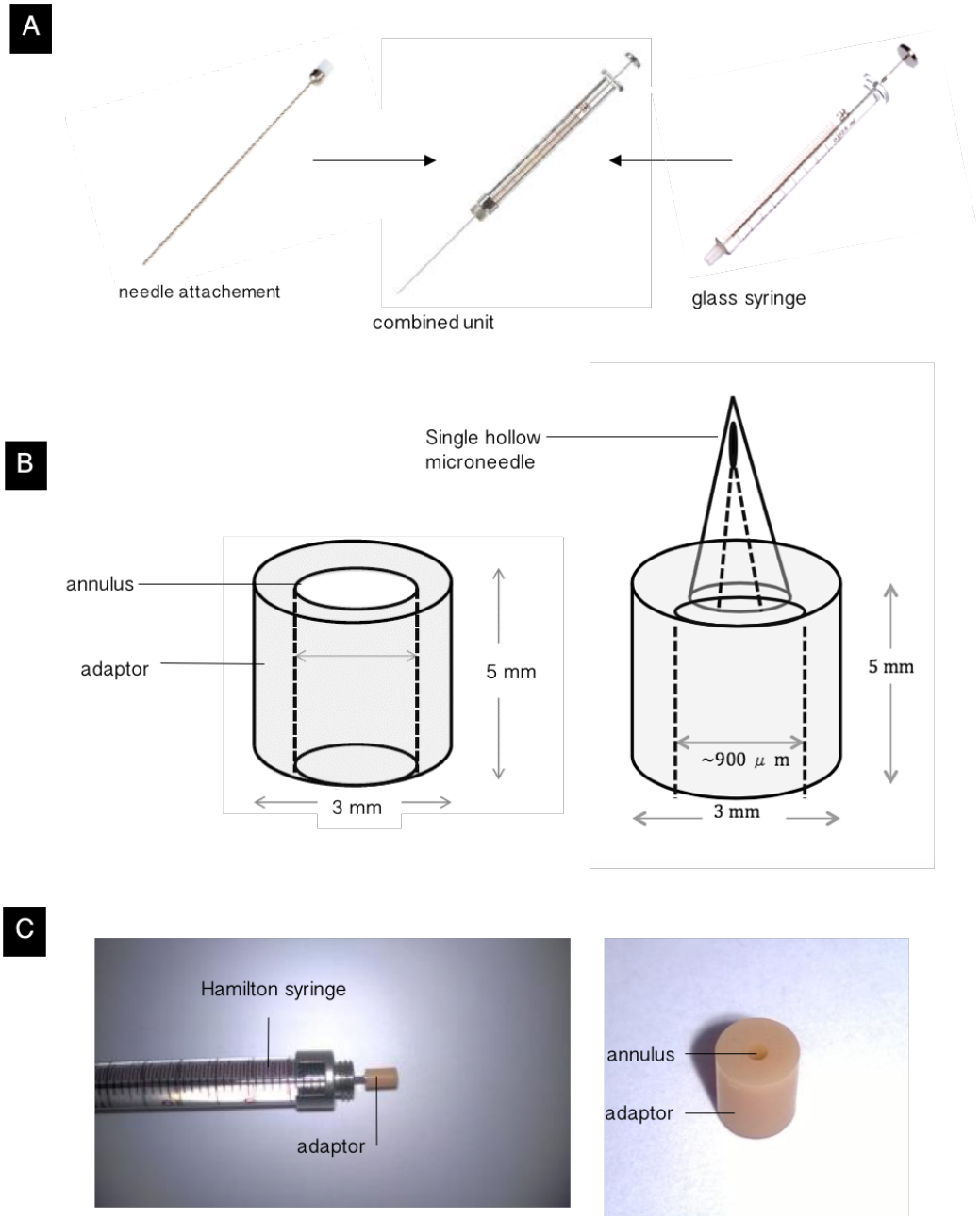

Figure 8.1 — Development of a single microneedle adaptor unit compatible with a Hamilton syringe: (A) Modular design of the Hamilton needles and syringes. **(B)** Schematic representation of the UDMA-based adaptor and its measurements for compatibility with the Hamilton syringe *(left),* the proposed adaptor with the single hollow microneedle included (*right).* **(C)** Photographs of the UDMA-based adapted produced at the Joint Department of Biomedical Engineering (University of North State University, Georgia, USA).

Appendix B — Impregnating various wound dressings with doxycycline solution

A series of experiments were carried out to assess the ability of different adhesive wound dressings to become saturated with doxycycline solution. The concept behind this was that wound dressings impregnated with doxycycline could be applied to early stage pressure ulcer sites that had been permeabilised by microneedle application. Once applied they act as a drug reservoir for a more controlled release of the drug rather than an immediate bolus delivery. Three commercially available wound dressings were assessed: (i) Elastoplast water resistant plaster (Beiersdorf UK, Birmingham, UK) — typically used on small wounds and cuts, (ii) Comfeel® wound dressing (Coloplast, Peterborough, UK) — a hydrocolloid dressing for the sealing and protection of wounds, and (iii) Cilguard® (SudMed, Glossop, UK) — a polyurethane foam dressing with soft silicone adhesion. Each wound dressing was cut to the same volume (1 cm x 1 cm x 1 mm).

The samples were immersed in wells that contained 10 ml of 10 mg/ml doxycycline solution (Alfa Aesar, Massachusetts, USA). The volume of doxycycline that was absorbed and retained was measured by periodically weighing the dressings. Dressing saturation was indicated when the mass plateaued. The dressings were blotted with filter paper before weighing to remove any excess moisture. Volume for volume, the Elastoplast dressing became saturated most rapidly and the Comfeel® dressing was the most absorbent **(Figure 8.2**). The next step is to see whether the dressings release their absorbed load once saturated, to what extent and over what sort of time frame.

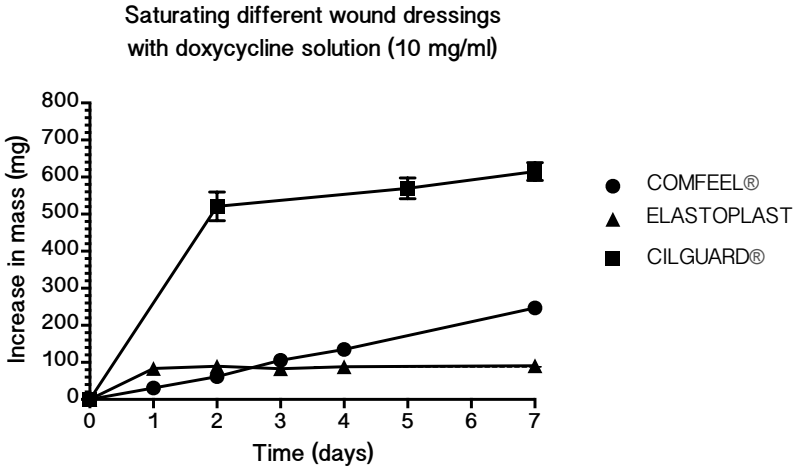

Figure 8.2 — Absorption and saturation of Comfeel®, Cilguard ® and Elastoplast wound dressings by monitoring their mass until it plateaued.

Appendix C — Development of an MMP-cleavable protein-based smart gel

Introduction

Research project

During my Ph.D., I undertook an Institute of Biomedical Engineering (IBME)-funded trip to Yale University, USA where I worked on a collaborative project as part of the IBME-led Yale-UCL Medical Technologies Collaborative (MTC) for two months. The general idea behind these funded collaborations is to develop innovative technologies to solve medical challenges. I was one of two Ph.D. students to be funded under their research theme of 'Biomaterials and Drug Delivery'. I carried out my research at the Department of Molecular Biophysics and Biochemistry in collaboration with the principal investigator Professor Lynne Regan whose research specialises in the protein chemistry of gels. My main aim was to provide an application of their fundamental research on polymeric gels to a real-world medical problem. Consequently, I worked on the development of a smart gel for chronic wound healing. The entire body of work described here was carried out by myself (unless otherwise credited) under the supervision and guidance of Ashley Schloss (Ph.D. student) and Professor Lynne Regan.

Smart gels for controlled drug delivery in situ

Hydrogels are a hydrophilic networks of polymer chains that are used in several medical and research applications. A relatively new subtype are environmentally-sensitive hydrogels also known as smart gels[330,331]. In recent years, smart gels have become of increasing interest for controlled drug release applications. Smart gels have the ability to "sense" changes in their environment, such as changes in metabolite concentration, and can release an encapsulated load as result of this detected change. In this project, the smart gel's environmental cue would be an increase in matrix metalloproteinase (MMP) levels which would be responsible for cleaving a structural component of the gel. This then results in the release of trapped drugs, potentially MMP inhibitors such as doxycycline, from within the gel network. The drug can then act at the site of chronic wound: (i) to regulate MMP activity, (ii) to curb pressure ulcer development and (iii) to facilitate the wound healing process. For wounds where the skin has not yet been exposed, it is possible that individual gel components could be delivered separately *via* microneedles and will only form the gel once delivered and combined *in situ*.

The MMP recognition site (MMPRS)

The MMP recognition site, or the MMPRS, is the novel component of the proposed smart gel. It is a consensus sequence of eight amino acids, *VPMSMRGG*, cleavable (or with close to

optimal cleavage) by human MMPs 1 and 9, which have been shown to be aberrantly up-regulated in human chronic wounds through clinical investigations of wound fluid and exudate[105,114]. This sequence was investigated by Ashley Schloss and chosen from a library of MMP cleavage site consensus sequences[332]. The MMP 1 consensus sequence was chosen as it had relatively low MMP 7 activity, an MMP for which literature evidence for its presence in chronic wound was not found. The MMPRS can be targeted by MMPs for cleavage and thus provides the degradable component of the gel. For interactions with itself or other proteins and peptides, the MMPRS peptide can be terminally functionalised with amino acids such as cysteine to allow for covalent di-sulphide bond formation.

Approaches to MMP-degradable smart gels

There were three possible approaches to producing MMP-degradable smart gels, all using covalent bonds between peptide-protein or peptide-peptide components and all containing the MMP-cleavable peptide sequence, MMPRS. These were: (i) multi-arm polyethylene glycol and MMPRS peptide gels, (ii) MMPRS concatenated polypeptide gels and (iii) SpyTag-SpyCatcher gels. The unifying feature of these gels is that the protein-peptide/peptide-peptide components are covalently bonded and this union is only broken through cleavage of the MMPRS. Each approach presents potential advantages and disadvantages.

(i) Multi-arm polyethylene glycol and MMPRS peptide gel

Polyethylene glycol, or PEG, is an FDA-approved synthetic polymer used in many biomedical applications including drug delivery[330,331,333]. It comes in a range of molecular weights which can be selected to best suit a specific application. A multi-arm PEG unit can be used as a branching scaffold to build individual units of peptides onto to create a gel network. To covalently bond PEG to the MMPRS peptide for gel formation, both components need to be terminally functionalised. In this approach, the MMPRS is functionalised with two terminal cysteine residues, while a four-arm PEG molecule is functionalised with vinyl sulfone (**Figure 8.3 – A**). Under oxidising conditions, these functional groups can form covalent bonds. The MMPRS peptide can be further modified to increase the reactivity of the cysteines through the addition of two lysine residues which reduces the pKa of the disulphide bond formation. The non-lysine modified peptide is referred to as the ‘nK’ MMPRS subtype, whilst the lysine-modified peptide is referred to as the ‘K’ MMPRS subtype (**Table 9**).

Table 9 — Amino acid sequences of MMPRS peptide subtypes. The nK peptide sequence is flanked on its N-terminal and C-terminal with CYGG and GGC residues, respectively, while the K peptide sequence is flanked on its N-terminal and C-terminal with CKYGG and GGKC residues, respectively.

Peptide subtype	Additional amino acids	Amino acid sequence
MMPRS peptide	None	VPMSMRGG
nK MMPRS peptide	2x cysteine	CYGGVPMSMRGGC
K MMPRS peptide	2x cysteine, 2 x lysine	CKYGGVPMSMRGGKC

(ii) MMPRS concatenated polypeptide gel

Since the MMPRS peptide is functionalised with cysteine residues at either end it can form cysteine-cysteine disulphide bonds with itself under oxidising conditions thus creating a concatenated polypeptide (**Figure 8.3 – B**). This removes the need for an intermediate protein scaffold like PEG. However, because of the linearity of the polypeptides formed, gel formation may not be optimal due to a lack of branching which is otherwise exhibited when using a PEG scaffold. Nonetheless, it is possible that chain folding could result in a gel-like substance.

(iii) SpyTag-SpyCatcher gel

SpyTag-SpyCatcher is a highly-reactive, genetically encoded protein-peptide pair developed by Howarth *et al*. (2010)[334] and structurally investigated by Arnold and colleagues (2013)[335]. SpyCatcher is a 12 kDa peptide with a reactive 255 lysine residue that can covalently bond to the reactive 20th aspartic acid residue of the 1.1 kDa SpyTag peptide. In their paper, Arnold *et al.* (2013) investigated different protein structures that could be made with this interactive pair[335]. Their work inspired the idea of SpyTag-SpyCatcher based MMP-degradable smart gels. The idea behind this gel is to have a terminally functionalised MMPRS peptide with SpyTag on either end and a concatenated SpyCatcher arranged as a four-unit protein. These two separate components can then interact to create the gel network (**Figure 8.3 – C**). Note how the cleavable element of the gel, the MMPRS, is flanked by SpyTag.

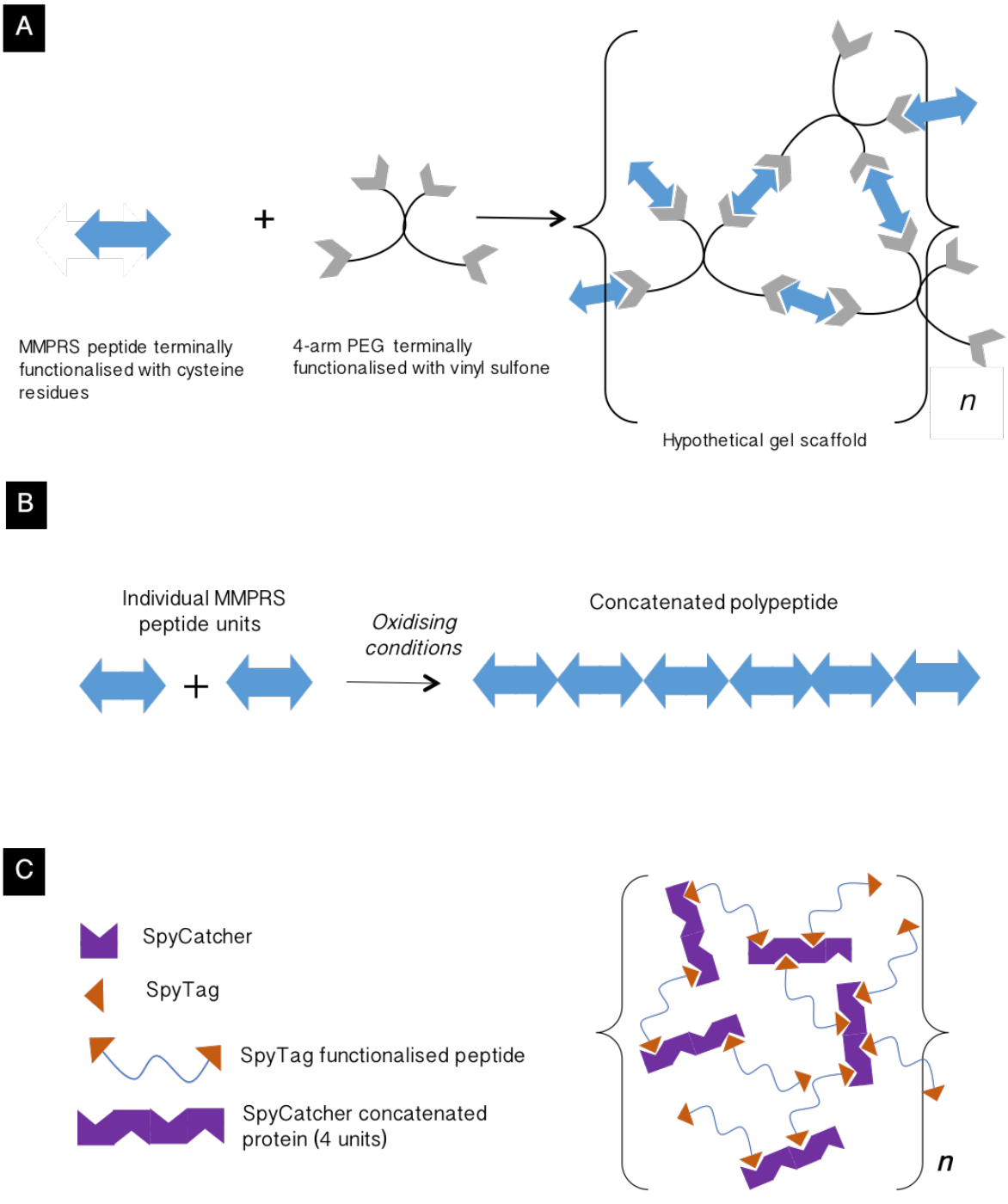

Figure 8.3 — Schematic representation of the three approaches towards MMP-cleavable smart gels: (A) The MMPRS peptide-PEG reaction resulting in a hypothetical MMP-degradable hydrogel scaffold with chemically cross-linked PEG and MMPRS units. **(B)** MMPRS peptide concatenation reaction. Individual MMPRS peptide units can be concatenated under oxidising conditions such as basic pH and aeration to form a linear polypeptide chain that should demonstrate different physiochemical properties. **(C)** Hypothetical SpyTag-SpyCatcher smart gel using homotelechelically-modified SpyTag and SpyCatcher proteins.

Research outline

The body of work presented here aimed to investigate whether MMP-degradable protein-peptide based smart gels could be used to encapsulate and release drugs in a controlled manner for the treatment of chronic wounds. The major aims were: (i) express, purify and characterise the two subtypes of MMPRS peptide (nK and K), (ii) to concatenate purified MMPRS peptides to form a polypeptide and (iii) to clone SpyCatcher and SpyTag into competent bacteria.

Methods and materials

Table 10 — Recipes for reagents and buffers used in protein synthesis and purification.

Autoclaved Broth and Nutrient Mixture (for 500 ml)

Solution	Constituents	Volume for 500 ml
20% 5XZY		100 ml
2% 50x5052	0.5% glycerol, 0.05% glucose, 0.2% α-lactose	10 ml
2% 50xM	1.25 M $NaHPO_4$, 1.25 M KH_2PO_4, 2.5 M NH_4CL, 0.25 M $NaSO_4$	10 ml
0.02% $FeCl_3$		100 µm
0.2% $MgSO_4$		1 ml

Resuspension solution (for 20 ml)

Solution	Constituents	Volume for 20ml
Buffer A	150 mM NaCl, 50 mM Tris at 7.4 pH	20 ml
Protease (EDTA free)		1 tablet
Lysozyme		20mg
BME (2-metacarphonel)		7 µl
DNase1		

Buffers

Buffer	Constituents (by molarity)
Buffer A	150 mM NaCl, 50 mM Tris at 7.4 pH
Buffer B	300 mM NaCl, 50 mM Tris at 7.4 pH

Sep-Pak SPE solutions

Solution	Constituents (by volume)
Conditioning Solution	90% Methanol/Water with 0.1% TFA
Loading/ Equilibrium Solution	0.1% TFA in water
Desalting Solution	5% Methanol/ Water with 0.1% TFA
Elution Solution	80% ACN/Water with 0.1% TFA

TFA = trifluoroacetic acid ; ACN = acetonitrile

Approach 1 — Multi-arm PEG and MMPRS peptide gel

Cloning and Molecular Biology

Cloning of the MMPRS peptides into BL21 *E. Coli* was carried out prior to this study by Ashley Schloss.

Protein synthesis

Colonies were selected from K and nK MMPRS peptide plates and transferred to culture tubes. 5 mL of L-Broth and 5 µl of ampicillin were added to the colonies. Colonies were placed on a shaker for s 5h at 37^{o}C. Each resulting culture was transferred to a flask of 500 ml Autoclaved Broth & Nutrient Mixture (**Table 10**) and 1 ml ampicillin (Sigma-Aldrich). Flasks were shaken overnight at 37^{o}C. Cultures were transferred to 500 ml centrifuge tubes and centrifuged at 6000 rpm at 4^{o}C. The supernatant was decanted and cell pellets re-suspended in 20 ml Resuspension Solution (**Table 10**) then transferred to 50 ml Falcon tubes and incubated on ice for 30 minutes. Solutions were sonicated on ice for 15 runs of 10 seconds on and 20 seconds off. This was repeated twice for each sample until the solutions cleared. Samples were transferred to 500 µl centrifuge containers and the re-suspended solutions centrifuged for 1 hour at 17 000 rpm and 4^{o}C. The supernatant containing the protein was collected for purification and the pellet containing dead cells and waste removed.

Protein purification

Nickel affinity chromatography purification

Five ml of nickel resin (HisPur Ni-NTA Resin; Thermo Fisher Scientific, Massachusetts, USA) was added to chromatography columns and the storage ethanol drained. Columns were washed twice with Ultrapure water and 20 mL of Buffer A + 20 mM imidazole (**Table 10**). The resin was then equilibrated with the samples through repeated inversions for 1 hour. For initial purification from contaminants, the MBP-MMPRS protein was washed through with 20 ml of buffer A + 20 mM imidazole and five times with 20 ml Buffer B (**Table 10**). The protein was eluted with buffer B + 250 mM imidazole (**Table 10**). Elution solution was dialysed in 5 mM Tris and 30 mM NaCl using dialysis tubing. The dialysis tubing was stirred at 4^{o}C overnight.

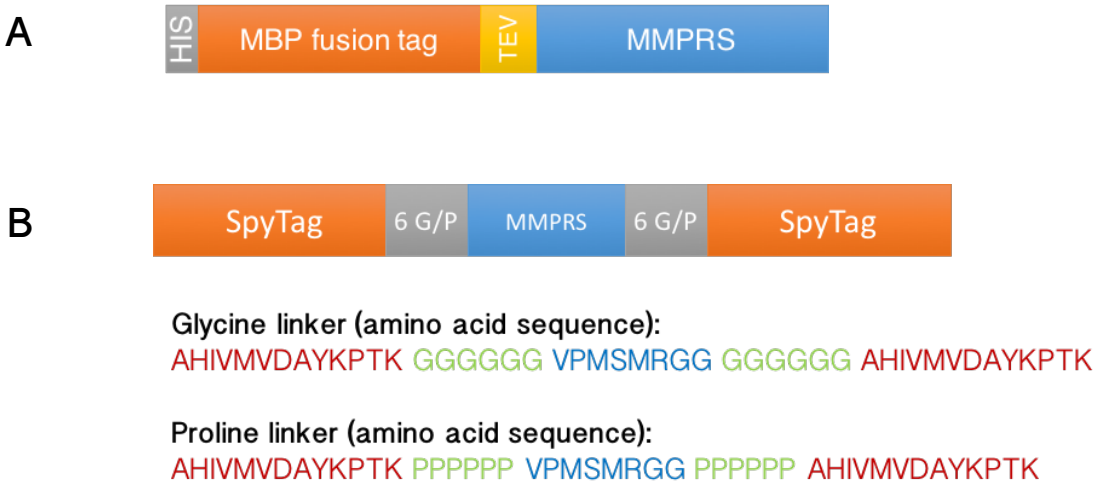

Figure 8.4 — Schematic representations of peptides cloned into the *E. Coli*: (A) The MMPRS (Matrix metalloproteinase recognistion site) peptide is cleavable by certain MMPs. It is coded with a His-Tag, TEV (Tobacco Etch virus) enzyme cleavable peptide and MBP (maltose-binding protein] fusion tag). His-Tag is a six histidine-long tag which allows for protein purification by nickel affinity chromatography. The histidine is out-competed by imidazole during elution steps. The MBP acts as a fusion tag for expressing the MMPRS peptide which enhances solubility, increases protein expression in *E. Coli* and increases the yield of desired product. The TEV enzyme-cleavable peptide has an amino acid sequence of '*ENLYFQC*' and is cleaved at the '*QC*' by the TEV enzyme to separate the MBP protein from the MMPRS peptide. **(B)** In the SpyTag-SpyCatcher approach to gel formation, the MMPRS peptide is coded with SpyTag and an amino acid linker. The SpyTag flags the MMPRS sequence forming a homotelechelic terminally functionalised peptide. 6 G/P (6 glycine or proline) refers to the six amino acid-long linker which comes in two subtypes, glycine and proline.

TEV cleavage reaction

Samples were transferred from the dialysis tubing to 50 ml Falcon tubes. 1 ml of Tobacco Etch virus (TEV) enzyme was added per 20 ml of dialysed sample and shaken overnight for the TEV cleavage reaction to occur.

Nickel affinity chromatography and purification of the MMPRS peptide

The solution from the TEV reaction underwent a second nickel affinity chromatography step to separate the MMPRS peptide from the MBP fusion tag. Nickel resin (10-20 ml) was added to chromatography columns and the storage ethanol drained. Columns were washed once with

Ultrapure water followed by 20 ml of buffer A. The resin was then equilibrated with the samples through repeated inversions for 1 hour. To separate the MMPRS peptide from the MBP fusion tag, the solution was first passed through the column and the flow-through collected as the MMPRS peptide. To elute the MBP protein, 20 ml of buffer B + 250 mM imidazole (**Table 10**) was passed through the column and the elution collected for characterisation.

Protein characterisation

SDS-PAGE protein characterisation

Sodium dodecyl sulphate polyacrylamide gel electrophoresis (SDS-PAGE) was used to determine the success of each nickel affinity chromatography step. Twenty ml of each solution to be characterised was added to 5 ml of dye and pipetted into a 15% SDS gel. A standard protein ladder (SDS-PAGE polypeptide standards, BioRad) was run alongside the samples. The gels were run at 160 V until the indicator dye reached the bottom of the gel. This took approximately 1 to 1.5 hours. The gels were removed and stained with Coomassie Blue stain and de-stained with Destain Solution (10% (v/v) acetic acid, 50% (v/v) methanol and 40% (v/v) water). Gels were imaged using a shielded light box and a camera. Any gels that had extra bands indicating contamination with a product other than the desired peptide were re-run through the corresponding purification step. Any samples that did not show the peptide of interest were discarded.

Sep-Pak Solid Phase Extraction (SPE)

Solid phase extraction (SPE) using Sep-Pak Cartridges (Waters, Massachusetts, USA) was used to separate the remaining components of the flow-through collected from the second nickel affinity chromatography step based on their chemical properties. The desired MMPRS peptide was retained on the stationary phase during the runs and could then be eluted. To condition the SPE cartridge, 3 ml of Conditioning Solution was passed through the packing bed without air entering the cartridge material. The SPE cartridge was equilibrated by passing 2 ml of Equilibration/ Load Solution through the packing bed. The sample was slowly passed through the cartridge (no faster than 1 drop per second) and this was repeated seven times in total. 500 µl of the sample could be taken between each run for further analyses. To desalt the sample, 1 ml Desalting Solution was passed through the cartridge. To elute the sample, 1 ml of Elution Solution was passed slowly through the cartridge and the eluent collected in a 1.5 ml Eppendorf which had been previously weighed.

Freeze drying and lyophilisation

In preparation for lyophilisation, the sample was freeze dried. The lid of the Eppendorf was pierced prior to allow the solvent to evaporate. The sample was then rapidly cooled in a liquid nitrogen bath. Samples were lyophilised overnight.

Analytical High-Performance Liquid Chromatography (HPLC)

Analytical HPLC is a sampling technique used to separate components of solutions based on their chemical properties. Samples were loaded into a modular HPLC system using a 20–80 % gradient over 30 minutes. Insulin was used as a standard that has a characteristic chromatographic peak at 21 minutes.

HPLC fraction collection

1 ml fractions were collected from HPLC at selected chromatographic peaks believed to correspond with the analyte of interest and stored at 4^{o}C.

Matrix-assisted laser ionization-time of flight (MALDI-TOF) mass spectrometry

MALDI-TOF mass spectrometry was used to confirm the presence of the MMPRS peptides based on their expected molecular weights. These were calculated from their amino acid sequences. During sample preparation, equal volumes of ACCA solution (50% α-cyano-4-hydroxy-3-methoxycinnamic acid, 25% TFA and 25% Ultrapure water by weight) and the sample were mixed, vortexed and spotted as 1 μL droplet onto a MALDI-TOF plate. 'ACCA solution only' and 'ACCA solution + a non-analyte fraction' acted as negative controls and 'ACCA solution + insulin' acted as a standard of known molecular weight.

Approach 2 — MMPRS peptide concatenation

Disulphide bond induction

MMPRS peptides can be covalently bonded *via* their terminal cysteine residues by inducing disulphide bond formation. This reaction forms a concatenated polypeptide built from the individual MMPRS units. Not only can disulphide bond induction be used to initiate gel formation, it can also be used to confirm the presence of MMPRS peptides in samples. A concatenated polypeptide will show different physiochemical properties compared with

individual peptides and the corresponding changes in hydrophobicity and molecular mass will be detectable by analytical HPLC and mass spectrometry respectively. To induce disulphide bond formation, oxidising conditions are required and can be provided using a basic pH and aerating the sample. After lyophilisation, the purified samples were reconstituted with sterilised water. Equal volumes of 2M Tris buffer (pH 10.2) and the reconstituted sample were added together in an Eppendorf. Samples were placed on a shaker overnight to allow them to aerate. Samples were then run under analytical HPLC and MALDI-TOF mass spectrometry.

Approach 3 — MMPRS peptide concatenation

Cloning and molecular biology

The SpyTag gene was ordered from GeneScript. Plasmids were transformed into a competent *Escherichia coli* strain, DH10β, using electroporation. 20 µL of sterilised water was used to dissolve the lyophilised DNA. 1 µL of DNA was transferred to 50 µL of DH10β cells and transferred to an electroporation cuvette. The cuvette was pulsed at 2.5 µL (MicroPulser, BioRad), 500 µL of L-Broth immediately to the cells. Cells were shaken for several hours at 37^{o}C. 1 µL of cells were plated on agar plates and incubated overnight at 37^{o}C.

Results

Multi-arm PEG and MMPRS peptide gel

Protein purification and expression

For both subtypes the MBP-MMPRS protein was successfully eluted from the nickel column indicated by 'Elut.' (**Figure 8.5 – A**). The elution was dialysed and the TEV enzyme added for to the TEV cleavage reaction. The TEV reaction was used to cleave the MMPRS peptide from its MBP fusion tag. The gels show that MBP is present both before ('Elut.') and after ('TEV') the TEV reaction (**Figure 8.5 – B**). The MMPRS peptide is not observed as it is of very low molecular weight (~1.5 kDa). After the MMPRS peptide had been cleaved from the MBP protein, it no longer bound to the nickel. Thus, when the sample was passed through the column it could be collected as flow-through ('FT') (**Figure 8.5 – C**). To elute the MBP protein, an imidazole-containing buffer was used ('Wash B'). Presence of MBP in the flow-through suggested not enough nickel had been used in the column so these samples were re-run using 10-20 mL nickel/run until MBP could no longer be detected.

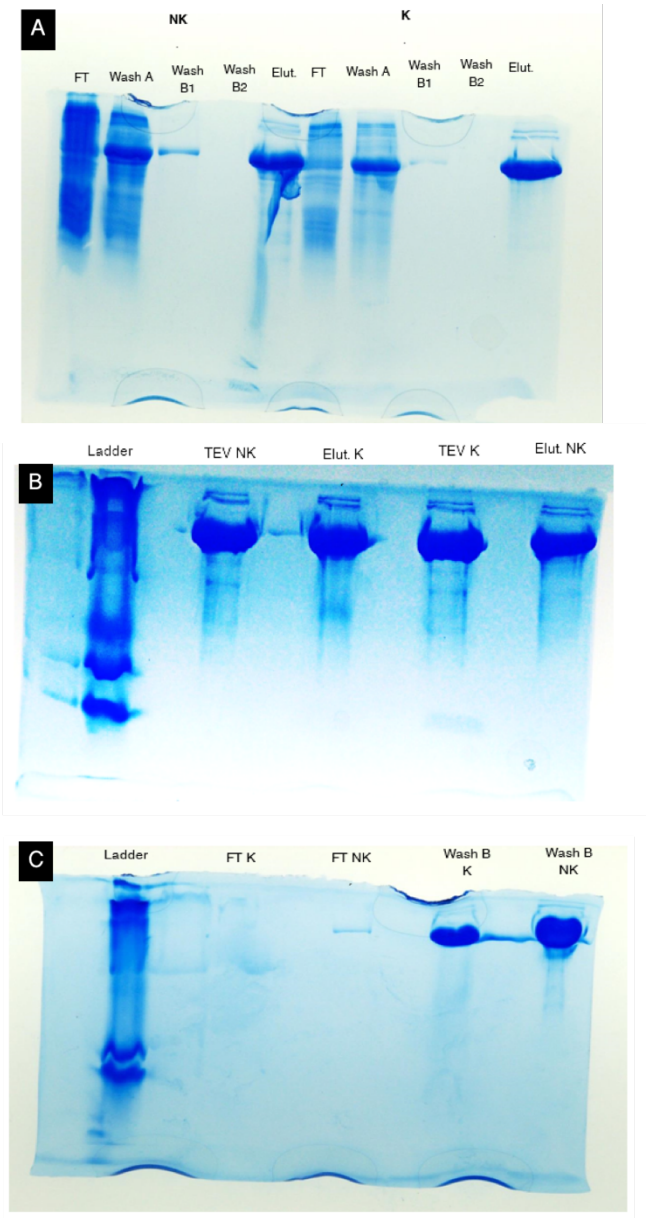

Figure 8.5 — (A) SDS-PAGE gel of nickel purification step one: separating the MMPRS-MBP protein from contaminants. **(B)** SDS-PAGE gel of TEV reaction compared with the elution. **(C)** SDS-PAGE gel of the second nickel purification step — separation of the MMPRs peptide from the MBP fusion tags**.**

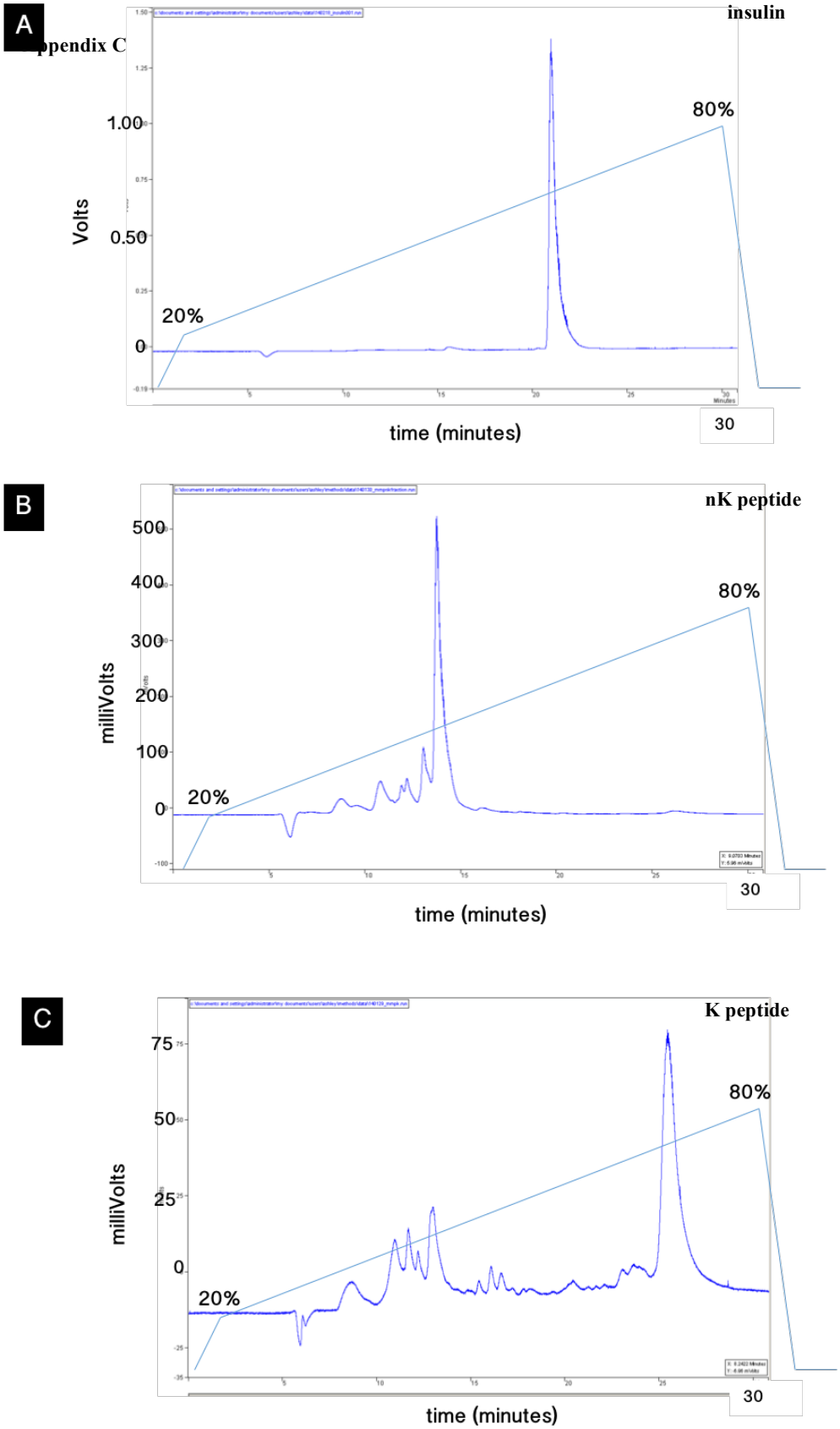

Figure 8.6 — Analytical HPLC traces of MMPRS peptide samples: (A) Analytical HPLC trace of 200mg human insulin gives a characteristic, strong monodisperse peak at 21 minutes. **(B)** Analytical HPLC trace of the nK MMPRS peptide gives a strong peak at 15 minutes. **(C)** Analytical HPLC trace of K MMPRS peptide gives a relatively weaker peak at 27 minutes.

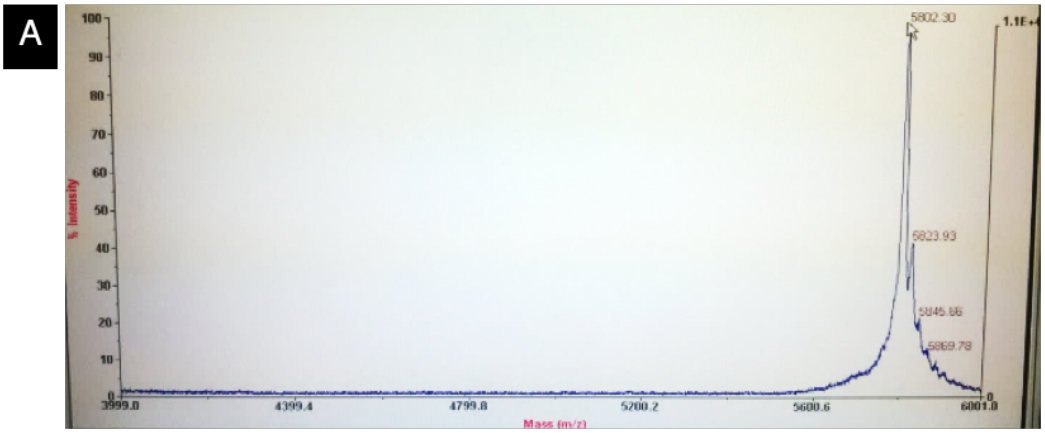

insulin

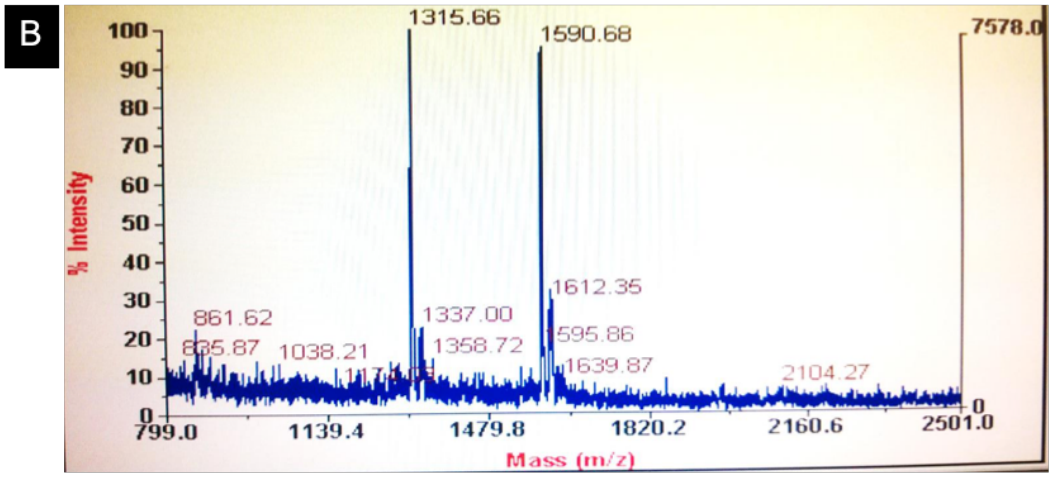

nK peptide

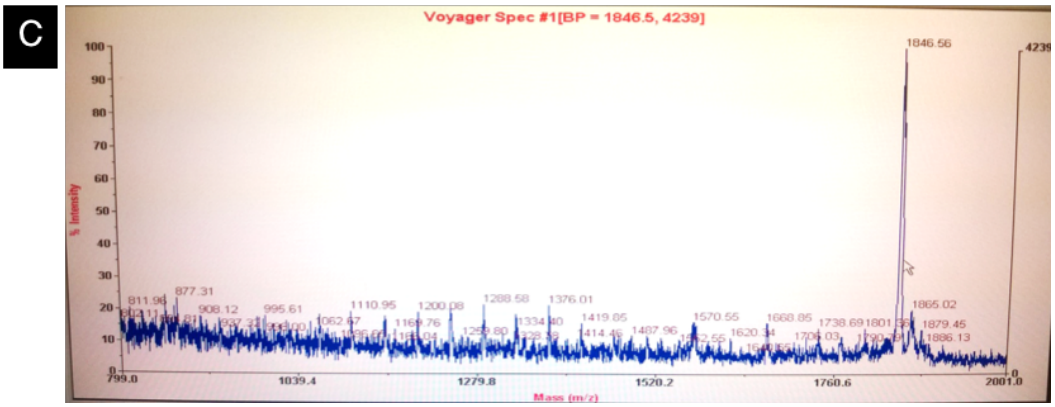

K peptide

Figure 8.7 — MALDI-TOF mass spectrometry graphs for: (A) Human insulin. **(B)** nK MMPRS peptide subtype**. (C)** K MMPRS peptide subtype**.**

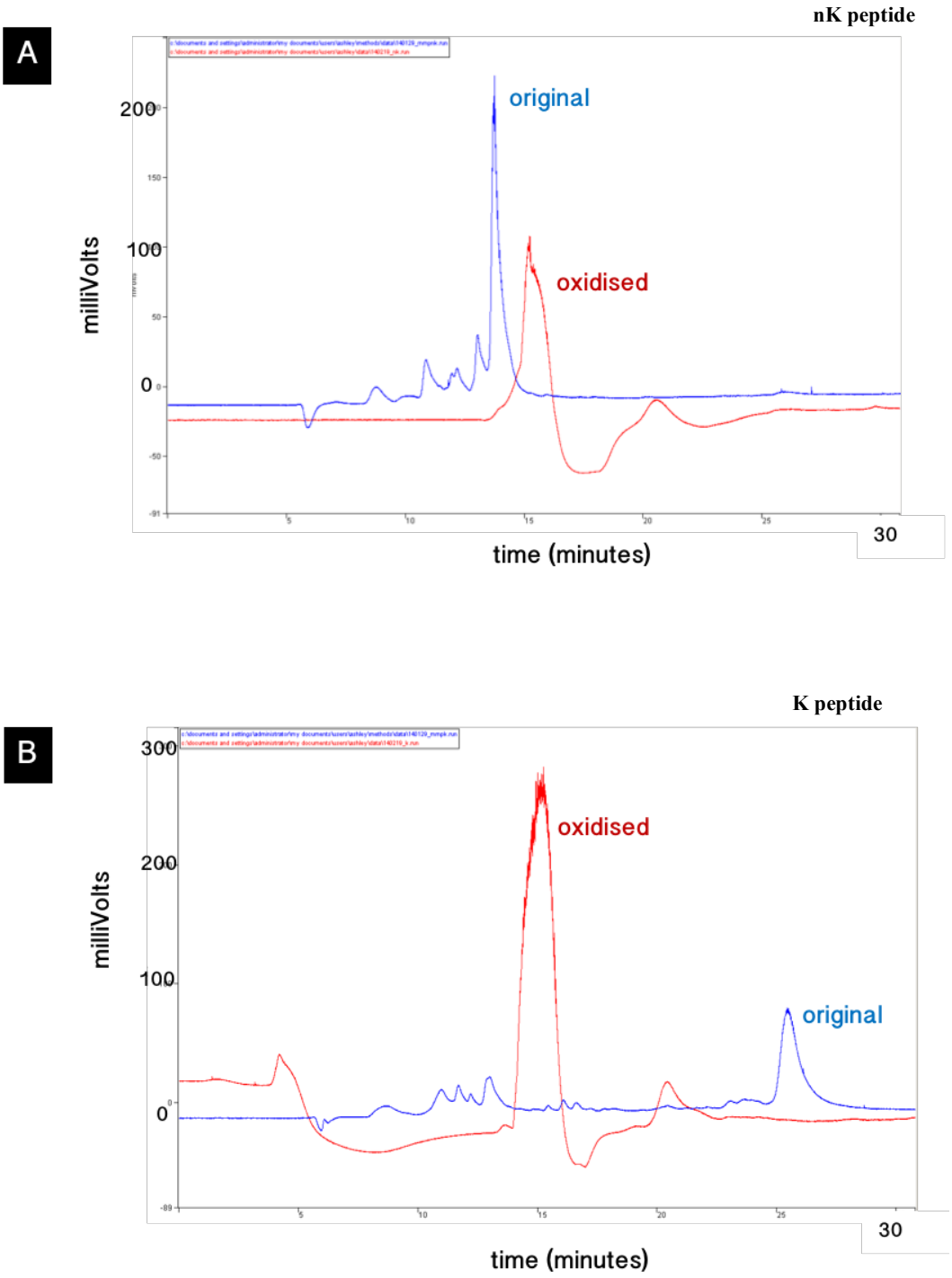

Figure 8.8 —Analytical HPLC traces of oxidised MMPRS peptide samples: (A) nK MMPRS peptide subtype. **(B)** K MMPRS peptide subtype.

Table 11 — Expected and observed peptide masses based on amino acid sequences.

Protein sample	*Observed Mass (Da)*	*Expected mass (Da)*
nK peptide	1316 (and 1591)	1317
K peptide	1847	1573
Human insulin standard	5802	5808

Discussion

The MMPRS peptide was successfully cleaved and purified from its MBP fusion tag

The TEV reaction was responsible for cleaving the MBP fusion tag from the MMPRS peptide. During the second nickel affinity chromatography step, the His-Tag binds the MBP to the column while MMPRS is collected in the flow-through. The results show that when sufficient nickel is used in the column, there are no bands on the SDS-PAGE gel to indicate MBP is present in the flow-through (the MMPRS peptide is itself too small to show up on the SDS-PAGE gel) (**Figure 8.5 – C**). To confirm the presence of the MBP protein, the column contents were eluted using imidazole. The results show that the MBP protein was indeed present and this is indicated by a thick band in the SDS-PAGE gel (**Figure 8.5 – C**). For gels which indicated that MBP was present in the MMPRS flow-through, the flow-through was re-run through the nickel column until the MBP could no longer be detected. Each re-run used between 10–20 mL of nickel resin.

Analytical HPLC on the samples suggested the presence of the two different MMPRS subtypes

Analytical HPLC was used to determine: (i) the chromatographic peak corresponding to each of the MMPRS peptides, (ii) the relative amount of the sample and, (iii) the purity of the sample. The protein standard, human insulin, produced a strong and monodisperse peak at 21 minutes. The trace for nK peptide was not monodisperse but there was a strong peak between 200 - 500mV at 14 minutes (**Figure 8.6 – B**). The trace for K peptide was also not monodisperse and the peak of interest was not as strong at nK, with a measurement of around 75mV at 26 minutes **(Figure 8.6 – C**). Positive indication of the presence of the MMPRS peptides in the samples is the two different peaks. This suggests that two different molecules are present. This is expected as HPLC separates molecules based on their polarity and the nK peptide and K peptides differ by two lysine residues in their amino acid sequences which change the polarity of the K peptide: at pH 7, lysine residues are positively charged. A more hydrophobic peptide is expected to produce a peak later, explaining the nK peptides later time-point. Furthermore, the results

suggest that there was a lower concentration of K than nK in the purified samples and contaminants peaks on the trace could be from salts which were used during the purification steps.

MALDI-TOF mass spectrometry confirmed the presence of the nK MMPRS peptide and suggested the presence of a modified K MMPRS peptide

Both nK and K peptide samples were flown under mass spectrometry to determine the molecular weights of proteins in the sample. These values were compared with the expected molecular weights of the peptides, which are 1317 and 1573, for nK and K respectively. Interestingly, nK samples consistently produced a dual peak (**Figure 8.7 – B**), one at 1316 which is the expected molecular weight and another at 1591, 274 Da greater than the expected molecular weight. The K sample produced a monodisperse peak at 1847 **(Figure 8.7 – C**), which is 275 Da greater than the expected molecular weight. The fact that peaks of different values were consistently obtained for the two different subtypes ruled out contaminants being responsible for the results and heavily suggested the presence of the peptides. However, the dual peak obtained for nK raised the question of potential modifications to the peptides, especially seeing as the difference between expected and observed were comparable, at around 274 Da. Suggestions for the discrepancies include post-translational modifications by the bacteria or some form of oxidation reaction occurring at the cysteine residues. The dual peaks for nK and the single peak for K indicate that there are two species of nK in the samples and a single species of K. This could be explained by the fact that the K peptide is more reactive due to its two additional lysine residues. Thus any modification reactions causing the shift in weight are more likely to go to completion for the more reactive peptide, K. At present, the chemical modification has not been attributed to any reaction.

MMPRS concatenation results are currently inconclusive but could be used to identify presence of MMPRS peptides

The unexpected peaks from the initial mass spec. analyses, with 274Da greater mass than expected, led to the uncertainty of the presence of the MMPRS peptides in the samples. An MMPRS concatenation reaction was thus used to confirm the presence of the peptides, as under oxidising conditions individual peptide units would covalently bond to form a linear polypeptide chain that had different physiochemical properties. However, a major limitation of the oxidisation reaction was the addition of Tris buffer. This caused a rise in pH of the solution interfering with the ACCA matrix and rendering the spotted sample unanalysable by mass spectrometry. To overcome this, for future experiments, the solution can be neutralised carefully with hydrochloric acid after the concatenation reaction which should not interfere

with the disulphide bonds. The oxidised samples were also run under HPLC. For both the K and nK samples, there were peaks at 15 minutes (**Figure 8.8 – A and B**). Neither of the peaks overlapped with the unoxidised samples suggesting a different species in the oxidised sample compared with the unoxidised sample. However, these results were not reproducible. Thus, at present, the analytical HPLC traces for the MMPRS concatenation *suggest* the presence of polypeptide chains but are not conclusive.

SpyTag-SpyCatcher presents a promising approach to MMP-cleavable protein-based gel formation

The SpyTag and SpyCatcher elements are in the process of being expressed and purified. Concatenation of the SpyCatcher is currently being carried out by Ashley Schloss.

Future work

The work carried out in this research collaboration shows promising results in working towards the development of an MMP-cleavable protein-peptide smart gel but requires further work to see it to completion. This includes: (i) the continued characterisation of the MMPRS peptide, (ii) gel formation using functionalised PEG and purified MMPRS peptide and (iii) expression, purification and characterisation of the MMPRS-modified SpyTag peptide and concatenated SpyCatcher protein.

Conclusion

MMP-degradable protein-peptide based smart gels present an interesting and innovative method for delivering drugs in a controlled manner. In chronic wounds, these gels could be used to deliver therapeutics that inhibit the MMPs responsible for preventing the wound from healing properly. There are multiple approaches to gel formation, each with their own advantages and limitations. The unifying features amongst these approaches are that they involve covalently bonded protein-peptide units and an MMP-cleavable component. This MMP cleavable component, known as the MMPRS, has been designed based upon a consensus amino acid sequence that is a natural enzymatic target of the MMPs believed to be upregulated in the chronic wound environment. The MMPRS peptide-PEG gel approach has shown promising results in the production of the individual gel components; however, it appears that the SpyTag-SpyCatcher will be the more successful avenue. In all, this international collaboration has brought together approaches from two different disciplines to address an important clinical problem in an innovative way.

Appendix D — MMP zymography of FPCL supernatant

Introduction

As previously outlined in the main body of the thesis, an up-regulation in MMP activity and/or expression is believed to be responsible for the ECM degradation seen in IR injury tissue. One method for assessing the effect of MMP on the ECM at an injury site is zymography, which is used for the detection of enzyme activity alongside the MMP activity assay. In fact, zymography uses MMP activity to help detect MMP expression. Excised tissue that has undergone IR injury can be liquefied and homogenised and the supernatant used to determine levels of MMPs present in the tissue. Data from these analyses could be used to determine how the activity and/or expression of MMPs correlates with ECM degradation.

Methods and materials

Zymography assay function

Zymography is a technique that uses the intrinsic function of an enzyme to digest molecules to monitor its expression, activation and activity within a solution. Solutions containing the MMP are supplemented with a loading buffer, free of reducing agent, that has several functions which include providing a tracking dye and denaturing the proteins to linearise them. The buffer is loaded into a zymographic gel that contains an MMP substrate such as gelatin. An electric current is passed across the gel which has been immersed in running buffer that is designed to provide a constant migration rate. The current causes proteins to migrate, with the distance of migration being inversely correlated to the protein's molecular weight (that is, smaller proteins will migrate further than larger ones in a given time).

After migration, the gel is bathed in renaturing buffer which allows the proteins to regain their tertiary structure required for enzymatic activity and is then bathed in denaturing buffer which is designed to allow the proteases to digest their substrates. A dye is then applied to the gel is to stain the MMP substrate and the gel is then washed to remove any excess dye. Areas of digestion appear as clear bands in the gel and the clearer the band the more concentrated the protease. Band staining intensity can be determined by a technique known as densitometry which can be carried out using the imaging software, ImageJ® (National Institutes of Health [NIH], Maryland, USA). Once normalised to controls the results can provide information on the expression of MMPs and their pro-MMPs in a solution over a specified period of time.

Sample collection

Supernatant samples (75 µl) were collected from FPCL culture medium on days 0, 3 and 7 and stored at 20^{o}C.

Zymogram gel electrophoresis

Samples were analysed using the Novex^{TM} 10% Zymogram (Gelatin) Gel with the manufacturer's recommended buffers. The manufacturer's claim the gel has a sensitive level of 5 x 10^{-6} units of collagenase. Triplicate samples were combined into a single 1.5 ml Eppendorf. Combined samples (15 µl) and 15 µl of 2x sample Tris-Glycine SDS buffer were added together in a separate 1.5 ml Eppendorf. The gels (10% Zymogram Gelatin Protein Gels, 1.0 mm, 10 well) were rinsed under water, added to the gel box and supplemented with 500 ml of Tris-Glycine SDS running buffer. Individual wells of the gel were cleaned using a 1 ml Pasteur pipette to remove residue. The standard protein ladder was centrifuged and 5 µl loaded into the first well of each gel. Each sample (28 µl) was then loaded into an individual well. The gels were run at 125 V for 90 minutes.

Renaturing and developing zymogram gels

Gels were carefully removed from the gel box and placed into individual washing containers. Fifty ml of 1x zymogram renaturing buffer was added to each gel. The gels were agitated for 30 minutes at room temperature on a plate shaker and the renaturing buffer decanted off. Zymogram 1x Developing Buffer (50 ml) was then added to the gels which were agitated for a further 30 minutes. The developing buffer was decanted replaced with fresh developing buffer and the gels were incubated overnight at 37^{o}C. After 16 hours the developing buffer was drained off and 50 ml of de-iodinated water was added to gels. Gels were agitated for 10 minutes and the water decanted. This step was repeated twice more. The SimplyBlue^{TM} SafeBlue stain (Life Technologies, Paisley, UK) was added directly to the gels (~50 ml per gel) and incubated for an hour with gentle agitation. The stain was drained off and the gels washed with deiodinated water. The gels were imaged under UV light and images were saved electronically for densitometric analysis.

Analysis of zymograms by densitometry

Clear bands appeared on the gels at areas of protease digestion. A protein ladder had been run on the gel so that these bands could be matched to the MMP standard and be identified. To determine the respective concentration of MMP in each band, the band density needed to be determined. This was achieved through densitometry using ImageJ® software. Firstly, the images were converted to 8-bit grey scale files. The 'rectangular selection tool' was used to outline the first band. The band was then numbered and using its outline was moved to the next

band. This was repeated until all the bands were selected. A profile plot of band intensity was generated for each band The 'straight line selection' tool was used to delineate the peaks of interest within separately enclosed areas. The 'wand tool', when clicked inside each peak, selected that peak and gave the corresponding intensity value. Zymographic bands from control and doxycycline-treated FPCLs were normalised to media controls which were complete DMEM only and 416 μM doxycycline (in DMEM), respectively. The normalisation removed the basal MMP expression levels and allowed statistical significance of results to be determined when pooling values from replicate gels.

Results

MMP 2 expression was reduced in doxycycline treated FPCLs.

Doxycycline treatment (416 μM) caused a significant reduction in MMP 2 expression and/or activity by day 7 in the FPCL supernatant. The zymograms of the supernatant collected from the FPCLs yielded four major bands, MMP 2 (63 kDa) and MMP 9 (82 kDa) and their respective zymogens, pro-MMP 2 (72 kDa) and pro-MMP 9 (92 kDa) **(Figure 8.9**). Despite inconclusive results for days 0 and 3, it was evident from triplicate experiments that either the activity, expression or both of MMP 2 was significantly attenuated by day 7 when FPCLs were treated with 416 μM doxycycline (**Figure 8.10**).

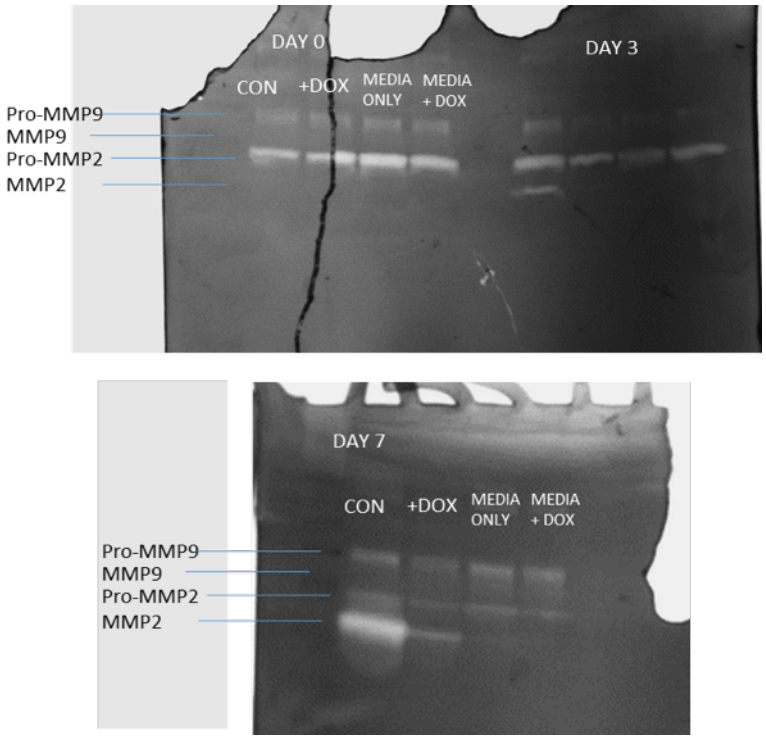

Figure 8.9 — Zymograms showing the band intensity of the gel media at three different time points (days 0, 3 and 7). Pro-MMP 9, MMP 9, pro-MMP 2 and MMP 2 can be detected as determined by the standard protein ladder.

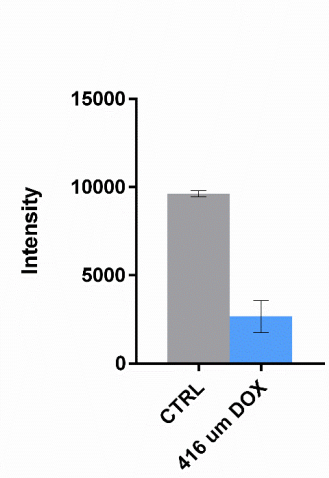

Figure 8.10 — MMP 2 levels were significantly reduced by doxycycline treatment by day 7 (n=3). The bar graph plots the pooled relative band intensities of untreated and FPCLs treated with 416 µM of doxycycline, normalised to media controls. Statisical analysis was carried out using a two-paired parametric *t*-test. Levels of MMP 2 were significantly reduced in FPCL supernatant treated with 416 µM doxycycline by day 7 ($p < 0.001$). *Error bars indicate the standard error of the mean.*

Appendix E — OCT images of drug delivery through a hollow microneedle array

In a preliminary investigation, the insertion of hollow microneedle array into excised murine tissue and its ability to delivery fluids were assessed using OCT. The 4 mm x 5 mm 16 microneedle array (**Figure 8.11**) was synthesised from urethane dimethacrylate (UDMA) and produced by the research group headed by Dr Roger Narayan (Joint Department of Biomedical Engineering, University of North State University, Georgia, USA). The microneedle array was applied by hand onto the apical surface of excised murine dorsum and imaged before, during and after application (**Figure 8.12**). Fluid delivery through the microneedle annuli was visualised using titanium dioxide nanoparticles (5-20 nm) suspended in PBS to provide contrast enhancement in OCT imaging (**Figure 8.13**). From the images obtained it is feasible that OCT could be used to monitor microneedle insertion into the skin and to visualise fluid delivery through the hollow microneedles. OCT, as previously observed with magnetic compression, is also able to detect changes caused by stress and strains to the skin layers.

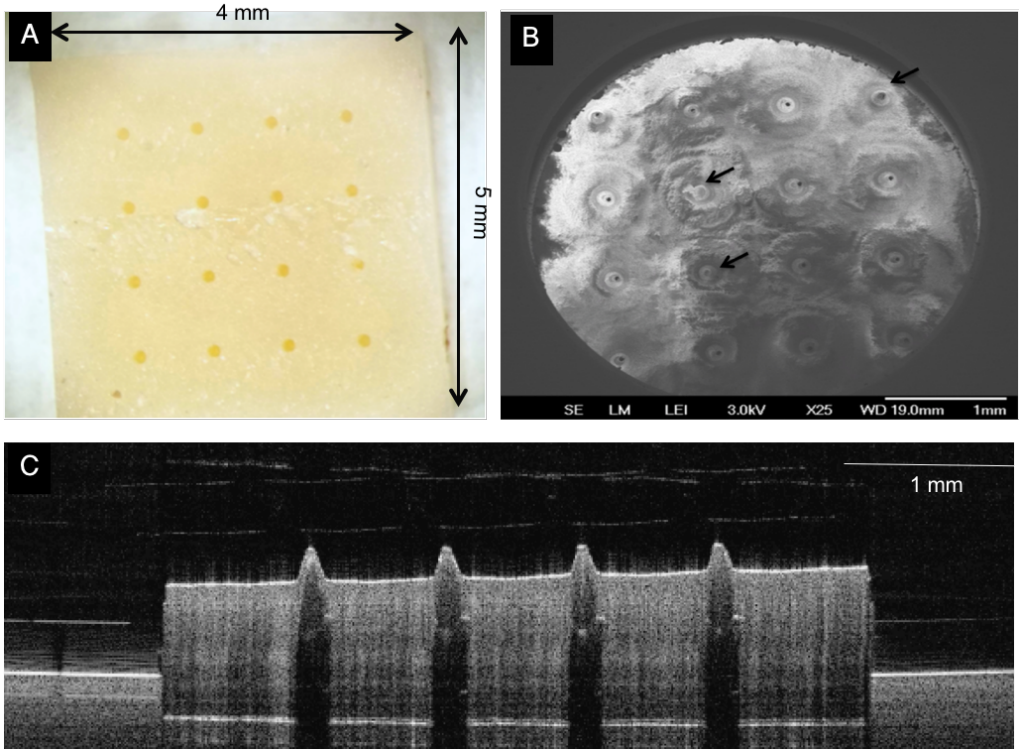

Figure 8.11 — UDMA-based hollow microneedle array: (A) Photograph of the base of the 4 mm x 5 mm array containing 16 microneedles. **(B)** Top-down scannining electron micrograph showing the array's microneedle and their annuli. (**C**) OCT cross-section through the microneedle array.

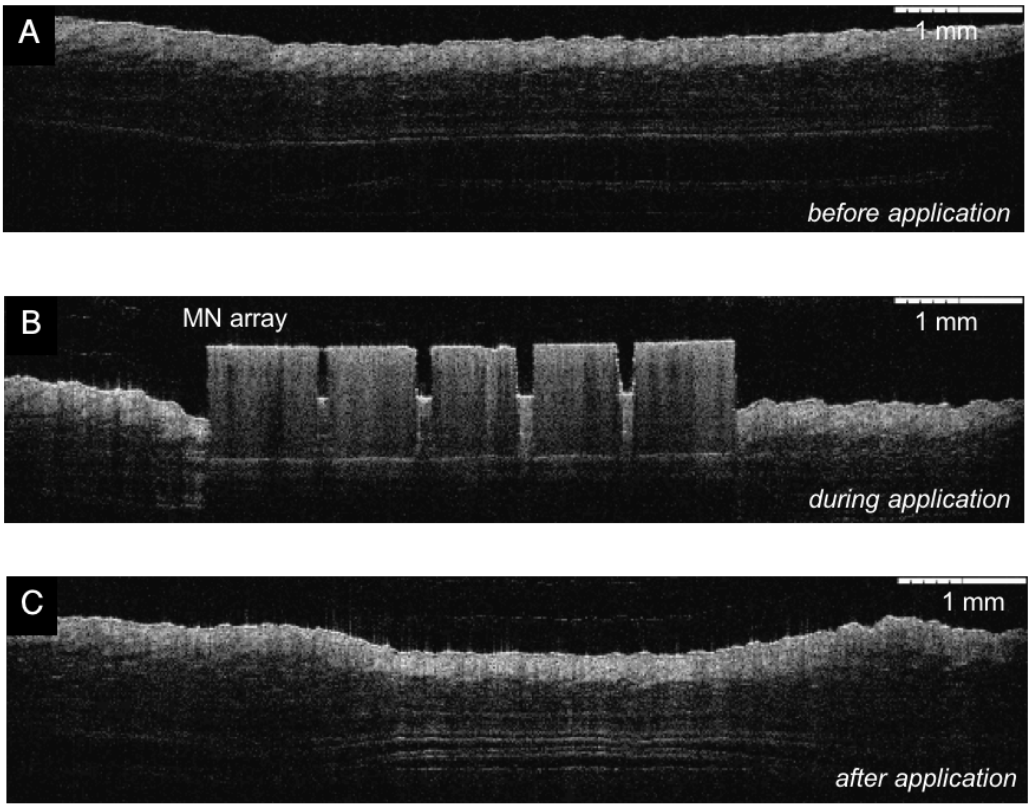

Figure 8.12 — Application of the hollow microneedle array onto excised murine dorsum as visualised by OCT: (A) Skin before array application. **(B)** The microneedle array was applied by hand onto the apical surface of skin. **(C)** At the site of microneedle application, compression of the skin's striations was observed.

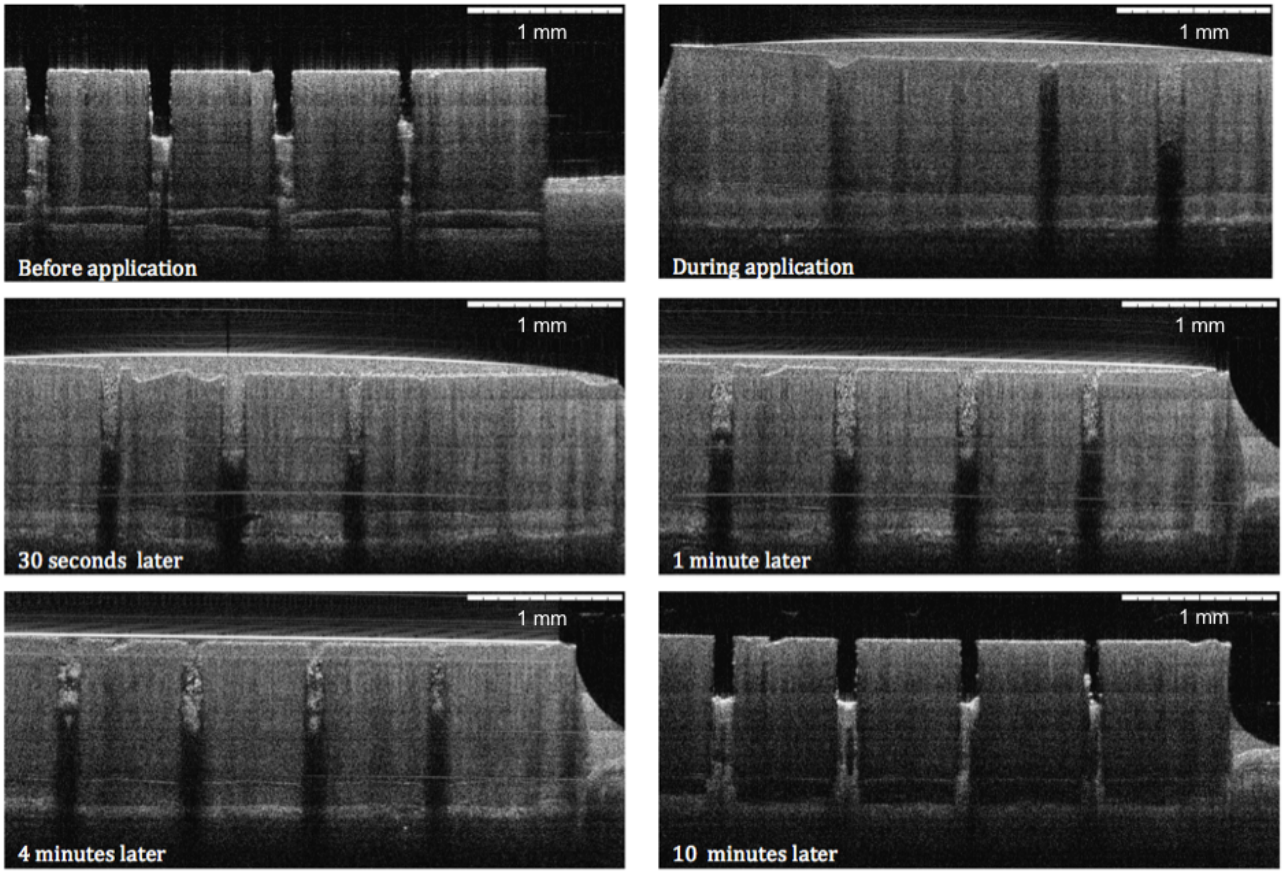

Figure 8.13 — Delivery of titanium dioxide nanoparticles suspended in PBS through hollow microneedles as visualised by OCT.